



UNIVERSITÀ
DEGLI STUDI
DI PADOVA

Università degli Studi di Padova

Dipartimento di Scienze Biomediche

CORSO DI DOTTORATO DI RICERCA IN SCIENZE BIOMEDICHE
31° CICLO

CRITICAL ROLE OF THE THIOREDOXIN AND THE GLUTATHIONE SYSTEMS IN MITOCHONDRIAL PATHOPHYSIOLOGY

Coordinatore: Ch.mo Prof. Paolo Bernardi

Supervisore: Ch.ma Prof. Maria Pia Rigobello

Co-Supervisore: Ch.mo Prof. Alberto Bindoli

Dottoranda: Valeria Scalcon

ACKNOWLEDGEMENTS

First of all, I would like to thank and to express my gratitude to my supervisor Prof. **Maria Pia Rigobello**. Thanks for having been a dedicated guide, being always present and curious of my work along these three years. Thanks also for helping me keeping the right direction, for encouraging me to present my work at several international conferences and for introducing me to the academic community.

I want to thank also my co-supervisor Prof. **Alberto Bindoli** for teaching me a lot, for the various stimulating discussions and for reading thoroughly this thesis. Both my supervisors transmitted me the passion for redox biology and I will always be grateful to them for this.

I thank my colleagues **Alessandra** and **Federica** for creating a nice work environment and for always being helpful and friendly and also for the fun we had during these years.

I thank all the collaborators around Europe in particular Prof. **Anne Vessières** and Prof. **Arne Holmgren** and their groups. I would like to thank especially Prof. **Angela Casini** for the very fruitful collaboration and for being a great example of a talented woman in science.

Thanks to Dr. **Tito Cali** for introducing me into molecular biology and for the support and for the useful advices.

I want to thank also the Master students **Manuela**, **Jurriaan**, **Debora** and **Giulia** because they have been always very helpful, involved in research and “challenged” me to move my first steps in teaching.

Thanks to my friend **Irene** for the enthusiasm and the interest you showed me for my research along these last three years motivating me to do my best.

I thank my parents, **Arrigo** and **Matilde** for the encouragement, the interest and for supporting me in my decision to move to Padua to follow my dreams.

Thanks to my little brother **Davide** to believe in me and to somehow follow my footsteps in the academic field, I wish you a brilliant future.

Last but not the least, my heartfelt thanks to my fiancée **Manuel**. Thank you for all the unconditioned support, for the patience and for taking care of me every day making me feel safe and loved. Words cannot explain how grateful and proud I am to have you beside my side.

Thank you!

Valeria

RESEARCH SUMMARY

The thioredoxin and the glutathione systems are important thiol redox regulating networks. The mitochondrial thioredoxin system is composed by NADPH, thioredoxin reductase 2 (TrxR2) and thioredoxin 2 (Trx2) that, in turn, can reduce peroxiredoxin 3 (Prx3) which has a hydroperoxide scavenging activity.

Cyclophilin D (CypD) is a small protein of the mitochondrial matrix having a crucial role in the control of the mitochondrial membrane permeability transition. CypD activity and redox state were found to be subjected to thioredoxin system-mediated reduction in both isolated rat heart mitochondria and in human cell lines. Furthermore, CypD interaction with Trx2 and Prx3 was observed with both the co-immunoprecipitation technique and with a molecular docking prediction. Thus, CypD can be redox modulated by the mitochondrial thioredoxin system.

The thiol redox regulating systems, especially TrxR2, are often overexpressed in cancer cells to counteract the increased ROS level due to cancer progression. Therefore, the search for specific TrxR2 inhibitors is a possible new anticancer strategy. Several novel compounds, obtained in the frame of different international collaborations, were studied. In particular, a new Au(III) complex bearing a bidentate N-donor ligand, various cyclometalated 2,6-diphenylpyridine Au(III) complexes and a series of mono and bis N-heterocyclic carbene Au(I) complexes were synthesized and were found to inhibit selectively thioredoxin reductase, disrupting the overall cellular redox homeostasis in human ovarian cancer cell lines.

Afterwards, a class of non-gold based metallodrugs, derived from tamoxifen and called tamoxifen-like metallocifens (TLMs), were studied. Interestingly, TLMs act as pro-drugs. In fact, upon enzymatic oxidation, they can be transformed into new oxidized derivatives endowed with remarkable TrxR2 inhibitory properties. In the lymphoblastoid cell line Jurkat, TLMs-mediated TrxR2 inhibition stimulated Trx2 oxidation, ROS production and intrinsic apoptotic pathway activation.

The effects of TrxR2 genetic depletion was also investigated in different cancer cell lines utilizing the Crispr/Cas9 method. Notably, an inverse correlation between TrxR2 protein level and cellular ROS production was observed, indicating the strong pro-oxidizing condition derived from TrxR2 depletion.

Then, the research was focused on glutaredoxin 2 (Grx2). Grx2 was reported to link the thioredoxin and the glutathione systems, but its specific role in redox signaling events is unclear. Grx2 catalyzes protein de-glutathionylations and can also coordinate an iron-sulfur cluster, forming dimers. Grx2 monomeric and dimeric state was analyzed upon HeLa cells treatment with different oxidizing conditions. Grx2 stayed principally as an inactive dimer, while it dissociated, and its activity was stimulated specifically in the mitochondrial compartment, only upon the combined hindering of both the glutathione and the thioredoxin systems. A large increase of free iron ions in the mitochondrial matrix, induction of lipid peroxidation and decrease of the mitochondrial membrane potential were also observed, indicating that Grx2 monomerization implied the release of the iron-sulfur cluster.

In collaboration with Prof. A. Holmgren's group at the Karolinska Institutet, the role of Grx2 in mitochondria has been further studied in a murine model knockout for Grx2 in mitochondria (mGrx2 KO). The overall redox state of mitochondria isolated from different organs of WT or mGrx2 KO mice at three months of age was assessed and interestingly it was not affected from Grx2 deletion. However, a significant increase of mitochondrial ROS production was noted in the liver associated to a decrease of the mitochondrial respiratory capacity, to a reduction of the mitochondrial membrane potential and to an increased sensitivity to calcium ions. Altogether, these results suggest that Grx2 deletion in mouse mitochondria affects mainly the mitochondrial functioning in the liver.

SOMMARIO DELLA RICERCA

I sistemi della tioredossina e del glutathione sono importanti nella regolazione redox cellulare. Il sistema tioredossinico mitocondriale è composto da NADPH, tioredossina reduttasi 2 (TrxR2) e tioredossina 2 (Trx2) che, a sua volta, può ridurre la perossiredossina 3 (Prx3) la quale detossifica dagli idroperossidi.

La ciclofilina D (CypD) è una proteina di matrice mitocondriale che ha un ruolo cruciale nel controllo della transizione di permeabilità di membrana mitocondriale. È stato visto che l'attività e lo stato redox di CypD sono soggetti a riduzione mediata dal sistema tioredossinico sia in mitocondri isolati che in linee cellulari umane. Inoltre, l'interazione di CypD con Trx2 e Prx3 è stata osservata sia tramite co-immunoprecipitazione che con una *molecular docking prediction*. Pertanto, CypD viene regolata redox dal sistema tioredossinico mitocondriale.

I sistemi di regolazione redox, e specialmente la TrxR2, sono spesso sovraespressi in cellule tumorali per contrastare l'aumento dei ROS causato dalla progressione tumorale. Pertanto, la ricerca di inibitori specifici della TrxR2 è una possibile strategia antitumorale. Sono stati studiati diversi nuovi composti nell'ambito di varie collaborazioni internazionali. In particolare, un complesso di oro(III) recante un ligando N-bidentato, vari complessi 2,6-difenilpiridinici di oro(III) e una serie di complessi carbenici di oro(I) sono stati sintetizzati e si sono rivelati in grado di inibire selettivamente la tioredossina reduttasi in linee cellulari tumorali ovariche, alterando l'intero equilibrio redox cellulare. In seguito sono stati studiati una classe di composti metallorganici derivati dal tamoxifene denominati tamoxifen-like metallocifens (TLMs). I TLMs sono profarmaci. Infatti, tramite ossidazione enzimatica, possono essere trasformati in derivati dotati di notevoli proprietà inibitorie sulla TrxR2. Nella linea cellulare linfoblastoide Jurkat, l'inibizione di TrxR2 indotta dai TLMs porta all'ossidazione di Trx2, alla produzione di ROS e all'attivazione della via apoptotica intrinseca.

Utilizzando il metodo Crispr/Cas9, sono stati anche studiati gli effetti della deplezione genetica di TrxR2 in diverse linee cellulari tumorali. Nei cloni knockdown per TrxR2 è stata osservata una correlazione inversa tra il livello di TrxR2 e la produzione di ROS. Ciò indica la forte condizione pro-ossidante derivante dalla mancanza di TrxR2.

Successivamente la ricerca si è focalizzata sulla glutaredossina 2 (Grx2). La Grx2 collega i sistemi tioredossinico e del glutathione, ma il suo ruolo specifico nella segnalazione redox non è stato ancora chiarito. Grx2 catalizza processi di de-glutathionilazione e può anche coordinare un centro ferro-zolfo, formando dimeri inattivi. Per prima cosa lo stato monomero e dimerico di Grx2 è stato analizzato a seguito del trattamento di cellule HeLa con differenti condizioni ossidanti. Grx2 è stata osservata principalmente come dimero inattivo, mentre può dissociare ed attivarsi specificatamente nel compartimento mitocondriale, solo in seguito all'inibizione di entrambi i sistemi tiolici. Ciò porta ad un aumento del ferro labile nella matrice mitocondriale e conseguenti perossidazione lipidica e diminuzione del potenziale di membrana mitocondriale.

In collaborazione con il gruppo del Prof. A. Holmgren presso il Karolinska Institutet, il ruolo di Grx2 nei mitocondri è stato ulteriormente studiato in un modello murino knockout per Grx2 nel comparto mitocondriale (mGrx2 KO). Lo stato redox di mitocondri deficitari di Grx2 non è stato trovato alterato nei diversi organi isolati da animali mGrx2 KO a tre mesi di età. Tuttavia, a livello epatico, sono stati osservati un aumento significativo della produzione mitocondriale di ROS, una diminuzione della capacità respiratoria e del potenziale di membrana mitocondriale associati ad una maggiore sensibilità degli stessi mitocondri agli ioni calcio. Complessivamente, questi risultati suggeriscono che, nel modello murino, il fegato è il principale organo affetto dalla delezione mitocondriale di Grx2.

INDEX

1. Introduction	9
1.1 ROS, oxidative stress and redox signaling	9
1.1.1 Reactive oxygen species: general introduction	9
1.1.2 Significance of ROS in the cell	9
1.1.3 Redox regulated proteins	11
1.2 Cellular sources of ROS	12
1.2.1 NADPH oxidase	12
1.2.2 Mitochondria	13
1.3 Thiol redox regulating systems	13
1.3.1 The thioredoxin system	14
<i>1.3.1.1 Thioredoxin reductases</i>	14
<i>1.3.1.2 Thioredoxins</i>	17
<i>1.3.1.3 Peroxiredoxins</i>	18
<i>1.3.1.4 Thioredoxin interacting protein</i>	19
1.3.2 The glutathione system	20
<i>1.3.2.1 Glutathione reductase</i>	20
<i>1.3.2.2 Glutathione</i>	21
<i>1.3.2.3 Glutathione peroxidases</i>	22
<i>1.3.2.4 Glutaredoxins</i>	23
<i>1.3.2.5 Glutathione S-transferases</i>	25
1.4 Oxidative stress and diseases	26
1.4.1 Cancer	26
<i>1.4.1.1 Targeting mitochondria for anticancer therapy</i>	27
<i>1.4.1.2 Targeting antioxidant systems for anticancer therapy</i>	28
1.4.2 Metabolic syndrome	32
2. Aims	35

3. Materials and Methods	37
3.1 Enzymes	37
3.2 Cell lines	37
3.3 Animal models	37
3.4 Enzymatic activities and BIAM assay	38
3.4.1 Thioredoxin reductase activity	38
3.4.2 Glutathione reductase activity	39
3.4.3 Glutaredoxin activity	39
3.4.4 BIAM assay	39
3.5 Experiments performed in cultured cells	39
3.5.1 MTT assay	39
3.5.2 Preparation of cell lysates	40
3.5.3 Preparation of cytosolic and mitochondrial cell fractions	40
3.5.4 Determination of cellular ROS production	40
3.5.5 Determination of total thiols	40
3.5.6 Estimation of total and oxidized glutathione	41
3.5.7 Evaluation of the redox state of Trx1, Trx2 and CypD	41
3.5.8 Determination of the monomer/dimer ratio of Prx3 and Grx2	41
3.5.9 Mitochondrial thioredoxin reductase depletion	42
3.5.10 Trx2 overexpression	42
3.5.11 Co-immunoprecipitation of CypD with Trx2 from Trx2 overexpressing HeLa cells	43
3.5.12 Flow cytometric analysis of the mitochondrial membrane potential	43
3.5.13 Flow cytometric analysis of the mitochondrial superoxide production	43
3.5.14 Determination of lipid peroxidation in HeLa cells	43
3.5.15 Estimation of cytochrome c release and caspase 3 activation	44
3.5.16 Determination of PARP-1 activity	44
3.5.17 ICP-OES metal quantification in Jurkat cells	44

3.5.18 Quantification of the labile iron pool in HeLa cells mitochondrial fractions	45
3.6 Experiments performed on isolated mitochondria	45
3.6.1 Mitochondria isolation and preparation of mitochondrial matrix	45
3.6.2 Measurement of CypD, Trx2 and Prx3 amount in rat heart and liver mitochondrial matrix	46
3.6.3 Determination of ROS production	46
3.6.4 Evaluation of the redox state of Trx2 and CypD	46
3.6.5 Measurement of the mitochondrial membrane potential	47
3.6.6 Estimation of mitochondrial swelling	47
3.6.7 Determination of the oxygen consumption	47
3.6.8 Assessment of total thiols	47
3.6.9 Estimation of the total and oxidized glutathione	47
3.6.10 Estimation of CypD PPIase activity	47
3.6.11 Co-immunoprecipitation of CypD with Trx2 and Prx3	48
3.7 RNA isolation and RT-qPCR analysis of Grx2 RNA	48
3.8 Western blot procedure and list of the primary antibodies	49
3.9 Molecular modelling of the interaction of CypD with Prx3 or Trx2	49
3.10 Enzymatic oxidation of TLMs by the HRP/H₂O₂ mixture	50
3.11 EPR spectroscopy studies on ansaFc	50
3.12 Statistical analysis	50
4. Results and Discussion	51
4.1 Targets of the mitochondrial thioredoxin system	51
4.1.1 CypD isomerase activity is induced by the thioredoxin system	51
4.1.2 Inhibition of the thioredoxin system triggers CypD oxidation	52
4.1.3 Molecular modelling of the interaction of CypD with Prx3 and Trx2	55
4.1.4 Co-immunoprecipitation of CypD with Trx2 and Prx3	55

4.2 Thioredoxin reductase as a target in cancer therapy	58
4.2.1 Thioredoxin reductase 2 genetic depletion	58
4.2.2 Thioredoxin reductase inhibitors as potential anticancer drugs	59
4.2.2.1 <i>Benzimidazole-4-carboxamide Au(III) complex</i>	60
4.2.2.2 <i>Diphenylpyridine Au(III) complexes</i>	63
4.2.2.3 <i>N-heterocyclic carbene (NHC) Au(I) complexes</i>	65
4.2.2.4 <i>Tamoxifen-like metallocifens</i>	69
4.3 Glutaredoxin 2 in the mitochondrial compartment: interplay between thioredoxin and glutathione systems	82
4.3.1 Grx2 response to oxidative stress in a cellular model	82
4.3.2 Effects deriving from mitochondrial Grx2 deletion in mice	86
4.3.2.1 <i>Determination of Grx2 amount and activity in mGrx2 KO mouse mitochondria</i>	86
4.3.2.2 <i>Analysis of the mitochondrial redox state</i>	88
4.3.2.3 <i>Study of liver mitochondria functioning</i>	90
5. Conclusions	92
5.1 Mitochondrial thioredoxin system mediates redox regulation	92
5.2 TrxR2 inhibition and consequences in cancer cells	92
5.3 Role of Grx2 in mitochondrial thiol redox regulation	94
6. List of publications	96
7. Abbreviations	97
8. References	99

1. Introduction

1

1.1 ROS, oxidative stress and redox signaling

1.1.1 Reactive oxygen species: general introduction

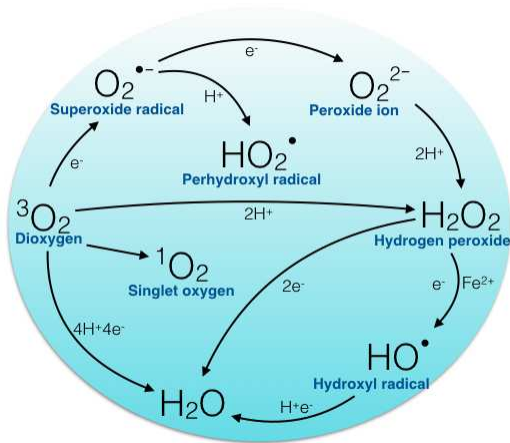


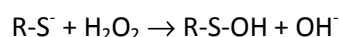
Fig. 1 ROS generation chain.

ROS, acronym of reactive oxygen species, indicates a group of moieties deriving from dioxygen (O₂) reduction. Of note, O₂ can accept only one electron at a time and thus its complete reduction to water requires different consecutive steps with the formation of reactive intermediates. In Fig. 1 the scheme of generation of the various ROS species is reported. In general, ROS can be divided into two major subgroups: radicals (superoxide anion, hydroxyl radical and perhydroxyl radical) that are highly reactive, and non-radicals (hydrogen peroxide and peroxides) which are more stable. In addition, ROS comprise singlet oxygen that is an excited form of dioxygen and which is formed, for instance, in the photodynamic process. ROS are generally endowed with a

high reactivity. In the biological context, all the cellular components namely lipids, proteins, sugars and nucleic acids can be affected and stably modified by these species. The effects of these modifications might be deleterious since they can affect DNA replication, membrane composition, enzymatic activities and key biochemical processes. Thus, all aerobic organisms that rely on O₂ consumption for their metabolism and energy production have to face ROS species and need to control their amount to avoid cell damage.

1.1.2 Significance of ROS in the cell

The excessive increase of ROS in cells is known as oxidative stress, which has been defined as a “disturbance in the prooxidant-antioxidant balance in favor of the former”.¹ However, in the last decades, many growth factors and hormones were shown to induce transient intracellular increases of hydrogen peroxide (H₂O₂) as a consequence of their signaling cascade. Platelet-derived growth factor,² epidermal growth factor,³ vascular endothelial growth factor (VEGF),⁴ tumor necrosis factor alpha (TNF-α),⁵ and insulin⁶ are the most prominent examples but also some neurotransmitters and cytokines are able to generate localized intracellular H₂O₂ fluxes.⁷ Therefore, ROS are not only deleterious species for the cell, but they can also be involved in signaling processes, known as redox signaling, that are essentially mediated by H₂O₂.^{8,9} It is important to underline that, in oxidative stress conditions, there is an uncontrolled and permanent increase of ROS which eventually damage cell components. Instead, in redox signaling events, the ROS production is transient, localized and limited to H₂O₂. Like other second messengers, H₂O₂ needs specific targets to evoke a peculiar response to the initial stimulus. In addition, the modification must be reversible in order to control the signal transduction. In redox signaling, it is largely recognized that H₂O₂ reacts specifically with protein thiols, with the generation of sulfenic acid as shown in the following equation:



This reaction is very fast since it is not kinetically hindered and in line with the velocity of a signaling event.¹⁰ Cell thiols were found to undergo continuous oxidation at a rate of about 0.5% of the total thiol pool per minute.¹¹ The oxidation of thiols by H₂O₂ has been known for a long time.¹² However, not all protein thiols, namely all the cysteine residues (Cys), present the same rate of reaction. Indeed, Cys show different reactivities according to the protein structure, hydrophobicity, and electronic environment.¹⁰ To reach high rate constants, the Cys needs to be in the nucleophilic dissociated form (thiolate). Next to basic amino acids, Cys become extremely reactive at physiological pH, due to a lowering of their pKa from typically eight to five/seven.¹³ It is interesting to note that the number of proteins containing at least one Cys increases along with evolution, indicating a development of signaling and regulatory functions of this amino acid.¹⁴

In comparison with other ROS species, H₂O₂ is relatively stable. Of note, H₂O₂ is able to cross cell membranes through channels called aquaporins diffusing into the cell environment to target the reactive Cys of the effector protein.^{8, 15} Consequently, H₂O₂ can be very selective in targeting certain protein Cys transiently generating sulfenic groups. Once oxidized, sulfenic cysteines can react with another protein thiol forming an intra- or inter-protein disulfide bond or can undergo glutathionylation through the formation of a disulfide bridge with glutathione (GSH). These bonds affect protein conformation and/or

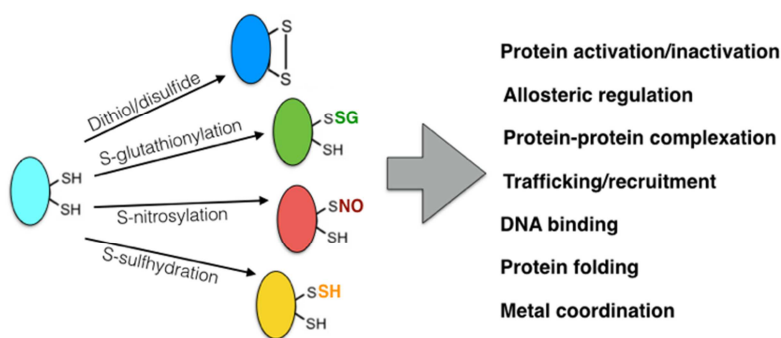


Fig. 2 Principal Cys redox modifications and functions modulated by alterations of protein thiol redox state.

activity. Single Cys redox reactivity is not limited to H₂O₂ interaction. In fact, they can also be nitrosylated by nitric oxide (NO), acylated by acetyl-CoA, sulphydrated by sulfidric acid, they can form thiohemiacetals in the presence of aldehydes or they can coordinate iron-sulfur (Fe-S) clusters.^{16, 17} Protein CoAlation is emerging as a novel post translational redox modification and consists in the Cys derivatization

mediated by coenzyme A (CoA). Recent findings suggest that the amount of CoAlated proteins could be influenced by nutrient availability.¹⁸ Each thiol modification can change the protein function through three different mechanisms: by alkylating Cys in the active site, by influencing its interactions with other macromolecules and by modulating the enzymatic activity through modification of allosteric Cys.¹¹ Fig. 2 shows the major Cys modifications occurring in proteins and the functions that can be affected by these derivatizations. Of note, different modifications can occur concomitantly on various Cys residues present on the same protein for a fine modulation of its function.

Together with reactive Cys, selenocysteines (Sec) are also highly reactive towards H₂O₂. Indeed, Sec possess a pKa around 5 that enables them to easily dissociate at physiological pH conferring high reactivity with H₂O₂. Moreover, their catalytic efficiency is higher with respect to Cys.¹⁹ Table 1 highlights the principal differences between Cys and Sec. Sec is considered the 21st protein amino acid and it is generated by the post-translational modification of the protein mediated by a complex machinery which incorporates a selenium atom into a serine.^{20, 21} In the human genome only 25 selenoproteins are present and many of them have a role in the control of cellular redox regulation.^{22, 23}

Table 1: Properties of the amino acids cysteine and selenocysteine (adapted from²⁴)

	<i>Cysteine</i>	<i>Selenocysteine</i>
<i>pKa</i>	8.3	5.2
<i>redox potential</i>	-233 mV	-488 mV
<i>codons</i>	UGU and UGC	UGA + hairpin structure

1.1.3 Redox regulated proteins

In the last decades, thanks to the “omics” approach, many proteins subjected to redox regulation have been identified. Recognized targets of H₂O₂ include transcription factors, molecular chaperones, peptidases, metabolic enzymes, protein kinases and phosphatases and many others.¹⁰

Focusing on the mitochondrial compartment, many redox regulated proteins have been identified. For instance, superoxide dismutase 1 (SOD1 or Cu/Zn SOD), the cytosolic isoform of the protein that is also present in the mitochondrial intermembrane space, was reported to be activated by low concentrations of H₂O₂ through the oxidation of two Cys present in its active site.²⁵ In addition, the small mitochondrial peptidyl prolyl *cis-trans* isomerase cyclophilin D (CypD) was reported to be a redox sensor. Indeed, CypD was shown to be nitrosylated on Cys203 and this modification was hypothesized to inhibit the opening of the permeability transition pore.^{26, 27} This hypothesis was confirmed by the observation that mouse liver mitochondria expressing the CypD mutant Cys203Ser were insensitive to Ca²⁺ induced mitochondrial permeability transition.²⁸ Also F₀F₁-ATP synthase is sensitive to ROS. In particular, oxidation of certain Cys in F₀ subunit resulted in complete and reversible uncoupling in bovine heart mitochondria.^{29, 30} In addition, Wang and colleagues found that Cys294 in the ATP α subunit of F₀F₁-ATP synthase can form an intermolecular disulfide bond with Cys103 of the ATP γ subunit in canine heart. However, these two Cys are located in distant positions in the assembled complex suggesting that these residue may bind only in misfolded/aggregated enzymes.^{27, 31} Cys294 was also reported to undergo nitrosylation and glutathionylation.³¹ Via quantitative proteomics, an increased Cys oxidation was reported in murine cardiomyocytes, during ischemia and reperfusion, at several subunits of F₀F₁-ATP synthase, including in the CypD binding site indicating a pathophysiological relevance of specific Cys redox modifications which can cause profound conformational changes of F₀F₁-ATP synthase complex leading to modulation of its activity.³² Moreover, F₀F₁-ATP synthase is activated by deacetylation mediated by sirtuin 3 (Sirt3). ROS can modulate Sirt3 expression and in turn F₀F₁-ATP synthase activity.³³

Since many cellular proteins are subjected to redox modulation of their activity, during evolution, a complex network of proteins able to produce and to remove ROS, enabling a controlled redox regulation, have been developed by the cell. In the next two paragraphs the cellular ROS sources and scavengers are presented with a focus on the thiol scavenging systems.

1.2 Cellular sources of ROS

The major cellular ROS generators are NADPH oxidases and mitochondria. However, many other sources are present such as xanthine oxidase, lipoxygenases, cyclooxygenases, D-amino acid oxidase, cytochromes P450, peroxisomes, ER-stress and many others (Fig. 3).³⁴⁻⁴¹

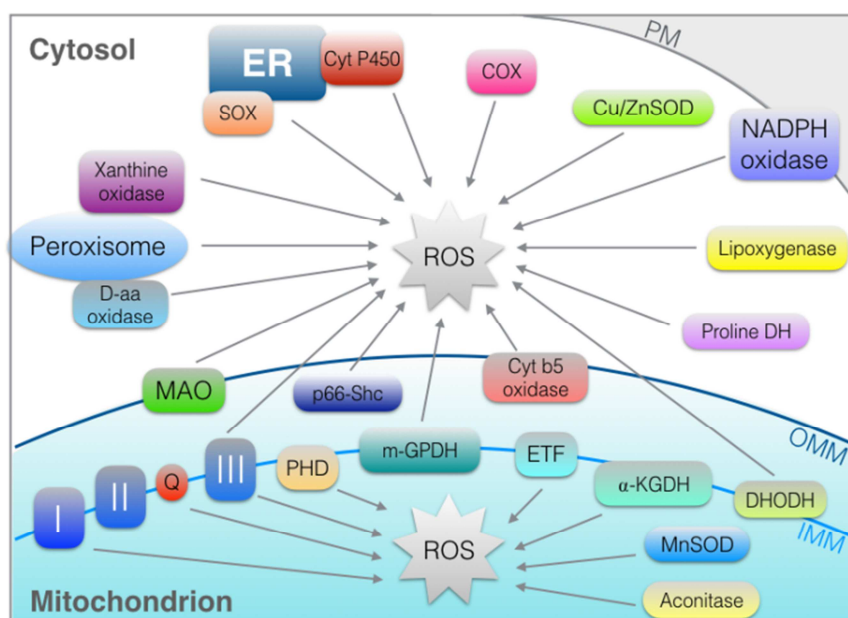


Fig. 3 Cellular sources of ROS. In the cytosol ROS are produced by: NADPH oxidase, proline dehydrogenase (Proline DH), lipoxygenase, xanthine oxidase, D-amino acid oxidase (D-aa oxidase), peroxisomal fatty acid oxidation, cytochrome P450 (Cyt P450), sulfhydryl oxidases (SOX), endoplasmic reticulum stress (ER) cyclooxygenases (COX), superoxide dismutase 1 (Cu/Zn SOD). In mitochondria the ROS generators are: complex I (I), complex II (II), complex III (III) of the respiratory chain, coenzyme Q (Q), pyruvate dehydrogenase (PDH), mitochondrial glycerophosphate dehydrogenase (mGPDH), electron transfer flavoprotein (ETF), alpha-ketoglutarate dehydrogenases (α -KGDH), dihydroorotate dehydrogenase (DHODH), aconitase, superoxide dismutase 2 (MnSOD), protein p66-Shc, cytochrome b5 oxidase (Cyt b5 oxidase),

monoamine oxidase (MAO). PM: plasma membrane, OMM: outer mitochondrial membrane, IMM: inner mitochondrial membrane. The arrows indicate the direction of ROS production.

1.2.1 NADPH oxidase

NADPH oxidase is a multimeric protein complex initially discovered in phagocytic cells such as neutrophils and macrophages. It is responsible for the so called “respiratory burst” an oxygen-consuming process that produces ROS against invading pathogens.⁴²⁻⁴⁴ Phagocytic NADPH oxidase is formed by a catalytic subunit, gp91phox that, along with the p22phox subunit, forms a heterodimer called Nox2, associated to the plasma membrane.^{42, 43} The complex has many cytosolic regulatory subunits such as p47phox, p67phox, and the small GTPases Rac1 or Rac2 which are necessary for its activation. In the catalytic process, two heme-groups of gp91phox transfer the electrons from NADPH, through the flavin prosthetic group, to oxygen, generating superoxide anion ($O_2^{\bullet-}$). Other non-phagocytic oxidases are Nox1, Nox3, Nox4, Nox5 and the dual oxidases Duox1 and Duox2.⁴⁵ The latter two oxidases are found mainly in the thyroid gland. The non-phagocytic NADPH oxidases can be activated by the regulatory subunits or by calcium ions as in the case of Nox5 and Duox1/2.⁴⁶ Therefore, NADPH oxidases offer the unique ability of forming ROS upon specific stimuli in a highly regulated manner, as required in signaling processes, by rapidly generating low concentrations of $O_2^{\bullet-}$, and easily stopping when the complex gets degraded.⁴⁷ NADPH oxidases have been associated with cell survival, proliferation, differentiation and migration signaling.^{43, 48} NADPH oxidase is not only localized on the plasma membrane, as specific isoforms are also found in endoplasmic reticulum (ER), nucleus, and mitochondria^{46, 49} and might be associated to different redox signaling pathways.

1.2.2 Mitochondria

Mitochondrial respiration produces a large amount of ROS through the electron leakage from the respiratory chain especially from complex I and III.^{50, 51} In fact, 2% of oxygen gets transformed into $O_2^{\bullet-}$,⁵² which is then rapidly dismutated by MnSOD to H_2O_2 .⁵³ However, mitochondrial ROS are not only a by-product of the electron transport chain. On the contrary, they are actively produced by many enzymes as summarized in Fig. 3. In the inner mitochondrial membrane, glycerolphosphate dehydrogenase (m-GPDH) and dihydroorotate dehydrogenase generate H_2O_2 and $O_2^{\bullet-}$ both directed towards the cytosol,^{54, 55} instead electron transfer flavoprotein (ETF) and alfa-ketoglutarate dehydrogenase (α -KGDH) produce ROS principally addressed to the mitochondrial matrix.^{56, 57} In the outer mitochondrial membrane two other sources of ROS have been identified, cytochrome b5 reductase⁵⁸ and monoamine oxidase.⁵⁹ In the intermembrane space, H_2O_2 is generated also by p66Shc, an apoptosis and lifespan regulator.⁸ Finally, in the matrix, aconitase utilizes H_2O_2 to form hydroxyl radicals.⁶⁰

Cardiolipin, the principal component of the mitochondrial inner membrane, is affected by ROS and its peroxidation leads to the release of cytochrome c (Cyt c).⁶¹ Of note, it is Cyt c itself that catalyzes H_2O_2 -dependent cardiolipin peroxidation which, in turn, facilitates its detachment from the outer surface of the inner mitochondrial membrane.⁶² As apparent, in mitochondria many ROS sources are present. Moreover, a specific isoform of NADPH oxidase, Nox4, presents also a mitochondrial localization⁶³ and it was shown to affect the thiol redox state of many mitochondrial proteins such as adenine nucleotide translocase, key components of the respiratory chain and enzymes of the Krebs cycle.⁶⁴ These findings lead to the conclusion that probably thiol redox regulation needs to be tightly controlled in this subcellular organelle. In addition, the spread of ROS towards opposite directions across mitochondrial membranes suggests different targets that are for the great majority largely unknown.

1.3 Thiol redox regulating systems

In order to balance ROS concentration, together with ROS producers, multiple scavenging systems are present in the cell. These systems are both enzymatic and non-enzymatic. The non-enzymatic ones are principally the vitamins α -tocopherol and ascorbic acid, which are lipophilic and hydrophilic, respectively. However, the main actors for the control of the cellular ROS balance are the antioxidant enzymes. As already mentioned in the previous paragraph, SODs are present both in the cytosol and in mitochondria to transform the reactive $O_2^{\bullet-}$ in H_2O_2 .⁵³ Once H_2O_2 is formed, it gets detoxified principally by catalase and by two enzymatic thiol redox regulating systems namely the thioredoxin and the glutathione systems. Catalase decomposes H_2O_2 to water utilizing a heme prosthetic group, and presents mainly a peroxisomal localization while it shows a low expression in mitochondria.⁶⁵

The thioredoxin and the glutathione systems are present both in the cytosolic and in the mitochondrial compartments and both receive reducing equivalents from NADPH (Fig. 4). $NADP^+$ is reduced by the pentose phosphate pathway in the cytosol and by the nicotinamide nucleotide transhydrogenase in mitochondria.¹⁰ In addition, glutamate and isocitrate dehydrogenases utilize both NAD^+ and $NADP^+$ for the oxidation of their substrates, providing a further source of NADPH.⁶⁶ The NADPH/ $NADP^+$ ratio is fundamental to maintain these systems active. Consequently, strong oxidizing conditions cannot be managed by the cell. This concept further supports the idea that these systems are principally involved in signaling events more than in simple scavenging pathways.

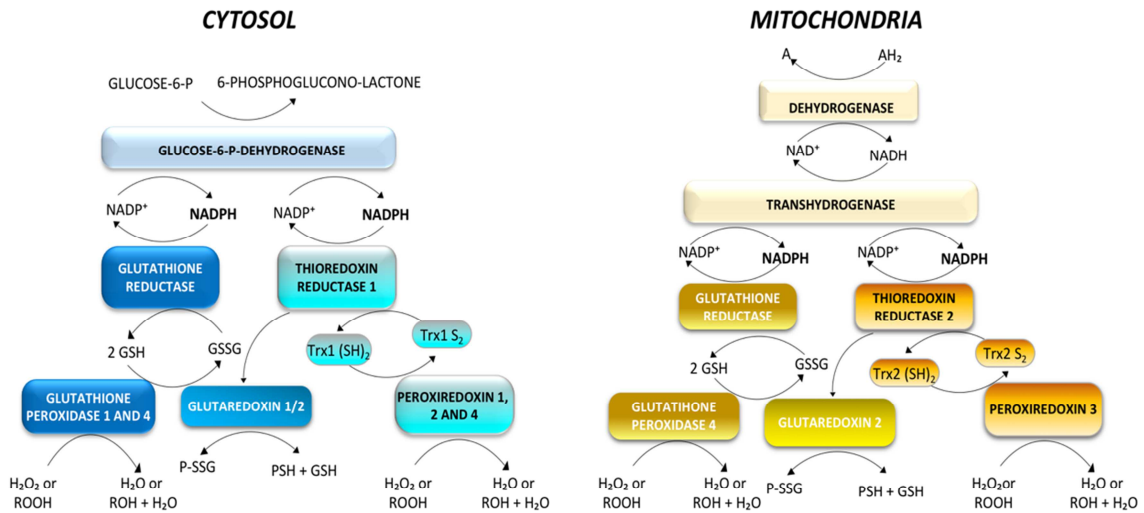


Fig. 4 Cytosolic and mitochondrial thiol redox regulating systems.

The thioredoxin system

The mammalian thioredoxin system consists of NADPH, thioredoxin reductase (TrxR), and thioredoxin (Trx) (Fig. 4). The cytosolic and the mitochondrial systems are formed by different isoenzymes encoded by genes located in separate chromosomes.^{10, 67} In particular, human cytosolic thioredoxin reductase, also known as thioredoxin reductase 1 (TrxR1) is encoded by TXNRD1 gene located on chromosomes 12q23.3 and cytosolic thioredoxin, thioredoxin 1 (Trx1) by TXN gene on chromosome 9q31.3. On the other hand, the mitochondrial protein isoforms namely thioredoxin reductase 2 (TrxR2) and thioredoxin 2 (Trx2) have both their genes set on chromosome 22 (22q11.21 for TXNRD2 and 22q12.3 for TXN2). The Trx system is mainly devoted to the transfer of electrons to peroxiredoxins (Prxs) for their antioxidant activity. However, the cytosolic and the mitochondrial thioredoxin systems possess other functions and targets which are discussed thoroughly in the next subparagraphs. Together with TrxR1 and TrxR2, thioredoxin glutathione reductase (TGR), encoded by the TXNRD3 gene (chr 3q21.3), is another member of the family possessing both glutathione and glutaredoxin reductase activity.^{68, 69} This enzyme is expressed only in early spermatids while it is absent in mature sperm and its expression is highly tissue-specific.⁷⁰

1.3.1.1 Thioredoxin reductases

Mammalian cytosolic and mitochondrial thioredoxin reductases are selenium-containing homodimeric flavoproteins constituted by two subunits of 55-56 kDa.

TrxR1 was first purified by Arne Holmgren in 1977 from calf liver and thymus,⁷¹ whereas mitochondrial thioredoxin reductase, TrxR2, was isolated for the first time twenty years later by Rigobello *et al.* from rat liver mitochondria.⁷² TrxR2 gene localization and complete sequence have been reported later in 1999.^{73, 74} Both protein isoforms were found to possess several splicing variants and to have a large sequence homology.⁷⁵ TrxR2 holds 36 additional amino acids at the N-terminus, which are necessary for the mitochondrial targeting. Interestingly, TrxR1 was detected also in the mitochondrial intermembrane space, where it probably counteracts the activation of Cu/Zn SOD.⁷⁶ TrxR monomers are composed by a NADPH binding site, a FAD prosthetic group, a dimerization domain, and two catalytic sites localized at the N- and C- termini.⁷⁷ The crystal structure of TrxR1 and of the human thioredoxin reductase-thioredoxin complex,

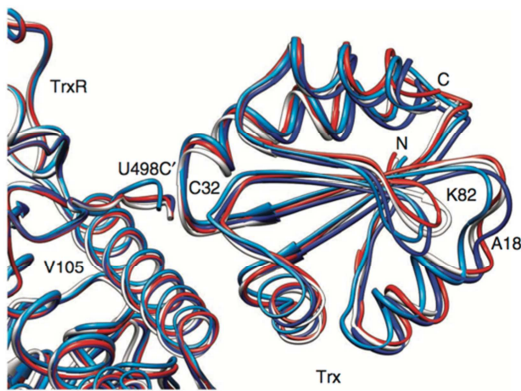


Fig. 5 Structure of the human TrxR-Trx complex from ref.⁷⁹ The interaction occurs between the Cys32 of Trx and the second catalytic site of TrxR.

obtained by two different groups, were crucial for the clarification of TrxR catalytic mechanism and of the interaction with its substrate, thioredoxin, as reported in Fig. 5.^{78, 79} A Cys-Val-Asn-Val-Gly-Cys motif, characterized by the presence of two active Cys, is present at the N-terminus, whereas the second active site, constituted by a Sec/Cys couple, is set on a protein flexible arm at the C-terminus. The two monomers of TrxR are associated in a head-to-tail fashion in order to make the first catalytic site of one subunit interact with the second active site of the other monomer (Fig. 6). From NADPH, the reducing equivalents are shuttled through the FAD prosthetic group to the first catalytic site of one TrxR subunit and then to the

second catalytic center on the other subunit. Finally, the second active site is responsible for thioredoxin reduction. As shown in Fig. 5, the flexible arm, endowed with the second active site (Cys/Sec couple), is solvent exposed and is crucial for the interaction with thioredoxin. The Sec residue has a fundamental catalytic function. Indeed, the recombinant enzyme lacking Sec was shown to dramatically decrease the catalytic rate.⁸⁰ The cytosolic and the mitochondrial TrxRs are very similar in their structure as reported by Biterova *et al.*⁸¹ However, Cys483, which is highly conserved in the interface domain of both TrxRs, was found to form an intersubunit disulfide bond only in the mitochondrial enzyme.⁸¹ Moreover, several amino acids around the active site were reported to be different between the two TrxR isoforms indicating a possible impact on the enzymatic activity. Interestingly, the two TrxRs display different sensitivities to calcium ions. In fact, the cytosolic isoform is inhibited by Ca^{2+} in the nanomolar range of concentrations and undergoes conformational changes, whereas the mitochondrial TrxR is hardly affected.⁸² Their different sensitivities could be due to their distinctive sequences with TrxR1 being more acidic than TrxR2 and, since mitochondria are known to accumulate calcium, suggests a possible physiological significance. In addition, Rackham *et al.* outlined that TrxR2 possesses a stronger affinity for its native substrate Trx2 with respect to TrxR1 for Trx1, and its catalytic efficiency is higher at pH 8, a more basic value in comparison to TrxR1.⁸³ This finding may reflect the adaptation of TrxR2 to the pH of the mitochondrial matrix which is generally higher in comparison to the cytosolic one that is usually set around 7.4. Except from their principal substrate, TrxRs can also reduce other targets, including selenite, tellurite, lipoic acid, lipid hydroperoxides, dehydroascorbic acid, tocopherol, ubiquinone and enzymes such as glutaredoxins (Grxs) and protein-disulfide isomerase (PDI).^{75, 84-86} Of note, the affinity of TrxR2 for these other substrates is generally significantly lower than the observed affinity of TrxR1.⁸³

In order to study the significance of the two TrxRs *in vivo*, mouse models knockout (KO) for either TrxR1 or TrxR2 were generated. In both cases, embryonic lethality was observed indicating that the proteins are essential for the development of embryos. Of note, TrxR1 expression is essential during embryogenesis in most tissues except for the heart,^{87, 88} while TrxR2 is crucial in particular for hematopoiesis and heart function.⁸⁹ Conditional TrxR1 KO in neurons led to cerebellar hypoplasia and severe ataxia in mice, whereas TrxR2 deletion did not.⁹⁰ Interestingly, the phenotype was not due to the lack of TrxR1 in neurons themselves but from the fact that glial cells became unable to support the proliferation of neurons upon TrxR1 depletion. Accordingly, a Pro190Leu mutant form of TrxR1, that lowers its enzymatic activity, was reported to induce epilepsy in humans suggesting a prominent role of TrxR1 in the central nervous system.⁹¹ Liver specific conditional deletion of TrxR1 in mice increased the expression of the glutathione system improving the overall ROS scavenging capacity of the liver and preventing acetaminophen induced

acute hepatotoxicity.⁹² However, the lack of TrxR1 was shown to induce glycogen accumulation in the liver and strong Nrf2 activation leading to hepatomegaly.⁹³

Regarding the mitochondrial enzyme, heart specific conditional deletion of TrxR2 in mice was reported to induce systolic dysfunction, fractional shortening and reduction of ejection fraction due to cellular stress in aged KO hearts.⁹⁴ Thus, TrxR2 is essential in protecting from age-related functional cardiac decline. Of note, Sibbing *et al.* identified three patients diagnosed with dilated cardiomyopathy to be heterozygous carriers of mutations in TrxR2 gene that led to a decrease in TrxR2 enzymatic activity.⁹⁵ The conditional TrxR2 deletion in CD4 and CD19 positive T- and B-lymphocytes showed no particular phenotype⁹⁶ while deletion of TrxR1 prevented the expansion specifically of CD4 and CD8 negative thymocytes.⁹⁷ Moreover, the same authors found that TrxR1 is necessary for the expansion of activated T-cells upon viral or parasite infection. Conditional TrxR2 KO in vascular endothelial cells resulted in enhanced intravascular cell deposition and microthrombi formation upon femoral artery ligation in mice.⁹⁸ In chondrocytes, lack of TrxR2, achieved through shRNA depletion, promoted cell proliferation and stimulated the expression of extracellular matrix genes indicating a key role of TrxR2 also in cartilage homeostasis.⁹⁹

Therefore, TrxR1 and TrxR2 depletion in mice determines markedly different phenotypes with tissue or organ specific effects, suggesting peculiar functions of the two TrxRs in the various tissues. Of note, the complete absence of TrxR2 in seven consanguineous individuals affected by familiar glucocorticoid deficiency has been reported.¹⁰⁰ The lack of TrxR2 in humans causes a late onset adrenal insufficiency due to increased oxidative stress in mitochondria which impedes steroidogenesis. Thus, TrxR2 deficiency is not embryonically lethal in humans as for mice. In addition, any of the patients lacking TrxR2, presented cardiomyopathy as it was expected from the dramatic phenotype of heart-specific TrxR2 KO mice, highlighting substantial differences among species. Interestingly, upregulation of TrxR2 has also been correlated with longer lifespan from the observation of its higher expression and activity in long-lived animals.¹⁰¹

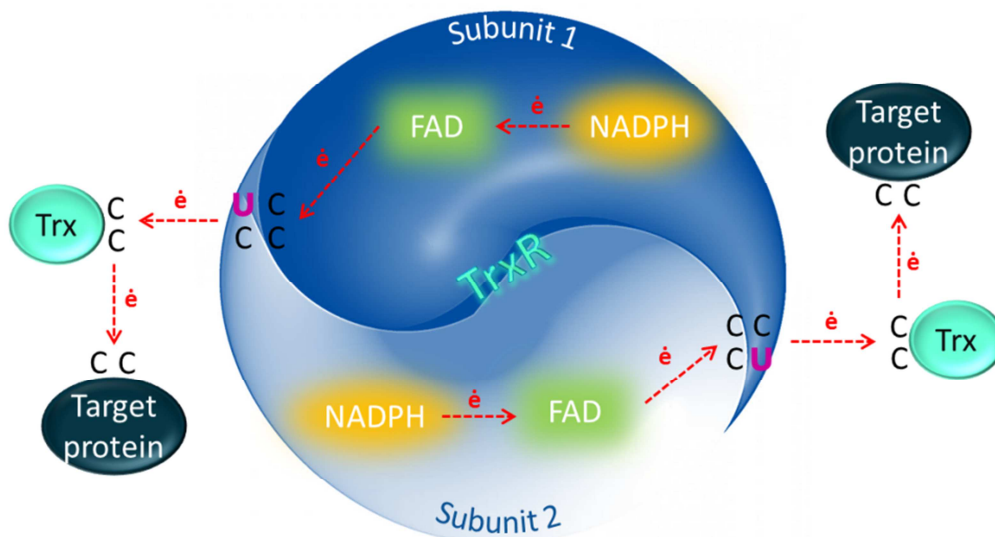


Fig. 6 Cartoon of the homodimeric structure of TrxR adapted from Ref.³¹⁷ Red arrows indicate the electron flow throughout the system. (C = cysteine; U = Selenocysteine; e⁻ = electron)

1.3.1.2 Thioredoxins

Thioredoxin was initially discovered as a cofactor of ribonucleotide reductase in *E. coli* and is evolutionally highly conserved.¹⁰² Both cytosolic (Trx1) and mitochondrial (Trx2) thioredoxins are small proteins of about 12 kDa that consist of a central β -sheet core surrounded by four α -helices, and are endowed with the conserved active site Cys-Gly-Pro-Cys.⁶⁷ Once reduced by TrxRs, the main function of thioredoxins is the the regeneration of antioxidant enzymes via reduction of disulfide bridges. The catalytic site, also known as cysteine box or thioredoxin fold (Cys-X-X-Cys), is formed by a couple of Cys, is highly conserved and is present also in other enzymes of the thioredoxin family which includes Grxs, Prxs, PDI, glutathione peroxidases (GPxs), glutathione S-transferases (GSTs) and chloride channels.¹⁰³

In human Trx1, the two active-site cysteines are Cys32 and Cys35. The residue at position 32 has a low pKa and it is called *attacking* cysteine since it is the one forming a mixed disulfide with the target protein, whereas Cys35 is implicated in the subsequent reduction of this disulfide bond and for this reason is called *resolving* cysteine. In addition to the two Cys of the active site, Trx1 presents other three cysteines in its sequence namely Cys62, Cys69 and Cys73. Through the modification of these residues the activity of Trx1 can be modulated.¹⁰⁴ Trx1 has been found to directly reduce hydroxyl radical and quench singlet oxygen.¹⁰⁵ However, the antioxidant function of Trx1 is mainly achieved through the regeneration of peroxiredoxins (Prxs), which can directly scavenge H₂O₂.¹⁰⁶

As already mentioned, Trx1 is able to provide reducing equivalents to ribonucleotide reductase but it was also shown to be a cofactor of other enzymes involved in biosynthetic processes such as methionine sulfoxide reductase and sulfate reductase.¹⁰⁷ Moreover, the cytosolic thioredoxin can enter the nucleus where it regulates the binding of several transcription factors to the DNA. Trx1 can act directly on transcription factors such as in the case of NF- κ B and of the glucocorticoid receptor, or indirectly via Ref-1 reduction as shown for AP-1, HIF-1 α , and p53.¹⁰⁸⁻¹¹¹ In addition, the transcriptional activity of the estrogen receptor was also reported to be sensitive to Trx1-mediated redox modulation.¹¹² In the cytosol, reduced Trx1 can bind and inhibit the kinase activity of ASK1 preventing ASK1-dependent apoptosis.¹¹³ Interestingly, Trx1 can modulate NO signaling by regulating NO synthases, but its redox activity can also be inhibited by nitrosylation on the structural Cys69.¹¹⁴ These findings suggest a fine cross-talk between the various redox signaling events. Trx1 can also be secreted by the cell under conditions of oxidative stress causing proinflammatory effects by potentiating the release of cytokines. Secreted Trx1 acts also as a chemotactic protein inducing migration of neutrophils, monocytes and T-cells. In addition, a truncated form of thioredoxin (Trx80), was found extracellularly at the surface of monocytic cells.¹⁰⁷

The mitochondrial thioredoxin, Trx2, is ubiquitously expressed and has a 35% sequence identity with Trx1. With respect to its cytosolic counterpart, Trx2 presents an N-terminal mitochondrial translocation signal of 60 amino acids, for the correct protein delivery to mitochondria. Cleavage of the leader peptide gives a mature protein of 12.2 kDa. Differently from Trx1, Trx2 lacks structural cysteines other than the two Cys present in the active site (Cys90 and 93 for the human enzyme).^{115, 116} Mitochondrial thioredoxin has a key role in antioxidant processes by either directly scavenging ROS or by reducing peroxiredoxin 3 (Prx3), the mitochondrial isoform of Prx family.¹⁰ Its reducing activity is crucial in mitochondria since these organelles are a major source of ROS. In addition, Trx2 has been shown to regulate both induction and inhibition of apoptosis. In fact, Trx2 downregulation was shown to lead to a decrease of the mitochondrial membrane potential ($\Delta\Psi_m$) and to an increased mitochondrial membrane permeability, inducing Cyt c release, caspases activation and apoptosis.^{116, 117} This effect was probably due to the increased mitochondrial ROS

level, due to a hindering of the detoxification mechanisms. This correlation was further supported by the finding that Trx2 can specifically scavenge ROS produced by TNF- α signaling, blocking NF- κ B activation and apoptosis.¹¹⁸ Trx2 was also shown to modulate caspase 3 activity via its denitrosylation,¹¹⁹ regulating both the apoptotic pathway and the cellular phenotype of microglia.^{120, 121} Both thioredoxin 1 and 2 are thus involved in the control of apoptosis, but with different mechanisms.

Animal models KO for Trx1 or Trx2 were generated to dissect the effect of their deficiency. Either Trx1 or Trx2 genetic deletion resulted to be embryonically lethal in mice. In particular, Trx1 is essential for early differentiation and embryonic morphogenesis.¹²² Instead, Trx2 KO mice showed increased apoptosis on day 12.5 coincident with the mitochondrial maturation phase.¹²³ In addition, conditional depletion of Trx2 in chicken B-cells was shown to induce the activation of the intrinsic apoptotic pathway.¹¹⁷ Thus, the two thioredoxins are both required in embryonic development and have a major function in the control of the redox balance and apoptosis in their cellular compartments.

1.3.1.3 Peroxiredoxins

The first peroxiredoxin (Prx) was discovered in 1968 by Harris.^{124, 125} Six isoforms of peroxiredoxins also known as thioredoxin peroxidases are present in mammalian cells.^{106, 126} The main function of Prxs is H₂O₂ detoxification, but they can also reduce peroxynitrite and organic hydroperoxides. Prxs present a high catalytic efficiency in H₂O₂ detoxification with a reaction rate of 10⁷-10⁸ M⁻¹s⁻¹.¹²⁷ Prxs are also abundant proteins and have been estimated to account for up to 1% of soluble cellular proteins.^{106, 128} Therefore, once H₂O₂ is produced, it will probably and quickly be scavenged by peroxiredoxins. It has been hypothesized that peroxiredoxins could be the principal sensors of the cellular redox condition and could transfer oxidative stimuli to target reactive Cys on other proteins after interaction with H₂O₂. In support of this idea, Stöcker *et al.* recently reported that deletion or depletion of cytosolic Prxs highly affect thiol oxidation upon H₂O₂ stimulation, indicating a probable role of Prxs in mediating H₂O₂ signaling.¹²⁹

Peroxiredoxins can be divided into three subgroups depending on the mechanism of activity: 2-Cys (Prx1 to Prx4), atypical 2-Cys (Prx5), and 1-Cys (Prx6).¹³⁰ The 2-Cys and atypical 2-Cys Prxs have two cysteine residues in their active site, namely an N-terminal *peroxidatic* Cys, endowed with a low pKa, and a C-terminal *resolving* one. The catalytic mechanism involves two steps. First, the *peroxidatic* Cys reacts with H₂O₂ via a nucleophilic attack forming a sulfenic acid. Then, the *resolving* Cys forms a disulfide bond with the *peroxidatic* Cys releasing a molecule of water. This disulfide bridge can be intermolecular with another monomer of Prx for typical 2-Cys Prxs, or intramolecular for atypical 2-Cys Prxs.¹³⁰ On the other hand, the 1-Cys peroxiredoxins possess only one reactive cysteine which undergoes oxidation reacting with H₂O₂. The recycling of peroxiredoxins back to their reduced state is performed by thioredoxins. Interestingly, Prx3, the mitochondrial isoform of peroxiredoxin family, is reduced by both Trx2 and glutaredoxin 2 (Grx2), which is part of the glutathione system, suggesting an interplay between the two thiol regulating networks in mitochondria.⁸⁶ It has been reported that, by transiently overexpressing Prx1 or 2 in cultured fibroblasts, it is possible to eliminate the intracellular H₂O₂ generated in response to growth factors and to block the H₂O₂-mediated activation of NF- κ B.¹³¹ These data further support the selective interaction of Prxs with H₂O₂.

Murine models KO for the different peroxiredoxins were generated. Prx1 KO mice were viable but were affected by hemolytic anemia from nine months of age and developed malignant cancers.¹³² In addition, Prx1 gene deletion significantly reduced the antioxidant capacity of lung tissue.¹³³ Prx2 KO mice were shown to be viable but developed splenomegaly caused by its congestion with morphologically altered

erythrocytes.¹³⁴ Moreover, Prx2 KO mice developed oxidative stress and insulin resistance in skeletal muscle suggesting that Prx2 has a crucial function in the maintenance of a normal redox status in skeletal muscles.¹³⁵ In addition, the absence of Prx2 in apolipoprotein E-deficient mice exacerbated atherosclerosis development through the increased immune cell adhesion and infiltration into the aortic intima.¹³⁶ The importance of Prx4 seems limited to spermatogenesis since spermatogenic cells lacking Prx4 are more susceptible to cell death via oxidative damage with respect to their wild-type (WT) counterparts.¹³⁷ Regarding the mitochondrial peroxiredoxin, in 2007, Prx3 KO mice were generated and were shown to develop normally but with a reduced body weight with respect to WT animals.¹³⁸ Moreover, they were more susceptible to lipopolysaccharide-induced lung damage probably because of their impairment in ROS handling capacity.¹³⁸ Another recent research pointed out that the deficiency of Prx3 in a murine model accelerated oxidative stress and mitochondrial impairment, resulting in the decline of physical strength with age.¹³⁹ Mice lacking Prx5 were viable and fertile but were more vulnerable to intraperitoneal injection of lipopolysaccharide, indicating that Prx5 may have a role in inflammation. Furthermore, at 14 months of age, 20% of Prx5 KO mice developed cancers.¹⁴⁰ Finally, the 1-Cys Prx6 was shown to protect keratinocytes from UV-induced cell damage as UV-mediated keratinocyte apoptosis was enhanced in Prx6-deficient mice.¹⁴¹

1.3.1.4 Thioredoxin interacting protein

Thioredoxin interacting protein (TXNIP) is a 50 kDa negative regulator of thioredoxin activity that can form a mixed disulfide bond with the two Cys present in Trx active site.^{142, 143} Usually TXNIP is located in the nucleus, but it can move to the cytosol or mitochondria to bind Trx1 or Trx2 in response to oxidative stress. TXNIP binding reduces ASK1 complexation with Trx1/Trx2 resulting in the activation of ASK1-mediated signaling pathway.¹⁴⁴ TXNIP overexpression in pancreatic β -cells was found to promote apoptosis by increasing the Bax/Bcl-2 ratio and caspase 3 expression.¹⁴⁵ Interestingly, the overexpression of TXNIP carrying a cysteine-serine mutation in its Trx binding site, inhibited glucose uptake in mature adipocytes as the WT protein suggesting peculiar functions of TXNIP not related to its Trx binding activity.¹⁴⁶ Furthermore, TXNIP inhibits adipogenesis and seems to have a central role in the overall glucose handling.¹⁴⁷ Two different groups observed that TXNIP regulates glucose metabolism and mediates high glucose-induced ROS generation.^{148, 149} TXNIP KO mice were reported to experience fasting hypoglycemia, increased glucose uptake in peripheral tissues and impaired lipid metabolism.^{147, 150, 151} Regarding mitochondria, TXNIP KO mice displayed altered heart mitochondria, but were more protected from ischemia-reperfusion injury. This latter observation was hypothesized to be due to the increased level of free Trx2.¹⁵² Moreover, TXNIP is induced by glucose, suppressed by insulin and upregulated in diabetic patients.¹⁵³ Therefore, TXNIP appears crucial in glucose and lipid metabolism via its own activity and in scavenging processes through its Trx binding capacity.

1.3.2 The glutathione system

The glutathione system is formed by NADPH, glutathione reductase (GR) and glutathione (Fig 4). In the cell, the ratio between reduced (GSH) and oxidized (GSSG) glutathione ranges from 30:1 to 100:1, and GR, using the reducing equivalents derived from NADPH, is the principal enzyme involved in the maintenance of this high pool of GSH.¹⁰ The glutathione system is expressed both in the cytosolic and in the mitochondrial cell compartments that are not in redox equilibrium with each other.¹⁵⁴ Reduced glutathione can provide electrons to a wide range of enzymes, including GPxs, GSTs and Grxs.^{10, 155} However, GSH can also react with other proteins not involved in ROS scavenging processes, that present reactive Cys in their sequence, generating reversible mixed disulfide bonds. This process of glutathionylation is part of the redox regulation and signaling mediated by GSH and can either activate or inhibit the activity of the target protein or modulate its binding with interacting partners.¹⁵⁵ For instance, mitochondrial complex I of the electron transport chain was shown to be glutathionylated¹⁵⁶ and this protein modification led to an increased production of O_2^{\bullet} by the protein itself.¹⁵⁷ In the following subparagraphs the different components of the glutathione system are described.

1.3.2.1 Glutathione reductase

Glutathione reductase (GR) was purified for the first time in 1955 from yeast and was immediately found to receive reducing equivalents from NADPH.¹⁵⁸ In fact, together with TrxRs, GR belongs to the pyridine nucleotide disulfide oxidoreductase family. In 1987, human GR crystal structure was solved from erythrocytes.¹⁵⁹ GR is a 52 kDa protein and its active form is a head-to-tail dimer with a large interface domain of more than 3000 Å. Like TrxRs, the reducing equivalents deriving from NADPH are transferred to

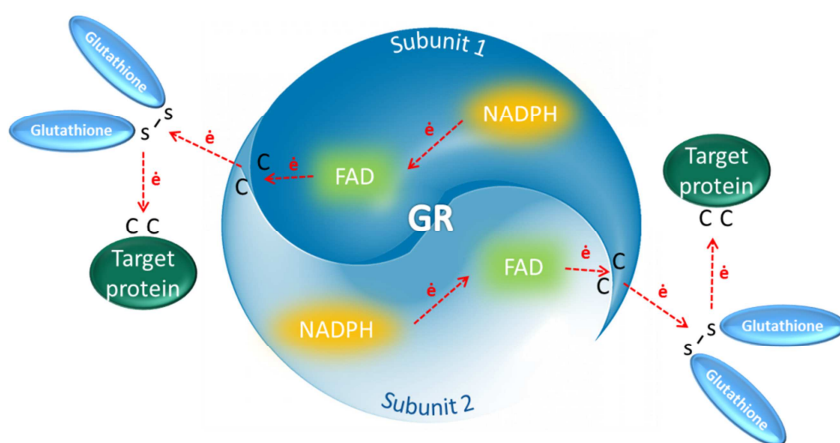


Fig. 7 Cartoon of the homodimeric structure of GR. Red arrows indicate the electron flow throughout the system. (C = cysteine; e⁻ = electrons)

the FAD prosthetic group and then to its active site formed by a couple of cysteines, Cys-Val-Asn-Val-Gly-Cys.¹⁶⁰ Through its activity, GR can reduce oxidized glutathione (GSSG) producing two molecules of GSH (Fig. 7). Thus, GR is fundamental to maintain the GSSG/GSH ratio and the GSSG-binding site is extremely conserved during evolution. Human GR is encoded by a single gene located on chromosome 8 at locus p21.1. However, different isoforms are present in the cytosolic and in the

mitochondrial cell compartments, which are encoded by two different in-frame starting codons present in the gene. Translation from the first codon generates the long mitochondrial GR isoform endowed with a mitochondrial targeting sequence, whereas the cytosolic form is encoded from the second starting codon.¹⁶¹ Of note, once the leader peptide is processed, the weight of the mature mitochondrial GR is equal to its cytosolic counterpart. The cytosolic GR is predominant in terms of total cellular amount, but the abundancies of the two isoforms in their own cell compartment is quite similar.¹⁶⁰

Interestingly, three patients with homozygous GR deficiency in blood cells were reported. These patients were in good health at about 50 years of age. The only clinical symptoms were restricted to a higher

susceptibility to hemolytic crisis after eating fava beans and development of cataract during early adulthood.^{162, 163} After this findings, a GR KO mouse model was generated. Interestingly, mice were viable and surprisingly not subjected to hemolytic anemia.^{164, 165} Curiously, even though the liver of GR deficient mice exhibited no GSSG-reductase activity, the amount of glutathione in the reduced form was maintained.¹⁶⁶ It was hypothesized that glutathione may rely on the thioredoxin system for its reduction through the mediation of glutaredoxins. However, in 2015 liver specific TrxR1/GR double KO mice were generated and were reported to be long term viable with normal hepatic activities.¹⁶⁷ Moreover, liver-specific TrxR1/Trx1/GR triple KO mice exhibited full recovery from surgical hepatic ischemia/reperfusion injury, indicating an effective antioxidant activity.¹⁶⁸ However, these mice were shown to be highly sensitive to pharmacological inhibition of GSH biosynthesis and to GSH depletion, indicating a strong dependence on glutathione *de novo* synthesis for the maintenance of the redox homeostasis.¹⁶⁸ In parallel, hepatocyte hyper-proliferation and increased tissue turnover were observed probably aimed to maintain a functional liver cell population.¹⁶⁸

1.3.2.2 Glutathione

Glutathione is the most abundant antioxidant in the cell reaching concentrations in the millimolar range.¹⁶⁹ It is a tripeptide consisting of glutamate, cysteine and glycine that can reduce either protein disulfide bonds in a reaction mediated by Grxs or scavenge ROS via GPxs. The reduction yields GSSG, that can be reduced back to two GSH by GR. GSH synthesis occurs only in the cytosol and involves two enzymatic steps both requiring ATP. The first step is rate limiting and is catalyzed by glutamate-cysteine ligase (GCL) also known as γ -glutamylcysteine synthetase. GCL is composed of two subunits of 73 kDa (catalytic one) and 31 kDa (modulatory one) respectively, encoded by different genes.¹⁷⁰ The large subunit is responsible for the enzymatic activity and mice lacking the catalytic subunit die before birth.¹⁷¹ The small modulatory subunit does not participate to the catalytic process but it increases the enzymatic efficiency. Indeed, mice KO for the regulatory subunit are viable but have markedly reduced tissue GSH levels.¹⁷² It has been reported that the holoenzyme is redox sensitive. In fact, it dissociates after treatment with the reducing agent dithiothreitol (DTT), while oxidative stress enhances holoenzyme formation.¹⁷³ GCL mutations leading to a lower protein expression have been reported in humans and were shown to determine hemolytic anemia, aminoaciduria and spinocerebellar degeneration.¹⁷³ The second step in GSH synthesis is catalyzed by glutathione synthetase (GS), which is formed by two identical subunits and finally generates γ -glutamylcysteinylglycine (GSH) by condensing glycine to the γ -glutamylcysteine. GS deficiency in humans is autosomal recessive and leads to severe symptoms such as hemolytic anemia, metabolic acidosis and neurological defects.¹⁷⁴ However, decreased GSH synthesis was reported also in aging, diabetes mellitus, fibrotic diseases, and hepatic disorders.¹⁷⁵⁻¹⁷⁷ As already mentioned, GSH is produced only in the cytosol, but it is also present in mitochondria and in other subcellular organelles such as the ER. Since GSH is negatively charged at physiological pH it cannot enter the mitochondrial matrix by simple diffusion. In fact, different carriers, such as 2-oxoglutarate or dicarboxylate and tricarboxylate carriers, transport GSH inside mitochondria.^{178, 179} The amount of glutathione in the mitochondrial matrix is 1 to 5 mM for the reduced form and 0.01 mM for the disulfide form. Interestingly, the basic pH of the matrix further decreases the reductive potential of GSH/GSSG to -280-340 mV compared to the -240 mV observed in the cytosol.¹⁸⁰

As the major redox buffer, GSH is involved in redox signal transduction of key cellular processes such as proliferation, differentiation, autophagy and apoptosis.^{181, 182} Regarding apoptosis, increased GSH levels were shown to prevent apoptotic cell death, whereas GSH depletion induced apoptosis in leukemia cells.¹⁸³ Changes in the GSH/GSSG ratio can influence also the activity of proteins undergoing glutathionylation.

In addition to redox signaling processes, GSH is also utilized to detoxify a variety of electrophilic substances by the phase II enzymes GSTs (see subparagraph 1.3.2.5) and is also involved in iron handling. Indeed, GSH depletion in *S. cerevisiae*, obtained via GCL deletion, was observed to affect iron metabolism but not the cell capacity to maintain the redox homeostasis.¹⁸⁴ Iron is necessary for the activity of many enzymes in the form of iron and sulfur clusters or heme complexes. However, free iron ions can generate dangerous radicals in the cell. Hidler and Kong were the first to report the affinity constant for GSH interaction with iron(II) and demonstrated that GSH binds iron(II) to a considerable extent at physiological pH avoiding undesired generation of radical species and making iron bio-available for its subsequent incorporation into iron-dependent enzymes.¹⁸⁵ Of note, GSH is endowed with the peculiar γ -carboxyl group which is resistant to intracellular degradation. The tripeptide can be hydrolyzed only by γ -glutamyltranspeptidase (GGT), an enzyme present on the external surface of certain cell types.¹⁸⁶

1.3.2.3 Glutathione peroxidases

Glutathione peroxidases (GPxs) are a family of enzymes that scavenge H_2O_2 and other peroxides using reduced glutathione as the electron source. The first GPx was discovered by Mills in 1957 from mammalian erythrocytes.¹⁸⁷ So far, eight GPxs have been identified in mammals of which GPx1-4 are selenoproteins (plus GPx6 in humans), while the other ones are endowed with Cys in their active site.¹⁸⁸ Functionally, GPxs can be classified as hydroperoxide or lipid-hydroperoxide oxidoreductases with different substrate specificities.¹⁶⁰ GPx1, 2, 3, 5 and 6 form active homotetramers, while GPx4, 7 and 8 are monomeric proteins.¹⁸⁹

GPx1 is widely expressed and localizes predominantly in the cytosol, and to a lower amount in the mitochondrial matrix.¹⁹⁰ Homozygous GPx1 KO mice are healthy and do not present increased content of protein carbonyl groups or lipid peroxides but are more susceptible to oxidative challenges.¹⁹¹ GPx2 is mainly expressed in the gastrointestinal tract and GPx1/GPx2 deficiency in mouse models led to inflammatory bowel disease with mucosal inflammation in the ileum and colon.¹⁹²

GPx3 is a secreted plasma protein synthesized mainly in the proximal convoluted tubule of the kidney.^{193, 194} GPx3 KO mice were found to be viable and did not show phenotypic alterations.¹⁹⁵

GPx4 exists in three different isoforms namely cytosolic GPx4 (expressed in the whole body), mitochondrial GPx4 and sperm-nuclear GPx4 (both expressed mainly in testis), all deriving from the same gene.¹⁶⁰ Each isoform localizes in its specific cell compartment and can be free or membrane-associated.¹⁸⁸ Interestingly, GPx4 can receive reducing equivalents not only from GSH but also from DTT, mercaptoethanol, cysteine and protein thiols.¹⁸⁹ Mice lacking GPx4 were reported to die in utero underlying a vital function of this selenoprotein.¹⁹⁶ The importance of this enzyme is not limited to embryonic development. In fact, lack of GPx4 in adult mice, achieved through the generation of a tamoxifen-inducible GPx4 KO strain, was also incompatible with life and led to death in just two weeks from tamoxifen administration.¹⁸⁹ GPx4 is also utilized as a structural protein during sperm maturation, being involved in the mitochondrial capsule formation.¹⁹⁷ Specific deletion of the mitochondrial GPx4 isoform gave rise to viable animals but males were completely infertile. On the other hand, sperm-nuclear GPx4 deficient mice were viable and fertile. Therefore, this latter isoform can be compensated by other enzymes.¹⁸⁹

GPx4 has been associated also with a new mechanism of cell death called ferroptosis. Ferroptosis is indeed defined as a process of cell death activated by missing GPx4 and that can be inhibited by iron-chelators or α -tocopherol supplementation. This process involves the iron-mediated peroxidation of lipids in cellular

membranes and cannot be rescued by inhibitors of apoptosis or of necroptosis. The precise mechanisms and the intermediates of the ferroptotic process are currently being studied and the possible occurrence of ferroptosis *in vivo* is still debated.¹⁹⁸ So far, truncated cardiolipin and 4-hydroxy-2-nonenal (HNE) have been suggested as possible species triggering ferroptosis.¹⁸⁹ In addition, acyl-CoA synthetase long chain family member 4 (ACSL4) has been recently identified as a key component of ferroptosis execution by mediating the insertion of long poly-unsaturated fatty acids into membranes.¹⁹⁹ Indeed GPx4/ACSL4 double KO cells were shown to be resistant to ferroptosis.

Going on with the other GPx isoforms, GPx5 has been reported as epididymis specific in many mammalian species and androgens control its expression.²⁰⁰ Mice lacking GPx5 are viable and fertile but display a high incidence of miscarriage and developmental deficits in the offspring especially when females are mated with old males.¹⁸⁹ GPx6 is a selenoprotein only in humans whereas it possesses a Cys in its active site in other mammalian species. This protein, homologous to GPx3, is expressed in the olfactory epithelium but it has not been purified yet.²⁰¹ Finally, GPx7 localizes in the cytosol and in the ER lumen and GPx8 is a membrane protein of the ER. GPx7 and GPx8 show low enzymatic activities and may have a role in protein folding in the ER.¹⁸⁹

1.3.2.4 Glutaredoxins

Glutaredoxin (Grx) was initially identified by Arne Holmgren in 1976 as a GSH-dependent electron donor for ribonucleotide reductase in an *E. coli* strain lacking thioredoxin.²⁰² Later on, the first mammalian glutaredoxin was purified from calf thymus in 1982.²⁰³ All Grxs belong to the thioredoxin superfamily and possess the thioredoxin fold.

Grxs are divided into two subgroups, dithiol and monothiol, depending on the number of Cys present in the active site. Dithiol isoforms are characterized by a Cys-Pro-Tyr-Cys catalytic site and catalyze the reduction of both protein disulfides and GSH mixed disulfides with proteins or low molecular weight thiols. Moreover, dithiol glutaredoxins can reduce also ascorbic acid protecting the cell from ROS induced apoptosis.²⁰⁴ For disulfide reduction both Cys of the active site participate to the catalysis. Instead, the reduction of GSH mixed disulfide with proteins requires the activity of only the N-terminal Cys. Interestingly, the cysteine to serine mutation of the C-terminal Cys in the active site of pig Grx1, increases the protein activity.²⁰⁵ Conversely, in *E. coli*, a Cys14Ser mutant of Grx1 displayed only 38% of GSH disulfide oxidoreductase activity compared to the WT protein.²⁰⁶ Monothiol Grxs possess a Cys-Gly-Phe-Ser active site. The majority of them is inactive in classical Grx activity assays and are mainly involved in the coordination of iron and sulfur clusters.¹⁶⁹ So far, four Grxs have been identified in mammalian cells, two dithiol glutaredoxins, Grx1 and Grx2, and two monothiol isoforms namely Grx3 and Grx5.²⁰⁷

Human Grx1 is encoded by GLRX1 gene set on chromosome 5q15 and its active site is constituted by the canonical sequence Cys-Pro-Tyr-Cys. Grx1 is a 12 kDa cytosolic protein but it can also enter the nucleus,²⁰⁸ be present in the mitochondrial intermembrane space,²⁰⁹ and be secreted into plasma.^{210, 211} Its catalytic activity is inhibited by oxidation and by pH lowering.²¹² Interestingly, Grx1 sequence contains other three Cys, apart from the ones forming the catalytic site, which may be involved in the observed protein inactivation during oxidative and nitrosative stress.²¹³ Grx1 KO mice displayed no peculiar phenotype,²¹⁴ but were shown to be protected from lipopolysaccharide-induced lung inflammation and from angiotensin II-triggered ROS production and cardiac hypertrophy.^{215, 216} Grx1 can also de-glutathionylate caspase 3 after TNF- α apoptosis induction.²¹⁷ Furthermore, high glucose levels were shown to increase Grx1 expression in

retinal Müller cells activating NF- κ B proinflammatory response and might be involved in the development of diabetic retinopathy.²¹⁸

Grx2 was identified in 2001 as another dithiol glutaredoxin.²¹⁹ Grx2 shows only 34% sequence identity

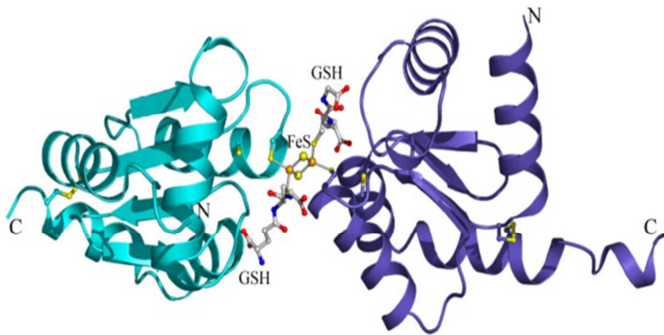


Fig. 8 Carbon trace of the Grx2 dimer. The dimer is bridged by a 2Fe-2S cluster. Monomers are the cyan and dark blue ribbon structures, while glutathione and protein cysteines are represented as sticks. From ref.²²⁴

compared to Grx1 and differs also in the size (18 kDa) and active site (Cys-Ser-Tyr-Cys).²¹⁹ In humans, the amount of Grx2 is generally 1:20 with respect to Grx1.²¹¹ Alternative splicing of Grx2 mRNA gives rise to various splice variants which are directed either to mitochondria or, in the absence of the N-terminal mitochondrial targeting sequence (19 amino acids), to the cytosol and nucleus.²²⁰ However, the expression of the cytosolic and nuclear isoforms is low apart from testis, immortalized cell lines and some cancer types.²²¹ As already mentioned, human Grx2 active site sequence is Cys-Ser-Tyr-

Cys. This particular sequence allows Grx2 to coordinate a 2Fe-2S cluster as discovered by Lillig *et al.* with Mössbauer spectroscopy (Fig. 8).²²² Of note, the proline residue in the active site of Grx1 was shown to be responsible for the inhibition of cluster coordination. In fact, the substitution of the proline with a serine in human Grx1 active site, increasing the flexibility, enables the protein to complex a 2Fe-2S cluster like Grx2.²²³ Insights into the mechanism of Grx2 cluster coordination revealed that the N-terminal cysteine (Cys37) of the active site is responsible for the iron binding and that the dimeric structure is further stabilized by two molecules of reduced glutathione which bind either iron non covalently and the two monomers of Grx2 by polar interactions (Fig. 8).²²⁴ The coordination of the cluster stabilizes Grx2 in a quiescent and enzymatically inactive dimer by sequestering its reactive Cys residues (Cys37 and Cys40).²²⁴ Cys40 is not required for deglutathionylation activities since its mutation was shown to increase Grx2 enzymatic activity.²²⁵ Notably, GSH bound to the complex is in dynamic equilibrium with free GSH and an increase of oxidized glutathione upon oxidative stimuli could destabilize the complex and free Grx2 monomers. Thus, the cluster may function as a redox sensor being able to release active monomeric Grx2 in case of a shift of the GSH/GSSG ratio toward a more oxidized condition. Accordingly, Grx2 is particularly expressed in tissues exposed to oxidative stress such as the heart, skeletal muscle and liver while it is not expressed at all in peripheral blood leukocytes.²²⁰ Grx2 sequence present another cysteine pair namely Cys28 and Cys113 which form a structural disulfide bridge far from the active site (Fig. 8). This second disulfide bond is highly conserved and increases protein stability by anchoring the N- and C- terminal α -helices. Indeed the mutation of these amino acids was shown to affect also dimer formation.²²²

It is important to note that Grx2 can be restored to its reduced state not only by GSH, but also by thioredoxin reductase as both TrxR isoforms were shown to be able to reduce human Grx2.²²⁶ This important finding underlines the connection between glutathione and thioredoxin pathways. Grx2 was hypothesized to be a sort of backup for the thioredoxin system being activated by oxidizing conditions and becoming important in the protection and recovery from oxidative stress. Indeed, Grx2 is resistant to oxidative inactivation and to electrophiles such as HNE,²²⁷ and may recycle Trx2 when TrxR2 is inactivated. Mitochondrial Grx2 overexpression was reported to make cell less susceptible to apoptosis induced by 2-deoxy-glucose and doxorubicin, by preventing Cyt c release and caspase activation.²²⁸ On the contrary, siRNA-mediated Grx2 depletion dramatically increased cell sensitivity toward apoptotic stimuli including

doxorubicin or phenylarsine oxide.²²⁹ In 2003, mitochondrial complex I was shown to be a target of Grx2 glutathionylation/deglutathionylation activity and to increase mitochondrial $O_2^{\bullet-}$ production when glutathionylated, thus supporting the idea of a role of Grx2 in redox signaling events.¹⁵⁷ In addition, Grx2 has recently been shown to inhibit peroxynitrite formation in oligodendrocytes.²³⁰ Interestingly, brain lesions of a mouse model of multiple sclerosis displayed decreased Grx2 expression and increased nitrotyrosine formation.²³⁰ Morpholino based knockdown of Grx2 in zebrafish impaired blood vessel network formation and axonal outgrowth leading to loss of neurons.^{231, 232} Moreover, Grx2 depletion in zebrafish affected correct heart looping.²³³ Grx2 deficient mice develop age dependent diseases including early cataract, heart hypertrophy and increased blood pressure.^{234, 235} Regarding Grx2 role in iron and sulfur cluster handling, its interaction with ISU scaffold proteins was observed in 2011.²³⁶ Furthermore, Grx2 was shown to be able to transfer 2Fe-2S clusters to apo ferredoxin 1 which is a mediator of electron-transfer reactions.²³⁷ Thus, Grx2 seems to be important also in cluster transfer pathways.

Moving to monothiol glutaredoxins, a cytosolic isoform Grx3, and a mitochondrial one Grx5, have been identified in mammalian cells. Both are involved in iron and sulfur cluster handling. Grx3 is a 37 kDa cytosolic protein endowed with an N-terminal inactive Trx domain and two C-terminal monothiol Grx domains both containing a Cys-Gly-Phe-Ser active site.²³⁸ It is an iron and sulfur cluster assembly factor, homologue to *S. cerevisiae* Grx3/Grx4.²³⁹ Interestingly, lack of Grx3 and 4 in yeast impaired the functioning of all iron-dependent enzymes because of a loss of bio-available iron necessary for their activity, despite accumulation of iron in the cell.²⁴⁰ Silencing of Grx3 in HeLa cells affected the activity of several cytosolic iron and sulfur proteins leading to a cell phenotype similar to iron starvation.²⁴¹ Moreover, in Jurkat cells, Grx3 was shown to translocate into the nucleus upon phosphorylation.²⁴² Grx3 deletion in murine models was reported to be embryonically lethal at day E12.5 and to cause morphological defects in embryos.²⁴³ By studying fibroblasts derived from Grx3 KO embryos it was shown that Grx3 deletion impaired cell growth and cell cycle progression during late mitosis.²⁴⁴ Monothiol Grx5 presents only one active site and is located exclusively in mitochondria.²⁴⁵ Grx5 is mainly implicated in iron and sulfur cluster biogenesis and has a role in heme biosynthesis.²⁴⁶ It was reported that patients carrying a homozygous mutation of Grx5 gene leading to decreased Grx5 levels, suffer of sideroblastic-like microcytic anemia and mitochondrial iron overload in erythroid cells due to impaired iron homeostasis and heme biosynthesis.²⁴⁷ Accordingly, yeast mutants lacking Grx5 are characterized by the accumulation of iron and inactivation of proteins containing iron and sulfur clusters.²⁴⁸

1.3.2.5 Glutathione S-transferases

Glutathione S-transferases (GSTs) are a family of GSH-dependent enzymes with overlapping conjugation activities for a variety of substrates.²⁴⁹ In fact, the predominant function of GSTs is the conjugation of GSH to a huge variety of electrophilic substances in order to reduce their toxicity or increase their solubility.¹⁶⁰ The glutathione-tagged molecules are finally metabolized and/or excreted. GSTs can be divided into three major subgroups, canonical soluble GSTs that usually reside in the cytosol, kappa soluble GSTs that can be targeted to the mitochondrial and/or peroxisomal compartments, and hydrophobic GSTs, also known as membrane-associated proteins with divergent functions in eicosanoid and glutathione metabolism (MAPEG), which are found in the microsomal fractions.¹⁶⁰ The mechanisms of GSH conjugations are extremely variable and depend on the GSTs class and on the specific substrate. Interestingly, GSTs and especially GSTP1 were shown to bind diglutathionyl dinitrosyl iron complexes and the binding of the cluster was reported to inhibit GSTs activity.²⁵⁰

1.4 Oxidative stress and diseases

In humans, oxidative stress was shown to be involved in a wide variety of pathologies, including cancer, type II diabetes, arteriosclerosis, chronic inflammatory processes, ischemia/reperfusion injury, metabolic syndrome and various neurodegenerative diseases.²⁵¹ Oxidative stress can be due to ROS overproduction through iperactivation/overexpression of ROS-producing enzymes such as NADPH oxidases, or to alteration/interruption of the electron transfer through the scavenging pathways. The common outcome is the disruption of the redox balance.¹¹

The permanent perturbation of redox homeostasis can lead to pro-inflammatory or cytotoxic conditions associated with acute and chronic diseases. Moreover, the continuous exposure of the cell to an excessive amount of ROS can further damage the DNA and other cellular components giving rise to a vicious cycle that may further trigger ROS production, exacerbating the outcome. Therefore, understanding the mechanisms involved in the dysregulation of redox signaling events, causing oxidative stress and leading to disease, is a compelling need. In the next subparagraphs the role of redox dysregulation with respect to two major pathologies affecting a large number of people worldwide, namely cancer and metabolic syndrome, is discussed.

1.4.1 Cancer

Cancer is a leading cause of morbidity and mortality worldwide. The World Health Organization estimated that in 2015, 8.8 million deaths were caused by cancer accounting for about 1:6 of total deaths. Unfortunately, the incidence increases every year and the number of new cases is expected to reach 22 million in 2022.²⁵²

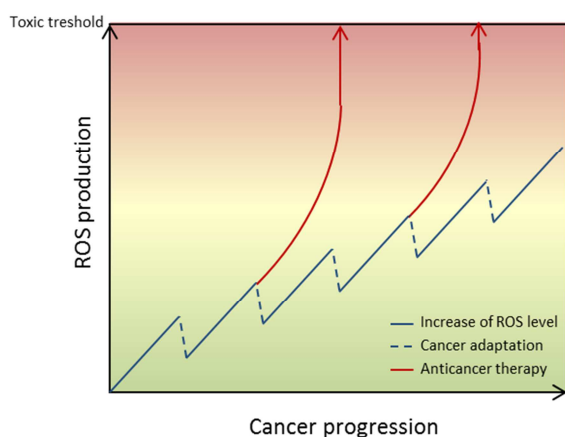


Fig. 9 ROS level during neoplastic transformation and possible effects deriving from the blockage of the cellular scavenging systems.

Cancer comprises a panel of hundreds of different forms characterized by distinctive origin, features and aggressiveness and derives from the neoplastic transformation of normal cells to cancerous cells through a multistep process. The neoplastic transformation is commonly divided into five consecutive stages: initiation, transformation, progression, local invasion and metastasis. The latter step, associated to the maximal tumor severity, consists in the colonization of a distant tissue by the cancer and correlates with a poor prognosis. The neoplastic transformation results from the dysregulation of DNA transcription with progressive loss of the features of a differentiated cell and it is associated to an enhanced proliferation and uncontrolled cell growth. Many are the

etiological causes of cancer and often the combination of many risk factors is necessary. The risk factors can be divided into physical carcinogens such as ultraviolet and ionizing radiations, chemical carcinogens such as alcohol abuse, tobacco smoke, asbestos, arsenic, and biological carcinogens, such as HPV or HBV infections and only a small proportion of the cases can be associated to genetic causes.²⁵³ The initiation process consists in a primary damage to the DNA but it is usually not sufficient for the development of cancer that, instead, is favored by the disruption of oncosuppressor genes such as p53, retinoblastoma protein (RB) and p16^{INK4A} which normally block the proliferation of mutated cells.²⁵⁴ As reported in Fig. 9, during the transition from normal tissue to invasive cancer, cells experience a progressive increase of ROS levels.²⁵⁵ In fact, increased amount of DNA oxidation products and of lipid peroxidation have been

measured in a large number of tumor samples including mammary ductal carcinoma, colorectal adenocarcinomas, renal cell carcinoma, gliomas and in blood samples of patients affected by leukemia.²⁵⁶ In addition, the amount of the DNA oxidative derivative 8-hydroxydeoxyguanosine in urine has been proposed as a marker of cancer.²⁵⁷ The origin of ROS overproduction probably resides in a combination of metabolic aberrations acquired following transformation, and of the immune response that further supports ROS increase.^{255, 258} The rise of ROS promotes tumor development with multiple mechanisms. Firstly, redox signaling is essential for the progression of cell cycle and thus for cell proliferation.²⁵⁴ In fact, an increased ROS amount was shown to positively affect the activity of different transcription factors such as ASK1 and FOXO and of cell cycle gatekeeper like RB or p53, sustaining cell proliferation and enabling the cancer cell to evade growth stops.²⁵⁴ Moreover, elevated ROS levels stimulate HIF-1 α stabilization and consequent transcription of VEGF which induces angiogenesis.²⁵⁹ Indeed, treatment with the free radical scavenger N-acetyl cysteine (NAC) or inhibition of NADPH oxidase were shown to block tumor vascularization.^{260, 261} Finally, high ROS levels have been detected in metastatic cells and have been associated with cancer dissemination.²⁵⁴ In fact, the inhibition of ROS by NAC was shown to restore adhesion of MDA-MB-435 breast cancer cells.²⁶² Therefore, ROS are exploited by cancer cells to promote growth and spreading.

However, the ROS increase was shown to induce also major changes in cancer cell functions by influencing key metabolic pathways. Already in 1926, Otto Warburg observed that cancer cells enhance their glucose uptake and rely mostly on glycolysis for their ATP production.^{263, 264} Amongst others, this metabolic switch increases the pentose phosphate pathway-mediated NADPH production furnishing reducing equivalents to the scavenging systems.²⁵⁴ In cancer cells, a reduction of oxidative phosphorylation is often associated with the concomitant formation of ROS by the electron transport chain.²⁶⁵ This large increase of ROS inside mitochondria can affect the mitochondrial DNA (mtDNA) which contains no introns and encodes for several components of the respiratory complexes, leading eventually to further mitochondrial dysfunctions. In fact, the occurrence of mutations in mtDNA have been reported in a wide variety of human tumors.²⁶⁶ Thus, cancer cells experience an increased ROS level especially in the mitochondrial compartment. This elevated ROS amount account for many aspects of cancer progression promoting cell growth and dissemination but it also affects cell metabolism reprogramming glucose utilization. These peculiarities of cancer cells can be exploited for the development of chemotherapeutic drugs targeting either dysfunctional mitochondria and/or increasing ROS production by exhausting the ROS-buffering capacity of cancer cells and triggering cell death.

1.4.1.1 Targeting mitochondria for anticancer therapy

Since long cancer cells were reported to show hyperpolarized mitochondria.^{267, 268} Interestingly, the increased $\Delta\psi_m$ is directly correlated to tumor aggressiveness and poor responsiveness to treatment.^{269, 270} Considering that mitochondria of many cancer cells, especially the ones resistant to standard chemotherapy, display both an elevated membrane potential and an increased ROS production,²⁵⁴ the selective targeting of cancerous mitochondria may be a possible successful therapeutic strategy in order to induce cancer cell death. For example, the susceptibility of mtDNA to ROS-induced mutation may be exacerbated by chemotherapeutic drugs.²⁷¹ mtDNA is more susceptible to ROS damage with respect to the nuclear DNA mainly because of the lack of introns and histones but also for its proximity to ROS generating sites and for the limited capacity of the mitochondrial DNA-repairing systems.²⁵⁶ It follows that a peak of ROS production in mitochondria can severely impact on cancer cell proliferation. In addition, the intrinsic apoptotic process is initiated in mitochondria by the release of pro-apoptotic factors into the cytosol. This

process was shown to be triggered by ROS increase.²⁷² Thus, by targeting hyperpolarized mitochondria, apoptosis could be selectively activated in cancer cells.

In order to discriminate between normal and dysfunctional mitochondria, the potential anticancer drug has to possess two main features: (I) be mitochondriotropic namely it has to accumulate mainly in the organelle with respect to the rest of the cell, and (II) distinguish between normal and cancer cells targeting only hyperpolarized mitochondria. An elegant study published in 2005 by Trapp and Horobin, using the

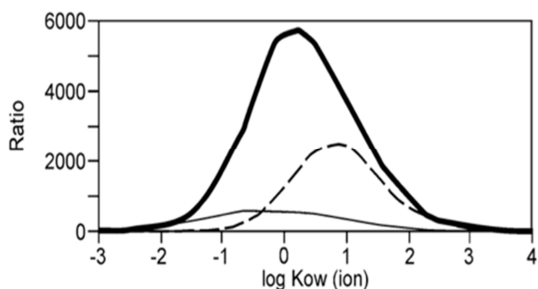


Fig. 10 Ratio between calculated mitochondrial and cytosolic concentrations of synthetic organic monovalent cations with different lipophilicity in cancer cells (thick line), in multidrug resistant cancer cells (dashed line) or in normal cells (thin line), considering 1 h exposure. Form ref.²⁷³

Fick-Nernst-Planck equation, identified the class of molecules which are more selectively targeted to cancer cell mitochondria.²⁷³ The study was based on the fact that the mitochondrial membrane potential is about 60 mV more negative in tumor cells with respect to normal cells. As reported in Fig. 10, monovalent cations with intermediate lipophilicity were found to possess the highest selectivity for cancer cell mitochondria.²⁷³

Moreover, this group of molecules seemed to accumulate also in mitochondria of cancer cells resistant to classic chemotherapy. Delocalized lipophilic cations (DLCs) are organic compounds with elevated lipophilicity which bear a positive charge that can be delocalized on different atoms.²⁷⁴ Accordingly with the article by Trapp and Horobin, DLCs are capable of crossing lipid membranes and, being positively-charged, accumulate in mitochondria exploiting the negative mitochondrial membrane potential generated by the respiratory chain. In addition, the increased $\Delta\psi_m$ can account for their selective gathering by cancer cells mitochondria. Rhodamine 123, which is currently utilized as a dye to measure the mitochondrial membrane potential, was the first DLC identified as an anticancer molecule. It was shown to inhibit the proliferation of cultured carcinoma cells *in vitro*, and to extend the survival of mice implanted with Ehrlich ascites tumor or with MB49 mouse bladder carcinoma cells.²⁷⁵⁻²⁷⁷ Later, a series of five linear cationic N-heterocyclic carbene (NHC) complexes with anticancer properties *in vitro* and inducing mitochondrial damage were synthesized by Berners-Price and co-workers.²⁷⁸ These compounds can be easily modified in the structure and thus their lipophilicity can be finely modulated. From the results obtained on normal and cancer breast cells, emerged that the degree of selectivity of the complexes towards cancer cells was correlated to their log P values with intermediate lipophilicity having again the best selectivity.²⁷⁸ Amongst others, the DLC MKT-077 was reported to significantly inhibit the proliferation of a panel of human cancer cell lines both *in vitro* and *in vivo*, being able to affect also tumors resistant to classic chemotherapeutics.^{279, 280} MKT-077 was also approved by the US Food and Drug Administration in clinical trials for the treatment of carcinoma. However, the trials were discontinued in phase II because of lack of efficacy. In conclusion, DLCs have been identified as selective mitochondriotropic agents able to target dysfunctional hyperpolarized mitochondria and were tested as possible anticancer agents. Unfortunately, none of the compounds developed so far has become a drug and thus further efforts should be done to identify an effective anticancer compound.

1.4.1.2 Targeting antioxidant systems for anticancer therapy

An excessive amount of ROS may lead to cell damage or even to death. Therefore, cancer cells need to maintain ROS levels in a certain range of concentration in order to avoid deleterious effects. It is widely recognized that cancer cells cope with the ROS rise by increasing their antioxidant defenses and, in particular, overexpressing the thioredoxin system.^{255, 281} In fact, both thioredoxins and thioredoxin reductases are highly expressed by many malignant cells and their expression correlates with tumor aggressiveness.²⁸¹ In particular, TrxR1 is upregulated in pleural mesotheliomas, melanomas, breast, thyroid, prostate, liver and colorectal cancers,²⁸²⁻²⁸⁸ whereas TrxR2 expression is particularly elevated in hepatocarcinoma, osteosarcoma, prostate, colon and rectal cancers.²⁸⁹⁻²⁹¹ Interestingly, TrxR2 is also involved in the progression of non-small-cell lung cancer and its inhibition was associated with a decrease of tumor proliferation and migration.²⁹² Regarding thioredoxins, their overexpression has been observed in lung, cervix, pancreatic, colorectal, hepatocellular, gastric and breast cancers.^{289, 293-298} In addition, Prx3 was shown to be upregulated in liver, cervical, prostate and colon cancers.^{289, 299-301} In tumor cells, the principal function of the thioredoxin system is to counteract the excessive amount of radical species in order to escape death. In HeLa cells, Trx2 was shown to reduce TNF- α -mediated mitochondrial ROS production with subsequent inhibition of apoptosis.³⁰² The scavenging activity of the thioredoxin system is also necessary to protect the transformed cell from the “oxygen burst” of immune cells and may contribute to the cancer capacity of escaping the immune system. In support of this anti-immune function, it has been reported that human TrxR can inactivate NK-lysin, a basic peptide produced by activated natural killer cells.³⁰³ Moreover, neoplastic cells, especially leukemia B- and T-cells, actively secrete thioredoxin and Trx-80, a truncated form of Trx1, as mitogenic cytokines to promote cell proliferation.^{304, 305} Furthermore, thioredoxin was shown to be capable of reducing and inactivate immunoglobulins *in vitro*.³⁰⁶ Thus, Trx1 secretion may be another defense mechanism against the immune system. It is worth highlighting that the thioredoxin system is also a source of reducing equivalents to ribonucleotide reductase and thus it can sustain cancer cell proliferation by providing key elements for DNA replication. The overexpression of the thioredoxin system has been also associated to the dramatic phenomenon of drug resistance. In fact, many tumors resistant to classic chemotherapeutics express high levels of both TrxR and Trx.³⁰⁷ In conclusion, the thioredoxin system can sustain tumorigenesis by many different ways including ROS detoxification, DNA replication and resistance to both the immune system and chemotherapy. Interestingly, both TrxR and Trx have been proposed as cancer biomarkers and could be useful in tumor diagnosis.³⁰⁸

As already mentioned, cancer cells show increased oxidative stress that is mainly due to neoplastic transformation, altered metabolism and impaired mitochondrial function. Therefore, they highly depend on their antioxidant systems for the control of ROS levels. As a consequence, cancer cells are more vulnerable with respect to normal cells to agents that further enhance oxidative stress or that lower their capacity to cope with ROS, because of their minor spare ability to sustain additional oxidative challenges (Fig 9).²⁸¹ Of note, a high ROS load also reduces the apoptotic threshold contributing to the vulnerability of tumors. Therefore, the inhibition of cellular antioxidant networks could be a way to target cancer cells, increasing the ROS level above the apoptotic threshold. This idea is supported by the fact that radiotherapy and many chemotherapeutics in clinical use rely on ROS accumulation to induce cancer cell death. For instance, etomoxir is able to increase ROS levels by depleting NADPH and ATP, and anthracyclines increase ROS production via redox-cycling and subsequent inhibition of the mitochondrial respiratory complexes.^{309, 310} Unfortunately, many pro-oxidizing chemotherapeutics induce also severe side effects such as cardiotoxicity and nephrotoxicity. Therefore, new ROS modulators with a safer therapeutic profile and a more specific cellular target need to be developed.³¹¹

Amongst the various scavenging enzymes, thioredoxin reductases have emerged as potential good targets for the development of anticancer drugs. This assumption is based on different points: (I) TrxRs are implicated in NADPH utilization upstream of Trx, Prx and Grx and, therefore, their inhibition impairs the flux of electrons in the whole system; (II) TrxRs are overexpressed in many cancer cells and tumors are more vulnerable to their inhibition; (III) Genetic depletion of either the cytosolic or the mitochondrial TrxR in cancer cells was shown to impair tumor progression;³¹² (IV) TrxRs confer tumor resistance to standard chemotherapeutic; (V) TrxRs can be selectively targeted through the binding of the selenocysteine present in their exposed active site.

In the last decades, more than 150 compounds have been found to target TrxRs ranging from natural products to metal ions or synthetic compounds.³¹³⁻³¹⁷ The majority of the inhibitors act by irreversibly alkylating Sec. However, organic compounds such as quinoids, anthracyclines and naphthoquinones, have been proposed to react with the FAD binding site.³¹⁵ Among the different classes of interacting molecules, gold compounds, and especially gold complexes, have emerged as particularly potent enzyme inhibitors. In 1997 Hill and colleagues reported for the first time the inhibitory effects of gold complexes such as aurothioglucose on thioredoxin reductase.³¹⁸ Then, Gromer *et al.* found that the enzyme was also inhibited by two drugs commonly used for the treatment of rheumatoid arthritis namely aurothioglucose and auranofin (Af).³¹⁹ These thiolate and phosphine Au(I) complexes were shown to be potent inhibitors of TrxR, in particular Af which displayed IC₅₀ value of inhibition of 4 nM. Interestingly, Af has recently passed phase II clinical trials for the treatment of chromatic lymphocytic leukemia and of prolymphocytic or small lymphocytic lymphomas.³²⁰

The good inhibitory capacity of gold complexes on TrxR can be explained by the “hard and soft acids and bases theory” which basically states that soft acids are more prone to react with soft bases and, accordingly, hard acids mainly react with hard bases. Selenolates fall under the soft bases category and thus are prone to complex with soft acids such as gold, silver, palladium, ruthenium and platinum. Thus, the research of TrxR inhibitors for anticancer therapy has focused principally on “soft” metal complexes. In the last years, efforts have been addressed to the synthesis of organometallic compounds in which the metal ion is coordinated by an organic scaffold that makes the molecule more stable in aqueous environment.³²¹ The family of organometallics comprises many different classes including metallocenes, metallo-carbenes (e.g. N-heterocyclic carbenes), metallo-arenes, metallo-carbonyls and alkynyl complexes.³²¹ Each class was found to benefit of some peculiarities which can be exploited to target tumors. For instance, carbonyl complexes, being highly lipophilic, are easily gathered by the cells.³²² However, the most studied and promising classes of organometallic complexes are the N-heterocyclic carbene (NHC) metal complexes and the metallocenes.

Regarding NHC compounds, they were initially developed in the late '90s as antibacterial drugs.³²³ The first NHC Au(I) complexes endowed with anticancer properties were synthesized by Berners-Price's group.²⁷⁸ As already reported in the previous subparagraph these complexes were able to enter into cancer cell mitochondria. The molecular target of these compounds was identified in the mitochondrial thioredoxin reductase and the mechanism of inhibition relied on the selective alkylation of the Sec present in TrxR active site.²⁷⁸ In the following years many differentially functionalized NHC Au(I) complexes have been synthesized. For example NHC Au(I) complexes with aminotriazole or xanthine ligands were shown to affect different cancer cell lines principally by inhibiting the activity of TrxR.^{324, 325} In the field of chemical synthesis, cyclometalation is a common way to generate metal complexes functionalized with various ligands. Of note, metals in different oxidation states can also be stabilized by the ring structure. Au(III) complexes are oxidizing agents that quickly react with thiols and are generally unspecific alkylators in

biological environments. Cyclometalation, however, can stabilize the metal atom and, by modulating the ring structure, can lead to a more targeted action. Already in 1996, a series of Au(III) complexes carrying a 2[dimethylamino)methyl]-phenyl backbone were shown to have strong cytotoxic properties on various cancer cell lines both *in vitro* and *in vivo* through inhibition of TrxR.³²⁶ In addition, a dimethylbenzyl-pyridine Au(III) complex, synthesized by Messori's group, was reported to be as effective as cisplatin in decreasing the viability of the ovarian cancer cell line A2780 by selectively inhibiting TrxR activity.³²⁷ Interestingly, the hydrolysis derivative of the complex was also shown to impair mitochondrial functions triggering apoptosis, suggesting a potential preference for TrxR2.³²⁸ Furthermore, dithiocarbamate Au(III) complexes were shown to affect mitochondria inducing ROS production.³²⁹

Moving to the metallocenes, the first complexes reported to induce toxicity via a redox mechanism were organometallic ruthenium(II) and osmium(II) arene complexes and iridium(III) cyclopentadienyl complexes.

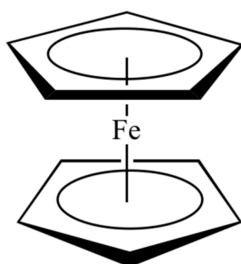


Fig. 11 Structure of the ferrocene unit.

In particular, these compounds were shown to target cancer cells leading to a redox imbalance in a combination therapy with L-buthionine sulfoximine (BSO), an inhibitor of GSH synthesis.^{330, 331} The majority of the metallocene compounds possessing an anticancer activity correlated to an imbalance of the cellular redox state, are ferrocene compounds.³³² The ferrocene unit, which is reported in Fig. 11, is formed by an iron center and two cyclopentadienyl ligands. The structure of ferrocene has several advantages with respect to other metallocenes for the synthesis of potential drugs: (I) it is a compact and stable molecule; (II) it has low toxicity and (III) it possesses reversible redox properties. The anticancer activity of ferrocenyl

compounds was already reported in 1978 by Brynes and co-workers who found for the first time that some ferrocene derivatives were able to kill lymphocytic leukemia cells.³³³ Of note, the neutral ferrocene complex itself is not cytotoxic whereas the ferricenium salts were active also *in vivo* being able to lead to the survival of up to 83% of the animals bearing Ehrlich ascites tumor with respect to untreated controls.³³⁴ Since ferrocene does not present DNA intercalating properties, its mechanism of action was supposed to be the generation of radical species, through the Fenton reaction mediated by the iron atom, leading to oxidative damage.³³⁵ A large number of ferrocene derivatives have been synthesized. Many of them are endowed with cytotoxic properties against specific cancer types and are well summarized in some recent reviews.^{332, 336} Amongst the ferrocenyl derivatives with anticancer activity, the family of ferrocifens deserves to be mentioned because of the promising results for breast cancer treatment. Ferrocifens were synthesized for the first time in 1996, by G. Jaouen and coworkers by substituting a phenyl ring of 4-OH-tamoxifen, the active metabolite of tamoxifen, with a ferrocene unit.³³⁷ Tamoxifen is a non-steroidal selective estrogen receptor modulator (SERM) which is commonly used to treat ER⁺ breast cancer.³³⁸ However, it is completely inactive on ER⁻ cancers which are associated to a worst prognosis and survival expectation. The functionalization of the tamoxifen moiety with the ferrocene unit was aimed to increase the potency of the drug possibly widening its efficacy to estrogen-insensitive cancer cells. Over the years, many derivatives were generated functionalizing the overall structure by modulating the stereochemistry, the length of the N,N-dimethylamino side chain, the position of both the phenol group and of the ferrocene unit.^{332, 339} Notably, hydroxyferrocifens were found to block the proliferation of both MCF-7 (ER⁺) and of MDA-MB-231 (ER⁻) breast cancer cells.³⁴⁰ Regarding the mechanism of action of ferrocifens on the two breast cancer cell lines, a large production of ROS was observed indicating again the potent redox properties of the ferrocene unit.³⁴¹ However, the exact mechanism of action and the cellular targets of these complexes needed to be defined. In 2014, Citta *et al.* identified that thioredoxin reductases are the principal targets of some of the ferrocifens in the lymphoblastoid Jurkat cell line, suggesting the mechanism involved in the ferrocifen-induced ROS production.³⁴²

Therefore, many different metal compounds can block the proliferation of cancer cells by targeting their scavenging systems, leading to ROS overproduction and eventually to cell death. Thioredoxin reductases seem to be good targets as they are often overexpressed in cancer cells. However, very few complexes specifically target one of the two TrxRs. Of note, TrxR2 inhibition in isolated rat liver mitochondria was associated with mitochondrial permeability transition and with Cyt c release.³⁴³⁻³⁴⁵ Thus, TrxR2 inhibition can directly affect $\Delta\psi_m$ leading to the activation of intrinsic apoptosis. Since cancer cells rely on TrxR for ROS detoxification especially in the mitochondrial compartment, TrxR2 inhibition could be exploited to selectively induce apoptosis in cancer cells. Isoform specific inhibitors are difficult to obtain because of the high similarity between the cytosolic and the mitochondrial TrxRs. However, their different cellular compartmentalization can potentially help to design a compound able to discriminate the two protein isoforms. For example, DLCs which are able to accumulate inside mitochondria, could be useful to specifically target TrxR2.

1.4.2 Metabolic syndrome

The pathophysiology of the metabolic syndrome is very complex and up to now no univocal causative factor has been identified yet. However, ROS have been associated to many aspects linked to its development.³⁴⁶ The metabolic syndrome is established if a patient shows three or more of the following factors: visceral obesity, elevated blood pressure, impaired glucose tolerance, increased triglyceride (TG) and decreased high-density lipoprotein (HDL) blood levels.³⁴⁶ Table 2 summarizes the criteria commonly utilized for the diagnosis of the disorder for both genders.

Table 2: Parameters for the diagnosis of the metabolic syndrome (fulfillment of three or more)

Parameter	Men	Women
Waist circumference	> 102 cm	> 88 cm
Blood pressure	> 130/85 mm Hg	> 130/85 mm Hg
Fasting plasma glucose levels	> 100 mg/L	> 100 mg/L
TG	> 150 mg/L	> 150 mg/L
HDL	< 40 mg/L	< 50 mg/L

Patients suffering from metabolic syndrome are often aged, obese, practice low physical activity and show insulin resistance. The excessive caloric intake in aged people is one of the major risk factors but there is also a genetic component.³⁴⁷ Visceral obesity may play an important role in the development of the syndrome. Upon macrophages infiltration, adipocytes release large amounts of cytokines inducing a chronic inflammatory state that may promote also oxidative stress. The resulting systemic inflammation favors the onset of other related pathologies such as cardiovascular disease (CVD) and diabetes.³⁴⁸ Accordingly, anti-inflammatory treatments such as statins, inhibitors of secretory phospholipase A2, inhibitors of lipoprotein-associated phospholipase A2 and inhibitors of angiotensin-converting enzyme were shown to reduce atherosclerosis progression.³⁴⁹ In general, the diagnosis of metabolic syndrome has been correlated to a 2-fold increase risk of CVD outcomes.³⁴⁷ Moreover, obesity promotes the development of colon, kidney, prostate, endometrial, and breast cancers and is associated to a worsened outcome for cancer treatment.³⁵⁰ Tumor proliferation is probably boosted by adipose tissue inflammation, hyperglycemia, hyperinsulinemia and increased insulin-like growth factor 1 levels.³⁵⁰ Furthermore,

metabolic syndrome is a risk factor for type II diabetes³⁴⁷ and can also be associated to nonalcoholic steatohepatitis (NASH).³⁵¹ All together, these observations point out that metabolic syndrome can favor the onset of many severe pathologies such as CVD, diabetes, NASH and cancer.

The different pathologic changes found in patients suffering from metabolic syndrome converge on oxidative stress induction which was found to be an early event in the progression of the disease.³⁴⁸ Therefore, the role of oxidative stress in metabolic syndrome is an emerging topic and, in literature, many papers have been published dealing with the contribution of specific scavenging enzymes to the protection from the disorder or with the role of ROS producing enzymes in the progression of the syndrome. It is important to remind that H₂O₂ formation is involved in insulin downstream signaling pathway.⁶ H₂O₂ itself was shown to increase glucose uptake by adipocytes and muscles, stimulating the translocation of GLUT4 to the membrane and the synthesis of lipid in adipocytes.³⁵² Interestingly, obese mice and humans experience a progressive increase of ROS production in adipose tissue, accompanied by NADPH oxidase overexpression. In addition, lipid peroxides and oxidized proteins measured in plasma and urine are also increased in obese patients.³⁴⁸ Among ROS producing enzymes, NADPH oxidases and myeloperoxidase are largely recognized to boost the progression of atherosclerosis.³⁵³ Regarding the antioxidant enzymes, Amirkhizi *et al.* reported a significant decrease of Cu/Zn SOD, total GPx and catalase activities in the erythrocytes of obese women compared to a normal weight group.³⁵⁴ Furthermore, obese patients displayed decreased amounts of vitamins A, C, E and of β -carotene.³⁵⁵ As a consequence, people affected from metabolic syndrome are more susceptible to oxidative stress. Therefore, the role of single antioxidant enzymes in relation to the syndrome and the specific redox signaling pathways affected by the increased ROS production are currently being investigated. For instance, Trx1 secreted in circulation was found to be higher in patients affected either by metabolic syndrome, hypercholesterolemia or diabetes, with respect to healthy controls³⁵⁶⁻³⁵⁸ and TrxR1 expression in adipose tissue is directly correlated to the percentage of fat mass in both human patients and obese mice.^{359, 360} However, TrxR1 knockdown in human undifferentiated adipocytes was shown to enhance adipose tissue differentiation indicating that TrxR1 overexpression does not have a role in adipocyte proliferation but probably deals with its ROS buffering activity.³⁶¹ TrxR2 expression was augmented in the heart of rats fed with a high-fat high-sucrose diet.³⁶² Moreover, mRNA levels of both thioredoxins and thioredoxin reductases were elevated in patients with hypertension.³⁶³ Of note, mice overexpressing Trx1 and fed with high-fat diet were shown to increase their adipose tissue mass similarly to the WT animals but did not develop glucose resistance,³⁶⁴ whereas human Trx2 overexpression in mice led to the prevention of angiotensin II induced hypertension.³⁶⁵ Interestingly, angiotensin II-triggered hypertension in WT mice increases Trx1 expression only in males and not in females, revealing a probable influence of estrogens.³⁶⁶ Altogether these data suggest that the upregulation of the thioredoxin system is probably a compensatory mechanism to reduce the oxidative burden derived from metabolic changes and from the inflammatory response. Accordingly, the cardioprotective effect of the antidiabetic agent metformin has been ascribed to an upregulation of Trx1 expression.³⁶⁷ Anyhow, alterations in the thioredoxin system do not seem to be involved in the pathogenesis of the metabolic disorder. In addition, the different mouse strains depleted or overexpressing enzymes of the thioredoxin system do not develop the metabolic syndrome.

On the contrary, recent advances in the field have emerged on the role of the other major thiol redox regulating system, namely the glutathione system, in relation to the metabolic syndrome. In fact, patients affected by type II diabetes display reduced levels of glutathione and significant oxidative stress in erythrocytes.^{368, 369} As already mentioned total GPx blood levels were decreased in obese women when compared to healthy subjects and this effect could be due to the decrease of GSH which is its substrate.

This hypothesis was confirmed in a rat model of oxidative stress. In fact, when glutathione biosynthesis was inhibited in rats by BSO administration and the glutathione levels were efficiently reduced, an impaired glucose homeostasis, associated with elevated adiposity and insulin resistance, was observed.³⁷⁰ In GPx1 KO mice, an increased deposition of atherosclerotic plaques was observed, while GPx4 overexpression decreased atherogenesis and delayed the progression of lesions suggesting a protective role of GPxs against atherosclerosis.^{371, 372} Accordingly, GPx3 activity measured in serum was diminished in patients affected by atrial fibrillation compared to healthy subjects, demonstrating that reduced levels of GPx increases the risk of CVD outcomes.³⁷³ In a study conducted in Japan on subjects affected by type II diabetes, emerged that individuals carrying a less-active mutated form of GPx1 (Pro198Leu variant) were more prone to atherosclerosis, vascular abnormalities and diabetic neuropathy with respect to the subjects having the more active Pro198 GPx1 variant.³⁷⁴ Of note the statin rosuvastatin, in addition to its lipid-lowering effect, was found to contrast atherosclerosis in rats by elevating the amount of glutathione and GPxs and enhancing the overall antioxidant capacity.³⁷⁵ Also GPx7 KO mice were reported to have higher body and fat-pad masses when fed on a 60% fat diet compared to WT mice.³⁷⁶ Thus, GPxs seem to be involved in the control of glucose metabolism and of the body weight and, in general, appear protective against the development of metabolic syndrome and related diseases.

Less than 0.2% of the total GSH pool is involved in protein S-glutathionylation.³⁷⁷ However, GSH-derivatization of Cys regulates the function of a plethora of different proteins. Thus, changes in the extent of this post-translational modification can be significant for numerous cell functions. Regarding the metabolic syndrome, levels of glutathionylated proteins are decreased in the liver and adipose tissue of obese rats compared to control animals. Interestingly, this decrease was associated with a parallel increase of Grx1 in the adipose tissue.³⁷⁸ In 2017, Shao *et al.* reported that Grx1 KO mice fed with normal diet spontaneously develop obesity, hyperlipidemia, and hepatic steatosis by 8 months of age.³⁷⁹ Authors identified that Grx1 KO mice exhibited upregulation of hepatic enzymes involved in lipid synthesis because of a decrease in sirtuin 1 activity due to its glutathionylation. The specific involvement of sirtuin 1 was supported by the observed lowering of lipid accumulation in the liver and of cholesterol levels in plasma of Grx1 KO mice after the hepatic expression of a mutant form of sirtuin 1 lacking cysteines (C61S + C318S + C613S).³⁷⁹ Downs *et al.* recently reported that only female mice deficient for Grx1 fed a normal chow diet develop the metabolic syndrome, characterized by atherosclerosis, mild hyperlipidemia, hyperglycemia and obesity.³⁸⁰ Aged female Grx1 KO mice display also macrophages activation with blood macrophages showing increased protein glutathionylation, overexpression of pro-inflammatory “M1”-associated genes and impaired autophagy. Therefore, monocytic Grx1 seems to be involved in the protection from atherosclerotic plaques deposition and chronic inflammatory diseases.³⁸⁰ More recently, Grx2 KO mice were shown to develop different features that can be associated to the metabolic syndrome.³⁸¹ Indeed, these mice display augmented body mass, increased blood pressure and heart hypertrophy.^{235, 381} Interestingly, Grx2 deletion does not induce Grx1 overexpression underlying different functions of the two isozymes which cannot be compensated by the other one. The proposed mechanism of metabolic syndrome induction in Grx2 KO mice is an altered mitochondrial respiration inducing $O_2^{\bullet-}/H_2O_2$ production and leading to a consequent oxidative stress especially in the liver and in the heart.³⁸¹ As already mentioned in paragraph 1.3.2.4, Grx2 has different splicing variants: a prevalent mitochondrial one, and other isoforms resident in the cytosol and in the nucleus able to regulate the redox state of transcription factors. Therefore, the impact of the deletion of single Grx2 isoforms should be evaluated in order to better clarify the mechanism of metabolic syndrome induction.

2. Aims of the research

The aim of this research was to investigate the role of different mitochondrial proteins involved in thiol redox regulation in relation to normal or dysregulated cell physiology. Redox regulation includes important signaling pathways that modulate key cellular functions such as proliferation or cell death. The exact mechanisms of redox signal cascades are often still unknown especially in the mitochondrial cell compartment and need to be elucidated.

In the first part of the research, I focused my attention on the mitochondrial thioredoxin system. The equivalents supplied by NADPH, are utilized by TrxR2 to reduce Trx2 that, in turn, reduces other substrates such as Prx3, devoted to the removal of H₂O₂ and other hydroperoxides. The purpose of the research was the identification of new mitochondrial proteins undergoing redox regulation by this system. Based on evidences in literature indicating that cyclophilins are sensitive to redox conditions,²⁶ we investigated whether cyclophilin D (CypD), a peptidyl prolyl *cis-trans* isomerase of the mitochondrial matrix, could be redox regulated by the thioredoxin system. To this aim, co-immunoprecipitation techniques, enzymatic activity assays, protein redox state determinations and *in silico* analysis were performed on both purified proteins, isolated rat heart mitochondria or different immortalized cell lines. In addition, using the co-immunoprecipitation method, CypD interaction with Trx2 was also investigated in a human cell line overexpressing Trx2 that has been successfully generated for this specific purpose.

In order to better clarify the peculiar function of thioredoxin reductase 2 (TrxR2) in mitochondria, I studied the effects of TrxR2 depletion in a cellular model. I started by utilizing the short-interfering RNA approach that can lead to a transient protein depletion and I analyzed the effect on Trx2 redox state. Then, I utilized the Crispr-Cas9 technique, which targets and cleaves the gene of interest, in order to generate a stable TrxR2 knockout cell line. Many different cancer cell models were employed and two DNA guides utilized. After expansion of single clones, the stable TrxR2-depleted cell lines were identified. Then, cellular ROS production was assessed in the various clones and were correlated to the expression level of the mitochondrial thioredoxin reductase.

The second part of the research was centered on the relation between thioredoxin reductases and cancer. Indeed, for their survival, invasion capacity and resistance to classic chemotherapeutic drugs, cancer cells are highly dependent on the thioredoxin system and in particular on thioredoxin reductases. For this reason, the design of new compounds able to affect the thioredoxin system is a possible strategy to hit cancer cells. In addition, cancer cells are often characterized by hyperpolarized mitochondria. Therefore, the aim was the identification of new anticancer drugs able to selectively target TrxR2 in mitochondria. Different classes of metal complexes, synthesized in the frame of various international collaborations, were investigated for their ability to inhibit TrxR activity. The mechanism of TrxR inhibition was characterized and the efficacy of the new compounds against different cancer cell lines was assessed. In addition, the effect of these complexes on the overall cellular redox state was measured. In particular, total thiols, amount of total and oxidized glutathione, thioredoxin and peroxiredoxins redox state, enzymatic activities of different redox active enzymes and ROS production were analyzed. Moreover, for the most promising complexes, their impact on mitochondrial functioning was assessed. Thus, mitochondrial membrane potential, mitochondrial ROS production, Cyt c release and caspase activation were determined. Finally, the subcellular localization of the complexes was also analyzed.

In the third part of the research, I focused on glutaredoxin 2 (Grx2), a mitochondrial protein that modulates protein glutathionylation and previously found to link the thioredoxin and the glutathione systems receiving reducing equivalents by both GSH and TrxRs.²²⁶ Grx2 can form enzymatically inactive dimers coordinating a 2Fe-2S cluster with its active site. Oxidative stress conditions were hypothesized to induce the disassembly of the dimer and to activate Grx2. In order to examine this hypothesis, I started by exploring the role of Grx2 in the mitochondrial response to oxidative stress in a cellular model. A classical chemical approach was utilized to establish oxidative stress, using principally micromolar concentrations of sodium selenite as a glutathione oxidizing agent. I first determined the concentration of sodium selenite able to almost completely oxidize the glutathione pool, inducing oxidative stress. In this condition, Grx2 monomeric/dimeric status and activity were analyzed. Mitochondria were isolated from selenite treated or control cells, and the specific glutaredoxin activity was estimated in both the cytosolic and the mitochondrial cell compartments at different time points from sodium selenite administration in order to monitor Grx2 activity over time. The impact of sodium selenite on TrxRs enzymatic activities was also evaluated in the two cell fractions. I further assessed whether oxidative stress, by affecting Grx2 monomer/dimer ratio, could determine the release of the 2Fe-2S cluster into mitochondria. Therefore, the free iron pool was measured in the cellular mitochondrial fractions. In the same conditions, the lipid peroxidation level was assessed with two different techniques as it may represent an indirect measurement of fluctuations of the free iron concentrations. Finally, the mitochondrial membrane potential was investigated in order to see possible effects of iron release on mitochondrial functioning.

In the very last part of the research, the effect of mitochondrial Grx2 deletion was investigated in a whole-body mGrx2 knockout C57bl/6 mouse model, in collaboration with Prof. Holmgren's group of the Karolinska Institutet. In the mouse strain, the mitochondrial-targeting sequence of Grx2 was deleted and thus the protein can be expressed, but cannot enter the mitochondrial compartment. Firstly, we investigated whether the absence of Grx2 in mitochondria can affect the redox state of the organelle. For this purpose, we isolated mitochondria from the liver, kidney, brain and heart and assessed the mitochondrial redox state measuring total thiols, glutathione amount and the enzymatic activities of glutaredoxin, thioredoxin reductases and glutathione reductase. Afterwards, since mGrx2 depleted mice displayed fatty liver from three months of age, we analyzed mGrx2 KO mouse liver mitochondria for their overall functioning. Hence, ROS production, oxygen consumption using different substrates and mitochondrial membrane potential status were measured. Eventually, mitochondrial sensitivity to calcium was also determined by means of the swelling assay.

3. Materials and Methods

3.1 Enzymes

- *Thioredoxin reductase 1 and 2*
Cytosolic rat liver thioredoxin reductase (TrxR1) was purified according to Luthman and Holmgren and mitochondrial rat liver thioredoxin reductase (TrxR2) according to Rigobello *et al.*^{72, 382}
- *Thioredoxin*
Human recombinant thioredoxin 1 (expressed and isolated from *E. coli* > 5 Units/mg of protein) was purchased from Sigma-Aldrich (Därmstadt, D).
- *Glutathione reductase*
Yeast glutathione reductase (from *S. cerevisiae* 500 Units/mg of protein) was purchased from Sigma-Aldrich (Därmstadt, D).
- *Glutaredoxin 2*
Human recombinant glutaredoxin 2 (expressed and isolated from *E. coli* > 5 Units/mg of protein) was kindly provided by Prof. A. Fernandez (Karolinska Institutet, Stockholm, S).

3.2 Cell lines

Table 3: List of the different cell lines utilized

Name	Cell type	Culture medium
Jurkat	lymphoblastoid cells	RPMI-1640
CEM-R	leukemic lymphoid cells (vinblastine resistant)	RPMI-1640
HeLa	epithelioid cervix carcinoma cells	high glucose DMEM
A2780	ovarian cancer cells	high glucose DMEM
A2780R	ovarian cancer cells (cisplatin resistant)	high glucose DMEM
SKOV-3	ovarian cancer cells	high glucose DMEM
2008	ovarian cancer cells	RPMI-1640
C13	ovarian cancer cells (cisplatin resistant)	RPMI-1640
A549	lung carcinoma cells	high glucose DMEM
HEK 293	embryonic kidney cells	RPMI-1640

The various human cell lines were obtained either by ECACC or by ATCC. Cells were cultured in RPMI-1640 medium or in high glucose DMEM medium (Gibco, Waltham, MA, USA) supplemented with 10% fetal calf serum (FCS), 2 mM glutamine and 1% penicillin/streptomycin (Invitrogen, Carlsbad, CA, USA) at 37°C in a humidified atmosphere of 95% air and 5% CO₂.

3.3 Animal models

- *mGrx2 KO mouse model*
The inbred C57bl/6 mouse strain lacking mitochondrial Grx2 (mGrx2 KO) was obtained from the Karolinska Institutet (Stockholm, S). The mouse model was generated at the Central Institute for Experimental Animals (Kawasaki, J) by targeting exons 1c, 1a and 2 in *GLRX2* gene, located on chromosome 1:143.72-143.75, and replacing them by a neomycin cassette which was subsequently

excised (Fig. 12). The deleted exons encode for Grx2 mitochondrial targeting sequence. Thus, in mGrx2 KO mice Grx2 is expressed but cannot enter the mitochondrial matrix and its expression is restricted to the cytosolic compartment. mGrx2 KO mice show no suffering phenotype and grow normally. However, they develop a metabolic syndrome in the adulthood with increased body weight and fatty liver. 10 to 13 weeks old mice were utilized for the reported experiments.

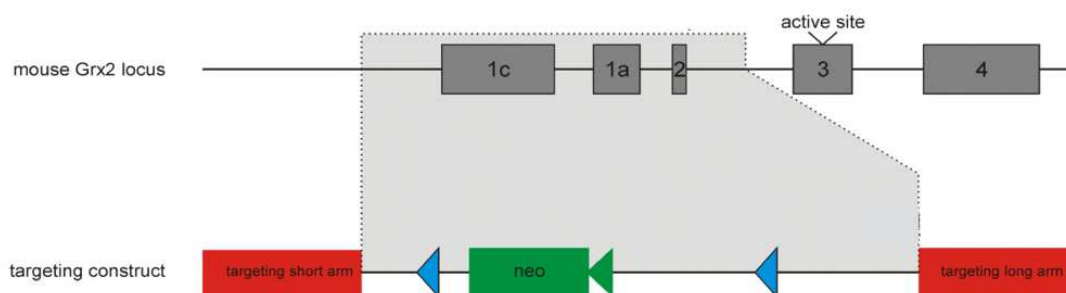


Fig. 12 Scheme of the targeting construct on mouse Grx2 locus.

- *Wistar rats*

Adult Wistar albino WT rats were bred in standard conditions and sacrificed at 7-8 weeks of age ($\cong 250$ g of body weight). Liver and heart were explanted and rapidly processed for mitochondria isolation.

All the animals utilized were kept in climate-controlled rooms ($21 \pm 2^\circ\text{C}$ and 50% of humidity) on a 12 h of light/12 h of dark day cycle and fed with a standard chow diet.

3.4 Enzymatic activities and BIAM assay

3.4.1 Thioredoxin reductase activity

Isolated rat liver thioredoxin reductase 1 and 2 activities were determined by estimating the dithiobis(2-nitrobenzoic acid) (DTNB) reduction kinetics in the presence of NADPH. Aliquots of highly purified TrxR1 or TrxR2 (70 nM) were preincubated for 5 min with the studied compounds in 0.2 M sodium/potassium phosphate (NaKPi) buffer (pH 7.4), 5 mM EDTA and 0.25 mM NADPH. The reaction was initiated with 1 mM DTNB and followed spectrophotometrically at 412 nm for about 10 min on a Lambda2 spectrophotometer (PerkinElmer, Waltham, MA, USA).

For the estimation of the total TrxR activity in cellular or mitochondrial lysates, aliquots (50 μg proteins) were added to 0.2 M NaKPi buffer (pH 7.4), 5 mM EDTA, and 2 mM DTNB in a final volume of 250 μL . After 2 min the reaction was started with 0.4 mM NADPH and DTNB reduction was followed spectrophotometrically at 412 nm for 10 min.

In addition, to measure TrxR activity in cellular lysates, the insulin assay was also employed. Briefly, aliquots of lysates (12 μg proteins) were incubated for 40 min in a final volume of 50 μL in 100 mM Hepes-Tris buffer (pH 7.6) in the presence of 15 mM EDTA, 1.5 mM NADPH, 0.20 mM insulin, and 0.1 mM Trx from *E. coli*. The reaction was stopped by adding 0.2 mL of 1 mM DTNB in 0.2 M Tris-HCl buffer (pH 8.1) containing 1 mM EDTA and 7.2 M guanidine, and the absorbance of the samples was estimated at 412 nm on a Tecan Infinite M200 PRO plate reader (Tecan, Mannedorf, CH).³⁸³

3.4.2 Glutathione reductase activity

Glutathione reductase activity was measured in 0.2 M Tris-HCl buffer (pH 8.1), 1 mM EDTA and 0.25 mM NADPH. After 5 min of preincubation of GR (70 nM) with the various compounds, the assay was started by the addition of 1 mM oxidized glutathione (GSSG) and NADPH consumption was measured at 340 nm using a Lambda2 spectrophotometer. In cellular and mitochondrial lysates, GR specific activity was estimated on 80 µg of proteins.

3.4.3 Glutaredoxin activity

The standard assay for Grx2 activity relies on the procedure developed by Mieyal *et al.*³⁸⁴ as modified by Raghavachari and Lou.³⁸⁵ Basically, recombinant human Grx2 (70 nM) was preincubated for 5 min with increasing concentrations of sodium selenite (1-20 µM) in 0.2 M NaKPi buffer (pH 7.4), 5 mM EDTA, 0.5 mM GSH, 70 nM GR and 0.2 mM NADPH. Then, the enzymatic activity was assessed at 30°C with 2 mM hydroxyethyl disulfide (HEDS) as Grx2 substrate. NADPH decrease was followed at 340 nm with a Lambda2 spectrophotometer. To determine Grx2 activity, the slope of the linear portion of the NADPH consumption curve was utilized. In cellular and mitochondrial lysates, Grx specific activity was estimated on 50 µg of proteins.

3.4.4 BIAM assay

This assay allows the detection of irreversible cysteine and selenocysteine alkylation in proteins. In particular, the differential derivatization of TrxRs' cysteine and selenocysteine by newly developed inhibitors can be studied. Rat liver TrxR1 (1 µM) pre-reduced in the presence of 60 µM NADPH was incubated with the studied compounds for 30 min at room temperature in 50 mM Tris-HCl buffer (pH 7.4) containing 200 µM NADPH and 1 mM EDTA. After incubation, 8 µL of the reaction mixture were added to 8 µL of 100 µM biotinylated iodoacetamide (BIAM) in either 0.1 M Tris-HCl (pH 8.5) or in 0.1 M Hepes-Tris (pH 6.0) buffer.³⁸⁶ The samples were incubated at room temperature for an additional 30 min to allow BIAM alkylation of free SH/SeH groups. Then, samples were subjected to sodium dodecyl sulphate-polyacrylamide gel electrophoresis (SDS-PAGE) on a 10% acrylamide/bis(acrylamide) gel, and transferred to a nitrocellulose membrane. BIAM labelled enzyme was detected with the chemiluminescence deriving from streptavidin-conjugated horseradish peroxidase (HRP) activity.

3.5 Experiments performed in cultured cells

3.5.1 MTT assay

Cell proliferation was determined with the 3-[4,5-dimethylthiazol-2-yl]-2,5-diphenyltetrazolium bromide (MTT) reduction assay. Cells (1×10^4) were plated on a 96 well plate and treated with increasing concentrations of the different compounds for 24, 48 or 72 h. At the end of incubation, 0.5 mg/mL MTT dissolved in phosphate-buffered saline (PBS) was added to the cells for 3 h at 37°C. Afterward, MTT solution was removed and 100 µL of stop solution (90% isopropanol, 10% DMSO) were added to each well. After 15 min and complete formazan dissolution, the absorbance at 595 nm and 690 nm was estimated using a Tecan Infinite M200 PRO plate reader.

3.5.2 Preparation of cell lysates

After treatment, cells (2×10^6) were harvested, washed with PBS and lysed with a modified RIPA buffer constituted by 50 mM Tris-HCl buffer (pH 7.4), 150 mM NaCl, 1 mM EDTA, 0.1% SDS, 1% Triton X100, 0.5% DOC, 1 mM NaF, 0.1 mM phenylmethylsulfonyl fluoride (PMSF) and supplemented with an antiprotease cocktail (Complete, Roche, Mannheim, D). After 40 min of incubation at 4°C, lysates were centrifuged at 14000g for 5 min and aliquots of the supernatants were utilized for protein determination with the Lowry assay.³⁸⁷

3.5.3 Preparation of cytosolic and mitochondrial cell fractions

Cells were sub-fractionated essentially following the protocol of Clayton and Shadel.³⁸⁸ Briefly, cells (3×10^7 per condition) were collected, washed with PBS and subjected to hypo-osmotic treatment with 2 mL of 10 mM NaCl, 1.5 mM $MgCl_2$, 10 mM Tris-HCl buffer (pH 7.5) for 5 min and gently homogenized using a Dounce tissue grinder. Afterwards, 1.4 mL of 525 mM mannitol, 175 mM sucrose, 2.5 mM EDTA, 12.5 mM Tris-HCl buffer (pH 7.5) were rapidly added. The homogenate was diluted to a final volume of 5 mL with 210 mM mannitol, 70 mM sucrose, 1 mM EDTA, 5 mM Tris-HCl buffer (pH 7.5) and subjected to differential centrifugation. The first step was carried out at 1300g for 5 min at 4°C to discard nuclei and non-disrupted cells. The mitochondrial fraction was pulled down from the supernatant at 15800g for 15 min at 4°C and washed twice. The crude soluble supernatant obtained from the mitochondrial isolation step was further centrifuged at 105000g for 15 min at 4°C to obtain the cytosolic fraction. Mitochondrial fractions were lysed using a modified RIPA buffer containing 50 mM Tris-HCl (pH 7.4), 150 mM NaCl, 1 mM EDTA, 1% Triton X100, 0.1% SDS, 0.5% DOC, 1 mM NaF, supplemented with an antiprotease cocktail and 0.1 mM PMSF and subjected to protein determination with the Lowry assay.³⁸⁷ The presence of cytochrome oxidase and Cyt c as mitochondrial markers was assessed by Western blot analysis in the mitochondrial fraction.

3.5.4 Determination of cellular ROS production

Adherent cells (1×10^4 per well) were seeded in a 96 well plate in complete medium in a volume of 100 μ L per well. The following day cells were washed with PBS/10 mM glucose and then incubated for 1 h with 10 μ M 5-(and-6)-chloromethyl-2',7'-dichlorodihydrofluorescein diacetate acetyl ester (CM-H2DCFDA) (ThermoFisher, Waltham, MA, USA) at 37°C, 5% CO_2 . Afterwards, the medium was removed and 100 μ L PBS/10 mM glucose supplemented with the various compounds was added to each well. ROS production was estimated by monitoring the fluorescence increase of the probe (λ_{Ex} = 485 nm, λ_{Em} = 527 nm) for 1.5-2 h using an Infinite M200 PRO plate reader. The protocol was also adapted for cells in suspension. In this case, Jurkat cells (4×10^4 per well) were seeded in PBS/10 mM glucose. After 1 h, cells were loaded with 1 μ M CM-H2DCFDA and with increasing concentrations of the compounds. Then, fluorescence was followed for 2 h as reported above.

3.5.5 Determination of total thiols

Cells (4.5×10^5 per well) were plated in a 6 well plate and incubated in the different conditions. Afterwards, cells were washed with PBS and dissolved with 7.2 M guanidine in a 0.2 M Tris-HCl buffer (pH 8.1), 5 mM EDTA. Then, 3 mM DTNB was added to titrate the thiol groups and the absorbance increase was monitored at 412 nm for 5 min on a Lambda2 spectrophotometer.

3.5.6 Estimation of total and oxidized glutathione

Cells (4.5×10^5) were incubated with the indicated compounds, then washed with cold PBS and deproteinized with 6% meta-phosphoric acid. After 20 min at 4°C, samples were collected and centrifuged at 15800g for 10 min at 4°C. Supernatants were neutralized with 15% Na_3PO_4 and utilized for total glutathione estimation.³⁸⁹ For the measurement of oxidized glutathione, sample aliquots were treated with 2-vinylpyridine for 40 min before performing the assay.³⁹⁰ The pellets obtained after centrifugation were washed with 1 mL of ice-cold acetone, centrifuged at 11000g, dried, and then dissolved in 62.5 mM Tris-HCl buffer (pH 8.1) containing 1% SDS for protein determination by means of the Lowry assay.³⁸⁷

3.5.7 Evaluation of the redox state of Trx1, Trx2 and CypD

In cells, the thiol redox state of the proteins of interest was estimated according to the method developed by Bersani *et al.* as modified by Du *et al.*^{391, 392} After treatment, cells (2×10^6) were washed with PBS and lysed with 100 μL of urea lysis buffer composed by 8 M urea, 1 mM EDTA, 100 mM Tris-HCl (pH 8.3), containing 10 mM iodoacetamide (IAM) in order to alkylate free thiols. Incubation was carried out at 37°C for 20 min. Then, cell lysates were spun down and precipitated by ice-cold acetone-1M HCl (98:2). The pellets were washed twice with ice-cold acetone-1M HCl- H_2O (98:2:10), dissolved in 60 mL of urea lysis buffer including 3.5 mM dithiothreitol (DTT), and incubated for 30 min at 37°C to reduce the disulfide bonds. Afterwards, 3 μL of 600 mM iodoacetic acid (IAA, final concentration 30 mM) were added to the samples, followed by incubation for 30 min at 37°C. The protein concentration was determined using the Lowry assay³⁸⁷ and 20 μg of each sample were separated by urea-PAGE (7% acrylamide/bis(acrylamide), 7 M urea) in non-reducing conditions and blotted. The membranes were probed with the primary antibodies for Trx1, Trx2 and CypD. A peroxidase conjugated secondary antibody and chemiluminescence were used to detect the immunoreactive bands.

3.5.8 Determination of the monomer/dimer ratio of Prx3 and Grx2

For Prx3 and Grx2 redox state estimation, the procedure of Stanley *et al.*³⁹³ with modification, was utilized. After incubation in the different conditions, cells were centrifuged at 500g for 5 min, washed with cold PBS and then treated with 1 mL of 10% trichloroacetic acid. Samples were kept at 4°C for 30 min, centrifuged at 10000g for 10 min at 4°C, and resuspended in 0.5 mL of ice-cold acetone. After 10 min of incubation, samples were centrifuged again at 10000g for 10 min at 4°C. Then, the pellets obtained were dissolved in 670 mM Tris-HCl buffer (pH 7.5), 2% SDS and 1 mM EDTA, containing 10 mM AIS (4-acetamido-4'-((iodoacetyl) amino) stilbene-2,2'-disulfonic acid) (Invitrogen, Carlsbad, CA, USA), a thiol alkylating agent. Derivatization was carried out at room temperature for 20 min, followed by further 45 min at 37°C. 20 μg of proteins of each sample was loaded, without reducing agents, onto Bis-Tris Gel NuPAGE (12% acrylamide/bisacrylamide) and blotted. Anti-Prx3 and anti-Grx2 antibodies were used to detect the monomeric and dimeric form of the proteins in Western blot. A horseradish peroxidase conjugated secondary antibody was employed to detect the immunoreactive bands in chemiluminescence. Cellular mitochondrial fractions were processed in the same manner. Once obtained following the protocol of Clayton and Shadel which is reported in subparagraph 3.5.3,³⁸⁸ mitochondria were lysed with the AIS-containing buffer and processed following the same protocol described above.

3.5.9 Mitochondrial thioredoxin reductase depletion

- *Transient TrxR2 depletion (siRNA method)*

In order to obtain a transient TrxR2 knockdown cell line, the short interfering RNAs (siRNAs) were utilized. HeLa cells were seeded at 50% confluence in 6 well plates and transfected with 40-80 nM of two different commercially available TXNRD2 siRNAs (siGENOME, Dharmacon GE Healthcare, Little Chalfont, UK) using Attractene (Qiagen, Venlo, NL) as transfection reagent. Target sequences: siRNA **a**: GAAAGAGAUUCUGCUGUCA, siRNA **b**: GCCGAUCACAUCAUUG. Medium was replaced after 6 h, cells were harvested 48 h after transfection and subjected to the experiment.

- *Stable TrxR2 depletion (Crispr/Cas9 method)*

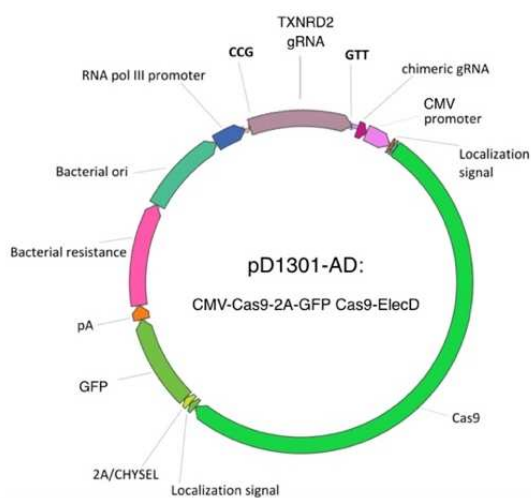


Fig. 13 Map of the all-in-one Crispr/Cas9 plasmid targeting TXNRD2 gene.

TrxR2 knockdown cell clones were generated with the Crispr/Cas9 technique. A549 cells were seeded at 80% confluence in a 6 well plate and transfected with 5 µg of commercially available all-in-one plasmid pD1301-AD: CMV-Cas9-2A-GFP,Cas9-ElecD expressing Cas9-DasherGFP and the sgRNA guides (ATUM, Newark, CA, USA) (Fig. 13) using lipofectamine 2000 as transfection agent (Invitrogen, Carlsbad, CA, USA). The gRNA guide sequence used were CTGGGGACACTCACGTGCGT and GATGCAGCCCACGTTGACGC. After 15 h cells were washed carefully with PBS and medium was replaced. Two days post-transfection, GFP positive cells were sorted in a 96 well plate using a FACS Aria II cell sorter (BD BioSciences, San Jose, CA, USA) and single clones were expanded.

To determine mitochondrial thioredoxin reductase depletion, cells ($\approx 1 \times 10^6$) were lysed with the modified RIPA buffer (see subparagraph 3.5.2) for 40 min at 4°C and centrifuged at 15800g for 10 min. Then, 25 µg of the supernatants were subjected to 10 % acrylamide/bisacrylamide SDS-PAGE and to Western blot analysis using a monoclonal anti-TrxR2 antibody. A peroxidase conjugated secondary antibody and chemiluminescence were used to detect the immunoreactive bands. For the loading control GAPDH amount was assessed.

3.5.10 Trx2 overexpression

Trx2 overexpression was established in Hela cells by means of a pcDNA3.1 plasmid coding for a FLAG-tagged form of human Trx2 (DYKDDDDK octapeptide linked at protein C-terminus) and bearing a G418 resistance (Invitrogen Carlsbad, CA, USA) (Fig. 14). Cells were seeded in a 6 well plate (4×10^5 cells/well) and transfected with 5 µg of DNA utilizing lipofectamine 2000 as transfection agent (Invitrogen, Carlsbad, CA, USA). After 15 h medium was replaced. Selection of the transfected cells was

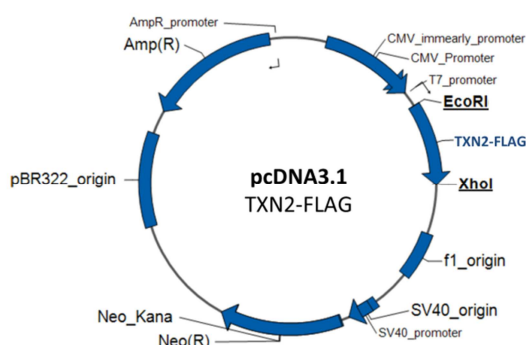


Fig. 14 Map of the plasmid utilized for Trx2 overexpression.

performed with 0.6 mg/mL geneticin (Gibco, Waltham, MA, USA). Afterwards, the protein overexpression was observed by Western blot analysis utilizing either an anti-Trx2 antibody and an anti-FLAG one.

3.5.11 Co-immunoprecipitation of CypD with Trx2 from Trx2 overexpressing HeLa cells

Trx2 overexpressing HeLa cells (1×10^6) were trypsinized, lysed for 30 min with 300 μ L of a 25 mM Hepes-Tris lysis buffer (pH 7.4), 150 mM NaCl, 1% Triton X100, 1mM EDTA containing a protease and phosphatase inhibitor cocktail, centrifuged at 20000g for 10 min at 4°C and diluted 1:1 with the same buffer without detergents. Pre-cleaning phase was performed using 20 μ L of A/G PLUS-Agarose beads (Santa Cruz Biotechnology, Dallas, TX, USA) for 45 min at 4°C with stirring. Pre-cleaned samples were centrifuged at 720g for 5 min and the supernatant was incubated with an anti-Trx2 antibody (Abfrontier) overnight at 4°C. A/G PLUS-Agarose beads (20 μ L) were added, incubated for 3 h at 4°C, centrifuged at 720g for 5 min and washed with ice-cold buffer (50 mM Tris-HCl (pH 7.4), 1 mM EDTA, 1 mM NaF and protease inhibitor). The pull down was resuspended in SDS loading buffer containing 100 mM DTT, boiled for 10 min, and then centrifuged at 17000g for 1 min. The supernatant was separated by SDS-PAGE (Mini-PROTEAN® TGX, any kD, Bio-Rad Lab. Inc., Hercules, CA, USA) and transferred onto a nitrocellulose membrane using Trans-Blot® Turbo Blotting System (Bio-Rad Lab Inc. Hercules, CA, USA). Membrane blots were probed with anti-Trx2 (Santa Cruz Biotechnology), anti-Prx3 (Abfrontier) and anti-CypD (ThermoFisher) antibodies and visualized by enhanced chemiluminescence.

3.5.12 Flow cytometric analysis of the mitochondrial membrane potential

The mitochondrial membrane potential was analyzed by flow cytometry with the fluorescent probe tetramethyl rhodamine methyl ester (TMRM) (Molecular Probes, Eugene, OR, USA). Cells (2×10^6) were incubated in the various conditions, then harvested and resuspended in PBS/10 mM glucose/25 nM TMRM for 20 min at 37°C in the dark. Changes of the membrane potential were estimated with a FACSCanto II flow cytometer (BD BioSciences, San Jose, CA, USA) using a blue laser at 488 nm. 30000 events were recorded for each sample.

3.5.13 Flow cytometric analysis of the mitochondrial superoxide production

Cells were probed for mitochondrial superoxide production utilizing the fluorescent probe MitoSOX Red™ (Molecular Probes, Eugene, OR, USA). Cells (2×10^6) treated under various conditions, were then incubated with 1 μ M MitoSOX Red in PBS/10 mM glucose for 25 min in the dark. Then cells were trypsinized, diluted (1:4) and fluorescence was recorded on the FL2 channel utilizing a FACSCanto II flow cytometer. 30000 events were recorded for each sample.

3.5.14 Determination of lipid peroxidation in HeLa cells

Lipid peroxidation was analyzed in cells either by flow cytometry and through the measurement of malondialdehyde (MDA) production. HeLa cells (3.5×10^5) were incubated for 18 h in the presence of 15 μ M sodium selenite. For the FACS estimation of lipid peroxidation, at the end of incubation, cells were loaded with 2 μ M BODIPY C-11 probe (Molecular Probes, Eugene, OR, USA) diluted in PBS/10 mM glucose, for 30 min at 37°C in the dark. Then, cells were trypsinized and resuspended in PBS/10 mM glucose at a concentration of 2.5×10^5 /mL. Lipid peroxidation was measured on the FITC-1 channel with a FACSCanto™ II flow cytometer (Becton-Dickinson, CA, USA) using a blue laser at 488 nm. 30000 events were recorded for each sample. For the MDA production, cells treated in the same conditions, were washed with PBS and

incubated with 1 mL of 50 mM H₂SO₄ and 150 µL of 10% phosphotungstic acid for 10 min at room temperature. Then, cells were collected and centrifuged at 15600g for 10 min at 4°C. The obtained pellets were washed with 1 mL of 50 mM H₂SO₄ and 150 µL of 10% phosphotungstic acid. Samples were incubated at room temperature for 5 min and centrifuged again at 15600g for 10 min at 4°C. Afterwards, the pellets were lysed with 350 µL of a buffer composed by 0.25% NONIDET P-40, 0.01% butylhydroxytoluene and 0.17% thiobarbituric acid and incubated at 95°C for 60 min. Samples were ice-cooled for 5 min and centrifuged at 15600g for 10 min. The pellets were washed with 500 µL of acetone/HCl solution (98:2) for 10 min at 4°C, centrifuged at 15600g for 10 min at 4°C, dissolved in 75 µL of RIPA buffer and subjected to protein determination.³⁸⁷ The supernatants were added with 400 µL of n-butanol, vigorously mixed and centrifuged at 15600g for 15 min. The fluorescence of the upper phase was analysed ($\lambda_{\text{Ex}}= 530 \text{ nm}$, $\lambda_{\text{Em}}= 590 \text{ nm}$) using a Tecan Infinite M200 PRO plate reader.

3.5.15 Estimation of cytochrome c release and caspase 3 activation

Cyt c release and caspase 3 activation were detected using the Western blot technique. After incubation, cells (2×10^6) were washed with PBS and treated for 15 min with a hypotonic lysis buffer constituted by 10 mM KCl, 1.5 mM MgCl₂, 1 mM EDTA, 1 mM EGTA, 20 mM Hepes-Tris buffer (pH 7.5) containing an antiprotease cocktail. Then, the suspension was centrifuged at 12500g for 10 min at 4°C. The supernatant was treated with 0.5 mM EGTA and 2.5 mM PMSF and centrifuged for 30 min at 105000g at 4°C to obtain the cytosolic fraction. The pellets obtained from the first centrifugation were lysed in the previously reported modified RIPA buffer. Aliquots of the supernatants or of the pellets (10 mg protein) were subjected to SDS-PAGE (15% acrylamide/bisacrylamide) followed by Western blot analysis using an anti- Cyt c and an anti-caspase 3 antibodies.

3.5.16 Determination of PARP-1 activity

Poly ADP-ribose polymerase 1 (PARP-1) activity was determined using Trevigen's HT Universal Colorimetric PARP Assay which measures the incorporation of biotinylated poly(ADP-ribose) onto histone proteins. Either recombinant human PARP-1 (supplied with the kit) or 50 µg of SKOV-3 cell lysates were used. Purified PARP-1 was incubated with the compounds for 1 h at room temperature prior to the assay, while cells were pre-treated with the compounds for 48 h. The TACS-SapphireTM (Helgerman Ct, Gaithersburg MD, USA), a horseradish peroxidase colorimetric substrate, was added and incubated in the dark for 30 min. At the end of incubation, absorbance was read at 630 nm using a Tecan Infinite M200 PRO plate reader.

3.5.17 ICP-OES metal quantification in Jurkat cells

For the estimation of cellular uptake of the osmium complexes Jurkat cells were incubated for 24 h in the presence of 50 µM **Oc-OH** or 15 µM **Oc-OH-Tam** and washed twice in PBS buffer. Pellets of cells (10^7 cells) were resuspended in 0.5 mL of HCl (37%, Fluka for trace analysis) and digested at 60°C in an ultrasound bath for 1 h. Then, samples were adjusted to HCl 2% by addition of 8.75 mL of water and filtered on a 0.2 µm filter. Quantification of osmium was performed at 225.585 nm. HNO₃ that is classically used for induced coupled plasma optical emission spectroscopy (ICP-OES) experiments, was substituted by HCl as HNO₃ leads to the formation of the very toxic and volatile OsO₄.

To measure the cellular distribution of TLMs, Jurkat cells (3×10^7) incubated for 24 h in the presence of 30 µM TLMs were subjected to cell fractionation, as reported in subparagraph 3.5.3. Then, mitochondria were dissolved in 0.54 mL HCl (37%, Fluka for trace analysis) and digested at 60°C in an ultrasound bath for 1 h.

The samples' volume was brought to 10 mL by the addition of water ([HCl] in the sample = 2%). The cytosolic fractions were adjusted to 2% HCl by the addition of appropriate volumes of 37% HCl and water (final volume = 10 mL). All the solutions were filtered on a 0.45 μm syringe filter. Quantification of iron, ruthenium and osmium was performed at 238.204, 267.876 and 225.585 nm, respectively, using an Agilent 5100 instrument (Agilent, Santa Clara, CA, USA). Metal standards (Fe, Ru and Os) were prepared from 1000 ppm stock solutions. The concentrations used for calibration were in all cases 0, 7.8, 15.6, 31.2, 62.5, 125, 250 and 500 ppb. The ICP-OES experiments were performed on the ALIPP6 platform at the University Pierre et Marie Curie, Paris, F.

3.5.18 Quantification of the labile iron pool in HeLa cells mitochondrial fractions

The amount of labile iron pool in mitochondria was measured after HeLa cells treatment with 15 μM sodium selenite for 18 h. After incubation, cells were subjected to mitochondria isolation as reported in subparagraph 3.5.3. Isolated mitochondria were treated with 600 μL of 6% meta-phosphoric acid for 20 min at 4°C in order to extract the labile iron pool. At the end of incubation, samples were centrifuged at 15800g for 10 min at 4°C. The pellets were subjected to protein determination.³⁸⁷ The supernatants were mineralized and the total amount of iron was estimated by atomic absorption spectroscopy. Briefly, supernatants were subjected to five 20 min freeze-thaw cycles at -20 +32°C and vortexed. Then, samples were mineralised in 200 μL of highly purified nitric acid (Fe: ≤ 0.01 mg/kg) and 200 μL H₂O₂. Afterwards, they were transferred into a microwave Teflon vessel before being subjected to the standard procedure using a speed wave MWS-3 Berghof instrument. After cooling, the Fe content of each sample was determined using a Varian AA Duo graphite furnace atomic absorption spectrometer (Varian, Palo Alto, CA, USA) at a wavelength of 248.3 nm. A calibration curve was obtained using standard solutions of known Fe concentrations.

3.6 Experiments performed on isolated mitochondria

3.6.1 Mitochondria isolation and preparation of mitochondrial matrix

Rat or mouse liver, heart and kidney mitochondria were isolated by differential centrifugation following the method of Myers and Slater.³⁹⁴ After an overnight starvation period, rodents were sacrificed by cervical dislocation. The different organs were explanted and dipped in ice-cold isolation buffer composed by 220 mM sucrose, 70 mM mannitol, 0.1 mM EDTA, 5 mM Hepes-Tris (pH 7.0). After 5-6 washes with the isolation buffer in order to remove blood, the various organs were minced using scissors and homogenized using a potter endowed with a teflon pestle. Only for the heart, the connective tissue was partially removed by fiberglass filtering. Afterwards, the homogenates were centrifuged at 700g for 10 min at 4°C. The supernatants obtained were poured to new ice-cold tubes and centrifuged again at 700g for 10 min at 4°C. The supernatant of the last centrifugation was transferred in new cold tubes and centrifuged at 10000g for 15 min at 4°C. The pellets, corresponding to the mitochondrial fractions, were resuspended in ice-cold isolation buffer and centrifuged at 10000g for 15 min at 4°C. The final pellets were dissolved in isolation buffer without EDTA and subjected to protein determination.

For isolation of brain mitochondria, the procedure utilized followed standard protocols.³⁹⁵ Briefly, mice were sacrificed by cervical dislocation, the complete brain was immediately removed and placed in an ice-cold beaker with extraction buffer composed by 125 mM sucrose, 250 mM mannitol, 10 mM EGTA, 0.01%

BSA, 1x protease inhibitors, 10 mM Hepes-Tris (pH 7.2) and rinsed twice. Then, the brain was minced using small scissors and gently homogenized using a dounce. Afterwards, the homogenate was centrifuged at 700g for 10 min at 4°C. Supernatant was poured to a new ice-cold tube and centrifuged again at 700g for 10 min at 4°C. The supernatant obtained was centrifuged at 10000g for 15 min at 4°C. The pellet was resuspended in ice-cold extraction buffer added with digitonin to a final concentration of 0.02%. The centrifugation at 10000g for 15 min at 4°C was repeated and the final pellet was dissolved in a small volume of extraction buffer and subjected to protein determination.

Mitochondrial proteins were estimated with the Bradford method to prevent possible interferences of lipids.³⁹⁶

Rat heart mitochondrial matrix was obtained by sonication (twice for 30 s each) of 20 mg/mL of a mitochondrial suspension diluted 1:4 with 25 mM Tris-HCl (pH 8.0), followed by centrifugation at 10000g for 10 min. Pellet was discarded and the supernatant centrifuged at 105000g for 30 min in order to separate sub-mitochondrial particles from the mitochondrial matrix. The latter was finally dialyzed overnight against 10 mM Tris-HCl buffer (pH 7.4), 1 mM EDTA.

3.6.2 Measurement of CypD, Trx2 and Prx3 amount in rat heart and liver mitochondrial matrix

Aliquots of 40 µg protein of rat heart and liver mitochondrial matrix were loaded onto Bis-Tris Gel NuPAGE (12% acrylamide/bisacrylamide) (Novex, Life Technology, Carlsbad, CA, USA) and then subjected to immunoblot detection using specific antibodies. Band quantification was performed utilizing Image J software.

3.6.3 Determination of ROS production

WT and mGrx2 KO mouse liver mitochondria (0.5 mg/mL) were incubated at 25°C in a 96-well plate with 20 mM Hepes-Tris buffer (pH 7.4) containing 100 mM sucrose, 50 mM KCl, 0.5 mM NaKPi and 5 mM succinate. Formation of H₂O₂ was detected with 20 µM AmplexRed (Invitrogen, Carlsbad, CA, USA) in the presence of 11 nM HRP ($\lambda_{\text{Ex}}= 530 \text{ nm}$, $\lambda_{\text{Em}}= 590 \text{ nm}$), using an Infinite M200 PRO plate reader.

3.6.4 Evaluation of the redox state of Trx2 and CypD

Trx2 and CypD redox state from rat heart mitochondria was estimated following an established method.³⁹¹ The procedure is slightly different with respect to the one described in subparagraph 3.5.7. Briefly, 200 µg of freshly prepared rat heart mitochondria were incubated in 220 mM mannitol, 70 mM sucrose, 1 mM EDTA, 5 mM Hepes-Tris (pH 7.4), 5 mM glutamate, 5 mM malate in a final volume of 50 µL in different conditions for 30 min. Then, 100 µL of 11 M urea, 1 mM EDTA, 50 mM Tris-HCl buffer (pH 8.3) containing 30 mM IAA were added and incubated for 30 min at 37°C to alkylate free thiols. Afterwards, proteins were precipitated by ice-cold acetone-1M HCl (98:2). The pellets obtained were washed with ice-cold acetone-1M HCl-H₂O (98:2:10), dissolved in 60 µL of lysis buffer composed by 8 M urea, 1 mM EDTA, 50 mM Tris-HCl (pH 8.3) additioned with 3.5 mM DTT, and incubated for 30 min at 37°C to reduce the disulfide bonds. Then, samples were treated with 10 mM IAM, for 20 min at 37°C in order to alkylate the newly exposed thiol groups. After protein determination,³⁸⁷ 20 µg of each sample were subjected to urea-PAGE electrophoresis (7% acrylamide/bis(acrylamide), 7 M urea) and blotted on a nitrocellulose membrane using a Trans-Blot® Turbo Blotting System (Bio-Rad Laboratories, Hercules, CA, USA). Finally, the membranes were probed for Trx2 and CypD with the respective primary antibodies. A peroxidase conjugated secondary antibody and chemiluminescence were used to detect the immunoreactive bands.

3.6.5 Measurement of the mitochondrial membrane potential

The mitochondrial membrane potential of WT or mGrx2 KO mouse liver mitochondria was estimated by means of the fluorescent dye rhodamine 123. Mitochondrial proteins (0.5 mg/mL) were incubated at 25°C in 20 mM Hepes-Tris buffer (pH 7.4), 100 mM sucrose, 50 mM KCl, 1 mM MgCl₂, 1 mM NaH₂PO₄ containing 12.5 μM rotenone. Mitochondria were treated with 5 mM succinate as an oxidizable substrate in the presence or absence of EGTA at the concentration of 20 μM or 1 mM. Fluorescence was estimated ($\lambda_{\text{ex}}=485$ nm, $\lambda_{\text{em}}=527$ nm) using an Infinite M200 PRO plate reader. The ratio between the fluorescence recorded before and after the addition of succinate was calculated and compared between WT and mGrx2 KO mice.

3.6.6 Estimation of mitochondrial swelling

Mitochondrial swelling was followed spectrophotometrically as decrease of the optical density at 540 nm. Briefly, WT or mGrx2 KO liver mitochondria (0.25 mg/mL) were incubated at 25°C in 5 mM Hepes-Tris buffer (pH 7.4), 213 mM mannitol, 71 mM sucrose, 20 μM EDTA, containing 5 mM succinate, 5 μM rotenone and 2.5 μM oligomycin in the presence or absence of 40 μM CaCl₂. The absorbance at 540 was monitored for about 20 min on a Lambda2 spectrophotometer.

3.6.7 Determination of the oxygen consumption

Oxygen consumption of WT or mGrx2 KO mouse liver mitochondria was measured polarographically, utilizing a Clark-type oxygen electrode inserted in a water jacketed chamber (25°C) with constant stirring. Mouse liver mitochondria (1 mg/mL) were incubated at 25°C in 20 mM Hepes-Tris buffer (pH 7.4), 100 mM sucrose, 50 mM KCl, 1 mM MgCl₂, 1 mM NaH₂PO₄ containing 20 μM EGTA. Respiration was started by the addition of 7.5 mM succinate or by the combination 7.5 mM glutamate + 3.75 mM malate (state 4). Then, 0.2 mM ADP was added (state 3). The consumption of dioxygen was calculated in nmoles of O₂·sec⁻¹·mg⁻¹ of protein and the respiratory control index (ratio between state 3/state 4 rates) was finally calculated in order to determine the tightness of the coupling between respiration and oxidative phosphorylation.

3.6.8 Assessment of total thiols

Liver, heart, brain and kidney mitochondria of WT or mGrx2 KO mice (0.25 mg of proteins) were diluted with 0.2 M Tris-HCl buffer (pH 8.1), 1% SDS, 10 mM EDTA to a final volume of 1 mL. Then, 3 mM DTNB was added to titrate thiol groups and the absorbance increase was monitored at 412 nm for 5 min on a Lambda2 spectrophotometer. The amount of thiols was determined by subtracting to the readings the background optical density observed before the addition of DTNB.

3.6.9 Estimation of the total and oxidized glutathione

Mitochondria (0.5 mg) were deproteinized with 2 mL of 6% meta-phosphoric acid. After 20 min at 4°C samples were collected and centrifuged at 15800g for 10 min at 4°C. Supernatants were neutralized with 15% Na₃PO₄ and utilized for total glutathione estimation as described in subparagraph 3.5.6.

3.6.10 Estimation of CypD PPIase activity

The peptidyl prolyl *cis-trans* isomerase (PPIase) activity of CypD was estimated essentially as described by Kofron *et al.* with modifications.³⁹⁷ Assays were performed at 5.5°C in 100 mM NaCl, 50 mM Hepes-Tris

buffer (pH 8.0). The peptide N-succinyl-Ala-Ala-Pro-Phe-*p*-nitroanilide was dissolved (3 mM) in trifluoroethanol containing 470 mM LiCl, while 2.4 mM α -chymotrypsin was dissolved in 1 mM HCl. Aliquots of mitochondrial matrix (30 μ g proteins) were preincubated for 15 min in a volume of 50 μ L in various conditions. The assay was performed in a final volume of 500 μ L by the addition, after 5 min of equilibration, of α -chymotrypsin (48 μ M, final conc) followed, after 1 min, by the peptide substrate (60 μ M, final conc). The reaction was followed spectrophotometrically at 390 nm as absorbance increase of *p*-nitroaniline resulting from the enzymatic cleavage by α -chymotrypsin of the peptide in the *trans* form. The acquired data were fitted to a first-order rate equation in order to obtain the corresponding rate constants (k_{obs} , s^{-1}).^{26, 28}

3.6.11 Co-immunoprecipitation of CypD with Trx2 and Prx3

Co-immunoprecipitation analysis was performed in isolated mitochondria employing a different method with respect to the one utilized for cell lysates (see subparagraph 3.5.11). Basically, rat heart mitochondrial matrix (0.2 mg proteins) was pre-reduced for 30 min at 37°C in 50 mM Tris-HCl buffer (pH 7.4) in the presence of 0.8 μ M TrxR1, 315 μ M NADPH and 1 mM EDTA in a final volume of 50 μ L with or without addition of 50 μ M cyclosporin A (CsA). Then, samples were diluted 1:1 with 50 mM Tris-HCl (pH 7.4), 50 mM NaCl, 1 mM NaF, 5 mM EDTA, 0.1 mM PMSF and protease inhibitor cocktail. Pre-cleaning phase was performed using 20 μ L of A/G PLUS-Agarose beads for 45 min at 4°C with stirring. Pre-cleaned samples were centrifuged at 720g for 5 min and the supernatant was incubated with anti-Trx2 (Abfrontier), anti-Prx3 (Santa Cruz Biotechnology) and anti-CypD (Fitzgerald) antibodies for 3 h at 4°C. A/G PLUS-Agarose beads (20 μ L) were added, incubated for 1 h at 4°C, centrifuged at 720g for 5 min and washed with ice-cold buffer (50 mM Tris-HCl (pH 7.4), 1 mM EDTA, 1 mM NaF and protease inhibitor). The pull down was resuspended in SDS loading buffer containing 100 mM DTT, boiled for 10 min, and then centrifuged at 17000g for 1 min. The supernatant was separated by SDS-PAGE (Mini-PROTEAN® TGX, any kD, Bio-Rad Lab. Inc., Hercules, CA, USA), transferred onto a nitrocellulose membrane using Trans-Blot® Turbo Blotting System (Bio-Rad Lab Inc. Hercules, CA, USA). Membrane blots were probed with anti-Trx2 (Santa Cruz Biotechnology), anti-Prx3 (Abfrontier) and anti-CypD (ThermoFisher) antibodies and visualized by enhanced chemiluminescence.

3.7 RNA isolation and RT-qPCR analysis of Grx2 RNA

Total RNA from liver and brain of WT or mGRX2 KO mice was isolated using TRIzol according to the manufacturer's procedure (Life Technologies, Carlsbad, CA, USA) and kept at -80°C. RNA concentration and purity was measured on a Nanodrop spectrophotometer (ThermoFisher, Waltham, MA, USA). Complementary DNA (cDNA) was synthesized from 2 μ g of total RNA by using a Maxima First Strand cDNA synthesis kit for RT-qPCR (ThermoFisher, Waltham, MA, USA). The cDNA was stored at -20°C. Reverse transcriptase PCR was performed using DreamTaq Green PCR Master Mix (2X) (ThermoFisher, Waltham, MA, USA) according to the manufacturer's procedure. Sequences of primer sets:

Exon1 sense: 5'- ATG GGA AAC AGC ACA TCG TCG -3' Exon4 antisense: 5'- CAG AGG CAG CAA TTT CCC -3'
Exon3 sense: 5'- CTA ACA ATT GTG TGG TGA TCT TC -3' Exon4 antisense: 5'- CAG AGG CAG CAA TTT CCC -3'

3.8 Western blot procedure and list of the primary antibodies

Once blotted, the membranes were saturated with 50 mM Tris-HCl buffer (pH 7.5), 150 mM NaCl, 3% BSA for 2 h at room temperature. Primary antibodies were diluted in 50 mM Tris-HCl buffer (pH 7.5), 150 mM NaCl, 1% BSA, 0.02% NaN₃, and added to the membranes. Following overnight incubation with primary antibodies at 4°C, membranes were washed three times for 10 min with the washing buffer composed by 50 mM Tris-HCl buffer (pH 7.5), 150 mM NaCl, 0.1% Tween20. Then, secondary antibodies conjugated to the reporter enzyme HRP (Santa Cruz Biotechnology, Dallas, TX USA) were diluted at the appropriate concentrations (from 1:10000 to 1:3000) in the same buffer utilized for the primary antibody and incubated with the membranes for 40 minutes at room temperature. Afterwards, the membranes were washed three times (10 min each). Protein bands were revealed using luminol as a HRP substrate in the presence of H₂O₂ taking advantage of UVITEC Alliance Q9 mini chemiluminescence imaging detector (UVITEC, Cambridge, UK) and analyzed using Image J or NineAlliance softwares for band quantification.

Table 4: List of the primary antibodies utilized

<i>Antibody</i>	<i>Brand</i>	<i>Commercial code</i>	<i>Clone</i>	<i>Species cross reactivity*</i>	<i>Secondary Ab dilution</i>
Trx1	Santa Cruz	sc-20146	FL-105	m, r, h	Rabbit 1:5000
Trx2	Abfrontier	LF-MA0079	4C5	m, r, h	Only For IP
Trx2	Santa Cruz	sc-50336	H75	m, r, h	Rabbit 1:5000
TrxR1	Santa Cruz	sc-28321	B-2	m, r, h	Mouse 1:3000
TrxR2	Santa Cruz	sc-166259	D-12	m, r, h	Mouse 1:3000
Prx3	Santa Cruz	sc-59663	4G10	m, r, h	Mouse 1:3000
Prx3	Abfrontier	LF-MA0044	12B	m, h	Mouse 1:5000
Grx2	IMCO	AGRX-02	n.a.	h	Rabbit 1:5000
Grx2	My Biosource	MBS176047	n.a.	m, r, h	Rabbit 1:10000
Caspase 3	Santa Cruz	sc-7148	H-277	m, r, h	Rabbit 1:5000
Cyt c	NovusBio	NB100-56503	7H8.2C12	m, r, h	Mouse 1:3000
Cyt c oxidase (subunit I)	Molecular Probes	A6403	1D6V	m, r, h	Mouse 1:3000
CypD	ThermoFisher	455900	E11AE12BD4	m, r, b, h	Mouse 1:10000
CypD	Fitzgerald	10R-1136	AT1F5	m, r, b, h	Mouse 1:3000
GAPDH	Santa Cruz	sc-32233	6C5	m, r, h	Mouse 1:3000
GSH	Santa Cruz	sc-52399	D8	m, r, b, h	Mouse 1:3000
FLAG	Sigma-Aldrich	F7425	FL	/	Rabbit 1:5000

* m= mouse; r= rat; b= bovine; h=human (n.a. = not available)

3.9 Molecular modelling of the interaction of CypD with Prx3 or Trx2

A molecular docking prediction using ClusPro 2.0 webserver was utilized.³⁹⁸ For CypD, Prx3, and Trx2 the protein structures present in PDB (Protein Data Bank), 2bit (human CypD), 1zye (bovine Prx3) and 1uvz (human Trx2) respectively were utilized. For Prx3, the bovine 1zye crystal structure that presents more than 88.8% identity with human sequence, was used.

3.10 Enzymatic oxidation of TLMs by the HRP/H₂O₂ mixture

Enzymatic oxidation of the compounds by HRP (46 nM) and H₂O₂ (200 mM) was performed in 0.2 M Tris-HCl buffer (pH 8.1), 1 mM EDTA. Briefly, HRP and H₂O₂ were added to the solution of the compounds. The solution was immediately transferred to a cuvette and the UV-Vis spectrum was recorded between 250 and 550 nm every 30 s on a Cary 50 spectrometer (Varian, Palo Alto, CA, USA).

3.11 EPR spectroscopy studies on ansaFc

X-band EPR spectra of ansaFc complex were recorded on a Bruker Elexsys 500 spectrometer equipped with an Oxford Instrument continuous-flow liquid helium cryostat and a temperature control system. 50 μM ansaFc was mixed with 46 nM HRP and 200 mM H₂O₂ in 0.2 M Tris-HCl buffer (pH 8.1), 1 mM EDTA, transferred in quartz tubes and incubated for different times (1, 2, 5, 10 min). At the end of incubation, the tubes were frozen in a liquid nitrogen bath and introduced in the EPR cavity. EPR experiments were performed at 10 K, using a microwave power of 0.159 mW (non-saturating conditions) with a modulation of 1 G.

3.12 Statistical analysis

All the experiments performed with WT and mGrx2 KO mice were made with matching-aged control animals. All the experimental data reported are the mean with their respective standard deviations (SD) of the indicated number of experiments. Comparisons between two groups were performed using non paired two-tailed Student's t-test. The statistical analyses of variance (ANOVA) were performed using the Tukey test with INSTAT 3.3 (GraphPad) software. A value of $p < 0.05$ was considered significant.

4. Results and Discussion

4.1 Targets of the mitochondrial thioredoxin system

The knowledge of the specific proteins undergoing redox regulation in mitochondria is still limited. Therefore, we aimed at identifying new proteins of the mitochondrial compartment able to interact with the thioredoxin system.

The family of cyclophilins comprises different proteins that catalyze the *cis-trans* isomerization of peptidyl-prolyl bonds (PPIase activity).³⁹⁹ Of note, long ago cyclophilins were found to possess redox properties. For instance, human T-cell cyclophilin 18 was shown to bind Prx3 stimulating its activity, while cyclophilin A can reduce and recycle Prx2.^{400, 401} Cyclophilin D (CypD) is the mitochondrial isoform of cyclophilins and has a key function in modulating the opening of the mitochondrial permeability transition pore.⁴⁰² Interestingly, the overexpression of CypD in HEK293 cells protects from *tert*-butylhydroperoxide induced permeability transition indicating redox properties.⁴⁰³ In addition, Linard *et al.* found that CypD conformation and activity are affected by the oxidation of the conserved Cys157 and Cys203 residues possibly through their condensation into a disulfide bond. In the same research, CypD oxidation was hypothesized to trigger the opening of the mitochondrial permeability transition pore.²⁶ This hypothesis was supported by the observed insensitivity of mouse liver mitochondria expressing the CypD mutant Cys203Ser, to Ca²⁺-induced swelling.²⁸

Considering that the principal regulator of the mitochondrial thiol redox state is the thioredoxin system and that other cyclophilins were already shown to be able to interact with peroxiredoxins, we investigated the possible interplay between CypD and the mitochondrial thioredoxin system.

4.1.1 CypD isomerase activity is induced by the thioredoxin system

First of all, we evaluated the relative amount of Prx3, Trx2 and CypD in rat heart and liver mitochondrial matrix. As reported in Fig. 15, all three enzymes are more abundant in heart mitochondria and thus, we chose this organ for our investigations. The PPIase activity of CypD was measured monitoring the absorbance increase of *p*-nitroaniline as described in the Materials and Methods section. Upon incubation of rat heart mitochondrial matrix in different experimental conditions, CypD activity was determined. In Fig. 16 the kinetic curves and the relative differences in first order rates between CypD activities incubated under various conditions with respect to the control are reported. The addition of NADPH did not affect CypD activity while the incubation of CypD with the complete thioredoxin system (NADPH, TrxR and Trx), stimulated both the rate and extent of PPIase activity. Interestingly, Af, the specific inhibitor of thioredoxin reductase,^{319, 343} completely prevented the observed stimulatory effect on CypD activity elicited by the thioredoxin system indicating that PPIase induction depends from the activity of the enzymatic system. Conversely, cyclosporin A (CsA), which is a specific inhibitor of CypD, inhibits PPIase activity, as previously reported.²⁸ Thus, the thioredoxin system, keeping CypD in its reduced form, increases its specific activity. Of note, diamide, a thiol-oxidizing agent, was also able to markedly inhibit CypD activity (data not shown) further suggesting that the redox state of CypD can modulate its activity.

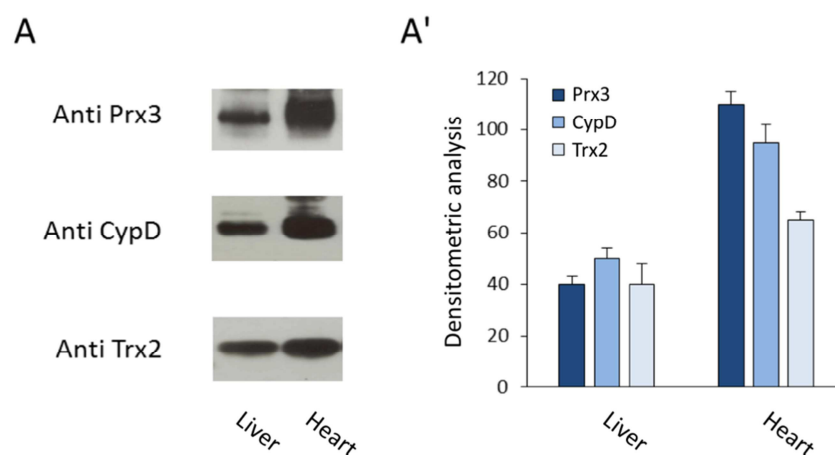


Fig. 15 Relative amount of Prx3, CypD and Trx2 in rat liver and heart mitochondrial matrix. (A) Western blot and (A') densitometric analysis performed with ImageJ software for the three proteins of interest.

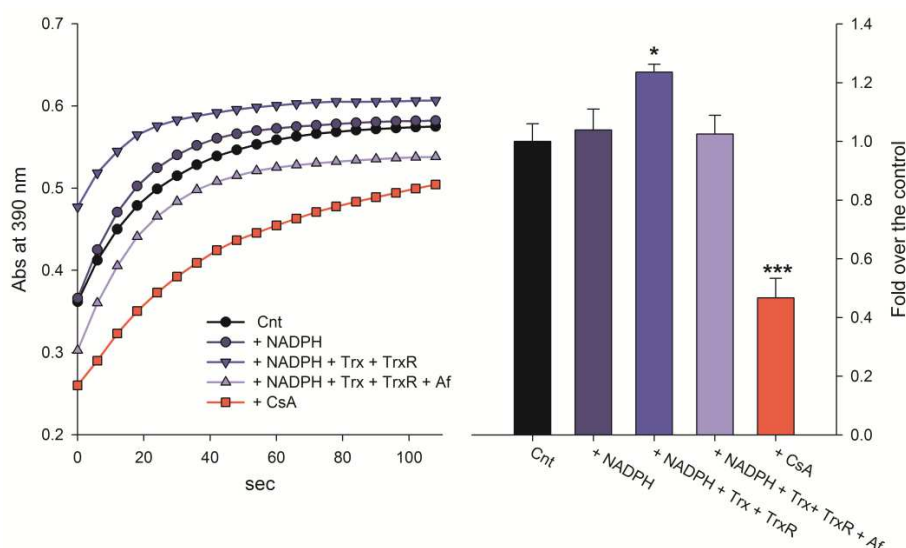


Fig. 16 PPLase activity of CypD incubated under different conditions. Rat heart mitochondrial matrix (30 μ g proteins) was preincubated in 100 mM NaCl, 50 mM HEPES-Tris buffer (pH 8.0) at 25°C for 15 min in the presence, where indicated, of 300 μ M NADPH, 0.4 μ M TrxR1 from rat liver, 3 μ M Trx from *E. coli*, 1 μ M Af or 1 μ M CsA. PPLase activity was estimated by a coupled assay utilizing α -chymotrypsin as described in the Materials and Methods section. The panel on the left reports the time course curves of PPLase activity. The panel on the right shows the relative differences of the rate constants in the various conditions with respect to the control (*= p <0.01; ***= p <0.001). Mean \pm SD of 3 experiments.

4.1.2 Inhibition of the thioredoxin system triggers CypD oxidation

In order to investigate the redox interaction between cyclophilin D and the thioredoxin system, Trx2, Prx3 and CypD redox state was assessed in both isolated rat heart mitochondria and cultured human cells upon TrxR2 inhibition or in the presence of reducing and oxidative stimuli utilizing the redox Western blot technique (see Materials and Methods section for details). This technique allows the detection of a number of bands corresponding to the number of thiols present in the enzyme plus one and related to the different oxidation states of the protein. Regarding Trx2, three major bands can be detected in accordance with the presence of only two Cys in Trx2 structure.²²⁷ As reported in Fig. 17, panel A at least 5 bands were apparent for CypD in isolated rat heart mitochondria, indicating the presence of 4 thiols potentially subjected to redox transition and consistent with the number of Cys present in CypD sequence.²⁶ Lane a of CypD redox Western blot displays the redox condition of CypD in homeostatic conditions. Of note, the protein is

present mainly in its reduced states and shows an oxidation pattern similar to N-acetyl cysteine (NAC) treated mitochondria, a thiol reducing agent (lane c). In these reducing conditions, also Trx2 and Prx3 are largely reduced (Fig 17, panel B and C). Prx3 redox state was determined through the measurement of its monomeric (reduced) and dimeric (oxidized) forms utilizing a different derivatization method as described in subparagraph 3.5.8. Incubation of mitochondria with CsA did not alter the redox state of CypD neither of Trx2 or Prx3 (lane d). On the contrary, oxidizing conditions achieved via diamide addition (lane b), shifted all the three proteins to their oxidized forms. Notably, the treatment of mitochondria with increasing concentrations of Af, the TrxR2 selective inhibitor, led to Trx2 oxidation, Prx3 dimerization and a concomitant shift of CypD to the more oxidized forms (lane e and f). Interestingly, the extent of CypD oxidation was correlated to the concentration of Af utilized and thus, seemed to be directly dependent on TrxR2 inhibition. Therefore, the oxidation of CypD in mitochondria is consistent with that of Trx2 and Prx3, and with the extent of TrxR2 inhibition suggesting a redox interplay between the thioredoxin system and CypD.

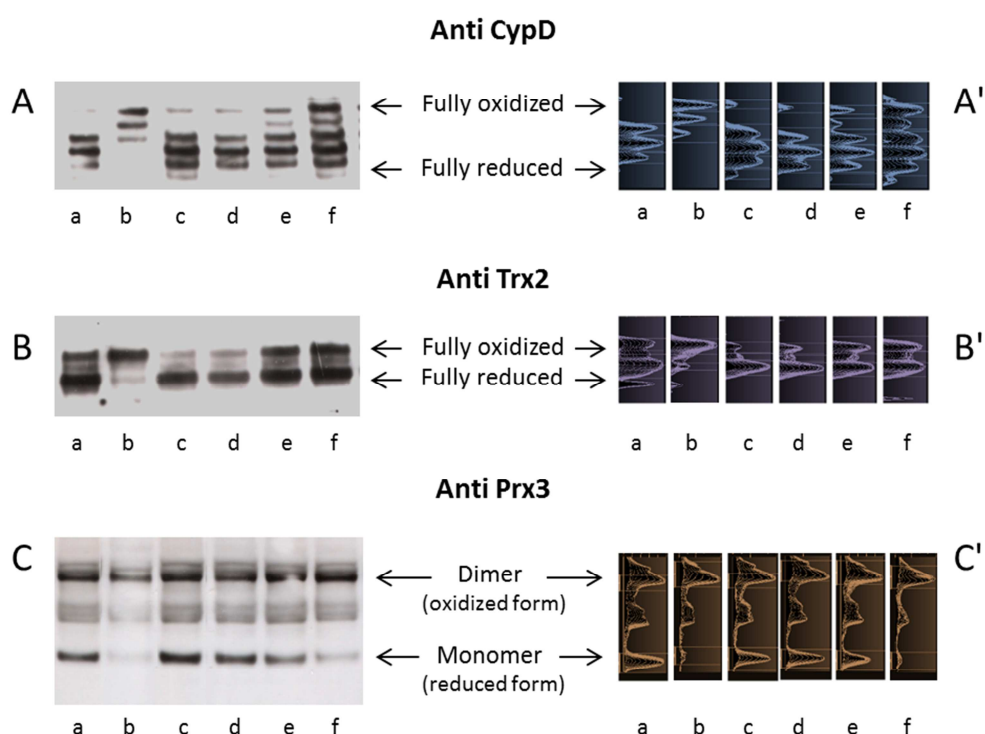


Fig. 17 Redox Western blot of CypD, Trx2 and Prx3 in rat heart mitochondria. Mitochondria (200 µg proteins) were incubated under various conditions at 25°C for 30 min. Then, the redox state of CypD (**A**), Trx2 (**B**), and Prx3 (**C**) were determined as described in the Materials and Methods section. **A'**, **B'** and **C'** report the densitometric analysis of the bands in **A**, **B** and **C** respectively, performed using the NineAlliance software. (a) Cnt; (b) 2 mM Diamide; (c) 2 mM NAC; (d) 1 µM CsA; (e) 5 µM Af; (f) 7 µM Af.

The redox states of Trx2 and CypD were also determined in two different human cell lines namely HeLa and CEM-R cancer cells. In this case, a modified redox Western blot analysis was employed in which the two thiol alkylating agents (IAA and IAM) are inverted with respect to the procedure used for isolated mitochondria (see Materials and Methods). Consequently, the upper Western blot band represents the fully reduced enzyme while the lowest corresponds to the completely oxidized form of the protein. In cells, in addition to Af, other compounds such as arsenic trioxide (ATO) and 1-chloro-2,4-dinitrobenzene (CDNB) were utilized as TrxR inhibitors.^{404, 405} As shown in Fig. 18, lanes b and g, both HeLa and CEM-R cell lines after treatment with NAC, displayed reduced states of CypD and Trx2 that look very similar to the

control conditions (lanes a and f). Thus, also in cells the proteins are mainly reduced in homeostatic conditions. Conversely, the two enzymes undergo concomitant oxidation upon TrxR inhibition mediated by Af (lanes c and i), ATO (lanes d and j), or CDNB (lanes e and k). Different concentrations of TrxR inhibitors were used in the two cell lines in accordance with their thioredoxin reductase expression levels.⁴⁰⁶ Moreover, for CEM-R cells, Prx3 redox state was also determined in the same conditions. As reported in Fig. 18, the monomer/dimer ratio of Prx3 is in accordance with the observed CypD and Trx2 redox states as previously seen in rat heart mitochondria (Fig. 17). In particular, the band corresponding to Prx3 monomer largely decreases in the presence of oxidizing conditions or upon inhibition of TrxR.

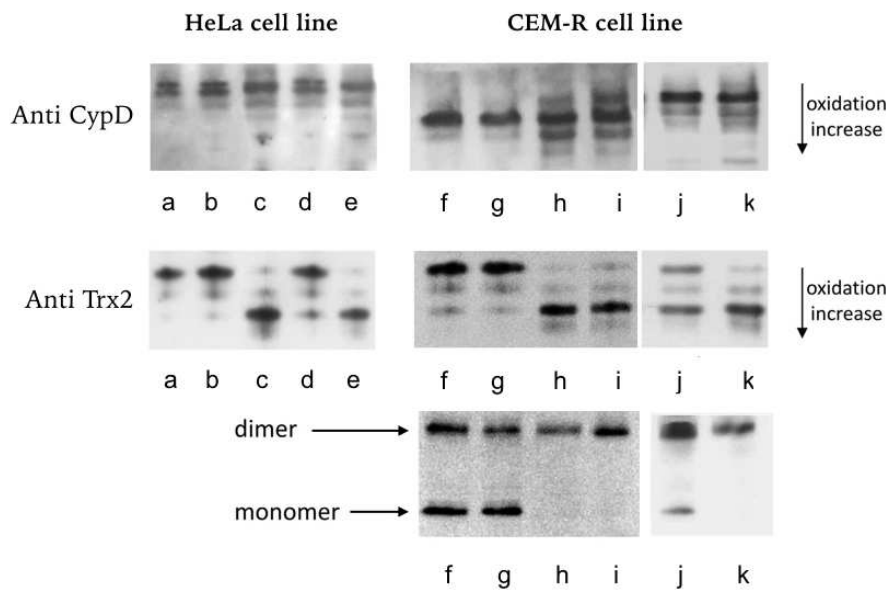


Fig. 18 Redox Western blot of CypD, Trx2 and Prx3 in cultured cells. HeLa and CEM-R cells (1×10^6) were treated for 18 h in various conditions, and then subjected to CypD and Trx2 redox state determination using a non-reducing urea-PAGE. For the estimation of the redox state of Prx3, CEM-R cell lysates were derivatized with 10 mM AIS and subjected to SDS-PAGE in non-reducing conditions. (a and f) Cnt; (b) 3 mM NAC; (c) 15 μ M Af; (d) 20 μ M ATO; (e) 20 μ M CDNB; (g) 2 mM NAC; (h) 2 mM diamide; (i) 3 μ M Af; (j) 15 μ M ATO; (k) 20 μ M CDNB.

To further prove the dependence of CypD on the thioredoxin system for its reduction and to avoid possible direct effects of oxidizing agents on CypD redox state, a short-interfering RNA (siRNA) mediated TrxR2 depletion was utilized. TrxR2 knockdown HeLa cells were obtained and subjected to redox Western blot analysis of both Trx2 and CypD. Although TrxR2 depletion was only partial, an induction of Trx2 oxidation was apparent and accompanied by a concomitant moderate oxidation of CypD (Fig. 19). Therefore, different oxidizing stimuli or direct thioredoxin system inhibition with either a pharmacological approach or RNA interference can induce a concurrent oxidation of Trx2, Prx3 and CypD, highlighting again the link between mitochondrial thioredoxin system and CypD.

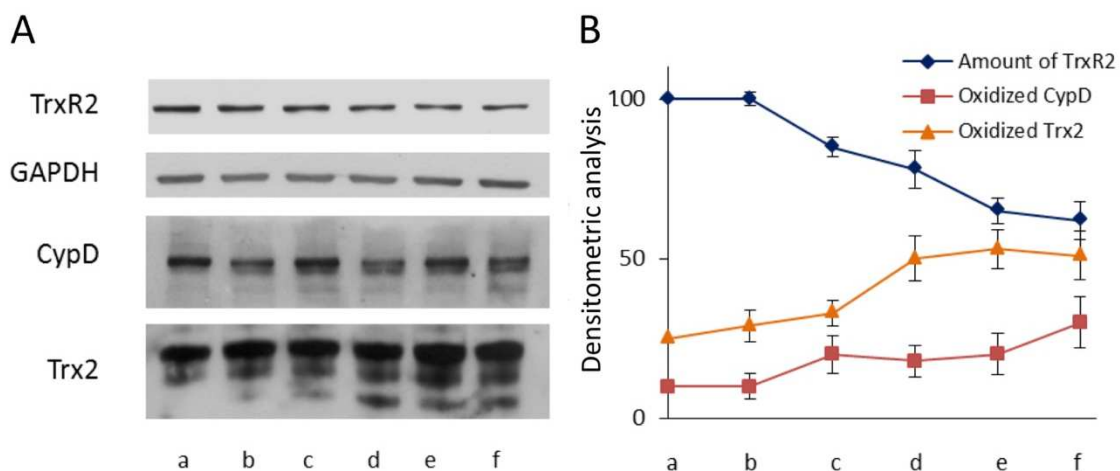


Fig. 19 Redox state of Trx2 and CypD upon TrxR2 silencing in HeLa cells. HeLa cells were transfected as reported in Materials and Methods (siRNA a targeting sequence: GAAAGAGAUUCUGCUGUCA, siRNA b targeting sequence: GCCGAUCACAUCAUUAUG) and

then subjected to the analysis of TrxR2 protein amount or Trx2 and CypD redox states. (A) TrxR2 protein level, GAPDH as loading control and redox state of CypD and Trx2. (B) Analysis of the correlation between TrxR2 depletion and Trx2 and CypD oxidation. (a) mock-treated; (b) non targeting siRNA; (c) 40 nM siRNA **a**; (d) 80 nM siRNA **a**; (e) 40 nM siRNA **b**; (f) 80 nM siRNA **b**.

4.1.3 Molecular modelling of the interaction of CypD with Prx3 and Trx2

A molecular docking prediction using ClusPro 2.0 webserver was employed to deepen the CypD interaction with Trx2 and Prx3.³⁹⁸ Interestingly, the majority of possible docking configurations for CypD require its CsA binding site. Indeed, CypD hydrophobic CsA-binding pocket is involved in the 96% of possible CypD-Trx2 interactions and in the 87% of predicted interplays between CypD and Prx3. Hydrophobic interactions and salt bridges are responsible for the stabilization of the complexes between proteins. Interestingly, Cys157 of CypD resides in the CsA binding pocket and, upon binding with both the redox active proteins, results in close proximity to reactive cysteines. In particular, its interaction with Cys90 of Trx2 active site and with the *peroxidatic* Cys109 of Prx3 can occur (Fig. 20) suggesting a possible involvement of this cysteine in the observed thioredoxin system-mediated redox regulation.

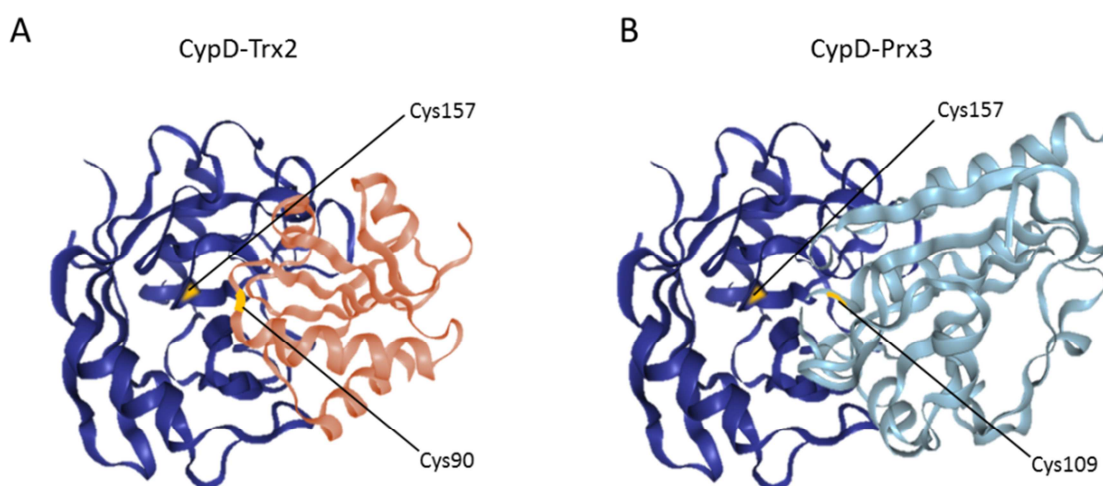


Fig. 20 Binding between CypD and Trx2 or between CypD and Prx3. PDB (Protein Data Bank), 2bit (human CypD), 1uvz (human Trx2) and 1zye (bovine Prx3) were utilized. (A) Global view of the best binding between CypD and Trx2. (B) Global view of the best predicted binding between CypD and Prx3. As one can see the Cys157 residue of CypD, present in the CsA binding pocket, is in close proximity to active Cys of Trx2 and Prx3. The amino acids residues are labelled according to the full-length protein sequences.

4.1.4 Co-immunoprecipitation of CypD with Trx2 and Prx3

The results obtained so far are consistent with a direct interaction of CypD with both Trx2 and Prx3. Therefore, the co-immunoprecipitation technique (Co-IP) was utilized to confirm the binding of CypD with proteins belonging to the thioredoxin system in both rat heart mitochondrial matrix and human cultured cells overexpressing Trx2. Pre-reduced rat heart mitochondrial matrix was incubated with either an anti-Trx2 or an anti-Prx3 antibody, immunoprecipitated and the pull-down protein pool was resolved onto a SDS-PAGE. CypD was detected in both cases in the co-IP protein pool (Fig. 21). Furthermore, the experiment was repeated utilizing an anti-CypD antibody to immunoprecipitate the proteins and CypD binding with both Trx2 and Prx3 was confirmed (data not shown). Since the molecular docking prediction indicated the highly probable involvement of the CsA binding pocket of CypD for its interaction with Trx2 and Prx3, the co-IP experiment was repeated in the presence of 50 μ M CsA. As apparent from Fig. 21, the addition of the CypD inhibitor partially hindered the binding between the proteins (19% reduction of the amount of CypD co-IP with Trx2 and 28% reduction of the binding between CypD and Prx3) supporting the data obtained from the molecular modelling.

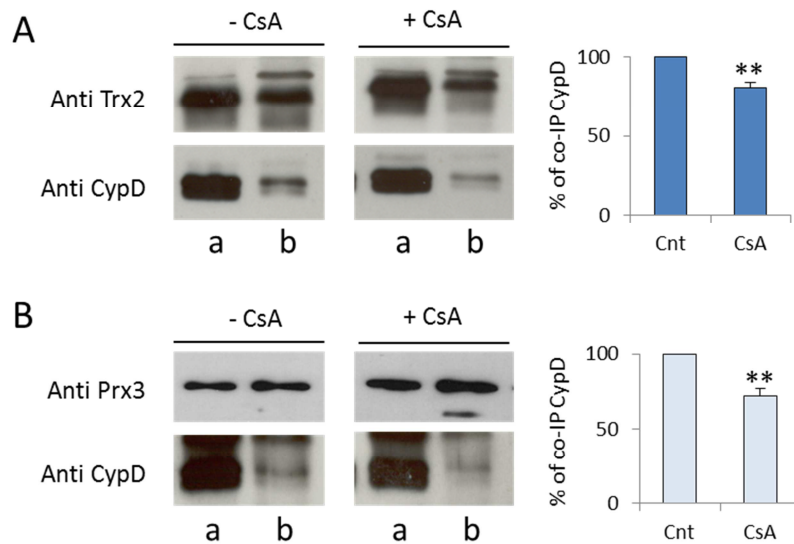


Fig. 21 Co-IP of CypD with Trx2 or with Prx3 from rat heart mitochondrial matrix. Pre-reduced rat heart mitochondrial matrix (200 μ g proteins), was incubated with antibodies anti-Trx2 or anti-Prx3 in the presence or absence of 50 μ M CsA, pulled down, separated by SDS-PAGE, blotted and probed with the specific antibodies as described in the Materials and Methods section. **(A)** Co-IP of CypD with Trx2. **(B)** Co-IP of CypD with Prx3. (a) aliquot of rat heart mitochondrial matrix (10 μ g protein); (b) immunoprecipitated proteins (** = $p < 0.01$).

Accordingly, CypD was successfully co-immunoprecipitated with Trx2 also from human cells. HeLa cells were transfected with a plasmid encoding for a FLAG-tagged form of human Trx2. The obtained cell line displayed an eight fold increase in Trx2 protein expression (Fig 22, panel A and A'). Then, CypD and Prx3 were efficiently co-immunoprecipitated with Trx2 from cell overexpressing Trx2, as shown in Fig. 22, panel B, confirming their binding properties also for the human protein isoforms.

Altogether, the co-immunoprecipitation experiments report that Trx2, Prx3 and CypD can physiologically interact, consistent with a functional relationship linking these proteins.

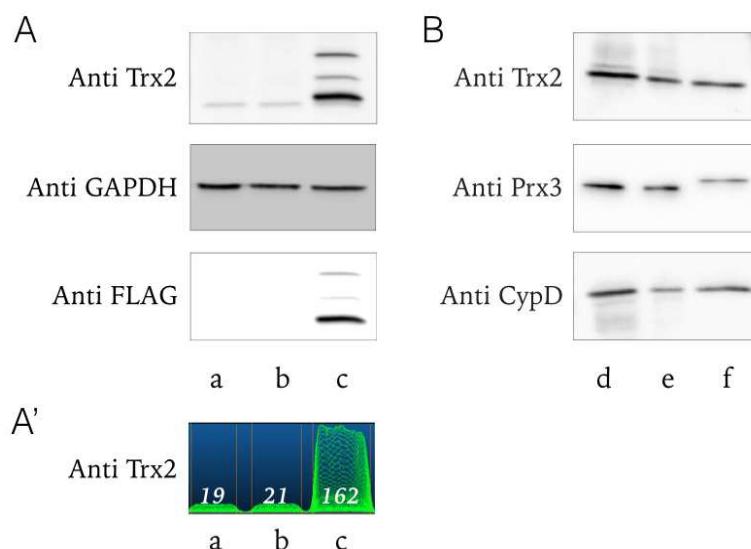


Fig. 22 Co-IP of CypD and Prx3 with Trx2 from Trx2 overexpressing HeLa cells. HeLa cells overexpressing a FLAG-tagged form of human Trx2 were lysed and incubated with an anti-Trx2 antibody, pulled down, separated by SDS-PAGE, blotted and probed with the specific antibodies. **(A)** Western blot analysis of FLAG-Trx2 overexpression, GAPDH is reported as a loading control; **(A')** Densitometric analysis of Trx2 protein level performed with NineAlliance software showing an 8 fold increase of Trx2 protein level. (a) mock-treated; (b) scrambled vector; (c) FLAG-Trx2 vector. **(B)** Co-IP of Prx3 and CypD with Trx2. (d) aliquot of HeLa cell lysate (10 μ g of protein); (e) aliquot of IP supernatant (10 μ g of protein); (f) immunoprecipitated proteins.

The results obtained in this first part of the research suggest a direct regulatory activity of the mitochondrial thioredoxin system on CypD. Interestingly, in physiological conditions, oxidation of CypD may be modulated by the action of Prx3 in the presence of H₂O₂, while thioredoxin or other reducing factors may reverse this process. This hypothesis arises from the fact that although Prxs preserve the majority of proteins from thiol oxidation, they were found to actively promote the oxidation of a subset of target proteins. For instance, Prx1 favors the oxidation of ASK1,⁴⁰⁷ and Prx2 of the transcription factor STAT3.⁴⁰⁸ Moreover, the deletion of all eight Prxs in yeast cells hindered the alteration of gene expression in response to H₂O₂, suggesting again their role in the transmission of redox events.⁴⁰⁹ Very recently, Dick and colleagues showed that the deletion or depletion of cytosolic Prx1 and 2 hinders the overall H₂O₂-dependent protein thiol oxidation in mammalian cells and that Prxs directly oxidize other proteins enabling redox signaling.¹²⁹ In the same paper, authors highlighted that, conversely, Trx1 depletion caused a slight increase in protein thiol oxidation after H₂O₂ addition independently from Prx1/2 expression level, suggesting a prevalent role of Trx1 as a thiol reducing protein. Notably, these results have been obtained on the cytosolic compartment and a direct translation of these findings to the mitochondria would be a too simplistic view but a possible oxidizing activity of Prx3 on CypD could be envisaged. In particular, a spark of H₂O₂ production in the mitochondrial matrix could be rapidly intercepted by Prx3 and transmitted to CypD.

Once oxidized, CypD may transfer the redox signaling to other mitochondrial proteins such as F₀F₁-ATP synthase, adenine nucleotide translocator, mitochondrial phosphate carrier and p53, which were all reported to possess reactive Cys in their structures.^{31, 410-414} Since CypD has a key function in the regulation of the mitochondrial permeability transition pore,⁴⁰² the modulation of its redox state could influence also the overall mitochondrial functioning. In particular, CypD may keep the permeability transition pore closed in its reduced state, while it could favor the pore opening when oxidized. Thus, further investigations on these redox interactions need to be carried out in order to elucidate the whole redox signaling cascade in mitochondria.

4.2 Thioredoxin reductase as a target in cancer therapy

Both cytosolic and mitochondrial thioredoxin reductases are overexpressed in cancer cells exerting proliferating and anti-apoptotic functions.^{281, 290} Together with their substrates thioredoxins, TrxRs have been reported as possible cancer diagnostic markers.^{308, 316} In addition, their enhanced expression was associated to the development of resistance to standard chemotherapeutics.³⁰⁷ Therefore, their inhibition could be useful in contrasting tumor progression and resistance. Some chemical compounds, especially gold complexes were reported to target TrxRs and to exert a noticeable cytotoxicity on cancer cells but without selectivity for one particular isoform of TrxR.³¹³⁻³¹⁷ In parallel to TrxRs overexpression, many cancer cells also display hyperpolarized mitochondria.^{267, 268} In order to specifically induce cytotoxicity in cancer cells with respect to normal cells, the defective mitochondria could be targeted. Therefore, the search for specific inhibitors of TrxR2 which may act specifically in cancer cells by exploiting the high mitochondrial membrane potential, was followed as a possible new anticancer strategy.

4.2.1 Thioredoxin reductase 2 genetic depletion

At first, the effects deriving from the selective TrxR2 depletion were studied in a cancer cellular model. In literature, several papers have been published dealing with TXNRD2 deletion in murine cells^{90, 94, 415, 416} and the majority of them investigated the effects of TrxR2 depletion on heart functioning. Interestingly, Hellfritsch *et al.* reported that TXNRD2 deletion in murine cancer cells was able to inhibit their proliferation via an altered mitochondrial redox balance.⁴¹⁶ However, data are completely lacking for human cancer cell lines and the effect of TrxR2 loss should be investigated as a potential approach in anticancer therapy.

As already reported in subparagraph 4.1.2, the siRNA-mediated transient depletion of TrxR2 highly affected Trx2 redox state. In particular, a large increase in the protein oxidation level was observed even for a slight decrease of TrxR2 protein amount (see Fig. 19). Therefore, we decided to utilize the Crispr-Cas9 technique in order to obtain a human cell line stably knockout for TrxR2. The Crispr/Cas9 technology consists in the deletion of the protein of interest via the targeted cleavage of the relative gene by Cas9 activity. Two different RNA guides for Cas9 were utilized targeting distinct exons of TXNRD2 gene and tested on a panel of cancer cell lines (see Materials and Methods for experimental details). After cell transfection, clonal selection was employed and more than 100 clones were screened in order to identify the ones in which the gene had been effectively cleaved. Although the complete TrxR2 deletion (TrxR2 KO) was not obtained in any of the cell lines used, we were able to generate different A549 stable TrxR2 knockdown clones. After clonal expansion, the cellular ROS production was assessed and compared to WT cells (Fig. 23).

Notably, we observed that the ROS level inversely correlated to TrxR2 protein expression, as shown in Fig. 23. In particular, the halving of TrxR2 protein level doubles both resting and antimycin-induced ROS production with respect to the control. These findings suggest that mitochondrial thioredoxin reductase possesses a key function in the control of the overall cellular redox homeostasis. Thus, selective inhibitors of the mitochondrial TrxR could be highly efficient in inducing cancer cell death through ROS overload.

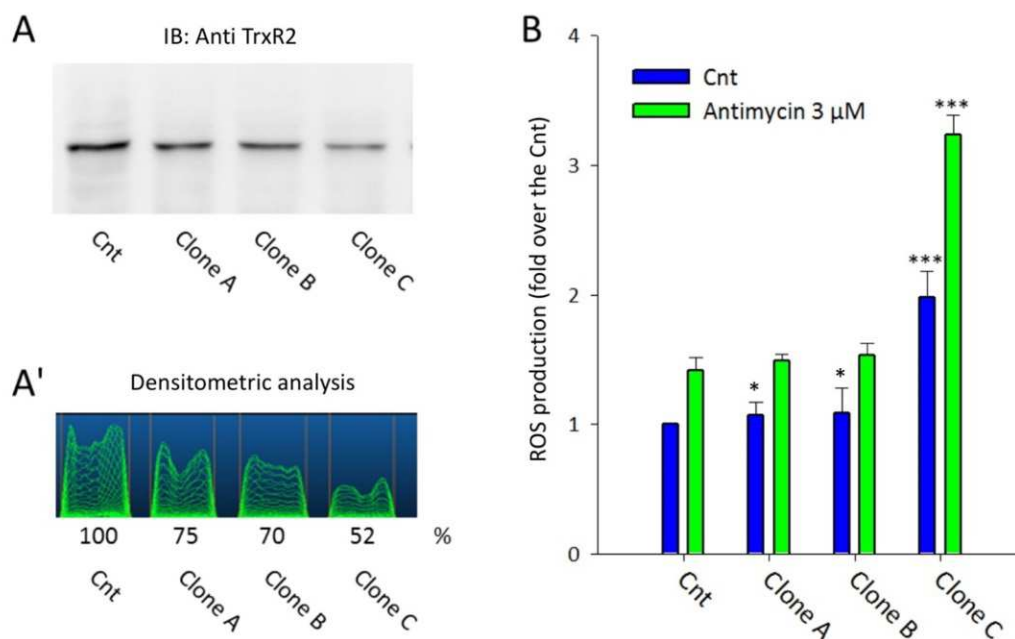


Fig. 23 Correlation between TrxR2 protein amount and ROS production. **(A)** Western blot analysis of TrxR2 in three different A549 knockdown clones (A-C) with respect to control cells; **(A')** Densitometric analysis of the Western blot bands shown in **A** using NineAlliance software. **(B)** Basal and antimycin-induced ROS production of the three TrxR2 depleted A549 clones, measured with the CM-H2DCFDA probe, reported as fold over the control after 2 h from the addition of the probe. Mean \pm SD of 3 experiments (*= $p < 0.05$; ***= $p < 0.001$).

4.2.2 Thioredoxin reductase inhibitors as potential anticancer drugs

Since TrxR2 depletion in human cells seemed to largely affect mitochondrial ROS handling capacity, we next aimed at finding compounds which could associate the TrxR2 inhibitory activity with a cancer cell targeting. Therefore, we focused on the identification of new TrxR inhibitors possibly having mitochondriotropic properties, namely being able to accumulate in the mitochondrial cell compartment exploiting the hyperpolarized status of cancer cell mitochondria. It is necessary to assess the selectivity of new families of complexes in order to avoid side-effects and to construct solid and reliable structure-activity relationships to address the design of targeted chemotherapeutic agents.

In the following subparagraphs, the different classes of metal complexes studied are presented. The compounds were synthesized in collaboration with different European groups of chemists from various universities. In particular, Prof. Angela Casini's group from the School of Chemistry of the Cardiff University (GB), Prof. Fritz Kühn's group from the faculty of Chemistry of the Technische Universität München (D) and Prof. Anne Vessières's group from the Department of Chemistry of the Sorbonne University in Paris (F). For each class the TrxR inhibitory activity, the mechanism of TrxR inhibition and the efficacy against different cancer cell lines were explored. In addition, their effects on the overall cellular redox state were also assessed.

4.2.2.1 Benzimidazole-4-carboxamide Au(III) complex

The first compound to be studied in collaboration with Prof. Casini's group, was an Au(III) complex bearing a 2-((2,2'-bipyridin)-5-yl)-1H-benzimidazol-4-carboxamide ligand. The ligand was specifically designed to inhibit the enzymatic activity of poly(adenosine diphosphate (ADP)-ribose) polymerase 1 (PARP-1), a zinc-finger protein involved in the repair of single-strand breaks in the DNA,⁴¹⁷ while the gold center was

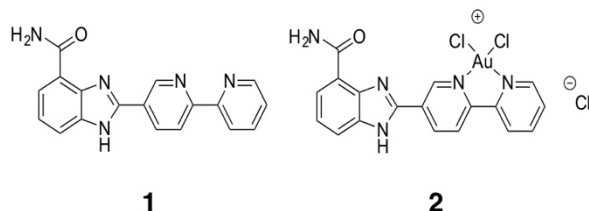


Chart 1: Structures of the benzimidazole-4-carboxamide ligand **1** and of the related Au(III) complex **2**.

conceived to target the Sec present in the active site of TrxR. Therefore, the inhibitory activities of both the Au(III) center and of the organic ligand may be synergic in leading to a cytotoxic effect in cancer cells. In addition, the inhibition of PARP-1 could be useful to potentiate the anticancer activity of DNA-intercalating agents.⁴¹⁸ In Chart 1 the structures of the gold complex (**2**) and of its ligand (**1**) are reported.

Firstly, the *in vitro* inhibition of purified enzymes (PARP-1, TrxR1 and GR) by the two compounds was determined as described in the Materials and Methods section. As expected, PARP-1 activity was highly inhibited by both compounds (Table 5). Of note, only complex **2** inhibited thioredoxin reductase activity (TrxR1) showing an IC₅₀ in the same range as Af (IC₅₀ of Af = 6.88±1.25 nM), whereas the ligand **1** was completely ineffective. This result fits with the lack of the Au(III) center in **1** able to bind the selenol group of TrxR. Furthermore, the inhibitory efficiency of complex **2** for GR is 28-fold lower than for TrxR1 as expected from the lack of Sec in GR structure (Table 5).

Table 5: Inhibitory effect of **1** and **2** on the different isolated enzymes *in vitro* (IC₅₀)

Compound	IC ₅₀ *		
	PARP-1 (nM)	TrxR1 (nM)	GR (μM)
1	5.0±2.1	>100	>10
2	6.0±1.3	14.32±1.62	0.40±0.06

*Mean ± SD of five experiments

Then, the complex and its ligand were tested for their antiproliferative activities in a small panel of cancer cell lines. To this aim the MTT assay was used (see Materials and Methods section). In particular, the human ovarian cancer cells SKOV-3, A2780 and A2780R (cisplatin resistant variant), as well as the human lung cancer line A549, were incubated with **1** or **2** at increasing concentrations for 72 h. Afterwards, their cytotoxicity was determined and compared to the one induced by cisplatin and Af. As reported in Table 6, the complex **2** was more efficient than the ligand **1** towards all tested cell lines. In addition, **2** was more effective than cisplatin on the cisplatin resistant A2780R cell line suggesting a different mechanism of action that can overcome the resistance. A549 cells were poorly sensitive to both the compounds, whereas the SKOV-3 cell line showed major differences in IC₅₀ values, with **2** being 4-fold more potent than **1**. The different sensitivities of the various cell lines could be due to several factors, including the transport mechanisms resulting in distinctive efficiencies in the uptake or efflux of the studied compounds. Af remained the most potent complex but it was highly unselective among the different cell lines.

Table 6: Cytotoxicity of compounds **1** and **2** (IC₅₀) on A2780, A2780R, A549, and SKOV-3 cancer cell lines after 72 h of treatment, compared to Af and cisplatin

Compound	IC ₅₀ (μM)*			
	A2780	A2780R	A549	SKOV-3
1	9.70±3.06	33.1±5.9	46.7±17.5	84.4±7.6
2	4.80±2.35	13.0±2.7	35.0±6.5	22.7±2.9
Af	1.25±0.5	1.5±0.3	2.5±0.7	1.8±0.4
cisplatin	5.2±1.9	35.0±5.9	10.8±2.8	13.2±3.5

*Mean ± SD of three experiments

SKOV-3 cells were selected for the characterization of the effects of compounds **1** and **2** in cells. First of all, total PARP-1, TrxR and GR activities were evaluated in SKOV-3 cells pre-treated with the two compounds for 48 hours. Interestingly, only the gold complex **2** (20 μM) was able to induce a 70% reduction of PARP-1 activity, while ligand **1** was almost totally ineffective (Fig. 24, panel A). Moreover, as shown in Fig. 24, panel B, **2** was also able to induce a 50% inhibition of the total TrxR activity at 40 μM (dark green bars) with a certain specificity over GR (light green bars), while **1** was inefficient on both the enzymes. Cell treatment with 3 μM Af led to a drop of the total TrxR activity to 20% indicating that **2** is less efficient than Af as TrxR inhibitor in cells. The effects of the new compounds on the various enzymatic activities are in line with the data on their cytotoxicity suggesting differences in the uptake mechanisms and in their cellular accumulation capacity. In fact, ligand **1**, which showed a high IC₅₀ value on SKOV-3 cells was unable to inhibit the three enzymes while **2** was either effective on the enzymes and cytotoxic.

In order to analyze the effect of **1** and **2** on the overall cellular redox state, the total glutathione content (reduced + oxidized) was measured in SKOV-3 cells, after their treatment with the two compounds for 48 h in comparison to Af. Fig. 24, panel C shows that no statistically significant variation of the total GSH content, as well as of the GSH/GSSG ratio occurred for Af or for ligand **1**, while **2** decreased the total glutathione amount and increased GSSG pool at the highest concentration tested (50 μM). This result indicates that the cytotoxic potency of the gold complex **2** does not particularly rely on the glutathione pathway and that its mechanism of toxicity is not due to a general oxidizing activity but on the targeting of specific enzymes in the cell.

Finally, we evaluated whether the Au(III) complex or its ligand could affect the mitochondrial membrane potential (MMP) in order to investigate possible mitochondriotropic properties. In fact, other Au(III) complexes were already reported to alter mitochondrial functioning and to induce apoptosis. For instance, an Au(III) meso-tetraarylporphyrin complex, that exhibited 100 fold stronger cytotoxicity than cisplatin against a panel of human cancer cell lines, was reported to induce a decrease of the MMP, release of Cyt c and activation of caspase 9 and caspase 3 of the apoptotic pathway.⁴¹⁹ In addition, a series of Au(III) anticancer agents showing dithiocarbamate ligands were found to induce ERK1/2 phosphorylation triggered by accumulation of ROS. Mitochondria have been suggested as a target of these gold complexes and the sustained ERK1/2 activation was hypothesized to lead to apoptosis.⁴²⁰ Thus, different Au(III) complex have mitochondria-based cellular targets and trigger mitochondrial dysfunctions.

Therefore, MMP of SKOV-3 cells treated for 18 h with 20 or 40 μM compounds **1** and **2** or with 10 μM Af was measured by cytofluorimetric analysis, using the probe tetramethyl rhodamine methyl ester (TMRM) according to established protocols (see Materials and Methods section for details) and compared to the MMP of cells incubated with 10 μM of the uncoupling agent carbonyl cyanide *m*-chlorophenyl hydrazone (CCCP). As apparent in Fig. 24, panel D, both complexes **1** and **2** did not alter the mitochondrial membrane potential with respect to their controls. Conversely, Af partially affected the MMP by inhibiting TrxRs activities while CCCP led to the drop of the MMP in the majority of the cells. This result clearly indicates that mitochondria are not affected by compounds **1** and **2** and that the complex and its ligand do not act on mitochondria to exert their anticancer activity.

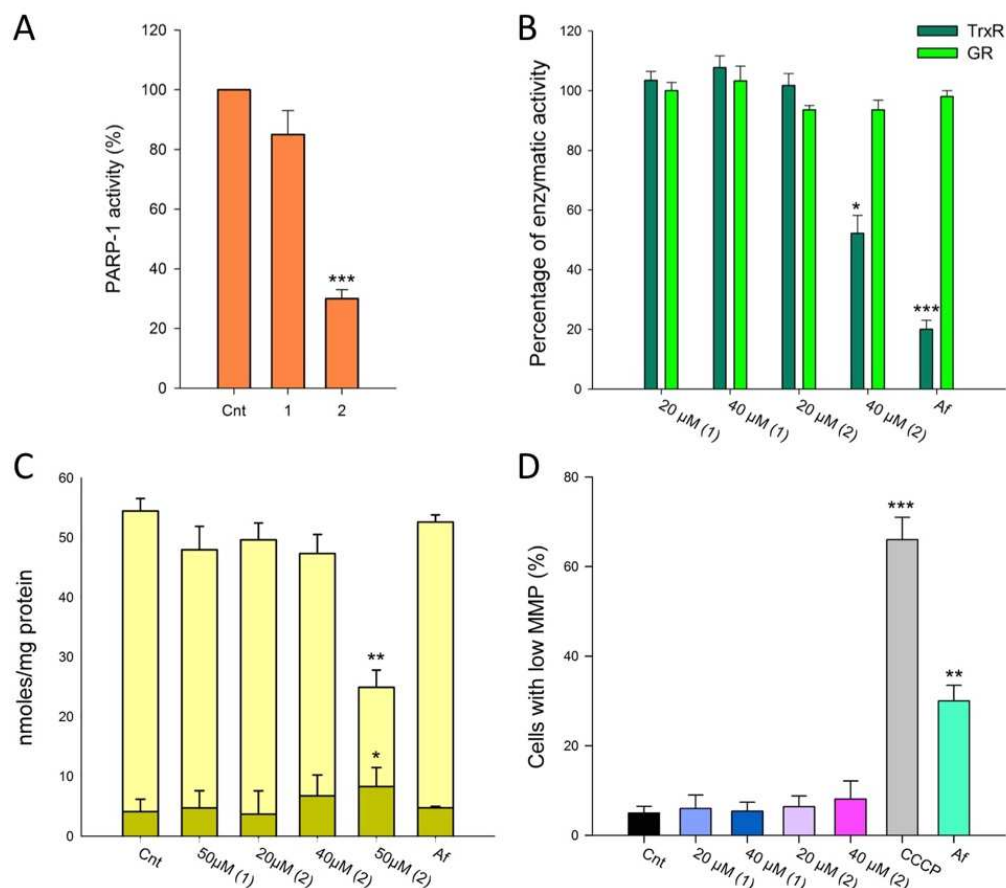


Fig. 24 Effects of the benzimidazole-4-carboxamide Au(III) complex (**2**) and of its ligand (**1**) on SKOV-3 cells. **(A)** PARP-1 activity estimation. SKOV-3 cells were treated with the compounds (20 μM) for 48 h and then subjected to the PARP-1 activity assay as described in Materials and Methods. **(B)** Effect of the compounds **1** and **2** on total TrxR and GR activities in cell lysates. SKOV-3 cells were treated for 48 h with 20 and 40 μM of **1** and **2** or with 3 μM Af, lysed and processed to determine the total TrxR (dark green bars) and GR (light green bars) activities. **(C)** Total and oxidized glutathione amount in SKOV-3 cells treated with **1**, **2** or Af. Glutathione levels were determined in SKOV-3 cells as described in Materials and Methods, after treatment with 50 μM **1**, 20-40-50 μM **2** or 3 μM Af for 48 h. **(D)** Mitochondrial membrane potential (MMP) of SKOV-3 cells treated for 18 h with the two compounds (20 or 40 μM). After treatment, cells were incubated with 25 nM TMRM for 20 min and then analysed by flow cytometry. 10 μM CCCP and 10 μM Af were used as positive controls for the induction of MMP collapse and for TrxR inhibition, respectively. Bars represent mean percentages \pm SD of SKOV-3 cells whose mitochondria showed low MMP. Data are the mean \pm SD of at least 3 replicates for each experiment (* = $p < 0.05$; ** = $p < 0.01$; *** = $p < 0.001$).

In conclusion, the Au(III) complex **2** possesses a potent PARP-1 inhibitory capacity on both the isolated enzyme and in cell lysates. In addition, the seleno-enzyme thioredoxin reductase is efficiently targeted by **2** but not from its ligand **1** which lacks the active gold center. The Au(III) compound displays a good cytotoxicity towards different ovarian cancer cell lines without major effects on both the MMP and the intracellular glutathione redox state suggesting a selective action on the two targeted proteins and a complete deficiency of mitochondriotropic properties.

4.2.2.2 Diphenylpyridine Au(III) complexes

Pursuing the search of novel Au(III) complexes endowed with TrxR inhibitory properties as well as anticancer activity, three new cyclometalated 2,6-diphenylpyridine Au(III) complexes were studied in collaboration with Prof. Kühn's group (Chart 2). The three complexes bear different ligands to the gold atom namely chloride for complex **1**, 1,3,5-triazaphosphaadamantane (PTA) for complex **2** and thio-β-D-glucose-tetraacetate (GluS⁻) for complex **3**. The PTA ligand was added to increase the hydrophilicity of complex **2**, while the GluS⁻ ligand was chosen to possibly enhance the uptake of **3** via the GLUT1 transporter.

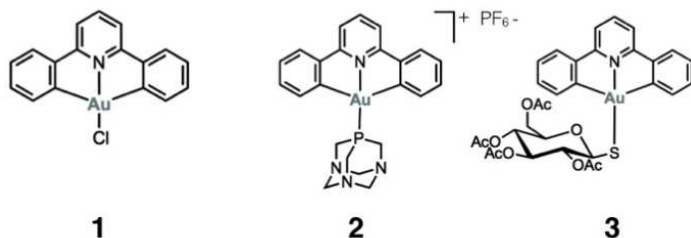


Chart 2: Structures of the three diphenylpyridine Au(III) complexes.

At first, *in vitro* inhibition of purified rat liver cytosolic and mitochondrial TrxRs by compounds **1-3** was investigated and compared to Af, using the DTNB assay described in Materials and Methods. As reported in Table 7, compounds **1-3** are good inhibitors of cytosolic thioredoxin reductase (TrxR1), with complex **3** being the most potent, showing an IC₅₀ value close to the one of Af. Instead, the mitochondrial TrxR activity is only slightly affected by the three complexes with compounds **1** and **3** showing a very similar inhibitory activity. Furthermore, the effect of the complexes on GR activity was also studied and, interestingly, their inhibitory capacity was at least 60-fold lower than for TrxR1 (Table 7).

Table 7: Inhibitory effect of compounds **1-3** (IC₅₀) on isolated TrxR1, TrxR2 and GR activities

Compound	IC ₅₀ (nM)*		
	TrxR1	TrxR2	GR
1	10±1	59±5	219±18
2	10±1	213±20	439±7
3	3±1	60±4	180±22
Af	0.9±0.3	3±1	>10 000

*Mean ± SD of three experiments

Afterwards, the gold complexes were tested for their cytotoxicity against A549, SKOV-3 and 2008 human cancer cell lines by means of the MTT assay (see Materials and Methods section) and compared to cisplatin. Of note, the cytotoxicity was assessed after 72 h of treatment with the complexes for A549 and SKOV-3 cells and after 48 h for 2008 cells. Table 8 reports the IC₅₀ values of **1-3** and of cisplatin on the cell viability. The compound displaying the highest potency was complex **3** in accordance to its good TrxR1 and GR inhibitory capacity observed *in vitro*, while the most sensitive cell line was the 2008 ovarian cancer.

Table 8: Cytotoxicity of the Au(III) compounds **1-3** and of cisplatin (IC₅₀) against A549, SKOV-3 (72 h incubation) and 2008 (48 h incubation) cells

Compound	IC ₅₀ (μM)*		
	A549	SKOV-3	2008
1	35±5	39±7	29±3
2	> 50	48.1±2.3	> 50
3	30.4±1.3	13.0±0.9	7.0±1.2
cisplatin	12±0.5	16.3±1.7	10.4±1.3

*Mean ± SD of three experiments

Then, we decided to analyse whether the complexes were able to target TrxR and GR in 2008 cells, the most sensitive cells to the compounds. Thus, the ovarian cancer cells were pre-treated for 48 h with **1-3** at increasing concentrations (10-50 μM) and subjected to the measurement of the two enzymatic activities (see Materials and Methods). As apparent from Fig. 25, panel A, complex **3** was the most effective in inhibiting the total thioredoxin reductase activity, followed by compound **2**. Conversely, complex **1** was almost inactive even at the highest concentration used (50 μM). In addition, GR activity was also determined and, as shown in Fig. 25, panel A', the enzyme was not inhibited by **1-3** confirming the different potency of the complexes on TrxR and GR already noted on the isolated enzymes.

In order to evaluate the effects deriving from TrxRs inhibition, the redox state of Trx1 and Trx2, the main substrates of TrxRs, was analysed in 2008 cells treated for 48 h with **1** and **3** (Fig. 25, panel B). The redox Western blot analysis already described in subparagraph 4.1.2 was utilized. As expected, only complex **3** induced the oxidation of Trx1 and Trx2, evidenced by the shift of the bands towards their more oxidized forms and, indirectly, confirmed that compound **3** is effective in inhibiting TrxR.

Finally, the overall cellular redox state was evaluated. To this aim, total thiols, total glutathione content and GSH/GSSG ratio were determined after incubation of 2008 cells (1×10^6) with **1-3** (25 μM and 50 μM) for 48 h. As shown in Fig. 25, panel C, the total amount of thiols in cells was unchanged upon treatment with complexes **1** and **2**, whereas complex **3** at the highest concentration (50 μM), was able to decrease thiols level of about 40%, suggesting that **3** affects the redox homeostasis of the cell. Regarding glutathione, a significant increase of oxidized glutathione was elicited only by complex **3** at 50 μM (Fig. 25, panel D). Therefore, complex **3**, by inhibiting thioredoxin reductase activity, induces oxidation of thioredoxins leading to a redox imbalance in the cell as shown from the decrease of total thiols and increase of the oxidized glutathione pool.

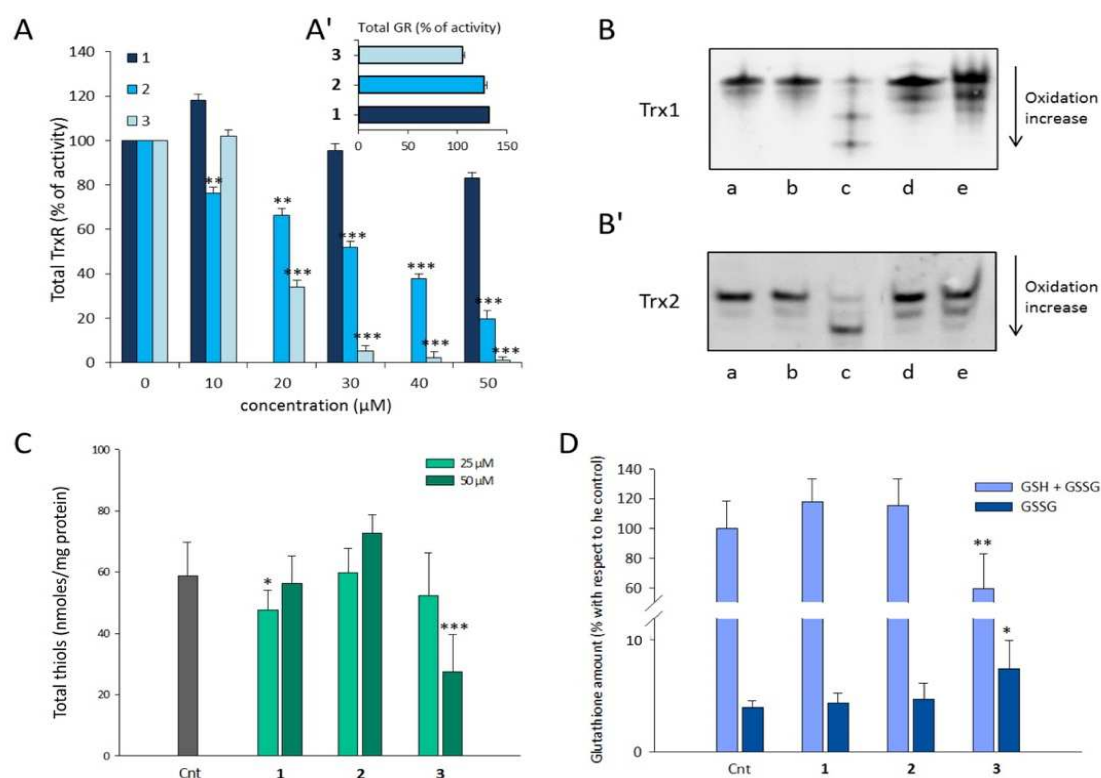


Fig. 25 Effects of the three Au(III) complexes in 2008 ovarian cancer cells. (A, A') Total TrxR and GR activities measured in 2008 ovarian cancer cells (1×10^6) after 48 h treatment with **1-3** as reported in the Materials and Methods section, mean \pm SD of 3 experiments. (A) Total TrxR activity estimation after cell treatment with **1-3** at the indicated concentrations; (A') GR activity

determination after cells treatment with 50 μM of each compound. (B) Redox Western blot of Trx1 and Trx2 in 2008 cells after incubation with **1** (40 μM) and **3** (20 μM) for 24 h; N-acetyl-cysteine (NAC) was used to achieve the fully reduced status, while diamide is taken as control for the totally oxidized protein form (a) Cnt; (b) 3mM NAC; (c) 2 mM diamide; (d) 40 μM compound **1**; (e) 20 μM compound **3**. (C) Total thiols in 2008 ovarian cancer cells after treatment with **1-3** for 48 h. Cells (5×10^5) were treated with the compounds (25 or 50 μM) and then subjected to total thiol determination, mean \pm SD of 5 experiments. (D) Total glutathione amount and redox state (GSSG/GSH ratio) after cell treatment with 50 μM of compounds **1-3** for 48 h, mean \pm SD of 3 experiments. (*= $p < 0.05$; **= $p < 0.01$; ***= $p < 0.001$).

In conclusion, the three novel Au(III) complexes have been examined for their TrxR and GR inhibitory capacity and for their antiproliferative effects in a small panel of human cancer cells. The complexes are nanomolar inhibitors of isolated cytosolic and mitochondrial TrxRs, with a more potent activity on the cytosolic isoform of the enzyme while they scarcely affect the activity of GR. In general, these compounds are poorly toxic, with the exception of compound **3**, which was particularly active against the 2008 ovarian cancer cell line. The preferential inhibition of TrxR over GR was confirmed also in 2008 cells and supported by the observed oxidation of Trxs after cell incubation with compound **3**. Furthermore, complex **3** was shown to be particularly effective in disrupting the cellular redox state by decreasing the level of thiols and augmenting glutathione oxidation. However, the Au(III) complexes need to be further optimized for biological applications, especially in terms of potency on cancer cells.

4.2.2.3 N-heterocyclic carbene (NHC) Au(I) complexes

In 2008, Berners-Price and coworkers synthesized a series of cationic N-heterocyclic carbene (NHC) Au(I) complexes endowed with remarkable cytotoxicity and able to induce mitochondrial damage.²⁷⁸ Since then, the research for novel organometallic NHC Au(I) complexes as potential anticancer agents has largely increased.⁴²¹ The fine-tuning of the hydrophilic/lipophilic character can highly affect the stability of the complex in physiologic media, its capacity to enter cancer cells and its inhibitory properties. Thereafter, we decided to characterize a series of new differentially functionalized mono- and bis- NHC Au(I) complexes for their cytotoxic activity and enzymatic inhibitory capacity. In addition, a dinuclear NHC Au(I) complex was also tested. The structures of the compounds synthesized in collaboration with Prof. Casini's group, are reported in Chart 3. Notably, the NHC ligands are endowed with sulfonate or hydroxyl groups in order to increase the hydrophilicity of the complexes. In addition, in the mono- and bis-carbenic series, R is substituted with groups endowed with increasing lipophilicity (lipophilic character of R: **1**<**2**<**3** and **5**<**6**<**7**).

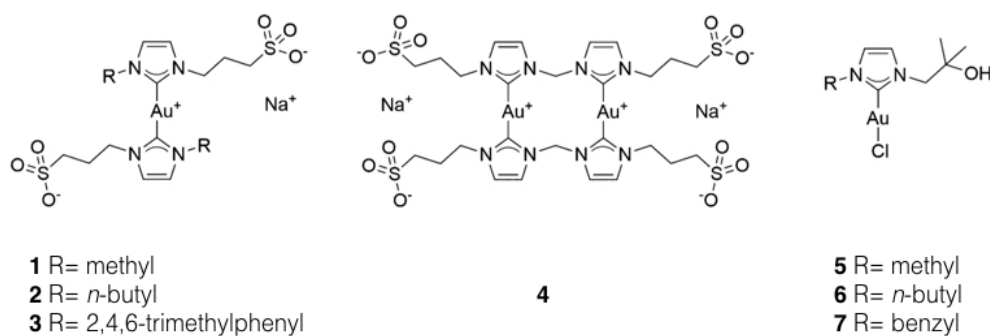


Chart 3: Structures of the hydrophilic N-heterocyclic carbene Au(I) complexes.

Initially, the seven NHC Au(I) complexes were evaluated for their inhibitory potential toward both isolated cytosolic (TrxR1) and mitochondrial (TrxR2) rat liver TrxRs, according to established protocols as described in the Materials and Methods section. In Table 9 the half-maximal inhibitory concentrations (IC_{50}) of the

NHC Au(I) complexes on the two enzymes are reported in comparison to Af as a benchmark. The monometallic bis-carbenic complexes **1-3** were able to inhibit cytosolic TrxR in the micromolar range of concentrations (4.8-23 μ M), while the mono-carbenic compounds **5-7** were much more efficient showing lower IC₅₀ values (0.018-0.073 μ M). These results are probably due to the greater stability of the bis-carbenic compounds **1-3** and to their lower nucleophilicity with respect to the mono-carbenic complexes **5-7** which, instead, easily undergo ligand exchange with Cys and/or Sec residues of TrxR. Of note, the bimetallic bis-carbenic gold complex **4** is slightly more potent than **1-3**, thanks probably to the two gold centers. In addition, TrxR activities were not inhibited by the isolated ligands demonstrating the requirement of gold centers for TrxR inhibition (data not shown). All three mono-carbenic Au(I) complexes were able to inhibit TrxR1 in the nanomolar range of concentrations as Af (TrxR1 inhibition potency: **6>7>5**). Regarding TrxR2, the inhibitory capacity of **5-7** was lower with respect to Af and the efficiency between the three complexes was slightly different than for TrxR1 (TrxR2 inhibition potency: **6>5>7**). Moreover, the complexes were tested for their inhibitory activity toward isolated glutathione reductase. GR activity was found to be inhibited at higher concentrations with respect to TrxRs (>10 μ M for all the complexes), indicating a preferential effect on TrxRs.

Table 9: Inhibitory effect (IC₅₀) of the NHC Au(I) complexes against isolated cytosolic (TrxR1) and mitochondrial (TrxR2) thioredoxin reductases

<i>Compound</i>	IC ₅₀ (μ M)*	
	<i>TrxR1</i>	<i>TrxR2</i>
1	5.073±0.212	n.d.
2	23.167±1.623	n.d.
3	3.664±0.091	n.d.
4	0.409±0.051	3.257±0.091
5	0.073±0.002	0.313±0.041
6	0.018±0.001	0.267±0.022
7	0.025±0.003	0.561±0.102
Af	0.007±0.001	0.004±0.001

*Mean \pm SD of three experiments

In order to investigate the mechanism of inhibition of the complexes toward TrxR, the biotinylated-iodoacetamide (BIAM) assay was employed. Utilizing this method, it is possible to observe the binding of the complexes with the C-terminal redox-active centre of TrxR on the basis of the different pKa values of Cys (8.57) and Sec (5.27). In particular, at pH 6.0 only Sec (and low pKa Cys) can be alkylated by BIAM, whereas at pH 8.5 both Cys and Sec are modified. The labelled enzymes are then detected with horseradish peroxidase conjugated streptavidin, triggering chemiluminescence. The pretreatment of TrxR with thiol- and/or selenol- alkylating species can block BIAM binding and thus reduces the intensity of the chemiluminescent band (see Materials and Methods section for details). Thus, we pretreated isolated TrxR1 with the mono-carbenic complexes **5-7** in comparison with the bis-carbenic compounds **1-3** followed by BIAM derivatization at the two pH. The results are shown in Fig. 26, panel A and A'. Complexes **1-3** (100 μ M) were poor alkylators of both Cys and Sec. Conversely, compounds **5** and **6**, at the same concentration, almost completely hindered BIAM binding to the enzyme at both pH, indicating a strong affinity not only

towards selenol groups but also for thiols. Compound **7** was the most effective complex. Indeed, a low concentration (20 μM) was sufficient to significantly affect BIAM binding. Interestingly, a certain selectivity for selenol groups was also detected (Fig. 26, panel A': 42% of residual band intensity for lane d vs 58% for lane d'). Therefore, the three mono-carbenic Au(I) complexes **5-7**, can alkylate TrxR and show a slight binding preference for Sec. On the contrary, complexes **1-3**, according to their low enzyme inhibitory capacity, do not target thiols nor selenols suggesting again that they hardly undergo ligand exchange reactions.

Then, the mono-carbenic Au(I) complexes (**5-7**) were evaluated for their antiproliferative effects on the 2008 ovarian cancer cell line. The dinuclear complex **4** was also included because of its stronger TrxR inhibitory activity in comparison to the other bis-carbenic compounds. To this end, 2008 cells were treated with compounds **4-7** at increasing concentrations and then cell viabilities were quantified using the MTT assay, as described in the Materials and Methods section. As reported in Fig. 26, panel B, the three mono-carbenic Au(I) complexes were highly efficient, displaying IC_{50} values of cytotoxicity in the low-micromolar range (13.2 \pm 3.5, 17.5 \pm 1.5, and 24.5 \pm 4.2 μM for **5**, **6** and **7**, respectively) already after only 1 h of incubation with cells. Conversely, complex **4** was not toxic even at the highest concentration used. Interestingly, compounds' cytotoxicity did not display significant differences at 24 h, suggesting that they could be inactivated with time. In support of this hypothesis, Ott and co-workers reported that the bioavailability of other NHC Au(I) complexes could be negatively affected by serum components.⁴²² This hypothesis may possibly explain the acute and transient effect on cell viability of our new Au(I) complexes.

Afterwards, the total TrxR and GR activities were assessed in 2008 cells pretreated with compounds **4-7** (20, 40, and 60 μM) for 3 h (Fig. 26, panel C and C'). For the dinuclear bis-carbenic complex **4**, a slight decrease of both enzymatic activities was apparent only at the highest concentration examined (60 μM), in accordance to its low cytotoxicity. Whereas, the mono-carbenic complexes **5-7** induced a significant decrease of the total thioredoxin reductase activity (>70%) even at the lowest concentration used (20 μM), showing an inhibitory effect following the same order of their antiproliferative activity **5**>**6**>**7**. At higher concentrations, TrxR activity largely declined, reaching 90% inhibition at 60 μM . In contrast, GR activity was clearly less affected by **5-7** with a maximal 70% inhibition of complex **5** at the concentration of 60 μM (Fig. 26, panel C'). These results are in agreement with the previously observed selectivity of **5-7** for TrxR as well as with their cytotoxicity, which appears to be correlated with their TrxR inhibitory capacity.

Finally, ROS production was evaluated upon 2008 cell treatment with the various NHC Au(I) complexes. In fact, TrxR inhibition, by altering the cellular redox homeostasis, increases H_2O_2 concentration that can be measured as a direct proof of redox imbalance. Thus, the effect of gold compounds **4-7** (20 μM) on ROS production was measured in 2008 ovarian cancer cells over a period of 2 h using the peroxide-sensitive fluorescent probe CM-H2DCFDA (see Materials and Methods section). As shown in Fig. 26, panel D, all three mono-carbenic Au(I) complexes stimulated ROS formation with complex **5** being the most effective, in accordance with its strongest inhibitory effect on TrxR. On the other hand, complex **4** did not elicit ROS production as expected from its poor activity *in cellulo*.

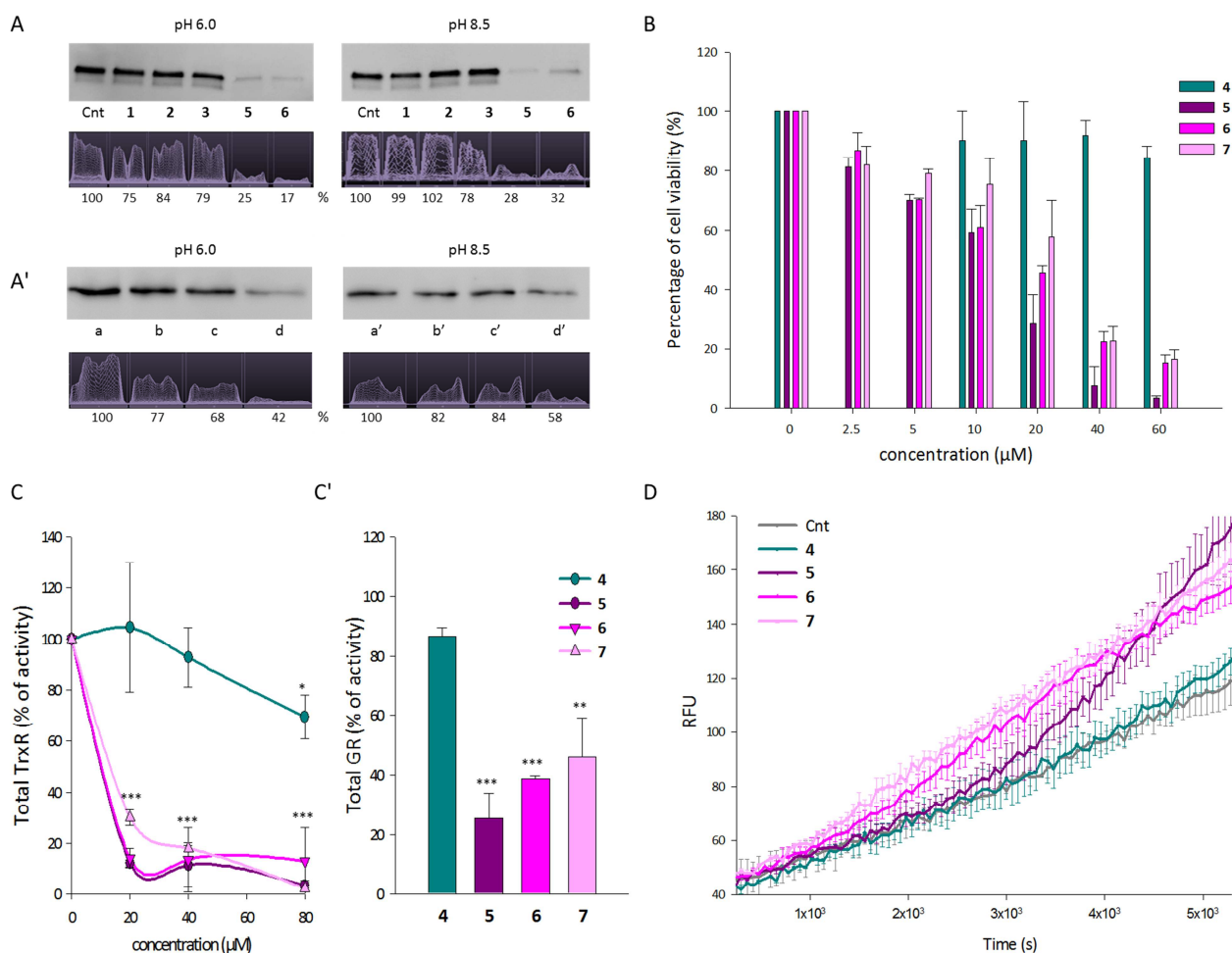


Fig. 26 Effects of the NHC Au(I) complexes *in vitro* on isolated enzymes and on cancer cells. (**A, A'**) BIAM assay on reduced TrxR1 pre-incubated with 100 μM complexes **1-3** and **5-6** (**A**) or with 5, 10 and 20 μM complex **7** (**A'**) (see Materials and Methods section for details). Densitometric analysis performed with NineAlliance software is reported. (**B**) Cell proliferation assessed with the MTT assay after 1 h incubation of 2008 cells (1×10^4) with increasing concentrations of **4-7**, mean \pm SD of 3 experiments. All the bars relative to cells treated with complexes **5-7** (2.5-60 μM) are significant with respect to the control with $p < 0.01$. (**C**) 2008 cells (1×10^6) were treated with complexes **4-7** at increasing concentrations (20, 40 and 60 μM) for 3 h, lysed and then subjected to total TrxR activity measurement as described in Materials and Methods, mean \pm SD of 4 experiments; (**C'**) 2008 cells (1×10^6) were treated with 60 μM complexes **4-7** for 3 h, lysed and total GR activity assessed (see Materials and Methods), mean \pm SD of 4 experiments. (**D**) ROS production of 2008 cancer cells (1×10^4) upon treatment with 20 μM complexes **4-7** utilizing the probe CM-H2DCFDA, RFU = relative fluorescent units, mean \pm SD of 4 experiments (*= $p < 0.05$; **= $p < 0.01$; ***= $p < 0.001$).

In conclusion, a series of novel mono- and bis-carbenic and one dinuclear Au(I) complexes were screened for their inhibitory effects on purified TrxR and GR and on 2008 cells. The three mono-carbenic complexes were the most effective in targeting TrxR over GR by preferentially binding preferentially to the Sec present in TrxR active site. In addition, the mono-carbenic compounds were tested for their antiproliferative effects, TrxR inhibitory activity and oxidative stress induction on the human ovarian cancer cell line 2008. The results clearly indicate a correlation between cytotoxicity, TrxR inhibition and ROS production in cancer cells. However, cell culture media components (including serum proteins) probably influence the metallodrug speciation and possibly induce deactivation of the complexes over time.

4.2.2.4 Tamoxifen-like metallocifens

The last class of metal complexes that have been studied as possible thioredoxin reductase inhibitors are the tamoxifen-like metallocifens (TLMs). Tamoxifen is a chemotherapeutic drug utilized to treat patients

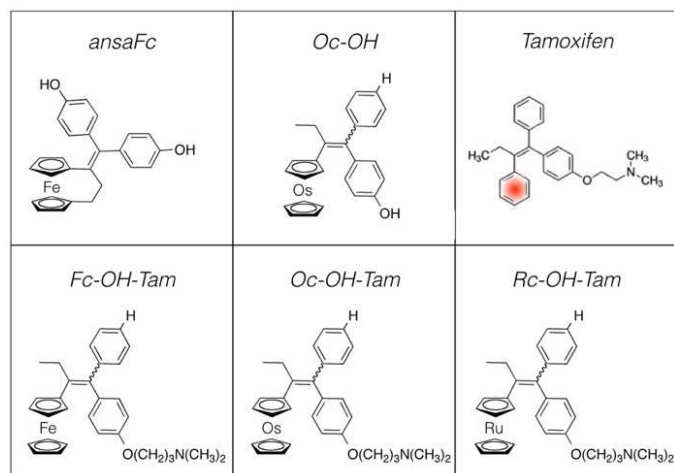


Chart 4: Structures of the various TLMs studied.

affected by ER⁺ breast cancer.³³⁸ The new complexes derive from the substitution of one of the phenyl rings in the structure of tamoxifen (indicated with a red dot in Chart 4) by a metallocene unit and modifications/excision of the lateral amino-chain. As already mentioned in Introduction, the metallocene unit presents reversible redox properties and long ago has been associated to an anticancer activity.³³³ Thus, TLMs were synthesized by Prof. Vessières's group to combine the estrogen modulatory properties of the tamoxifen structure with the redox activity of the metallocene unit. In addition, it has been shown that tamoxifen is able to affect mitochondria by interfering with oxidative phosphorylation leading to mitochondria uncoupling and to the perturbation of the MMP.⁴²³ Thus, TLMs could possibly associate the mitochondrial targeting capacity to a redox activity. Many different derivatives have been synthesized. In 2014, Citta *et al.* studied two TLMs of iron (**Fc-OH** and **Fc-OH-Tam**) with respect to their possible inhibitory activity on TrxR, GR and GPx and reported that the complexes were able to selectively target TrxR, while GR or GPx were not affected.³⁴² Interestingly, metallocifens need to be enzymatically transformed into oxidized derivatives (with the combination H₂O₂/HRP) to be able to alkylate the Sec present in the active site of TrxR. These derivatives were identified as quinone methides (QMs). **Fc-OH** and **Fc-OH-Tam** inhibitory effect on TrxR was confirmed also in the lymphoblastoid Jurkat cell line. Therefore, we decided to further analyze the effects of this class of complexes on both isolated enzymes and cancer cells. In particular, other TLMs were tested for their TrxRs inhibitory capacity and insights were obtained into the mechanism of cancer cell death induction. Moreover, since tamoxifen was found to target mitochondria we also investigated the possible tropism for mitochondria of some TLMs. Chart 4 reports the structure of the different TLMs studied.

The first compound to be investigated was the ansa-ferrocenyl compound (**ansaFc**). As apparent in Chart 4, differently from **Fc-OH-Tam**, the amino-chain has been substituted by a hydroxyl group and the ferrocene unit is covalently linked to the rest of the complex by both the cyclopentadienyl rings.

Since the active metabolites of the previously studied iron complexes were obtained through the enzymatic oxidation mediated by the HRP/H₂O₂ mixture, we initially investigated whether **ansaFc** could be also transformed into a quinone methide. Thus, the UV-Vis spectrum of the compound (50 μM) was recorded in the presence of 46 nM HRP and 200 μM H₂O₂ in 0.2 M Tris-HCl buffer (pH 8.1), 1 mM EDTA as described in the Materials and Methods section. The time evolution of the UV-Vis spectrum of **ansaFc** upon HRP/H₂O₂ addition is shown in Fig. 27, panel A. Two short-lived bands rapidly appeared at 368 and 273 nm. Then, a band at 560 nm emerged and was associated with the coloring of the solution in bright pink. The intensity of this band reached a maximum of absorbance at 15 min, then rapidly decreased (t_{1/2} = 8 min). The transient species observed initially could be a radical of the compound (**ansaFc•**) probably resulting from one electron oxidation and one proton abstraction. To prove this hypothesis EPR spectroscopy was

employed and confirmed the formation of a transient organic radical (Fig. 27, panel B). In fact, kinetic studies in the range 1-10 min showed the formation of a peak at $g = 2.0205$ characteristic of an organic radical that reached a maximum after 2 min and then slowly decreased but remained detectable after 10 min. Instead, the pink species was attributed to the quinone methide formation. This species seems to be also poorly stable as shown by the disappearance of the band after 90 min along with the appearance of insoluble species, associated to an increase of the baseline (Fig. 27, panel A).

In the previous studies performed in the ferrocifen series, the QMs obtained by enzymatic oxidation were characterized as strong inhibitors of thioredoxin reductase, whereas the parent complexes were less efficient inhibitors.³⁴² Thus, we decided to evaluate the inhibitory capacity of both **ansaFc** and **ansaFc•** on TrxR1. Since the radical derivative **ansaFc•** is not stable, its inhibitory activity on TrxR was measured after different pre-incubation times of **ansaFc** with the HRP/H₂O₂ mixture (0.5-60 min) and a 5 min incubation with TrxR1 prior to the enzymatic activity measurement. The results summarized in Fig. 27, panel C, show that the extent of TrxR1 inhibition highly depend on the time of **ansaFc** pre-incubation with HRP/H₂O₂. In fact, TrxR1 activity decreased between 0.5 and 5 min pre-incubation times and reached a minimum (14% of residual activity) at 5 min. However, the inhibitory effect decreased for longer pre-incubation times, i.e. when the QM is formed, indicating that **ansaFc•** is the active metabolite of **ansaFc** responsible for TrxR1 inhibition.

Then, the inhibitory capacity of **ansaFc** on TrxR1 and GR in comparison with **ansaFc•** (obtained after 5 min preincubation in the presence of the HRP/H₂O₂ mixture where the inhibitory potency of the species is maximal), was studied (Fig. 27, panel D). Regarding TrxR1, **ansaFc** alone only slightly inhibited TrxR1 (IC₅₀ around 7 μ M) while a significantly lower IC₅₀ value (around 0.15 μ M) was found for **ansaFc•**. Interestingly, GR which is structurally homologous to TrxR, was not significantly inhibited by both the compounds as shown in Fig. 27, panel D.

This result suggests that **ansaFc•** may target the Sec at the C-terminal of TrxR that is not present in GR. In order to verify the alkylation of the selenol in TrxR by the **ansaFc** derivative, the BIAM assay was performed. As apparent from Fig. 27, panel E, **ansaFc**, at relatively high concentration (50 μ M), was not able to interact with the Sec. Indeed, the amount of TrxR detected was almost identical to the control. On the contrary, **ansaFc•** at a very low concentration (2 μ M), was able to react with both Sec and Cys. These results are in good agreement with the respective potency of **ansaFc** and **ansaFc•** as TrxR inhibitors (Fig. 27, panel D). However, the BIAM assay revealed also that **ansaFc•** binds not only the Sec residue but also thiols indicating a high reactivity.

Ab-initio calculations performed at Density Functional Theory (DFT) level showed the possibility of delocalization of the unpaired electron of **ansaFc•** between the C α position and the deprotonated phenol ring (Fig. 27, panel F). The possibility of an intramolecular resonance stabilizes the organic radical and thus renders it visible in both the UV-Vis and in the EPR spectra.

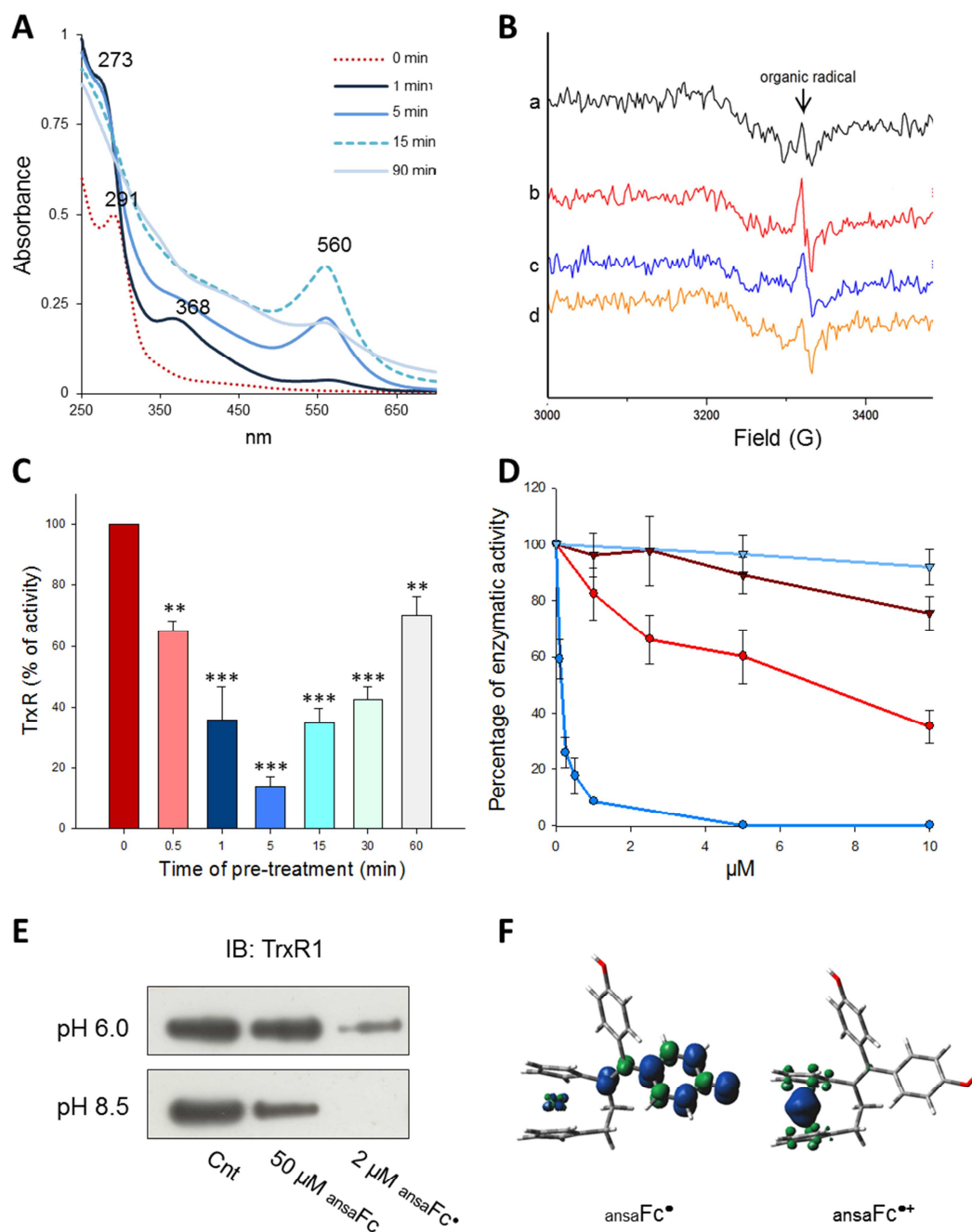


Fig. 27 Effects of **ansaFc**, enzymatic transformation, characterization of the derivative, and inhibitory properties. **(A)** Time evolution of the UV-Vis spectrum of **ansaFc** (50 μM) incubated in the presence of 46 nM HRP/200 μM H_2O_2 in 0.2 M Tris-HCl buffer (pH 8.1), 1 mM EDTA at 25°C. **(B)** X-band EPR (microwave frequency = 9.3944 GHz) of frozen solution of **ansaFc•**: evolution of the peak at $g=2.0205$, corresponding to the organic radical, at the indicated reaction times (a) 1 min; (b) 2 min; (c) 5 min; (d) 10 min. **(C)** Kinetics of inhibition of cytosolic thioredoxin reductase (TrxR1) *in vitro* by **ansaFc•**. **Ansafc** (0.25 μM) was first preincubated for different times (0.5-60 min) with the HRP/ H_2O_2 mixture. Then, aliquots of highly purified TrxR1 (60 nM) were added and incubated for 5 min in 0.2 M Tris-HCl buffer (pH 8.1), 1 mM EDTA and NADPH (0.25 mM). Percentage of remaining TrxR1 activity was determined by estimating the DTNB-reducing property of the enzyme as described in Materials and Methods section, mean \pm SD of 3 experiments. **(D)** Percentage of TrxR1 and GR activities. Purified enzymes were incubated for 5 min in the presence of various concentrations of **ansaFc** or **ansaFc•** (obtained by pretreatment of **ansaFc** with H_2O_2 /HRP for 5 min) and TrxR1 and GR activities were then measured, mean \pm SD of 3 experiments. Red curve: TrxR1 activity in the presence of **ansaFc**; Dark blue curve: TrxR1 activity in the presence of **ansaFc•**; Light blue curve: GR activity in the presence of **ansaFc**; Dark red curve: GR activity in the presence of **ansaFc•**. **(E)** BIAM assay of TrxR1 with **ansaFc** or **ansaFc•**. TrxR1 (1 μM), pre-reduced with NADPH (60 μM), was incubated for 30 min with 50 μM **ansaFc** or 2 μM **ansaFc•** in 50 mM Tris-HCl buffer (pH 7.4) containing 0.2 mM NADPH, 1 mM EDTA. Then, samples were processed as described in Materials and Methods section (IB: immunoblot). **(F)** Computed Spin Density isosurfaces (isocontour value 0.025). Positive (blue) zones indicate regions where an excess of electron is present corresponding to the zones where the radical is localized (** = $p < 0.01$; *** = $p < 0.001$).

Next, we moved to assess the possible anticancer effect of **ansaFc** in Jurkat cells. We started by investigating its cytotoxicity, utilizing the MTT assay. Cells were incubated for 72 h with increasing concentration of **ansaFc** and then processed (see Materials and Methods for details). Fig. 28, panel A displays the viability curve and it is interesting to note that the compound is cytostatic more than cytotoxic.

We also evaluated the total TrxR and GR activities in Jurkat cell lysates after their incubation with **ansaFc** for 48 h. The complex led to a modest inhibition of TrxR and was completely ineffective on GR activity. We hypothesized that **ansaFc**, once oxidized to **ansaFc^o**, could be too reactive to be selective for TrxR and that it could possibly derivatize Cys residues of other proteins, inducing oxidative stress. The cellular ROS production upon addition of **ansaFc** was thus determined. The CM-H2DCFDA probe was utilized following established protocols (reported in Materials and Methods section) and the ROS level was measured from the addition of **ansaFc** to the cells and followed for 2 h. Notably, very low concentrations of **ansaFc** were found to largely increase ROS level (Fig. 28, panel C and C') proportionally to the amount of **ansaFc** administered. The high ROS production indicates an imbalance of the cell redox homeostasis. The amount of total cellular thiols was then analyzed after cell treatment with **ansaFc** and, consistently with the previous results, a dose-related decrease of thiol groups was determined (Fig. 28, panel D).

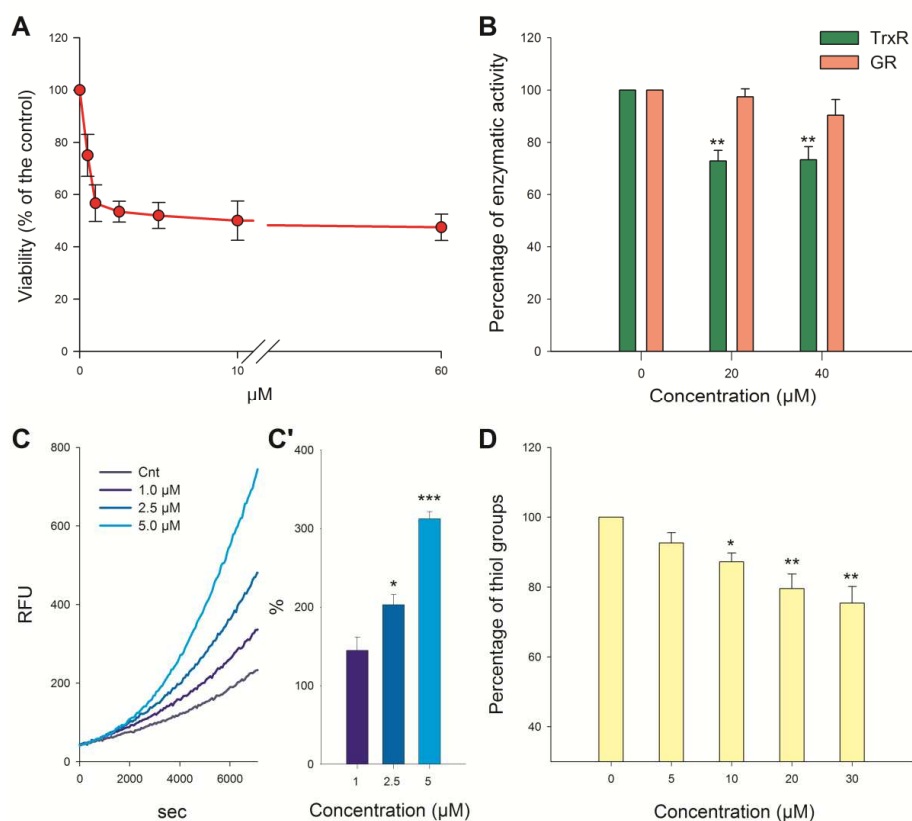


Fig. 28 Effect of **ansaFc** on Jurkat cells. **(A)** Cell proliferation assay performed on Jurkat cells using the MTT assay. Cells (4×10^4) were incubated with increasing concentrations of **ansaFc** for 72 h and then processed as reported in the Materials and Methods section. **(B)** Inhibitory activity of **ansaFc** on the total TrxR and GR activities in Jurkat cells. Cells (1×10^6) were incubated with the indicated concentrations of **ansaFc** for 48 h, lysed and subjected to the determination of the total TrxR (green bars) and GR (orange bars) activities. **(C)** Cellular ROS production after **ansaFc** administration. Jurkat cells (4×10^4) were treated with **ansaFc** at increasing concentrations and then ROS production was analyzed for 2 h using CM-H2DCFDA as reported in the Materials and Methods section, RFU = relative fluorescent units; **(C')** ROS level of cells incubated with increasing concentrations of **ansaFc** at 2 h from the treatment, as percentage with respect to the control. **(D)** Total thiols of Jurkat cells after **ansaFc** administration. Cells (1×10^6) were incubated for 48 h with increasing concentrations of **ansaFc**. Afterwards, total thiols were titrated utilizing DTNB. Mean \pm SD of 3 biological replicates are shown for each experiment (* = $p < 0.05$; ** = $p < 0.01$; *** = $p < 0.001$).

In conclusion, **ansaFc** can generate a very reactive derivative, **ansaFc•**, which has been characterized as an organic radical that can be stabilized by resonance. The oxidative derivative is a potent inhibitor of TrxR1 with respect to GR on the isolated enzyme showing reactivity towards both Sec and Cys. In Jurkat cells the compound is cytostatic and the mechanism involves an imbalance of the redox homeostasis of the cell. Indeed, a large ROS production and a decrease of total thiols were observed. However, the complex seems to be too much reactive and may unselectively target protein thiols when administered to cultured cells after the generation of the reactive radical. Thus, **ansaFc** probably needs to be optimized in order to exert a more targeted activity on cancer cells.

Continuing with the class of TLMs, we moved to the osmium derivatives namely **Oc-OH** and **Oc-OH-Tam** (see Chart 4). Osmium is an element of the group 8 of transition metals of the periodic table, together with iron and ruthenium. This heavy element is endowed with an excellent metal-to-ligand back-donation property at low oxidation states (+2, +3) and can form more stable complexes than those of iron in biological media.^{424, 425} Thus, we decided to study the potential anticancer activity of these organometallic complexes in order to see possible differences with the iron analogues previously studied by Citta *et al.*³⁴²

Aiming to see whether the osmium compounds can also be transformed in more active species upon enzymatic oxidation, we started by assessing their potential inhibitory activity on isolated thioredoxin reductases before and after incubation with HRP/H₂O₂, as previously performed for the iron series of compounds. Thus, we incubated the osmium complexes with 0.1 mM H₂O₂ and 22 nM HRP in 0.2 M Tris-HCl buffer (pH 8.1). After 5 min, TrxR activity was estimated as described in Materials and Methods. Of note, their respective quinone methides (QM), synthesized by chemical oxidation with freshly prepared Ag₂O, were also tested for their TrxR inhibitory activity. As reported in Table 10, both compounds are scarcely effective on the cytosolic thioredoxin reductase (TrxR1) up to a concentration of 20 μM, whereas a remarkable TrxR1 inhibition was apparent after their oxidation with the HRP/H₂O₂ system, with oxidized **Oc-OH-Tam** being a little more active than oxidized **Oc-OH**. The chemically synthesized quinone methides displayed also a good inhibitory capacity on TrxR1, but lower with respect to the derivatives resulting from HRP/H₂O₂ transformation. **Oc-OH**, **Oc-OH-Tam** and their enzymatically-formed derivatives were also tested on the isolated mitochondrial thioredoxin reductase (TrxR2). In accordance with the data obtained on the cytosolic enzyme, only the transformed compounds showed a significant inhibition of TrxR2. Moreover, a large difference in terms of potency on TrxR2 was seen between the two derivatives. In particular, the **Oc-OH-Tam** derivative was more than two fold better as TrxR2 inhibitor than the one generated from **Oc-OH**.

Table 10: Inhibitory effect of the osmium complexes alone, after enzymatic transformation, and of their chemically synthesized quinone methides (IC₅₀) on purified thioredoxin reductases

	IC ₅₀ (μM)*			
	TrxR1		TrxR2	
	<i>Oc-OH</i>	<i>Oc-OH-Tam</i>	<i>Oc-OH</i>	<i>Oc-OH-Tam</i>
Complex alone	≥ 20	> 20	≥ 20	> 20
Complex pre-treated with HRP/H ₂ O ₂	2.4±0.3	1.2±0.1	12.2±1.8	4.5±0.8
Quinone methide	5.4±0.7	3.6±0.2	n.d	n.d

*Mean ± SD of three experiments (n.d = not determined)

At this point we investigated the nature of the species obtained in the presence of the enzymatic oxidizing system HRP/H₂O₂. The formation of the new derivatives was followed by UV-Vis spectrometry upon HRP/H₂O₂ addition (Fig. 29, panel A and B). At first, we observed a rapid decrease of the shoulder around 300 nm, characteristic of **Oc-OH** and **Oc-OH-Tam**, together with the appearance of a peak at 323 nm in both spectra. The formation of these species was rapid ($t_{1/2}$ = 6.7 and 4.0 min for **Oc-OH** and **Oc-OH-Tam** derivatives, respectively). As apparent from Fig. 29, panel A and B, the UV-Vis spectra of the enzymatically-obtained species were also different from those of the corresponding quinone methides which showed peaks at 365 nm and 417 nm, respectively.

Since the two potent TrxR inhibitors obtained from **Oc-OH** and **Oc-OH-Tam** enzymatic transformation are not quinone methides, we hypothesized that a cessation of the reaction sequence at an earlier step than that of neutral quinone methide could be involved, and referable to a quinone methide cation (QM⁺) (Fig. 29, panel C). As already mentioned, osmium is the most effective element of the triad in stabilizing carbocations and radicals. Thus, QM⁺ can be obtained after a first oxidation of the complex, the removal of the phenolic proton and a second oxidation without the release of the last proton.

Taking into account the positive results obtained on the isolated enzyme, we moved to experiments *in cellulo*. The antiproliferative effect of the two complexes was determined on Jurkat cells in order to compare their activity to the one elicited by the previously studied TLMs. After 24 h incubation, **Oc-OH-Tam** exhibited a strong antiproliferative effect showing an IC₅₀ value of 7.4 μM, while **Oc-OH** was significantly less cytotoxic (IC₅₀ = 42 μM).

The effect of **Oc-OH** and of **Oc-OH-Tam** on the total TrxR and GR activities in Jurkat cells was then analyzed. In particular, based on the cytotoxic activity, Jurkat cells (2x10⁶) were incubated for 18 h with 50 μM of **Oc-OH** or 15 μM of **Oc-OH-Tam**, lysed and subjected to the estimation of the two enzymatic activities as described in Materials and Methods. As reported in Fig. 29, panel D, **Oc-OH-Tam** was far more effective than **Oc-OH** towards TrxR as, at 15 μM, it inhibited the enzyme activity by almost 70%, while **Oc-OH**, even at a higher concentration (50 μM), was only slightly effective. Conversely, the activity of GR was partially stimulated suggesting a selectivity of the two complexes for TrxR. The stimulatory effect on GR probably derived from the induction of its expression as a consequence of the cellular redox imbalance. Notably, the two osmium compounds, incubated in the same conditions described above, did not inhibit TrxR activity in the non-tumor cell line HEK293 (data not shown), indicating some selectivity for cancer cells. This result can be due to different uptake capacity of the two cellular models or, more probably, depend on the selective activation of the complexes to their active metabolites only in cancer cells, which are characterized by a higher basal ROS production.

Afterwards, the thiol redox state of both cytosolic and mitochondrial thioredoxins (Trx1 and Trx2), the principal substrates of TrxRs, was examined in Jurkat cells incubated in the same conditions utilized for the analysis of the enzymatic activities (50 μM **Oc-OH** or 15 μM **Oc-OH-Tam** for 18 h). The redox Western blot method, specific for thiol oxidation states, was used (see Materials and Methods). As shown in Fig. 29, panel E, **Oc-OH-Tam** appeared extremely effective in inducing the oxidation of both Trx1 and Trx2 while **Oc-OH** only partially increased their oxidation. Prx3 redox state was also determined in the same experimental conditions. Upon cell incubation with **Oc-OH-Tam**, the dimeric form of Prx3, corresponding to its oxidized state, was prevalent, as shown in Fig. 29, panel E. Conversely, **Oc-OH** was completely unable to stimulate the oxidation of Prx3.

Since the whole thioredoxin system seemed to be impaired, ROS production was estimated in Jurkat cells monitoring CM-H2DCFDA fluorescence over 2 h from the addition of the complexes to the cellular media (Fig. 29, panel F and F'). Accordingly to the results obtained so far, **Oc-OH-Tam** was more effective than **Oc-OH** in triggering ROS production as shown by both the kinetic curves (Fig. 29, panel F) and ROS quantification at 120 min (Fig. 29, panel F').

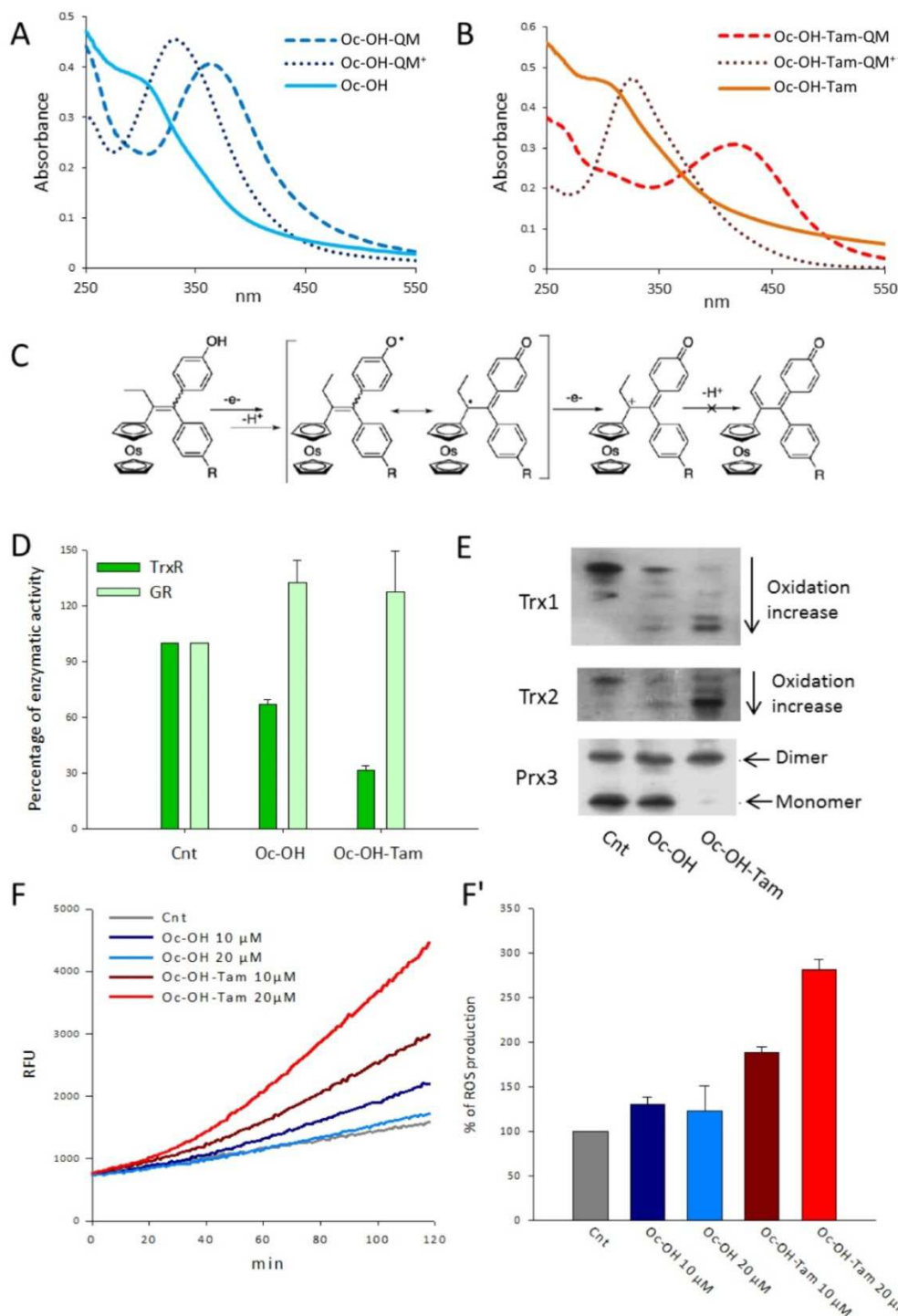


Fig. 29 Action of the osmium complexes and of their derivatives *in vitro* and in cancer cells. **(A)** Superimposition of the UV-Vis spectra of **Oc-OH**, **Oc-OH-QM** and of its derivative generated by enzymatic oxidation **Oc-OH-QM⁺**. **(B)** Superimposition of the UV-Vis spectra of **Oc-OH-Tam**, **Oc-OH-Tam-QM** and of the species formed by the HRP/H₂O₂ system **Oc-OH-Tam-QM⁺**. **(C)** Proposed scheme of the oxidation sequence of **Oc-OH** and **Oc-OH-Tam**. **(D)** TrxR (dark green bars) and GR (light green bars) activities in Jurkat cell lysates. Jurkat cells (2×10^6) were incubated for 18 h with **Oc-OH** (50 μM) or **Oc-OH-Tam** (15 μM), lysed and the activities of the two redox enzymes were estimated, mean \pm SD of 3 experiments. **(E)** Redox state of Trx1, Trx2 and Prx3. Jurkat cells (2×10^6), treated for 18 h with the two complexes in the same conditions reported in **D**, were subjected to redox Western blot analysis as

reported in Materials and Methods. The bands correspond to the different oxidation states of Trx1 or Trx2 and Prx3. (**F**, **F'**) Estimation of cellular ROS production after Jurkat cells treatment with the two osmium compounds. 4×10^4 cells were incubated in PBS/10 mM glucose medium in the presence of 1 μ M CM-H2DCFDA and osmium complexes at the indicated concentrations; (**F**) Kinetic curves of fluorescence increase, RFU = relative fluorescent units; (**F'**) Percentage of ROS production obtained after 120 min of incubation; mean \pm SD of 3 experiments (* = $p < 0.05$; ** = $p < 0.01$; *** = $p < 0.001$).

In order to determine whether mitochondria are targeted by the two complexes, their effect on the mitochondrial membrane potential (MMP) were studied in Jurkat cells. Interestingly, **Oc-OH-Tam** was effective in decreasing the MMP after 18 h of incubation at the concentration of 15 μ M (Table 11). **Oc-OH** (50 μ M) could also affect mitochondria but to a minor extent.

Table 11: Percentages of Jurkat cells with high and low MMP after treatment with 50 μ M **Oc-OH** or 15 μ M **Oc-OH-Tam** for 18 h

	Percentage of cells (%) [*]	
	high MMP	low MMP
Cnt	81.95 \pm 4.8	18.1 \pm 4.8
Oc-OH	61.5 \pm 10.9	38.8 \pm 10.6
Oc-OH-Tam	2.95 \pm 0.05	97.6 \pm 0.64

* Mean \pm SD of five experiments

Finally, we evaluated the cellular uptake of the two osmium complexes. In particular, quantification of osmium in whole cells (1×10^7) incubated for 24 h in the presence of **Oc-OH** (50 μ M) or **Oc-OH-Tam** (15 μ M) was performed by ICP-OES as described in Materials and Methods. Interestingly, the amount of osmium is higher in cells incubated with 15 μ M of **Oc-OH-Tam**, the most cytotoxic complex, than in cells incubated with 50 μ M of **Oc-OH** (Table 12). This result indicates that **Oc-OH-Tam** is more efficiently internalized by the cells and that probably the lateral amino-chain has a role in favoring the uptake of the complex in the cell.

Table 12: ICP-OES quantification of osmium in Jurkat cells after incubation with **Oc-OH** or **Oc-OH-Tam**

Compound	Amount of Os in the sample (ppb) [*]	Amount of Os per cell (fmol)
Oc-OH	796 \pm 6	3.9
Oc-OH-Tam	855 \pm 5	4.2

* Mean of 3 measurements, Cnt < 50 ppb

In conclusion, the results show that the two osmium complexes behave differently from their iron analogues. In fact, we observed the formation of quinone methide carbocations as active metabolites instead of quinone methides. In addition, the iron complexes had similar effects on cell viability, whereas, in the osmium series, **Oc-OH-Tam** displayed a higher cytotoxicity with respect to **Oc-OH**. The antiproliferative activity of the two compounds was dependent on their different cellular uptake. In fact, the entrance in the cell was shown to be larger for **Oc-OH-Tam** with respect to **Oc-OH** indicating that the amino-chain is important in the process of compounds' internalization. Once inside the cell, the two complexes can be converted into their active species able to inhibit TrxR activity. Of note, the difference in cytotoxicity between the two complexes was consistent with their differential inhibitory effect on TrxR that, therefore, appeared as a pivotal cellular target. The high TrxR inhibitory activity of **Oc-OH-Tam**, hindering the electron flow in the system, triggered the oxidation of Trx1, Trx2 and Prx3 and it was associated to an increase of ROS production and decrease of mitochondrial membrane potential eventually leading to the death of cancer cells.

In order to investigate the role played by the metallocene unit in the activity of TLMs, we decided to compare the biological effects of the iron, osmium and ruthenium complexes bearing the lateral amino-chain namely **Fc-OH-Tam**, **Oc-OH-Tam** and **Rc-OH-Tam** (see Chart 4), with those of tamoxifen (**Tam**) and of its main metabolite 4-OH-tamoxifen (**OH-Tam**) formed by **Tam** hydroxylation mediated by cytochromes P450 CYP2D6 and CYP3A.⁴²⁶ As already mentioned, the complexes endowed with the amino-chain are the most cytotoxic on cancer cells especially for the osmium series.

We started by assessing their effects on isolated TrxR1 and TrxR2 before and after transformation with the HRP/H₂O₂ mixture. As reported in Table 13, the organic **Tam** and **OH-Tam** were completely inactive on both TrxR1 and TrxR2. The ruthenium compound had never been tested before for its inhibitory effect on thioredoxin reductases. Interestingly, **Rc-OH-Tam** alone was even less active than the iron and the osmium complexes on both TrxR isoforms. Strikingly different results were obtained when the TLMs were enzymatically oxidized by 22 nM HRP and 0.1 mM H₂O₂ for 15 min prior to the incubation with TrxR. Indeed, upon oxidation, **Rc-OH-Tam** became a potent inhibitor of TrxR1 showing an IC₅₀ value of 0.42 μM in line with the values previously found for **Fc-OH-Tam** and **Oc-OH-Tam** derivatives. **Tam** remained inactive after treatment with HRP/H₂O₂ while **OH-Tam** enzymatic oxidation led to a partial inhibition of TrxR1 (see Table 13).

Table 13: Inhibitory effect of the three TLMs and of tamoxifen and OH-tamoxifen (IC₅₀) on isolated cytosolic (TrxR1) and mitochondrial (TrxR2) thioredoxin reductases

Compound	IC ₅₀ (μM)		IC ₅₀ (μM) ^a	
	TrxR1	TrxR2	TrxR1	TrxR2
Tam	> 100	> 100	> 10	> 10
OH-Tam	> 100	> 100	8.7±1.1	> 10
Fc-OH-Tam	15±2	32±3	0.06±0.02	10.9±1.2
Oc-OH-Tam	40±3.5	23±3	1.2±0.1	4.5±0.8
Rc-OH-Tam	62±2	> 100	0.42±0.08	4.6±0.1

a) Compounds were incubated in 0.2 M Tris-HCl buffer (pH 8.1), with 22 nM HRP and 0.1 mM H₂O₂ for 15 min at 25°C and then added to the enzyme. Mean ± SD of three experiments is reported for each compound

As for the osmium complexes, the enzymatic oxidation of **OH-Tam**, **Fc-OH-Tam** and **Rc-OH-Tam** by the HRP/H₂O₂ system was monitored by UV-Vis spectrometry in order to identify the active species generated by their enzymatic oxidation. **OH-Tam** treatment with HRP/H₂O₂ led to the rapid disappearance of its characteristic band at 279 nm but no new peak appeared on the spectrum (Fig. 30, panel A). Accordingly, **OH-Tam** was already shown to generate unstable radical species that tend to polymerize after HRP-mediated oxidation.⁴²⁷ Thus, the transient radical species could be involved in the increased TrxR1 inhibitory capacity shown for **OH-Tam** upon its enzymatic transformation (Table 13). For **Fc-OH-Tam**, an intense band at 402 nm appeared after transformation, corresponding to the one observed with the quinone methide synthesized by chemical oxidation with Ag₂O (Fig. 30, panel B). Thus **Fc-OH-Tam** active derivative is the quinone methide (**Fc-OH-Tam-QM**) as already reported in literature.³⁴² This conversion corresponds to a 2-electron, 2-proton abstraction pathway. Upon oxidation with HRP/H₂O₂, **Rc-OH-Tam** displayed a band at 418 nm (Fig. 30, panel C) which we assigned to the trace typical of a quinone methide. Therefore, also the ruthenium complex reactive derivative is a quinone methide. As it appears from the spectra recorded, oxidation of all the compounds is rapid, with a slightly faster rate observed for the iron complex.

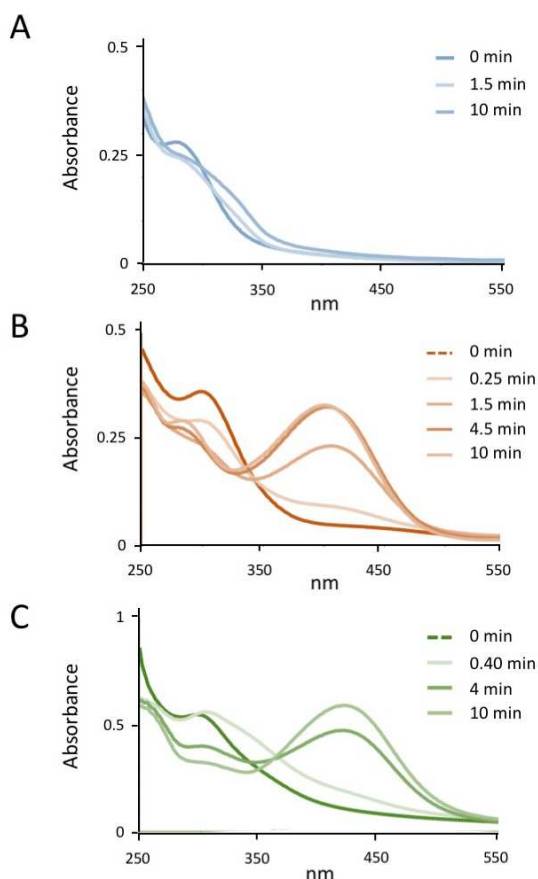


Fig. 30 UV-Vis spectra of **OH-Tam**, **Fc-OH-Tam** and **Rc-OH-Tam** and derivatives. Each complex was treated with 22 nM HRP and 0.1 mM H₂O₂ in 0.2 M Tris-HCl buffer (pH 8.1), 1 mM EDTA and the UV-Vis spectra were recorded at the indicated times (see Materials and Methods section for details). **(A)** Disappearance of the peak at 279 nm for **OH-Tam**. **(B)** Gradual appearance of a peak at 402 nm in the **Fc-OH-Tam** spectra characteristic of the QM. **(C)** Appearance of a peak at 418 nm in the **Rc-OH-Tam** spectra assigned to the formation of the quinone methide derivative.

To gain better insight into the mechanism of action of the three TLMs upon transformation by the HRP/H₂O₂ mixture, the BIAM assay was performed. Fig. 31, panel A and A' shows that very weak bands were observed for TrxR1 samples at pH 6 after treatment with the TLMs derivatives, while the organic analogues had no effect. This means that the three TLMs derivatives were able to interact with the selenol of TrxR. At pH 8.5, only oxidized **Oc-OH-Tam** partially decreased the band intensity, indicating an affinity also towards thiol groups. Of note, the HRP/H₂O₂ mixture alone had no effect on the ability of BIAM to alkylate TrxR1. Altogether the results obtained with the BIAM assay suggest that the three TLMs, once transformed into

their active derivatives, are able to target TrxRs by interacting with the Sec present in the catalytic site of the protein (and **Oc-OH-Tam** also with the Cys) whereas **Tam** and **OH-Tam** are almost completely ineffective, as expected from their inability of generating reactive species. The fact that the oxidation derivative of **Oc-OH-Tam** is a quinone methide carbocation and not the neutral quinone methide may provide a rationale for its higher reactivity with respect to the iron or ruthenium complexes.

At this point we compared the effects induced by the three TLMs with the ones elicited by their organic analogues **Tam** and **OH-Tam** against cancer cells. Jurkat cells (2×10^6) were incubated with each compound (15 μ M) for 18 h and the total TrxR activity was determined in cell lysates. A significant decrease of the total TrxR activity (60 to 95% inhibition) was observed in cells treated with the three TLMs while **Tam** and **OH-Tam** were not effective (data not shown). Next, we decided to measure separately the activity of TrxR1 and TrxR2 in order to investigate the potential different sensitivities of the two isoforms to the compounds *in cellulo*. For the isolation of the cellular mitochondrial fraction an important bulk of cells is necessary, thus we increased the amount of compounds in order to keep a ratio between the number of cells and the concentration of the complexes. The conditions were set at 30 μ M compounds on 3×10^7 Jurkat cells. At the end of incubation, cells were collected and subjected to sub-fractionation as reported in the Materials and Methods section. The cytosolic and mitochondrial cell fractions were then tested for TrxR1 and TrxR2 enzymatic activities, respectively. As apparent from Fig. 31, panel B, the effect of the three TLMs on TrxR1 was surprisingly modest, inducing only 25-36% of inhibition. In addition, the extent of TrxR1 hindrance was not much different from that of the organic compounds which led to a decrease of the enzymatic activity in the range of 12–21%. Conversely, a large inhibition of TrxR2 was observed for cells exposed to **Fc-OH-Tam** and **Rc-OH-Tam** (72% and 79.4% inhibition, respectively), followed by **Oc-OH-Tam** (44% inhibition). On the other hand, **Tam** and **OH-Tam** were significantly less effective on TrxR2 (up to 27% inhibition). This result is

particularly interesting because the extent of inhibition on the isolated enzymes was higher on TrxR1 for all the compounds, whereas in cells a striking selectivity towards TrxR2, especially for **Fc-OH-Tam** and **Rc-OH-Tam**, is apparent.

As the three TLMs induced a strong inhibition of TrxR2, the redox state of its main substrate, Trx2, was evaluated. Cells were incubated with each compound for 18 h (15 μ M on 2×10^6 cells) and subjected to the redox Western blot procedure (see Materials and Methods for details). In Fig. 31, panel C and C' the bands corresponding to the fully oxidized, the partially oxidized and the completely reduced form of Trx2 are shown. As one can see, the three TLMs induced Trx2 oxidation, especially **Fc-OH-Tam** for which almost all Trx2 was fully oxidized. Jurkat cells exposed to **Oc-OH-Tam** or **Rc-OH-Tam** displayed also a large Trx2 oxidation with more than 50% of the protein in the completely oxidized form for both the complexes. On the contrary, **Tam** and **OH-Tam** did not significantly alter Trx2 redox state and displayed a pattern of oxidation similar to the untreated cells. The data obtained for Trx2 redox state are in line with the previous results on TrxR2 inhibition with the organic tamoxifens being almost totally ineffective.

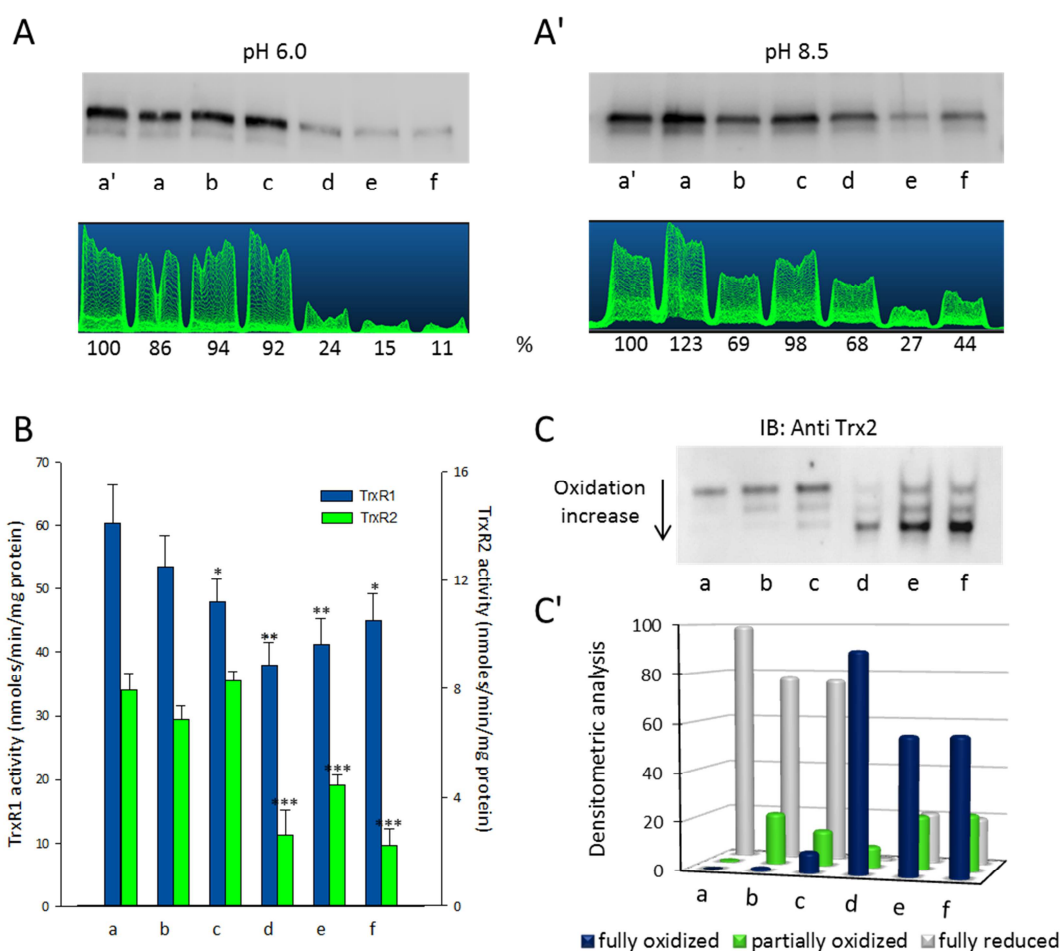


Fig. 31 Effect of TLMs on isolated TrxR1 and on cell lysates. (A, A') BIAM assay of TrxR1 treated with the various compounds after their oxidation with the HRP/H₂O₂ system. TLMs, **Tam** and **OH-Tam** (2 μ M) were treated with HRP/H₂O₂ for 15 min. A pre-reduced aliquot of TrxR1 was incubated with the oxidized derivatives and then with BIAM at pH 6.0 (A), or pH 8.5 (A'). BIAM conjugated enzyme was detected with a streptavidin-HRP conjugate as reported in the Materials and Methods section. (a') Cnt; (a) Cnt + HRP/H₂O₂; (b) **Tam** + HRP/H₂O₂; (c) **OH-Tam** + HRP/H₂O₂; (d) **Fc-OH-Tam** + HRP/H₂O₂; (e) **Oc-OH-Tam** + HRP/H₂O₂; (f) **Rc-OH-Tam** + HRP/H₂O₂. (B) TrxR1 and TrxR2 activities in Jurkat cells. Cytosolic and mitochondrial fractions were isolated from Jurkat cells treated with the various compounds (30 μ M/ 3×10^7 cells for 18 h), and TrxR1 (blue bars) and TrxR2 (green bars) activities were estimated as reported in the Materials and Methods section, mean \pm SD of 4 experiments (a) Cnt; (b) **Tam**; (c) **OH-Tam**; (d) **Fc-OH-Tam**; (e) **Oc-OH-Tam**; (f) **Rc-OH-Tam** (*= p<0.05; **= p<0.01; ***= p<0.001). (C) Redox state of Trx2 in treated cells. Jurkat cells (2×10^6) incubated for 18 h with 15 μ M TLMs or organic tamoxifens were lysed and subjected to IAM/IAA procedure to visualize the reduced, partially oxidized and fully oxidized protein, (a) Cnt; (b) **Tam**; (c) **OH-Tam**; (d) **Fc-OH-Tam**; (e) **Oc-OH-Tam**; (f) **Rc-OH-Tam**. (C') Densitometric analysis of the lanes shown in C performed using ImageJ software, mean \pm SD of 3 experiments.

Since the mitochondrial thioredoxin system was the most affected by TLMs in Jurkat cells, the effects of the compounds on the specific mitochondrial ROS production and on the mitochondrial membrane potential were determined. The mitochondrial superoxide production was measured by flow cytometric analysis using the MitoSOX Red probe. Cells were incubated with 15 μ M TLMs or organic tamoxifens for 18 h and then processed as reported in the Materials and Methods section. As apparent from Fig. 32, panel A, TLMs elicited a strong ROS production. **Fc-OH-Tam** was the most effective with 72% of cells analyzed showing high superoxide levels. Also in this case, the organic tamoxifens had no major effects in cells and did not significantly induce ROS production with respect to the control.

Then, the mitochondrial membrane potential (MMP) was evaluated by flow cytometry using the TMRM dye (Fig. 32, panel B). In particular, 2×10^6 cells were treated with the compounds (15 μ M) for different incubation times in order to see whether the effect of the complexes on mitochondrial functioning was an early or a late event after cell treatment. Interestingly, the impact of TLMs on mitochondria is gradual with **Fc-OH-Tam** being the most rapid, in accordance with its fast transformation into the active derivate and with its strong TrxR2 inhibitory activity in cells. Anyhow, after 18 h, the population of cells with a low MMP was close to 100% for cells incubated with each TLMs. Conversely, the organic tamoxifens affected the MMP to a much lower extent (up to 16% for OH-Tam at 18 h).

The collapse of the mitochondrial membrane potential is often associated to the release of pro-apoptotic factors into the cytosol and with the consequent activation of the intrinsic apoptotic pathway.²⁷² Therefore, localization of Cyt c and activation state of caspase 3 were examined in Jurkat cells exposed to 15 μ M TLMs or organic tamoxifens for 18 h. As clearly shown in Fig. 32, panel C, only TLMs triggered a massive release of Cyt c from mitochondria to the cytosol. In addition, pro-caspase 3 was no more detectable in cells exposed to TLMs as reported in Fig. 32, panel D, indicating that the enzyme had been activated by proteolytic cleavage. Thus, TLMs and not organic tamoxifens were able to trigger cell apoptosis by the activation of the intrinsic pathway.

Finally, the cellular distribution of the three TLMs was determined in order to confirm a potential mitochondrial accumulation capacity. In particular, the quantification of iron, osmium and ruthenium in the mitochondrial and cytosolic cell fractions was performed by ICP-OES analysis upon cell treatment with **Fc-OH-Tam**, **Oc-OH-Tam** or **Rc-OH-Tam**. Since iron is normally present in cells, its quantification was also assessed in untreated cells. The levels of iron, osmium and ruthenium relative to the single cell compartments were similar, indicating that the three TLMs were all able to enter the cell in comparable concentrations. As expected, the highest levels of the three metals were detected in mitochondria supporting a preferential accumulation in the mitochondrial cell fraction (Fig. 32, panel E).

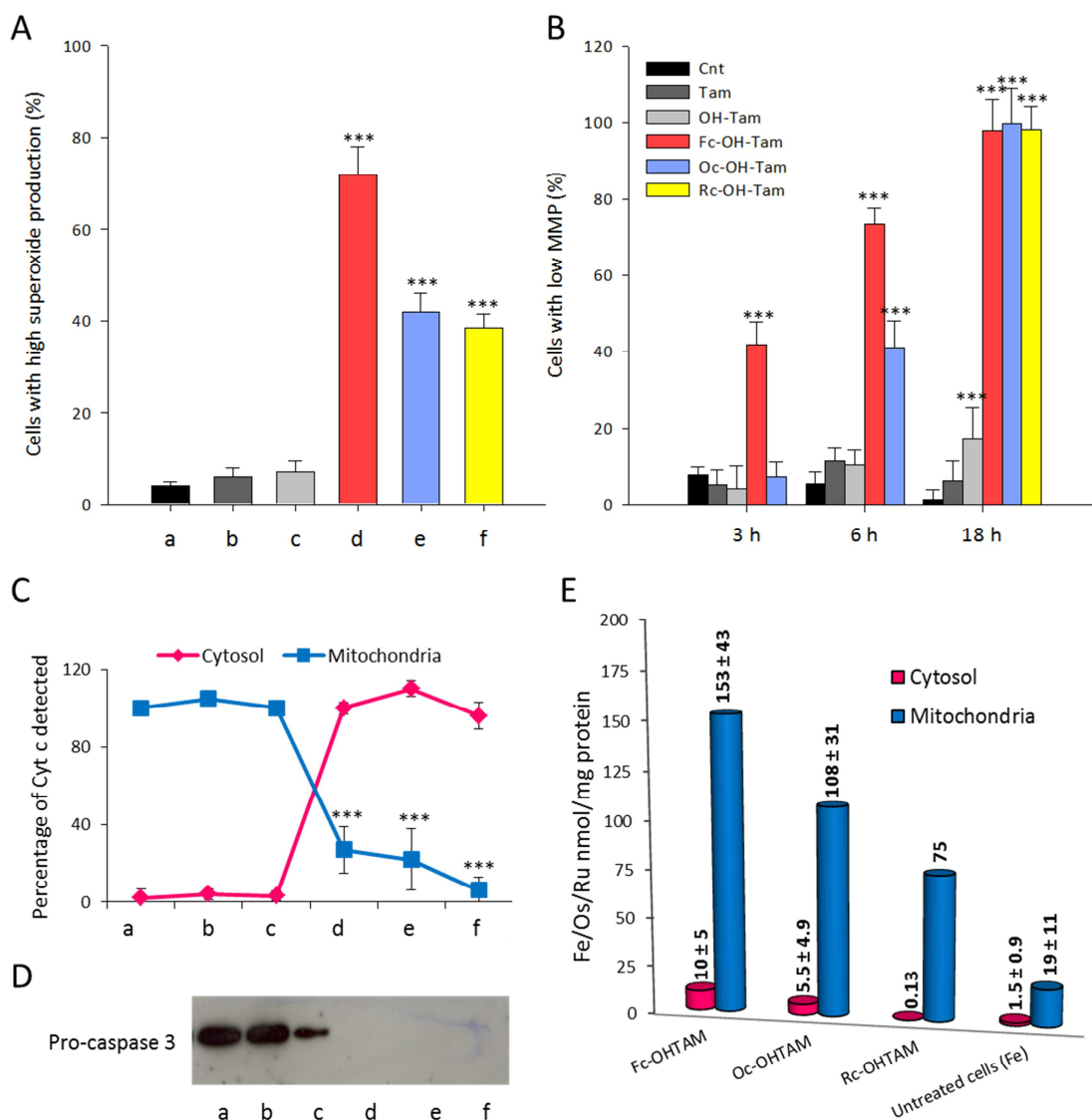


Fig. 32 Effects of TLMs and of organic tamoxifens on Jurkat cell mitochondria. **(A)** Consequences of TLMs and organic tamoxifens on mitochondrial superoxide production in Jurkat cells. Cells were treated for 18 h with the various compounds (15 μ M), then incubated in PBS/10 mM glucose in the presence of 1 μ M MitoSOX and subjected to the determination of superoxide production in flow cytometry. **(B)** Impact of TLMs and organic tamoxifens on mitochondrial membrane potential. Cells were treated with the compounds (15 μ M) for 3, 6 or 18 h. Then, aliquots of the cells were incubated in PBS/10 mM glucose in the presence of 25 nM TMRM and FACS analysis performed. **(C)** Release of Cyt c from mitochondria. Jurkat cells (2×10^6) were treated for 18 h in the presence of 15 μ M compounds. Afterwards, Cyt c localization was evaluated in both the cytosol and in mitochondria. **(D)** Western blot analysis of pro-caspase 3. (a) Cnt; (b) Tam; (c) OH-Tam; (d) Fc-OH-Tam; (e) Oc-OH-Tam; (f) Rc-OH-Tam. Mean \pm SD of 3 biological replicates for all the experiments was performed (*= $p < 0.05$; **= $p < 0.01$; ***= $p < 0.001$). **(E)** ICP-OES quantification of iron, osmium and ruthenium in the cytosol and mitochondria of Jurkat cells (3×10^7) incubated with 30 μ M Fc-OH-Tam, Oc-OH-Tam or Rc-OH-Tam for 18 h or of iron in untreated cells. Mean \pm SD of 3 replicates for Fc-OHTAM, two replicates of Oc-OHTAM and single experiment for Rc-OHTAM.

In conclusion, TLMs are mitochondriotropic complexes able to selectively target TrxR2 in Jurkat cancer cells. The dimethylamino group present in the lateral chain of TLMs is protonated at physiological pH, and is probably involved in their observed accumulation in mitochondria. In fact, the positive charge favors the translocation of the complexes into the negatively-charged mitochondrial matrix.²⁷⁴ The TLMs-mediated TrxR2 inhibition has been shown to trigger ROS production and mitochondrial dysfunction with the activation of the intrinsic apoptotic pathway. In contrast, organic tamoxifens are far less potent TrxR inhibitors and also less cytotoxic than metallocenes. This finding highlights the essential role of the metallocene unit for the biological activity of TLMs and for their pro-drug character.

4.3 Glutaredoxin 2 in the mitochondrial compartment: interplay between thioredoxin and glutathione systems

Glutaredoxin 2 (Grx2) is a small protein that modulates protein glutathionylation/de-glutathionylation processes.²¹⁹ The protein has mainly a mitochondrial localization but other splicing variants have been observed in the cytosolic and nuclear compartments.²²¹ In the mitochondrial matrix, Grx2 coordinates a 2Fe-2S cluster through its active site forming an inactive dimer stabilized by two molecules of glutathione. In addition, Grx2 was reported to connect the thioredoxin and the glutathione systems by receiving reducing equivalents by both GSH and TrxRs²²⁶ and by reducing, in turn, Trx2 and Prx3.²²⁷ Whether Grx2 is mostly active as a disulfide reductase or if it is mainly involved in the transport of iron and sulfur clusters is still not known. Therefore, we decided to study this enzyme in relation to the mitochondrial redox state in both cultured cells and in a mouse model specifically knockout for mitochondrial Grx2.

4.3.1 Grx2 response to oxidative stress in a cellular model

Based on evidences reporting a protective role of Grx2 from apoptosis,²²⁹ it has been hypothesized that this protein usually resides in the mitochondrial matrix as an inactive dimer and that it may sense redox imbalance getting activated upon oxidative stress induction. However, the protein redox state has never been observed in cells. Therefore, a classical pharmacological approach was utilized to establish oxidative stress in HeLa cells. In particular, the TrxRs inhibitor Af, the inhibitor of glutathione synthesis buthionine sulfoximine (BSO) and the glutathione depleting and oxidizing agent sodium selenite (Sel), were utilized alone or in combination in order to block the thioredoxin system, the glutathione system or both thiol redox regulating networks. Then, the monomeric and dimeric forms of the protein were detected by Western blot after cell lysis and thiol alkylation with AIS as reported in the Materials and Methods section. Untreated cells displayed Grx2 principally in the dimeric form (Fig. 33, lanes a and e) confirming the hypothesis of a dominant inactive condition of Grx2. Interestingly, the block of either the glutathione system by 1 mM BSO (lane b) or of the thioredoxin system by 1 μ M Af (lane c), did not significantly affect Grx2 redox state with respect to the control. Conversely, the concomitant inhibition of both thiol scavenging systems by the combination of BSO + Af or by 15 μ M Sel for 18 h, led to Grx2 monomerization as apparent from the increase intensity of the band corresponding to Grx2 monomer in lanes d and f. This result shows for the first time the redox state of Grx2 in cells and highlights that the hindering of both thiol redox systems is necessary for the induction of its monomerization.

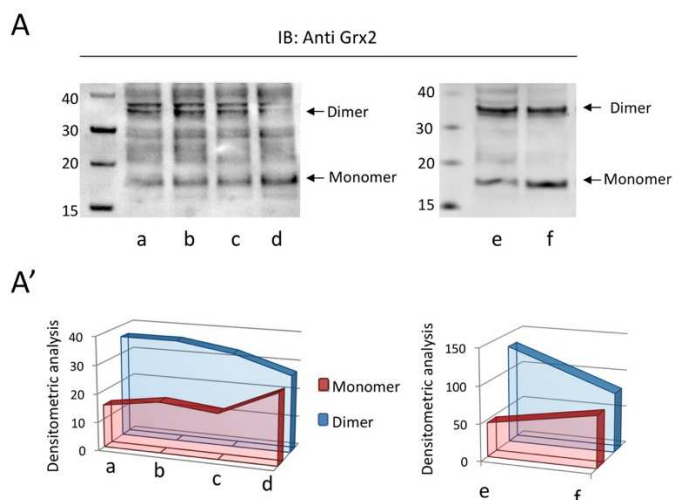


Fig. 33 Determination of Grx2 monomeric/dimeric state in HeLa cells under different oxidative conditions. HeLa cells (4.5×10^5) were treated for 18 h with 1 μ M Af, 1 mM BSO, the combination Af + BSO or with 15 μ M Sel. To analyze the monomerization of Grx2, whole cell samples incubated in the different conditions, were derivatized with 10 mM AIS, subjected to SDS-PAGE in non-reducing conditions and stained with an anti-Grx2 antibody (see Materials and Methods for details). (A) Western blot analysis of Grx2 monomer/dimer ratio; (A') Densitometric analysis of data reported in panel A performed with ImageJ software. (a, e) Cnt; (b) 1 mM BSO; (c) 1 μ M Af; (d) 1 mM BSO + 1 μ M Af; (f) 15 μ M Sel.

Treatment with Sel was the most effective in inducing Grx2 monomerization. Therefore, we decided to utilize it for the following experiments. In order to check Grx2 monomer/dimer ratio in the mitochondrial compartment avoiding possible interferences of the cytosolic/nuclear isoforms of the enzyme, we isolated the mitochondrial cell fraction from HeLa cells incubated with 15 μM Sel for 18 h, and subjected them to the same procedure utilized for the whole cell lysates. The result obtained is shown in Fig. 34, panel A and A'. In isolated mitochondria, the induction of Grx2 monomerization was even clearer since Sel treatment led to an almost complete conversion of the dimer into the monomeric form of the protein. This process is probably addressed to the rescue of the redox balance specifically in mitochondria and further supports the sensitive cross-talk between Grx2 and both the mitochondrial redox systems. The same Western blot membrane was also incubated with an antibody raised against glutathione. Interestingly, we observed that the glutathione moiety was detected only in correspondence to the dimeric form of Grx2 as expected from the fact that two molecules of glutathione are involved in the stabilization of the protein-cluster complex,²²² while no staining was shown for the monomer or in cells treated with Sel (Fig. 34, panel B). As GSH bound to the complex was reported to be in continuous exchange with the pool of free GSH,²²³ oxidative stress conditions, leading to an alteration of GSH/GSSG ratio, can likely cause the disassembly of the cluster. Thus, we determined the glutathione amount and redox state in HeLa cells treated for 18 h with increasing concentrations of Sel up to 20 μM . As shown in Fig. 34, panel C, a marked decrease of the total glutathione pool was measured, accompanied by a large increase of the relative amount of oxidized glutathione (GSSG). In addition, in cells treated in the same conditions also total thiols decreased (Fig. 34, panel D) in line with glutathione depletion. This indicates that glutathione oxidation induced by Sel can be sensed by Grx2 dimer possibly through the oxidation and removal of the two GSH molecules involved in the stabilization of the complex.

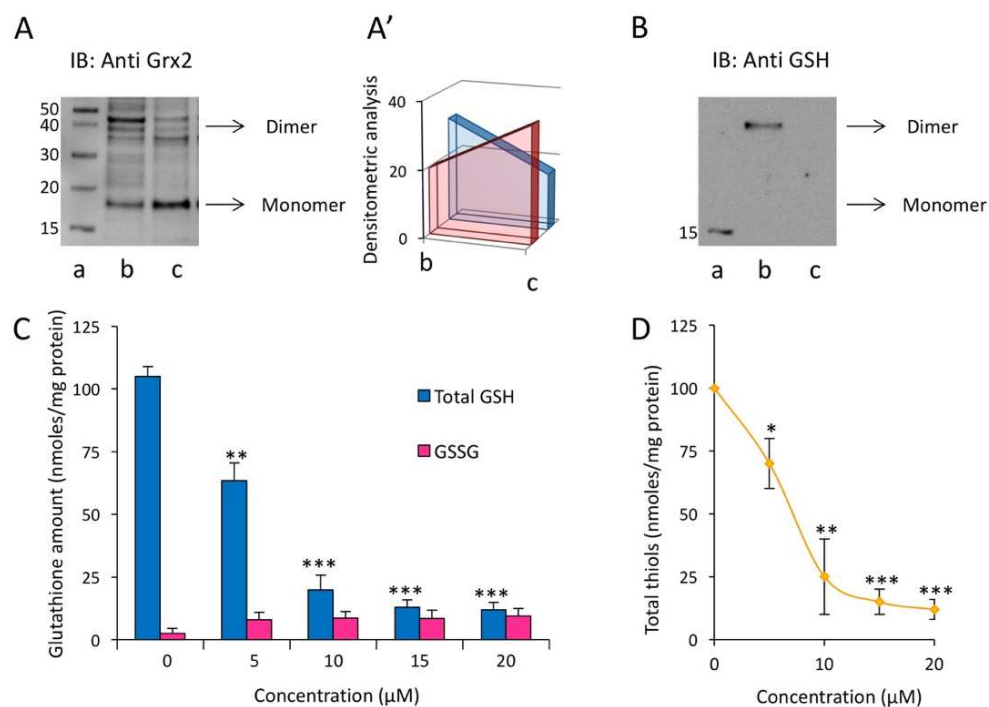


Fig. 34 Mechanism of Grx2 monomerization upon HeLa cells treatment with Sel. **(A)** Determination of Grx2 monomerization in mitochondrial cell fractions. HeLa cells (3×10^7) were treated for 18 h with 15 μM Sel. Then, mitochondria were isolated and derivatized with 10 mM AIS, subjected to SDS-PAGE in non-reducing conditions and analyzed by Western blot. (a) Markers; (b) Cnt; (c) 15 μM Sel; **(A')** Densitometric analysis of data reported in panel **A** performed with ImageJ software. **(B)** Determination of protein-bound glutathione. HeLa cells were processed as reported in **A** and the membrane was probed with an anti-GSH antibody. (a) Markers; (b) Cnt; (c) 15 μM Sel. **(C)** Determination of glutathione amount and redox state. HeLa cells (4.5×10^5) were treated for 18 h with increasing concentrations of Sel (5-20 μM). At the end of incubation, cells were processed and total (Total GSH) and oxidized (GSSG) glutathione levels were assessed, mean \pm SD of 3 experiments. **(D)** Measurement of total thiols in HeLa cells treated in the same conditions reported in **C**, mean \pm SD of 3 experiments. (*= $p < 0.05$, **= $p < 0.01$, ***= $p < 0.001$).

In order to see whether Grx2 gets activated upon monomerization, we analyzed its specific activity in mitochondria. Thus, mitochondria were isolated from Sel treated (15 μ M for 18 h) or control HeLa cells, and the specific glutaredoxin activity was determined in the mitochondrial cell compartment over time as described in the Materials and Methods section. In particular, Grx2 enzymatic activity was measured after 3, 6, 12 or 18 h from Sel administration in order to monitor its response to oxidative stress. Interestingly, Grx2 activity showed an initial slight decrease, followed by a significant increase of about 30% at 18 h (Fig. 35, panel A), which coincided with the time when protein monomerization occurred. The overall amount of protein did not change after Sel administration neither in the mitochondrial nor in the cytosolic cell compartments when cell fractions were lysed and subjected to SDS-PAGE in reducing conditions and Western blot analysis (Fig. 35, panel B). This finding further supported the idea that the observed increase of protein activity was due to the disassembly of Grx2 dimer and not from an increased protein expression. We also evaluated the impact of cell treatment with Sel on TrxR2 specific activity. As shown in Fig. 35, panel C, TrxR2 activity was initially stimulated but then dropped at longer incubation times. It is interesting to note that Grx2 activity inversely correlates with the one of TrxR2. In fact, the initial stimulation of TrxR2 was associated to a decrease of Grx2 activity, while the further progressive decrease of TrxR2 activity seemed to be balanced by an increase of Grx2 thiol reducing action. Once again these data suggest that Grx2 can sense the redox state of both the thioredoxin and the glutathione systems getting activated when the residual scavenging activity of both systems falls under a certain threshold. Notably, in the cytosol, the total glutaredoxin and TrxR1 activities were not remarkably affected (Fig. 35, panel D), indicating that the role of Grx2 in response to oxidative stress is probably limited to the mitochondrial compartment. We also evaluated the direct effect of Sel on purified human recombinant Grx2 activity and we observed that Sel treatment up to 20 μ M did not alter Grx2 activity (data not shown).

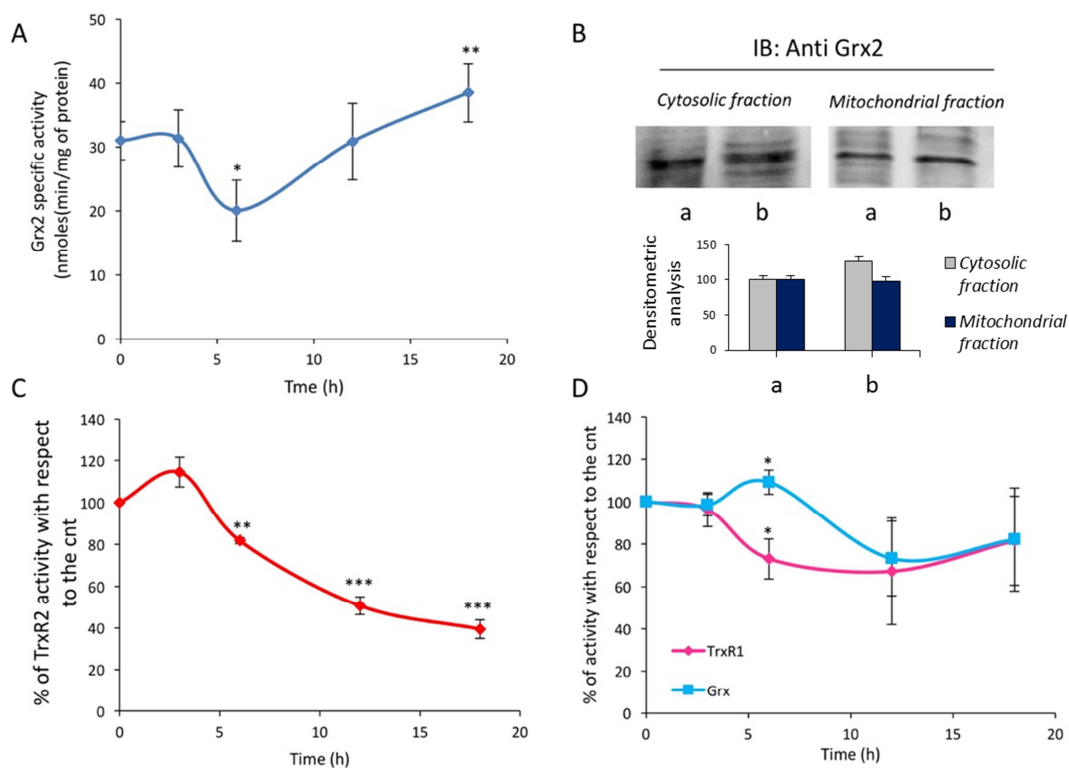


Fig. 35 Enzymatic activities and Grx2 amount in mitochondrial and cytosolic cell compartments of Sel treated or control HeLa cells. HeLa cells (3×10^7) were treated for 3, 6, 12 or 18 h with 15 μ M Sel and then subjected to cell sub-fractionation in order to obtain cytosol and mitochondria enriched fractions. **(A)** Grx activity in the mitochondrial cell fraction determined as reported in Materials and Methods, mean \pm SD of 5 experiments. **(B)** Grx2 overall protein level in the two cellular compartments. Densitometric analysis performed with NineAlliance software is reported. (a) Cnt; (b) 15 μ M Sel. **(C)** Time-scale analysis of TrxR2 activity in mitochondrial cell fractions, mean \pm SD of 5 experiments. **(D)** TrxR1 and total cytosolic glutaredoxin activities measured in Sel treated cells, mean \pm SD of 5 experiments. (*= $p < 0.05$, **= $p < 0.01$, ***= $p < 0.001$).

Since Grx2 activation implies the drop of the 2Fe-2S cluster, which is coordinated through a Cys in Grx2 active site, we decided to analyze whether the cluster is released inside the mitochondrion upon redox imbalance. Therefore, the labile iron pool, namely the amount of metal not bound to proteins, was measured in mitochondria isolated from Sel treated or control cells by atomic absorption as described in Materials and Methods. Graphite furnace atomic absorption involves the vaporisation of samples in a graphite coated furnace in order to atomise the sample. Free atoms of a specific element (for this study, iron) will absorb light at characteristic wavelengths and the absorption at this wavelength is linearly proportional to the amount of that element present in the specimen. Table 14 reports the quantity of free iron normalized for the protein content in the mitochondrial fraction of control or Sel treated (15 μ M for 18 h) cells. As one can note, the amount of free iron ions was extremely increased in mitochondria isolated from treated cells supporting our hypothesis of a release of the 2Fe-2S clusters, concomitantly with Grx2 monomerization.

Table 14: Amount of labile iron ions in the mitochondrial fractions of Sel treated (15 μ M for 18 h) or control HeLa cells

	μ g Fe/mg protein*
Cnt	11.8 \pm 6.3
Sel 15 μ M	24.1 \pm 15.1

* Mean \pm SD of three experiments

It is well known that free iron ions can have deleterious effects in the cell as they can easily induce lipid peroxidation. The increase of free iron and lipid peroxidation are associated to a particular mechanism of cell death called ferroptosis.¹⁶⁹ Thus, the lipid peroxidation level in HeLa cells after Sel treatment was estimated by flow cytometry technique utilizing the BODIPY-C11 fluorescent dye. In addition, the malondialdehyde production was also measured. As shown in Fig. 36, panel A and B, with both methods cells treated with 15 μ M Sel for 18 h displayed an increase in lipid peroxidation with respect to control cells. A different sensitivity between the two methods was observed and may be explained by the fact that malondialdehyde is a late product of the lipid peroxidation process and may need a longer incubation time. We further analyzed the status of the mitochondrial membrane potential (MMP) which is known to be affected by cardiolipin oxidation.⁶¹ As expected, the MMP was largely affected in Sel-treated cells (Fig. 36, panel C) probably as a result of the iron-induced peroxidation of lipids in the mitochondrial membrane.

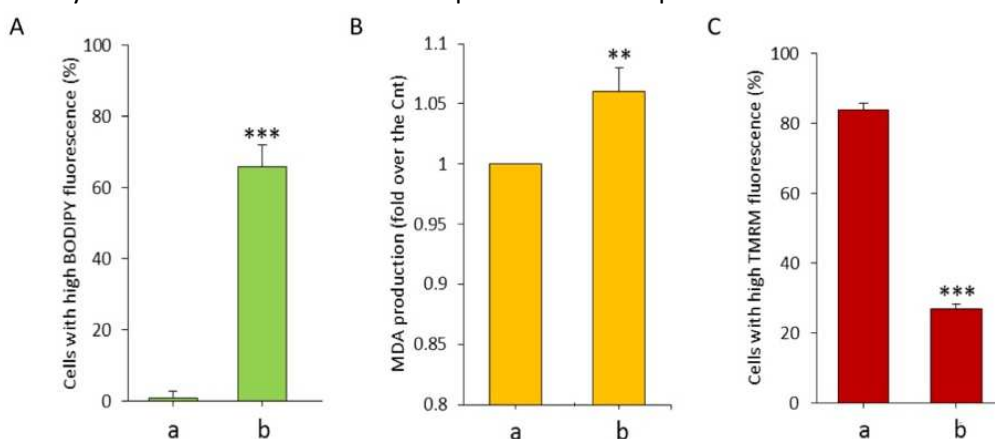


Fig. 36 Effects of iron release in mitochondria. HeLa cells (4×10^5) were treated with 15 μ M Sel for 18 h and then subjected to the different experiments. **(A)** FACS analysis of lipid peroxidation measured in HeLa cells with the BODIPY-C11 fluorescent dye (see Materials and Methods for details), the percentage of cells displaying high fluorescence corresponding to a high level of lipid peroxidation is shown. **(B)** MDA production measured in HeLa cells reported as fold over the control. **(C)** Percentage of HeLa cells with high MMP determined in flow cytometry using TMRM probe. (a) Cnt; (b) 15 μ M Sel. Mean \pm SD of 3 biological replicates for all the experiments. (**= $p < 0.01$, ***= $p < 0.001$).

In conclusion, we have found that, in cells, Grx2 resides in the mitochondrial matrix as an inactive dimer in homeostatic conditions, coordinating a 2Fe-2S cluster. Upon oxidative stress induction by the concomitant inhibition of the thioredoxin and the glutathione systems, the complex can sense the redox imbalance via the two molecules of glutathione that normally stabilize the dimer, and gets disassembled. The monomeric Grx2 was shown to be active as a disulfide reductase. The release of the iron and sulfur cluster instead, by increasing the amount of free iron ions in mitochondria, induced lipid peroxidation and, consequently, a drop of the mitochondrial membrane potential. This result is in agreement with a previous finding indicating that, in dopaminergic neurons, Grx2 knockdown by siRNA resulted in a significant increase of labile iron pool levels in mitochondria.²²³ In addition, disturbed iron homeostasis has been recently identified as cell death mechanism in Parkinson's disease.⁴²⁸ Therefore, mitochondrial Grx2 redox state and activity could be also involved in neurodegenerative disorders.

4.3.2 Effects deriving from mitochondrial Grx2 deletion in mice

Following the appealing results obtained in cultured cells we decided to delve more deeply into the role of Grx2 in mitochondria functioning moving to an *in vivo* murine model, in collaboration with Prof. A. Holmgren's group from the Department of Medical Biochemistry and Biophysics at the Karolinska Institutet in Stockholm (S). Therefore, the effects deriving from the specific deletion of mitochondrial Grx2 were investigated. The C57bl/6 inbred mouse strain was generated by the selective deletion of Grx2 mitochondrial-targeting sequence encoded by exons 1a, 1c and 2 in GRX2 gene, leading to a mouse model whole body knockout for Grx2 in the mitochondrial compartment (see Materials and Methods for details).

4.3.2.1 Determination of Grx2 amount and activity in mGrx2 KO mouse mitochondria

At first, we checked the actual absence of the protein in mitochondria. In particular, we performed both a RT-PCR of Grx2 mRNA in order to establish the effective deletion of the first exons, and a Western blot analysis to highlight the absence of the protein in the mitochondrial compartment. As reported in Fig. 37, panel A and A', Grx2 mRNA isolated from both the brain and the liver of mGrx2 KO mice, clearly lacked the first exons. In addition, as expected, the Western blot analysis confirmed the absence of Grx2 in mitochondria of mGrx2 KO mice (Fig. 37, panel B), whereas it was still expressed in the cytosol as in wild-type (WT) animals (Fig. 37, panel B'). Moreover, we measured the total glutaredoxin activity in both the mitochondrial and the cytosolic cell compartments after their isolation from the liver, brain, heart and kidneys of WT and KO mice at 3 months of age (see Materials and Methods for details). As apparent from Fig. 37, panel C, glutaredoxin activity was decreased in mGrx2 KO mitochondria with respect to their WT counterparts. Interestingly, Grx2 activity did not show the same extent of decrease in the mitochondrial fractions isolated from the various organs. In particular, mGrx2 KO heart mitochondria did not display statistically significant differences in glutaredoxin activity in comparison to the WT. This unexpected result might be explained by the fact that the assay can also titrate the activities of other 2-Cys glutaredoxins present in the mitochondrial lysate. In particular, glutaredoxin 1 (Grx1), which is the most abundant representative of the family of Grx enzymes, is highly efficient in catalyzing the reduction of HEDS, the synthetic substrate utilized in the activity assay. Grx1 usually resides in the cytosol but it can also enter the mitochondrial intermembrane space (IMS)²⁰⁹ and has a critical role specifically in heart mitochondria. Indeed, a decrease of Grx1 protein level in the IMS by 50-60% was reported in elderly rats and was associated to their increased susceptibility to ischemia/reperfusion damage.²¹⁴ Altogether these data may explain the residual Grx activity measured in the various mitochondrial fractions and particularly in the

heart. The total glutaredoxin activity was also measured in the cytosolic fractions of WT and mGrx2 KO mice and no significant differences were found for any of the organs studied (Fig. 37, panel C').

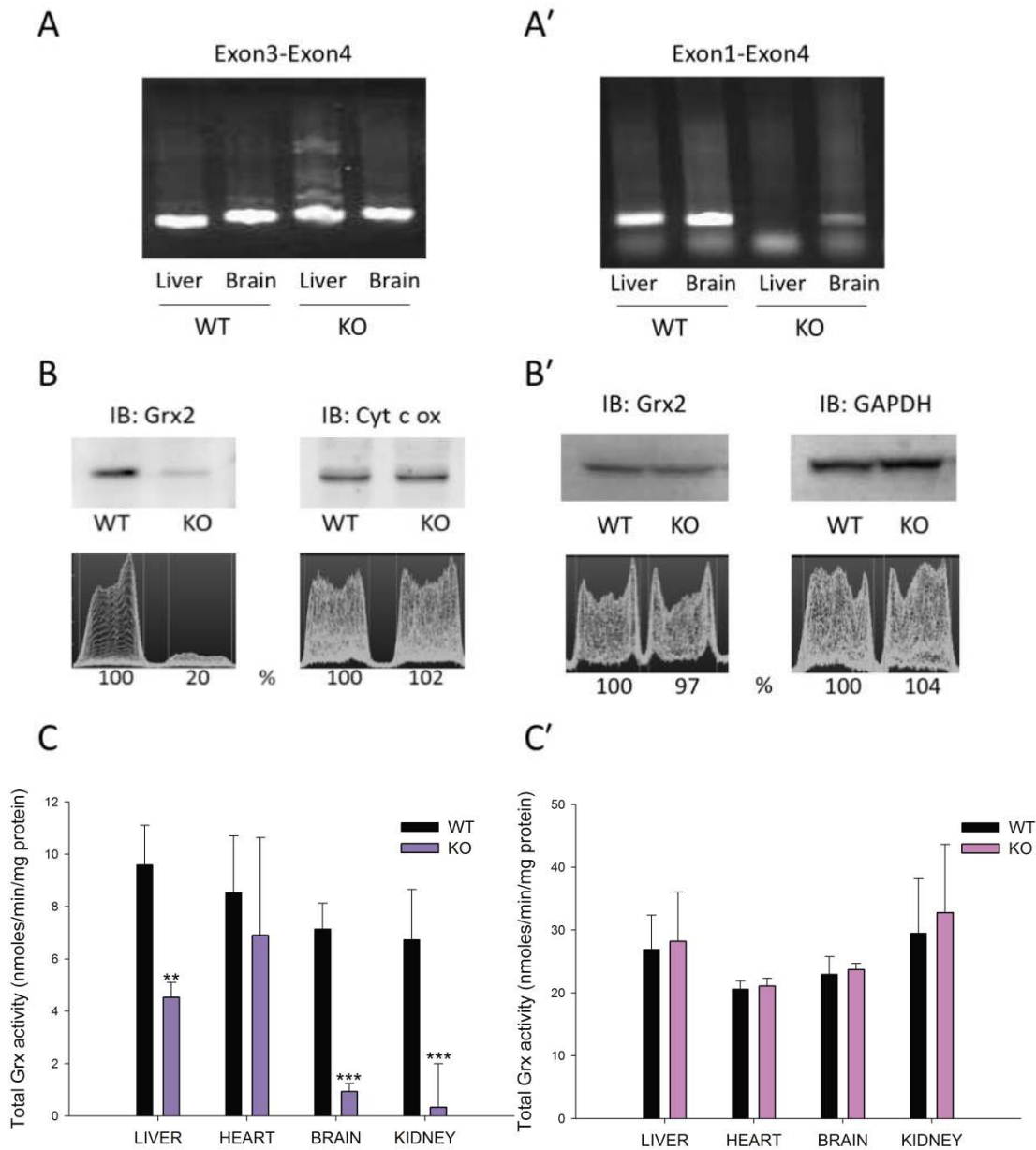


Fig. 37 Determination of Grx2 amount and activity in mGrx2 KO mice in comparison to WT animals. (**A, A'**) RT-PCR analysis of Grx2 mRNA (see Materials and Methods for details). (**A**) DNA bands corresponding to the exon 3-4 transcript; (**A'**) Bands corresponding to the exon 1-4 transcript. (**B, B'**) Western blot analysis and densitometric analysis of Grx2 protein level in the mitochondrial (**B**) and in the cytosolic (**B'**) mouse liver fractions. Cyt c oxidase and GAPDH are reported as loading controls for the mitochondrial or cytosolic compartments, respectively. (**C**) Total glutaredoxin activity of mouse mitochondria isolated from liver, heart, brain and kidneys of WT or mGrx2 KO mice. Mitochondria were isolated with differential centrifugations and Grx activity was assessed on 50 μ g of proteins as reported in the Materials and Methods section. Mean \pm SD of 8 experiments, n= 24; (**C'**) Total glutaredoxin activity of mouse cytosolic fractions isolated from liver, heart, brain and kidneys of WT or mGrx2 KO mice and assessed as reported in **C**. Mean \pm SD of 8 experiments, n= 24. (** = p<0.01; *** = p<0.001).

4.3.2.2 Analysis of the mitochondrial redox state

We next investigated whether the absence of Grx2 in mitochondria could affect the overall redox state of the subcellular organelle by determining total thiols and glutathione amount in mitochondria. Mice were sacrificed at 3 months of age, organs were explanted and subfractionated as described in Materials and Methods. As shown in Fig. 38 neither the total thiols nor the glutathione amount were significantly different between WT and mGrx2 KO mitochondria. However, both parameters are lower in mGrx2 KO mitochondria in all the organs analyzed, indicating a trend towards a more oxidized condition. Therefore, by increasing the size of the sample, a statistically significant difference between WT and mGrx2 KO mitochondria could possibly emerge.

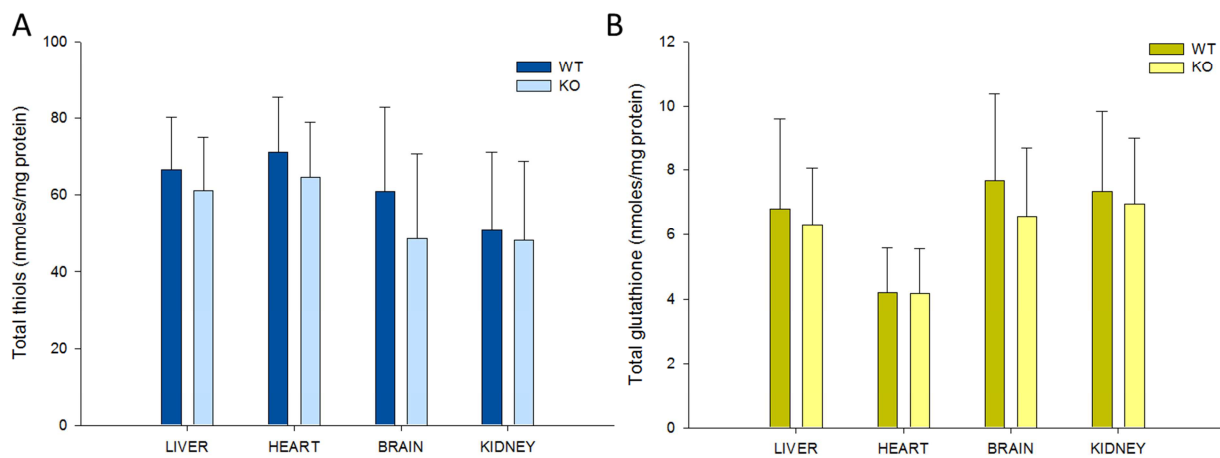


Fig. 38 Total thiols and glutathione amount of WT and mGrx2 KO mouse liver, heart, brain and kidney mitochondria. **(A)** Total thiols determined on 0.25 mg of mitochondrial proteins as described in Materials and Methods. **(B)** Glutathione content (GSH + GSSG) measured on 0.5 mg of mouse mitochondria. Mean \pm SD of 6 experiments, n= 18.

Since no major variations were observed in the overall mitochondrial redox state, we hypothesized that the absence of Grx2 could be compensated, in mGrx2 KO mice, by the increased expression/activity of other enzymes involved in thiol redox regulation. Thus, we measured the thioredoxin reductase and glutathione reductase activities in both the mitochondrial and the cytosolic compartments isolated from WT and mGrx2 KO liver, heart, brain and kidneys. As reported in Fig. 39 TrxR1, TrxR2 and GR activities were quite similar between WT and mGrx2 KO mice. Notably, a slight increase of both TrxR1 and GR activities were found in mGrx2 KO mice only in the kidneys, suggesting a possible organ-specific effect deriving from the lack of Grx2. The study of elderly mice could be useful in order to understand whether the mild effects on the overall redox state observed in young mice could worsen during aging. In fact, young animals are known to face better oxidative stress conditions with respect to the elderlies.

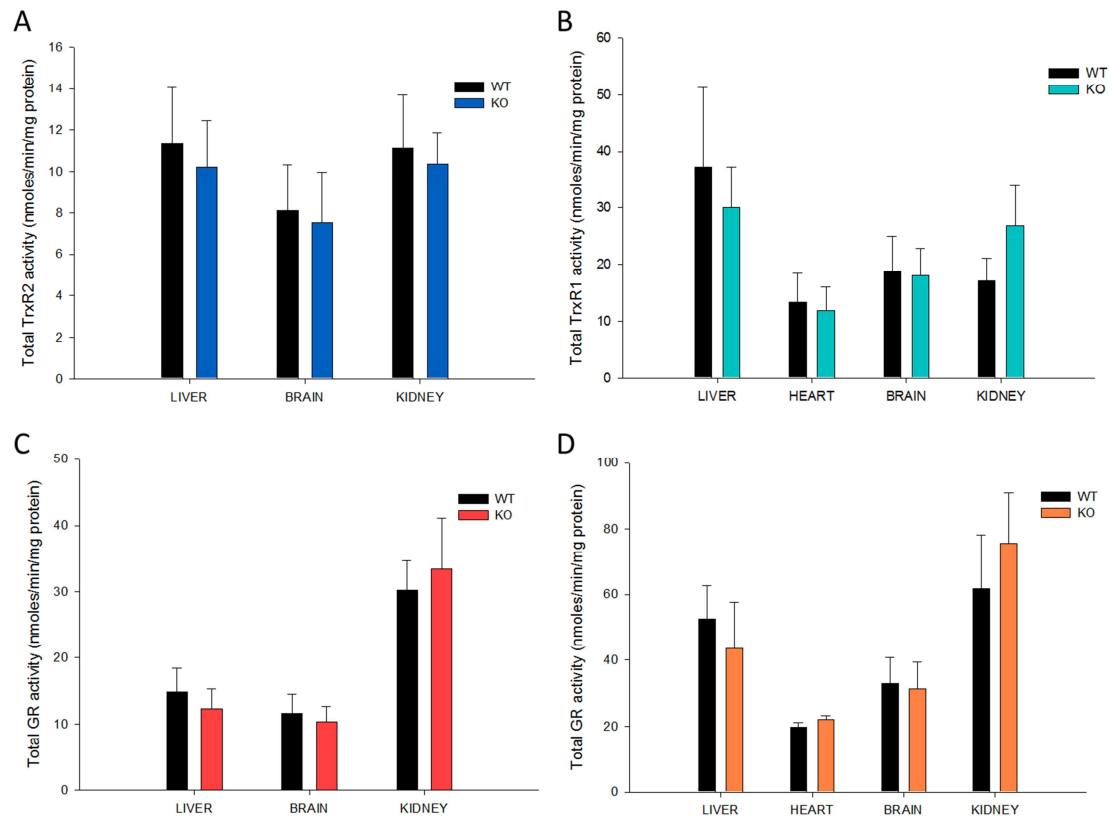


Fig. 39 TrxR and GR activities in the cytosolic and mitochondrial fractions. (A) TrxR2 specific activity determined in the mitochondrial fractions on 50 μ g of proteins (see Materials and Methods for details). (B) TrxR1 specific activity determined in the cytosolic fractions on 50 μ g of proteins. (C) GR specific activity determined in the mitochondrial fractions on 50 μ g of proteins. (D) GR specific activity determined in the cytosolic fractions on 50 μ g of proteins. Mean \pm SD of 8 experiments, n= 24.

Comparing the liver of mGrx2 KO mice at 3 months of age with the one of WT animals, we observed a clear increase in lipid deposition as apparent from its enlarged and off-white appearance (Fig. 40, panel A). Interestingly, we also observed that mGrx2 KO liver mitochondria showed an increased basal ROS production with respect to WT liver mitochondria (Fig. 40, panel B and B') indicating that the absence of Grx2 specifically impacts on the redox homeostasis of this organ. Therefore, we focused on the liver and we tried to understand the effects linking mGrx2 deletion to fatty liver development.

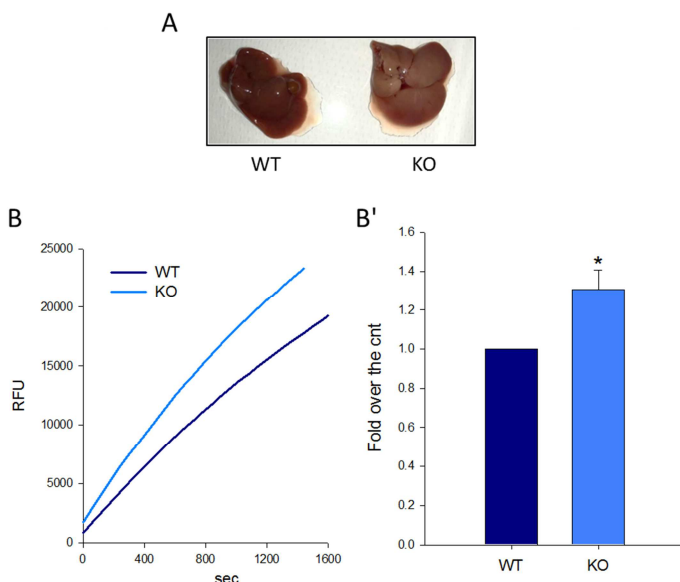


Fig. 40 Comparison of liver appearance and ROS production between WT and mGrx2 KO mice. (A) Picture of WT (left) and mGrx2 KO (right) livers explanted from mice at three months of age. (B, B') ROS production of WT and mGrx2 KO mouse liver mitochondria measured on 0.125 mg proteins using the AmplexRed dye as described in Materials and Methods section. (B) Kinetic curves of basal ROS production, RFU = relative fluorescent units; (B') Quantification of ROS levels reported in fold over the control (WT) after 1200 sec. Mean \pm SD of 3 experiments, n= 10 (* = p<0.01).

4.3.2.3 Study of liver mitochondria functioning

The functioning of mGrx2 KO mouse liver mitochondria was investigated. At first, the oxygen consumption of liver mitochondria was determined polarographically using a Clark electrode as described in Materials and Methods. Different substrates were employed and the control-index values (ratio between state 3/state 4 rates) were determined. This index outlines the tightness of the coupling between respiration and oxidative phosphorylation. mGrx2 KO mouse liver mitochondria showed a lower respiratory capacity with respect to WT mitochondria with both substrates (succinate or glutamate/malate) when assessed in the presence of low concentrations of EGTA (20 μ M), while their respiratory capacity was comparable to the WT when all the endogenous calcium was chelated (1 mM EGTA). Fig. 41, panel A, reports the control index values of WT or mGrx2 KO mouse liver mitochondria determined utilizing either succinate or glutamate + malate as oxidizable substrates in the presence of 20 μ M EGTA.

Accordingly, the mitochondrial membrane potential of mGrx2 KO liver mitochondria was lower with respect to WT mitochondria when assessed in the presence of low amount of EGTA or in the absence of the calcium chelator, while no statistically significant differences were observed in the presence of 1 mM EGTA (Fig. 41, panel B). This result fits perfectly with the data on mitochondrial respiration and suggests an increased sensitivity of mGrx2 KO mouse liver mitochondria to calcium ions.

Thereafter, the mitochondrial sensitivity to calcium was assessed by means of the swelling assay (see Materials and Methods for details). As apparent from Fig. 41, panel C and D, mGrx2 KO liver mitochondria are more easily subjected to swelling as shown from the rapid decrease of absorbance at 540 nm upon calcium addition (40 μ M CaCl_2 in buffer containing 20 μ M EGTA).

In conclusion, mGrx2 KO mice did not show major alterations in mitochondrial redox balance in most of the organs tested nor a compensatory increase of activity/expression of other enzymes involved in thiol redox regulation. However, the liver of these mice, already at three months of age, appeared filled up with lipid deposits. Measuring ROS production of liver mitochondria we observed a rise of the basal ROS level upon mGrx2 deletion. Moreover, an increased sensitivity to calcium ions of mGrx2 KO liver mitochondria with respect to WT was shown. The association to the metabolic syndrome of altered levels or dysregulated function of many proteins involved in redox regulation in mitochondria, is in accordance with the observed phenotype. However, the exact mechanism linking Grx2 deletion with the alterations in liver functions and fatty liver development has not been elucidated yet. A possible implication of sirtuins or of iron and sulfur cluster handling capacity could be envisaged and should be investigated.

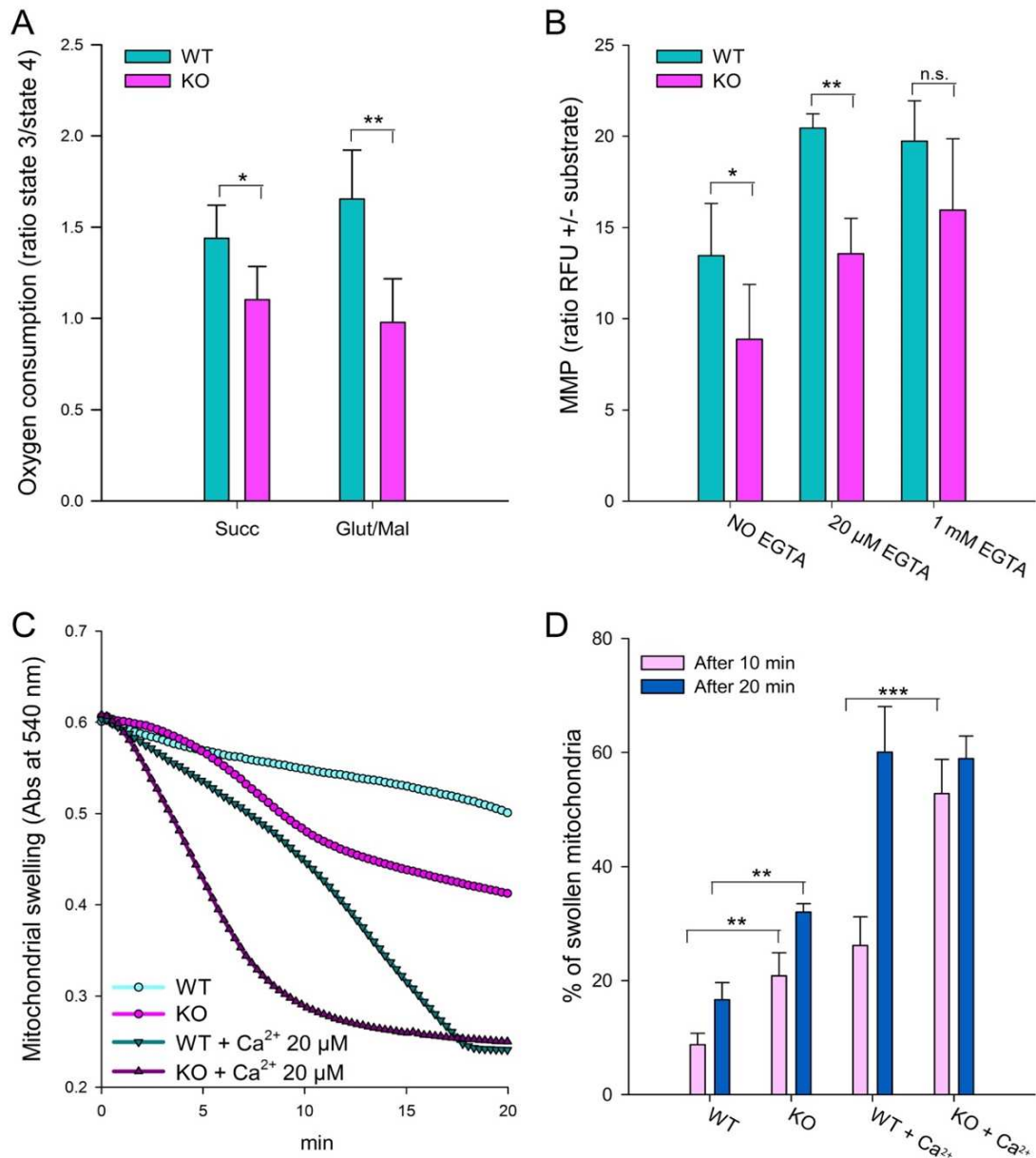


Fig. 41 Effect of mGrx2 deletion on mouse liver mitochondria functioning. **(A)** Mitochondrial respiratory capacity of WT and mGrx2 KO mouse liver mitochondria was measured polarographically on 1 mg proteins, as described in Materials and Methods. The control-index values obtained with either succinate (Succ) or glutamate/malate (Glut/Mal) in the presence of 20 μM EGTA are shown. **(B)** Mitochondrial membrane potential of mouse liver mitochondria measured on 0.125 mg of proteins, reported as ratio of relative fluorescence unit (RFU) of the probe rhodamine 123 before and after substrate addition (5 mM succinate) in the presence of increasing concentrations of EGTA (0-1 mM). **(C, D)** Swelling assay performed in the presence of 5 mM succinate, 20 μM EGTA on 0.25 mg of mouse liver mitochondria with or without treatment with 40 μM CaCl₂. Mean ± SD of 6 experiments, n = 18, (n.s. = not significant, * = p<0.05, ** = p<0.01, *** = p<0.001).

5. Conclusions

The role of different mitochondrial proteins involved in thiol redox regulation in relation to normal or dysregulated cell physiology was investigated. The principal conclusions obtained from the research presented in this thesis are outlined below.

5.1 Mitochondrial thioredoxin system mediates redox regulation

- *Cyclophilin D is redox regulated by the mitochondrial thioredoxin system*
The peptidyl prolyl *cis-trans* isomerase activity of CypD was stimulated by the presence of the complete thioredoxin system. In addition, analysis of CypD redox state highlighted that the inhibition or depletion of TrxR2 led to a concomitant oxidation of Trx2, Prx3 and CypD, suggesting a cross-talk between these proteins. This result was obtained in both rat heart mitochondria and cultured human cell lines. A molecular binding prediction was also performed and pointed out that CypD interacts with both Trx2 and Prx3 through its CsA binding pocket where a conserved Cys is located. Co-immunoprecipitation technique from rat heart mitochondrial matrix was employed to confirm the binding capacity of CypD with both Trx2 and Prx3. Interestingly, the addition of CsA partially hindered this interaction indicating the involvement of the CsA binding pocket of CypD. Moreover, CypD co-immunoprecipitated with Trx2 also from a Trx2-overexpressing cell line. Considering the importance of CypD as the unique recognized factor modulating the mitochondrial permeability transition, the redox control dependent on the thioredoxin system appears critical for the overall mitochondrial functioning.⁴²⁹
- *TrxR2 controls ROS production*
Taking advantage of the Crispr-Cas9 technique, a few stable TrxR2 knockdown cell lines were generated. The cellular ROS production was measured in the various TrxR2 knockdown clones and was observed to inversely correlate to the amount of TrxR2. The result indicates that TrxR2 depletion is promptly followed by a large increase of ROS species suggesting a direct involvement of TrxR2 in ROS handling.

5.2 TrxR2 inhibition and consequences in cancer cells

- *The benzimidazole-4-carboxamide Au(III) complex inhibits both PARP-1 and TrxRs*
The inhibitory capacity of a new cytotoxic benzimidazole-4-carboxamide Au(III) complex on PARP-1 and TrxRs activities was studied. Various biological and biochemical assays showed that the compound is a potent inhibitor of PARP-1 and, to a lower extent, of TrxR while it does not affect GR activity. Accordingly, the intracellular glutathione redox state was almost not affected. Notably, the double inhibition of PARP-1 and TrxR can be synergic in determining the observed cytotoxicity on cancer cells and may potentiates the activity of DNA-damaging agents, such as alkylators, platinum compounds, topoisomerase inhibitors, and radiation. Thus, this complex seems promising as a possible anticancer metallodrug with a double cellular target.⁴³⁰
- *Diphenylpyridine Au(III) complexes show different cytotoxicity depending on the ligand*
Three novel diphenylpyridine Au(III) complexes were studied for their TrxR and GR inhibitory capacity and for their antiproliferative effects in a small panel of human cancer cells. The

complexes appeared to selectively inhibit isolated cytosolic and mitochondrial TrxRs, with respect to the homologous enzyme GR. Notably, compound **3** was the only one showing good cytotoxic properties and was particularly active against the 2008 ovarian cancer cell line. In addition, compound **3** was able to inhibit TrxR in 2008 cells, increasing Trxs oxidation and leading to the disruption of the overall cellular redox state by decreasing the amount of free thiols and enhancing glutathione oxidation. Therefore, a central role of the ancillary ligands in the observed anticancer effects has been outlined and may be useful in the field of the metallodrugs' design.⁴³¹

- *Hydroxylated mono-carbenic Au(I) complexes display promising anticancer activities*
Different novel mono- and di-nuclear Au(I) complexes featuring sulfonated bis-carbenic ligands and a series of hydroxylated mono-carbenic Au(I) compounds were comparatively evaluated for their inhibitory activity on TrxR and GR. Notably, the sulfonated bis-carbenic Au(I) complexes were mild inhibitors of TrxR, whereas the mono-carbenic compounds (**5-7**) were selective against TrxR over GR, showing IC₅₀ values in the nanomolar range of concentrations. The mechanism of TrxR inhibition involved the binding of the Au(I) center to Sec in the enzyme active site as shown from the BIAM assay. The mono-carbenic compounds were tested also on the human ovarian cancer cell line 2008 and a correlation between TrxR binding capacity and the cytotoxic effect was observed.⁴³² However, a poor stability in cell culture media was outlined probably due to their inactivation mediated by serum proteins. Thus, in order to improve complex stability, the carbene scaffold could be derivatized with targeting molecules such as antibodies or proteins.
- *TLMs give rise to different active metabolites and behave as pro-drugs*
Various complexes deriving from tamoxifen structure and endowed with a metallocene unit were tested for their inhibitory activity on both TrxR isoforms. All the compounds analyzed were mild inhibitors of TrxRs but acquired a potent inhibitory capacity upon enzymatic oxidation with the HRP/H₂O₂ mixture. The oxidation derivative of **Fc-OH-Tam** was shown to be the most active, having an IC₅₀ value in the range of those measured for Au(I) complexes (IC₅₀=0.06 μM on isolated TrxR1). The active derivatives of the complexes were then identified and corresponded mostly to quinone methides except **ansaFc** and **Oc-OH-Tam** that originated a radical species and a quinone methide cation, respectively. The oxidation derivatives were able to alkylate the Sec in TrxR active site irreversibly, inhibiting the enzyme. It has also been shown that, once inside the cell, probably thanks to the activity of cytochrome P-450, the complexes effectively undergo conversion to their active species able to inhibit TrxR activity and thus TLMs can be defined as pro-drugs. This selective activation inside cancer cells could be a good strategy to avoid side-effects *in vivo*.⁴³³⁻⁴³⁵
- *TLMs bearing the amino-chain accumulate in mitochondria*
The first clue suggesting the importance of the amino-chain for the compounds' activity in cells was the observed higher cytotoxicity displayed by **Oc-OH-Tam** with respect to **Oc-OH**. In fact, the cytotoxicity of osmium compounds was found to depend on their cellular uptake from culture media that was larger for **Oc-OH-Tam** indicating that the amino-chain has a role in the process of compounds' internalization. The ICP-OES analysis of the TLMs distribution in the different cell compartments confirmed a mitochondrial accumulation for all the complexes endowed with the chain. Therefore, we can assume that the amino chain, positively-charged at physiological pH, favors their mitochondrial accumulation in a mitochondrial membrane potential-driven fashion. Thus, TLMs endowed with the amino-chain can be defined as mitochondriotropic agents.⁴³⁵

- *TLMs induce the activation of the intrinsic apoptotic pathway*
In Jurkat cells, TLMs were shown to preferentially inhibit the mitochondrial TrxR leading to the oxidation of its main substrate Trx2. Afterwards, their impact on mitochondrial functioning was assessed and alteration of the MMP, overproduction of ROS, release of Cyt c and activation of the caspase pathway were observed, indicating an induction of the intrinsic apoptotic pathway. This may have to do with CypD oxidation and its role in the regulation of the mitochondrial permeability transition process.⁴³⁵

5.3 Role of Grx2 in mitochondrial thiol redox regulation

- *Grx2 gets activated upon concomitant disruption of the thioredoxin and the glutathione systems*
For the first time in cells, Grx2 has been shown to be enzymatically inactive in homeostatic conditions forming dimers in mitochondria by coordinating a 2Fe-2S cluster. Oxidative stress was found to induce Grx2 activation through the disassembly of the dimer only in the mitochondrial compartment. Interestingly, Grx2 monomerization was induced by the concomitant impairment of both the thioredoxin and glutathione systems. Thus, Grx2 is able to sense the mitochondrial redox state and seems to get activated in strong oxidizing conditions probably through the detachment of the two molecules of glutathione involved in the stabilization of the dimer. Then, the labile iron pool was determined in order to analyze whether the 2Fe-2S was released from Grx2 dimer disassembly in mitochondria. As expected, the amount of free iron ions was largely increased upon Grx2 monomerization in the cellular mitochondrial fraction. In addition, the newly released iron ions were shown to induce lipid peroxidation and eventually to affect the mitochondrial membrane potential.
- *mGrx2 KO mice show fatty liver and impaired liver mitochondria functioning*
In order to determine the role of Grx2 in the mitochondrial redox balance, a C57bl/6 mouse strain knockout for Grx2 in mitochondria was characterized. The genetic excision of the mitochondrial targeting sequence of Grx2 was employed in order to generate the mouse model lacking Grx2 specifically in the mitochondrial compartment. No major alterations in the overall mitochondrial redox homeostasis were observed in different organs isolated from three months-old mice with respect to WT mice. Mitochondria isolated from the liver, kidney, brain and heart were subjected to the determination of total thiols, glutathione amount and enzymatic activities of TrxR2 and GR and no significant differences were observed between WT and mGrx2 KO animals. However, mGrx2 KO mice displayed fatty liver. Thus, mGrx2 KO mouse liver mitochondria were checked for their functioning. Notably, mGrx2 KO liver mitochondria were found to have an increased ROS production, decreased oxygen consumption capacity and decreased mitochondrial membrane potential in the absence of a calcium chelator. Interestingly, mGrx2 KO liver mitochondria displayed also a higher sensitivity to calcium as shown from the swelling assay. Altogether, these preliminary results indicate that the lack of Grx2 in the mitochondrial compartment is responsible for the development of an early-onset fatty liver in which a decrease of mitochondrial activity associated to an increased sensitivity to calcium is implicated. A possible alteration in lipid synthetic pathway or in their catabolism could be envisaged.

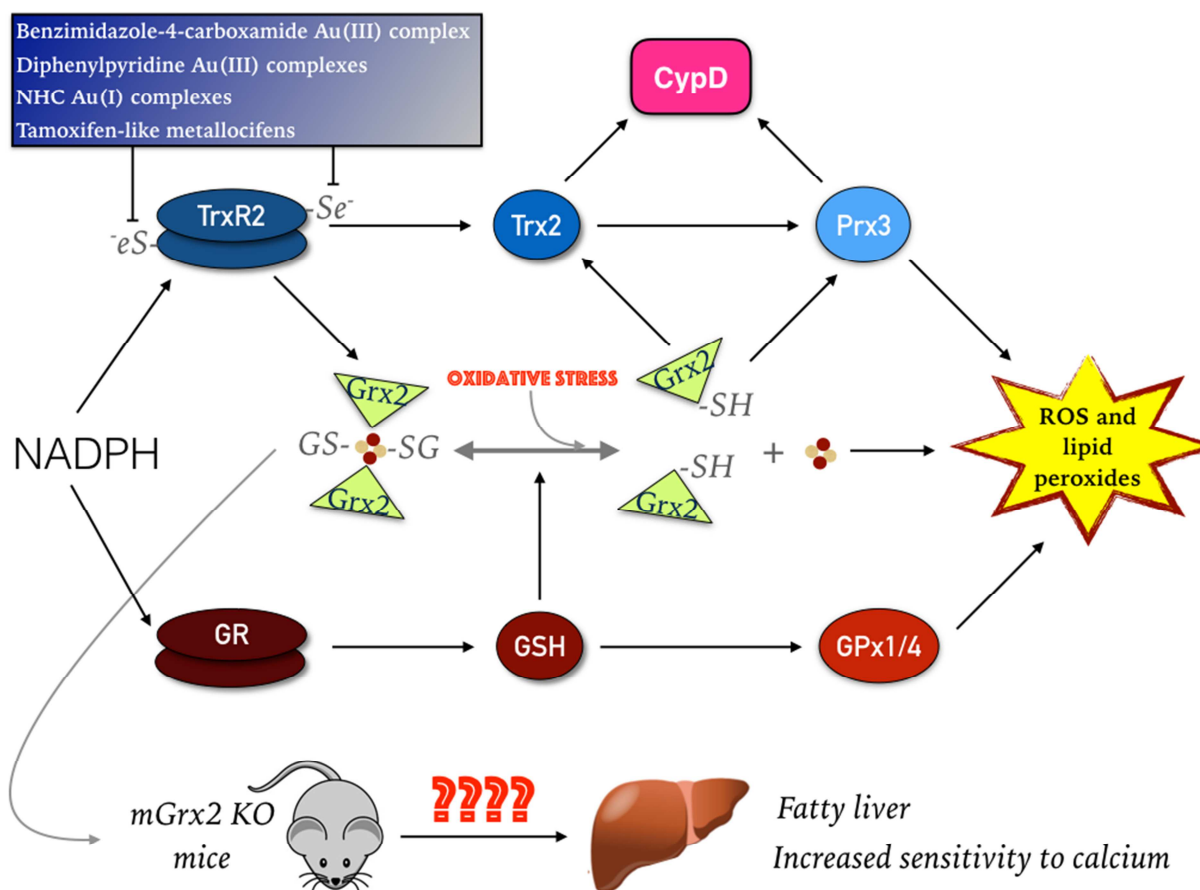


Fig. 42 Summary of the principal results presented in this thesis. The picture shows the two thiol redox regulating networks present in the mitochondrial cell compartment. The different classes of novel TrxR inhibitors studied are reported, and their interaction with the Sec present in the active site of TrxR is highlighted. The redox regulation of CypD by the mitochondrial thioredoxin system is displayed and, in particular, the observed interaction of CypD with both Trx2 and Prx3 is shown. Regarding Grx2, it has been found to get activated in mitochondria upon oxidative stress conditions and hindering of both the thioredoxin and the glutathione pathways. Its activation implies the release of the 2Fe-2S cluster leading to an increased lipid peroxidation. Finally, a mouse model KO for mGrx2 has been studied. Fatty liver and increased sensitivity to calcium, associated to an increase of ROS production, has been observed specifically for mouse liver mitochondria.

Part of the results presented in this thesis have already been published (see publication list) or are currently being processed for the preparation of manuscripts for later submission and publication. The future perspectives are principally aimed to earn a more complete knowledge on the significance of redox signaling in the mitochondrial compartment. The search for new proteins undergoing redox regulation by the thioredoxin system in mitochondria will be a major issue. In addition, the role of Grx2 in mitochondrial thiol redox regulation will be further explored in both cultured cells and mice. *In vivo*, we will study the mechanism linking Grx2 depletion to fatty liver development. The identification of this mechanism could possibly help also for the understanding of the metabolic syndrome etiopathogenesis. Finally, novel and more selective TrxR inhibitors will be tested for their possible application as anticancer drugs searching in particular for mitochondriotropic molecules.

6. List of publications

1. Folda A, Citta A, **Scalcon V**, Cali T, Zonta F, Scutari G, Bindoli A, Rigobello MP (2016). Mitochondrial Thioredoxin System as a Modulator of Cyclophilin D Redox State. *Sci. Rep.* 6:23071. doi: 10.1038/srep23071
2. **Scalcon V**, Top S, Lee HZ, Citta A, Folda A, Bindoli A, Leong WK, Salmain M, Vessières A, Jaouen G, Rigobello MP (2016). Osmocenyl-tamoxifen derivatives target the thioredoxin system leading to a redox imbalance in Jurkat cells. *J Inorg Biochem.* 160:296-304. doi: 10.1016/j.jinorgbio.2016.04.005
3. Citta A*, **Scalcon V***, Göbel P, Bertrand B, Wenzel M, Folda A, Rigobello MP, Meggers E, Casini A (2016). Toward anticancer gold-based compounds targeting PARP-1: a new case study. *RSC Advances.* 6:79147-79152. doi: 10.1039/c6ra11606j *these two authors contributed equally.
4. **Scalcon V**, Citta A, Folda A, Bindoli A, Salmain M, Ciofini I, Blanchard S, de Jesús Cázares-Marinero J, Wang Y, Pigeon P, Jaouen G, Vessières A, Rigobello MP (2016). Enzymatic oxidation of ansa-ferrocifen leads to strong and selective thioredoxin reductase inhibition in vitro. *J Inorg Biochem.* 165:146-151. doi: 10.1016/j.jinorgbio.2016.08.005.
5. **Scalcon V**, Salmain M, Folda A, Top S, Pigeon P, Shirley Lee HZ, Jaouen G, Bindoli A, Vessières A, Rigobello MP (2017) Tamoxifen-like metallocifens target the thioredoxin system determining mitochondrial impairment leading to apoptosis in Jurkat cells. *Metallomics.* 9:949-959. doi: 10.1039/c7mt00121e.
6. Jürgens S, **Scalcon V**, Estrada-Ortiz N, Folda A, Tonolo F, Jandl C, Browne DL, Rigobello MP, Kühn FE, Casini A (2017) Exploring the C^NC theme: synthesis and biological properties of tridentate cyclometalated gold(III) complexes. *Bioorgmedchem. Bioorg Med Chem.* 25:5452-5460. doi: 10.1016/j.bmc.2017.08.001.
7. Karaca Ö*, **Scalcon V***, Meier-Menches SM, Bonsignore R, Brouwer JM JL, Tonolo F, Folda A, Rigobello MP, Kühn FE, Casini A. (2017) Characterization of Hydrophilic Gold(I) N-Heterocyclic Carbene (NHC) Complexes as Potent TrxR Inhibitors Using Biochemical and Mass Spectrometric Approaches. *Inorg Chem.* 56:14237-14250. doi: 10.1021/acs.inorgchem.7b02345 *these two authors contributed equally.
8. **Scalcon V**[#], Bindoli A, Rigobello MP[#]. (2018) Significance of the mitochondrial thioredoxin reductase in cancer cells: An update on role, targets and inhibitors. *Free Radic Biol Med.* 127:62-79. doi: 10.1016/j.freeradbiomed.2018.03.043 [#]= co-corresponding authors
9. **Scalcon V**, Tonolo F, Gandin V, Folda A, Bindoli A, Rigobello MP. (2018) Glutaredoxin 2 senses selenite-induced changes of the redox condition and can get activated in mitochondria releasing iron-sulfur clusters. *Redox Biol. To be submitted*
10. Tonolo F, Folda A, **Scalcon V**, Salmain M, Bindoli A, Vessieres A, Rigobello MP. (2018) Differences in the cytotoxic activity between two metallocifen-stereoisomers in breast cancer cells. *Manuscript in preparation*
11. **Scalcon V**, Coppo L, Tonolo F, Folda A, Bindoli A, Rigobello MP, Holmgren A. (2018) Mitochondrial-specific deletion of Grx2 in mice leads to metabolic syndrome. *Manuscript in preparation*

7. Abbreviations

ACSL4	acyl-CoA synthetase long chain family member 4
Af	auranofin, (1-thio- β -D-glucopyranosato) (triethylphosphine)Au 2,3,4,6-tetraacetate
AIS	4-acetamido-4'-((iodoacetyl) amino) stilbene-2,2'-disulfonic acid
AP-1	activator protein 1
ASK1	apoptosis signal-regulating kinase 1
ATO	arsenic trioxide
BIAM	biotinylated iodoacetamide
BSA	bovine serum albumin
BSO	buthionine sulphoximine
CDNB	1-chloro-2,4-dinitrobenzene
CM-H2DCFDA	5-(and-6)-chloromethyl-2',7'-dichlorodihydrofluorescein diacetate acetyl ester
CoA	coenzyme A
CsA	cyclosporin A
CVD	cardiovascular diseases
CypD	cyclophilin D
Cys	cysteine
Cyt c	cytochrome c
DLCs	delocalized lipophilic cations
DOC	sodium deoxycholate
DTNB	5,5'-dithiobis (2-nitrobenzoic acid)
DTT	dithiothreitol
EDTA	ethylene diamine tetraacetic acid
EGTA	ethylene-bis(oxyethylenenitrilo) tetraacetic acid
EPR	electron paramagnetic resonance
ER	endoplasmic reticulum
FACS	fluorescence-activated cell sorting
FCS	fetal calf serum
2Fe-2S	iron and sulfur cluster
FLAG	Asp-Tyr-Lys-Asp-Asp-Asp-Lys octapeptide
FOXO	forkhead box O protein
GAPDH	glyceraldehyde 3-phosphate dehydrogenase
GCL	glutamate-cysteine ligase
GGT	γ -glutamyltranspeptidase
GLRX2	glutaredoxin 2 gene
GPx	glutathione peroxidase
GR	glutathione reductase
Grxs	glutaredoxins
Grx1	glutaredoxin 1
Grx2	glutaredoxin 2
GS	glutathione synthetase
GSH	glutathione (reduced)
GSSG	glutathione (oxidized)
GSTs	glutathione S-transferases
HEDS	hydroxyethylsulfide
Hepes	4-(2-Hydroxyethyl) piperazine-1-ethanesulfonic acid
HIF-1 α	hypoxia inducible factor 1 alfa
HNE	4-hydroxy-2-nonenal
H ₂ O ₂	hydrogen peroxide
HRP	horseradish peroxidase

IAA	iodoacetic acid
IAM	iodoacetamide
ICP-OES	inductively coupled plasma-atomic emission spectrometry
KO	knockout
MDA	malondialdehyde
mGrx2 KO	mitochondrial Grx2 knockout
MMP or $\Delta\Psi_m$	mitochondrial membrane potential (delta psi)
MTT	3-[4,5-dimethylthiazol-2-yl]-2,5-diphenyltetrazolium bromide
NAC	N-acetyl cysteine
NADPH	β -nicotinamide adenine dinucleotide
NaKPi	sodium/kalium phosphate
NASH	non alcoholic steatohepatitis
NHC	N-heterocyclic carbene
NF- κ B	nuclear factor kappa light chain enhancer of activated B cells
NO	nitric oxide
Nrf2	nuclear factor erythroid derived 2 like 2
O ₂	dioxygen
O ₂ ^{•-}	superoxide anion
PAGE	polyacrylamide gel electrophoresis
PARP-1	poly ADP-ribose polymerase 1
PBS	phosphate-buffered saline
PMSF	phenylmethylsulfonyl fluoride
PPIase	peptidyl prolyl <i>cis-trans</i> isomerase
Prx3	peroxiredoxin 3
Prxs	peroxiredoxins
Rac1/2	Ras-related C3 botulinum toxin substrate 1/2
ROS	reactive oxygen species
RT-qPCR	reverse transcriptase-polymerase chain reaction
SDS	sodium dodecyl sulfate
Sec	selenocysteine
Sel	sodium selenite
Sirt3	sirtuin 3
SODs	superoxide dismutases
SOD1/ Cu-Zn	superoxide dismutase 1 (cytosolic)
SOD2/Mn	superoxide dismutase 2 (mitochondrial)
TGR	thioredoxin glutathione reductase
TLMs	tamoxifen-like metalocifens
Tris	tris(hydroxymethyl)aminomethane
Trx1	thioredoxin 1
Trx2	thioredoxin 2
Trx80	truncated thioredoxin 1
TrxRs	thioredoxin reductases
TrxR1	thioredoxin reductase 1
TrxR2	thioredoxin reductase 2
TNF- α	tumor necrosis factor alfa
TXN	thioredoxin 1 gene
TXN2	thioredoxin 2 gene
TXNIP	thioredoxin interacting protein
TXNRD1	thioredoxin reductase 1 gene
TXNRD2	thioredoxin reductase 2 gene
TXNRD3	thioredoxin glutathione reductase gene
VEGF	vascular endothelial growth factor
WT	wild-type

8. References

1. Sies H., Berndt C., and Jones D.P. *Oxidative Stress*. Annu Rev Biochem, 2017. **86**: p. 715-48.
2. Sundaresan M., Yu Z.X., Ferrans V.J., Irani K., and Finkel T. *Requirement for generation of H₂O₂ for platelet-derived growth factor signal transduction*. Science, 1995. **270**(5234): p. 296-99.
3. Bae Y.S., Kang S.W., Seo M.S., Baines I.C., Tekle E., Chock P.B., and Rhee S.G. *Epidermal growth factor (EGF)-induced generation of hydrogen peroxide. Role in EGF receptor-mediated tyrosine phosphorylation*. J Biol Chem, 1997. **272**(1): p. 217-21.
4. Roy S., Khanna S., and Sen C.K. *Redox regulation of the VEGF signaling path and tissue vascularization: Hydrogen peroxide, the common link between physical exercise and cutaneous wound healing*. Free Radic Biol Med, 2008. **44**(2): p. 180-92.
5. Meier B., Radeke H.H., Selle S., Younes M., Sies H., Resch K., and Habermehl G.G. *Human fibroblasts release reactive oxygen species in response to interleukin-1 or tumour necrosis factor-alpha*. Biochem J, 1989. **263**(2): p. 539-45.
6. Mahadev K., Wu X., Zilbering A., Zhu L., Lawrence J.T., and Goldstein B.J. *Hydrogen peroxide generated during cellular insulin stimulation is integral to activation of the distal insulin signaling cascade in 3T3-L1 adipocytes*. J Biol Chem, 2001. **276**(52): p. 48662-69.
7. Pahl H.L. and Baeuerle P.A. *Oxygen and the control of gene expression*. Bioessays, 1994. **16**(7): p. 497-502.
8. Giorgio M., Trinei M., Migliaccio E., and Pelicci P.G. *Hydrogen peroxide: a metabolic by-product or a common mediator of ageing signals?* Nat Rev Mol Cell Biol, 2007. **8**(9): p. 722-28.
9. Rhee S.G. *Redox signaling: hydrogen peroxide as intracellular messenger*. Exp Mol Med, 1999. **31**(2): p. 53-59.
10. Bindoli A. and Rigobello M.P. *Principles in redox signaling: From chemistry to functional significance*. Antioxid Redox Signal, 2013. **18**(13): p. 1557-93.
11. Jones D.P. *Radical-free biology of oxidative stress*. Am J Physiol-Cell Ph, 2008. **295**(4): p. C849-C68.
12. Pascal I., Tarbell D.S. *The kinetics of the oxidation of a mercaptan to the corresponding disulfide by aqueous hydrogen peroxide*. J Am Chem Soc, 1957. **79**: p. 6015-20.
13. Foster M.W., Forrester M.T., and Stamler J.S. *A protein microarray-based analysis of S-nitrosylation*. Proc Natl Acad Sci U S A, 2009. **106**(45): p. 18948-53.
14. Miseta A. and Csutora P. *Relationship between the occurrence of cysteine in proteins and the complexity of organisms*. Mol Biol Evol, 2000. **17**(8): p. 1232-39.
15. Bienert G.P., Moller A.L.B., Kristiansen K.A., Schulz A., Moller I.M., Schjoerring J.K., and Jahn T.P. *Specific aquaporins facilitate the diffusion of hydrogen peroxide across membranes*. J Biol Chem, 2007. **282**(2): p. 1183-92.
16. Bindoli A., Fukuto J.M., and Forman H.J. *Thiol chemistry in peroxidase catalysis and redox signaling*. Antioxid Redox Signal, 2008. **10**(9): p. 1549-64.
17. Couturier J., Przybyla-Toscano J., Roret T., Didierjean C., and Rouhier N. *The roles of glutaredoxins ligating Fe-S clusters: Sensing, transfer or repair functions?* Bba-Mol Cell Res, 2015. **1853**(6): p. 1513-27.
18. Tsuchiya Y., Peak-Chew S.Y., Newell C., Miller-Aidoo S., Mangal S., Zhyvoloup A., Bakovic J., Malanchuk O., Pereira G.C., Kotiadis V., Szabadkai G., Duchon M.R., Campbell M., Cuenca S.R., Vidal-Puig A., James A.M., Murphy M.P., Filonenko V., Skehel M., and Gout I. *Protein*

- CoAlation: a redox-regulated protein modification by coenzyme A in mammalian cells.* Biochem J, 2017. **474**(14): p. 2489-508.
19. Stadtman T.C. *Biosynthesis and function of selenocysteine-containing enzymes.* J Biol Chem, 1991. **266**(25): p. 16257-60.
 20. Xu X.M., Carlson B.A., Mix H., Zhang Y., Saira K., Glass R.S., Berry M.J., Gladyshev V.N., and Hatfield D.L. *Biosynthesis of selenocysteine on its tRNA in eukaryotes.* PLoS Biol, 2007. **5**(1): p. e4.
 21. Low S.C. and Berry M.J. *Knowing when not to stop: selenocysteine incorporation in eukaryotes.* Trends Biochem Sci, 1996. **21**(6): p. 203-08.
 22. Kryukov G.V., Castellano S., Novoselov S.V., Lobanov A.V., Zehtab O., Guigo R., and Gladyshev V.N. *Characterization of mammalian selenoproteomes.* Science, 2003. **300**(5624): p. 1439-43.
 23. Schweizer U. and Fradejas-Villar N. *Why 21? The significance of selenoproteins for human health revealed by inborn errors of metabolism.* FASEB J, 2016. **30**(11): p. 3669-81.
 24. Johansson L., Gafvelin G., and Arner E.S. *Selenocysteine in proteins-properties and biotechnological use.* Biochim Biophys Acta, 2005. **1726**(1): p. 1-13.
 25. Inarrea P., Moini H., Rettori D., Han D., Martinez J., Garcia L., Fernandez-Vizarra E., Iturralde M., and Cadenas E. *Redox activation of mitochondrial intermembrane space Cu,Zn-superoxide dismutase.* Biochem J, 2005. **387**: p. 203-09.
 26. Linard D., Kandlbinder A., Degand H., Morsomme P., Dietz K.J., and Knoop B. *Redox characterization of human cyclophilin D: Identification of a new mammalian mitochondrial redox sensor?* Arch Biochem Biophys, 2009. **491**(1-2): p. 39-45.
 27. Bernardi P., Rasola A., Forte M., and Lippe G. *The mitochondrial permeability transition pore: channel formation by F-ATP synthase, integration in signal transduction, and role in pathophysiology.* Physiol Rev, 2015. **95**(4): p. 1111-55.
 28. Nguyen T.T., Stevens M.V., Kohr M., Steenbergen C., Sack M.N., and Murphy E. *Cysteine 203 of cyclophilin D is critical for cyclophilin D activation of the mitochondrial permeability transition pore.* J Biol Chem, 2011. **286**(46): p. 40184-92.
 29. Yagi T. and Hatefi Y. *Thiols in oxidative phosphorylation: inhibition and energy-potentiated uncoupling by monothiol and dithiol modifiers.* Biochemistry, 1984. **23**(11): p. 2449-55.
 30. Yagi T. and Hatefi Y. *Thiols in oxidative phosphorylation: thiols in the F₀ of ATP synthase essential for ATPase activity.* Arch Biochem Biophys, 1987. **254**(1): p. 102-09.
 31. Wang S.B., Foster D.B., Rucker J., O'Rourke B., Kass D.A., and Van Eyk J.E. *Redox regulation of mitochondrial ATP synthase: implications for cardiac resynchronization therapy.* Circ Res, 2011. **109**(7): p. 750-57.
 32. Fernandez-Sanz C., Ruiz-Meana M., Castellano J., Miro-Casas E., Nunez E., Inserte J., Vazquez J., and Garcia-Dorado D. *Altered FoF1 ATP synthase and susceptibility to mitochondrial permeability transition pore during ischaemia and reperfusion in aging cardiomyocytes.* Thromb Haemost, 2015. **113**(3): p. 441-51.
 33. Wu Y.T., Lee H.C., Liao C.C., and Wei Y.H. *Regulation of mitochondrial FoF1 ATPase activity by Sirt3-catalyzed deacetylation and its deficiency in human cells harboring 4977 bp deletion of mitochondrial DNA.* Bba-Mol Basis Dis, 2013. **1832**(1): p. 216-27.
 34. Holzerova E. and Prokisch H. *Mitochondria: Much ado about nothing? How dangerous is reactive oxygen species production?* Int J Biochem Cell Biol, 2015. **63**: p. 16-20.
 35. Cross A.R. and Jones O.T. *Enzymic mechanisms of superoxide production.* Biochim Biophys Acta, 1991. **1057**(3): p. 281-98.

36. O'Donnell V.B. and Azzi A. *High rates of extracellular superoxide generation by cultured human fibroblasts: involvement of a lipid-metabolizing enzyme.* Biochem J, 1996. **318** (Pt 3): p. 805-12.
37. Paolicchi A., Dominici S., Pieri L., Maellaro E., and Pompella A. *Glutathione catabolism as a signaling mechanism.* Biochem Pharmacol, 2002. **64**(5-6): p. 1027-35.
38. Schrader M. and Fahimi H.D. *Peroxisomes and oxidative stress.* Bba-Mol Cell Res, 2006. **1763**(12): p. 1755-66.
39. Sandri G., Panfili E., and Ernster L. *Hydrogen-peroxide production by monoamine-oxidase in isolated rat-brain mitochondria - Its effect on glutathione levels and Ca²⁺ efflux.* Biochim Biophys Acta, 1990. **1035**(3): p. 300-05.
40. Pizzinat N., Copin N., Vindis C., Parini A., and Cambon C. *Reactive oxygen species production by monoamine oxidases in intact cells.* Naunyn Schmiedebergs Arch Pharmacol, 1999. **359**(5): p. 428-31.
41. Seiler N. *Oxidation of polyamines and brain injury.* Neurochem Res, 2000. **25**(4): p. 471-90.
42. Cross A.R. and Segal A.W. *The NADPH oxidase of professional phagocytes - prototype of the NOX electron transport chain systems.* Bba-Bioenergetics, 2004. **1657**(1): p. 1-22.
43. Lambeth J.D. *Nox enzymes and the biology of reactive oxygen.* Nat Rev Immunol, 2004. **4**(3): p. 181-89.
44. Lambeth J.D., Kawahara T., and Diebold B. *Regulation of Nox and Duox enzymatic activity and expression.* Free Radic Biol Med, 2007. **43**(3): p. 319-31.
45. Geiszt M. and Leto T.L. *The Nox family of NAD(P)H oxidases: Host defense and beyond.* J Biol Chem, 2004. **279**(50): p. 51715-18.
46. Al Ghouleh I., Khoo N.K.H., Knaus U.G., Griendling K.K., Touyz R.M., Thannickal V.J., Barchowsky A., Nauseef W.M., Kelley E.E., Bauer P.M., Darley-Usmar V., Shiva S., Cifuentes-Pagano E., Freeman B.A., Gladwin M.T., and Pagano P.J. *Oxidases and peroxidases in cardiovascular and lung disease: New concepts in reactive oxygen species signaling.* Free Radic Biol Med, 2011. **51**(7): p. 1271-88.
47. Sauer H., Wartenberg M., and Hescheler J. *Reactive oxygen species as intracellular messengers during cell growth and differentiation.* Cell Physiol Biochem, 2001. **11**(4): p. 173-86.
48. Bedard K. and Krause K.H. *The NOX family of ROS-generating NADPH oxidases: Physiology and pathophysiology.* Physiol Rev, 2007. **87**(1): p. 245-313.
49. Brunati A.M., Pagano M.A., Bindoli A., and Rigobello M.P. *Thiol redox systems and protein kinases in hepatic stellate cell regulatory processes.* Free Radical Res, 2010. **44**(4): p. 363-78.
50. Cadenas E. and Davies K.J.A. *Mitochondrial free radical generation, oxidative stress, and aging.* Free Radic Biol Med, 2000. **29**(3-4): p. 222-30.
51. Brand M.D. *The sites and topology of mitochondrial superoxide production.* Exp Gerontol, 2010. **45**(7-8): p. 466-72.
52. Harman D. *The biologic clock: the mitochondria?* J Am Geriatr Soc, 1972. **20**(4): p. 145-47.
53. Okado-Matsumoto A. and Fridovich I. *Subcellular distribution of superoxide dismutases (SOD) in rat liver: Cu,Zn-SOD in mitochondria.* J Biol Chem, 2001. **276**(42): p. 38388-93.
54. Forman H.J. and Kennedy J. *Dihydroorotate-dependent superoxide production in rat brain and liver. A function of the primary dehydrogenase.* Arch Biochem Biophys, 1976. **173**(1): p. 219-24.
55. Drahotka Z., Chowdhury S.K., Floryk D., Mracek T., Wilhelm J., Rauchova H., Lenaz G., and Houstek J. *Glycerophosphate-dependent hydrogen peroxide production by brown adipose*

- tissue mitochondria and its activation by ferricyanide*. J Bioenerg Biomembr, 2002. **34**(2): p. 105-13.
56. Ruzicka F.J. and Beinert H. *A new iron-sulfur flavoprotein of the respiratory chain. A component of the fatty acid beta oxidation pathway*. J Biol Chem, 1977. **252**(23): p. 8440-45.
 57. Starkov A.A., Fiskum G., Chinopoulos C., Lorenzo B.J., Browne S.E., Patel M.S., and Beal M.F. *Mitochondrial alpha-ketoglutarate dehydrogenase complex generates reactive oxygen species*. J Neurosci, 2004. **24**(36): p. 7779-88.
 58. Whatley S.A., Curti D., Das Gupta F., Ferrier I.N., Jones S., Taylor C., and Marchbanks R.M. *Superoxide, neuroleptics and the ubiquinone and cytochrome b5 reductases in brain and lymphocytes from normals and schizophrenic patients*. Mol Psychiatry, 1998. **3**(3): p. 227-37.
 59. Kaludercic N., Carpi A., Menabo R., Di Lisa F., and Paolocci N. *Monoamine oxidases (MAO) in the pathogenesis of heart failure and ischemia/reperfusion injury*. Biochim Biophys Acta, 2011. **1813**(7): p. 1323-32.
 60. Vasquez-Vivar J., Kalyanaraman B., and Kennedy M.C. *Mitochondrial aconitase is a source of hydroxyl radical - An electron spin resonance investigation*. J Biol Chem, 2000. **275**(19): p. 14064-69.
 61. Montero J., Mari M., Colell A., Morales A., Basanez G., Garcia-Ruiz C., and Fernandez-Checa J.C. *Cholesterol and peroxidized cardiolipin in mitochondrial membrane properties, permeabilization and cell death*. Bba-Bioenergetics, 2010. **1797**(6-7): p. 1217-24.
 62. Kagan V.E., Tyurin V.A., Jiang J.F., Tyurina Y.Y., Ritov V.B., Amoscato A.A., Osipov A.N., Belikova N.A., Kapralov A.A., Kini V., Vlasova I.I., Zhao Q., Zou M.M., Di P., Svistunenko D.A., Kurnikov I.V., and Borisenko G.G. *Cytochrome c acts as a cardiolipin oxygenase required for release of proapoptotic factors*. Nat Chem Biol, 2005. **1**(4): p. 223-32.
 63. Block K., Gorin Y., and Abboud H.E. *Subcellular localization of Nox4 and regulation in diabetes*. Proc Natl Acad Sci U S A, 2009. **106**(34): p. 14385-90.
 64. Maejima Y., Kuroda J., Matsushima S., Ago T., and Sadoshima J. *Regulation of myocardial growth and death by NADPH oxidase*. J Mol Cell Cardiol, 2011. **50**(3): p. 408-16.
 65. Glorieux C. and Calderon P.B. *Catalase, a remarkable enzyme: targeting the oldest antioxidant enzyme to find a new cancer treatment approach*. Biol Chem, 2017. **398**(10): p. 1095-108.
 66. Holmgren A., Johansson C., Berndt C., Lonn M.E., Hudemann C., and Lillig C.H. *Thiol redox control via thioredoxin and glutaredoxin systems*. Biochem Soc Trans, 2005. **33**(Pt 6): p. 1375-77.
 67. Lillig C.H. and Holmgren A. *Thioredoxin and related molecules-from biology to health and disease*. Antioxid Redox Signal, 2007. **9**(1): p. 25-47.
 68. Sun Q.A., Kirnarsky L., Sherman S., and Gladyshev V.N. *Selenoprotein oxidoreductase with specificity for thioredoxin and glutathione systems*. Proc Natl Acad Sci U S A, 2001. **98**(7): p. 3673-78.
 69. Sun Q.A., Wu Y., Zappacosta F., Jeang K.T., Lee B.J., Hatfield D.L., and Gladyshev V.N. *Redox regulation of cell signaling by selenocysteine in mammalian thioredoxin reductases*. J Biol Chem, 1999. **274**(35): p. 24522-30.
 70. Sun Q.A., Su D., Novoselov S.V., Carlson B.A., Hatfield D.L., and Gladyshev V.N. *Reaction mechanism and regulation of mammalian thioredoxin/glutathione reductase*. Biochemistry, 2005. **44**(44): p. 14528-37.

71. Holmgren A. *Bovine thioredoxin system. Purification of thioredoxin reductase from calf liver and thymus and studies of its function in disulfide reduction.* J Biol Chem, 1977. **252**(13): p. 4600-06.
72. Rigobello M.P., Callegaro M.T., Barzon E., Benetti M., and Bindoli A. *Purification of mitochondrial thioredoxin reductase and its involvement in the redox regulation of membrane permeability.* Free Radic Biol Med, 1998. **24**(2): p. 370-76.
73. Miranda-Vizueté A., Damdimopoulos A.E., and Spyrou G. *cDNA cloning, expression and chromosomal localization of the mouse mitochondrial thioredoxin reductase gene(1).* Biochim Biophys Acta, 1999. **1447**(1): p. 113-18.
74. Lee S.R., Kim J.R., Kwon K.S., Yoon H.W., Levine R.L., Ginsburg A., and Rhee S.G. *Molecular cloning and characterization of a mitochondrial selenocysteine-containing thioredoxin reductase from rat liver.* J Biol Chem, 1999. **274**(8): p. 4722-34.
75. Arner E.S. *Focus on mammalian thioredoxin reductases-important selenoproteins with versatile functions.* Biochim Biophys Acta, 2009. **1790**(6): p. 495-526.
76. Inarrea P., Moini H., Han D., Rettori D., Aguilo I., Alava M.A., Iturralde M., and Cadenas E. *Mitochondrial respiratory chain and thioredoxin reductase regulate intermembrane Cu,Zn-superoxide dismutase activity: implications for mitochondrial energy metabolism and apoptosis.* Biochem J, 2007. **405**(1): p. 173-79.
77. Holmgren A. *Thioredoxin and glutaredoxin systems.* J Biol Chem, 1989. **264**(24): p. 13963-66.
78. Sandalova T., Zhong L., Lindqvist Y., Holmgren A., and Schneider G. *Three-dimensional structure of a mammalian thioredoxin reductase: implications for mechanism and evolution of a selenocysteine-dependent enzyme.* Proc Natl Acad Sci U S A, 2001. **98**(17): p. 9533-38.
79. Fritz-Wolf K., Kehr S., Stumpf M., Rahlfs S., and Becker K. *Crystal structure of the human thioredoxin reductase-thioredoxin complex.* Nat Commun, 2011. **2**: p. 383.
80. Zhong L. and Holmgren A. *Essential role of selenium in the catalytic activities of mammalian thioredoxin reductase revealed by characterization of recombinant enzymes with selenocysteine mutations.* J Biol Chem, 2000. **275**(24): p. 18121-28.
81. Biterova E.I., Turanov A.A., Gladyshev V.N., and Barycki J.J. *Crystal structures of oxidized and reduced mitochondrial thioredoxin reductase provide molecular details of the reaction mechanism.* Proc Natl Acad Sci U S A, 2005. **102**(42): p. 15018-23.
82. Rigobello M.P., Vianello F., Folda A., Roman C., Scutari G., and Bindoli A. *Differential effect of calcium ions on the cytosolic and mitochondrial thioredoxin reductase.* Biochem Biophys Res Commun, 2006. **343**(3): p. 873-78.
83. Rackham O., Shearwood A.M., Thyer R., McNamara E., Davies S.M., Callus B.A., Miranda-Vizueté A., Berners-Price S.J., Cheng Q., Arner E.S., and Filipovska A. *Substrate and inhibitor specificities differ between human cytosolic and mitochondrial thioredoxin reductases: Implications for development of specific inhibitors.* Free Radic Biol Med, 2011. **50**(6): p. 689-99.
84. Rigobello M.P., Folda A., Citta A., Scutari G., Gandin V., Fernandes A.P., Rundlof A.K., Marzano C., Bjornstedt M., and Bindoli A. *Interaction of selenite and tellurite with thiol-dependent redox enzymes: Kinetics and mitochondrial implications.* Free Radic Biol Med, 2011. **50**(11): p. 1620-29.
85. Nordberg J. and Arner E.S. *Reactive oxygen species, antioxidants, and the mammalian thioredoxin system.* Free Radic Biol Med, 2001. **31**(11): p. 1287-312.
86. Hanschmann E.M., Lonn M.E., Schutte L.D., Funke M., Godoy J.R., Eitner S., Hudemann C., and Lillig C.H. *Both thioredoxin 2 and glutaredoxin 2 contribute to the reduction of the mitochondrial 2-Cys peroxiredoxin Prx3.* J Biol Chem, 2010. **285**(52): p. 40699-705.

87. Jakupoglu C., Przemeck G.K., Schneider M., Moreno S.G., Mayr N., Hatzopoulos A.K., de Angelis M.H., Wurst W., Bornkamm G.W., Brielmeier M., and Conrad M. *Cytoplasmic thioredoxin reductase is essential for embryogenesis but dispensable for cardiac development*. Mol Cell Biol, 2005. **25**(5): p. 1980-88.
88. Bondareva A.A., Capecchi M.R., Iverson S.V., Li Y., Lopez N.I., Lucas O., Merrill G.F., Prigge J.R., Siders A.M., Wakamiya M., Wallin S.L., and Schmidt E.E. *Effects of thioredoxin reductase-1 deletion on embryogenesis and transcriptome*. Free Radic Biol Med, 2007. **43**(6): p. 911-23.
89. Conrad M., Jakupoglu C., Moreno S.G., Lippl S., Banjac A., Schneider M., Beck H., Hatzopoulos A.K., Just U., Sinowatz F., Schmahl W., Chien K.R., Wurst W., Bornkamm G.W., and Brielmeier M. *Essential role for mitochondrial thioredoxin reductase in hematopoiesis, heart development, and heart function*. Mol Cell Biol, 2004. **24**(21): p. 9414-23.
90. Soerensen J., Jakupoglu C., Beck H., Forster H., Schmidt J., Schmahl W., Schweizer U., Conrad M., and Brielmeier M. *The role of thioredoxin reductases in brain development*. PLoS One, 2008. **3**(3): p. e1813.
91. Kudin A.P., Baron G., Zsurka G., Hampel K.G., Elger C.E., Grote A., Weber Y., Lerche H., Thiele H., Nurnberg P., Schulz H., Ruppert A.K., Sander T., Cheng Q., Arner E.S., Schomburg L., Seeher S., Fradejas-Villar N., Schweizer U., and Kunz W.S. *Homozygous mutation in TXNRD1 is associated with genetic generalized epilepsy*. Free Radic Biol Med, 2017. **106**: p. 270-77.
92. Patterson A.D., Carlson B.A., Li F., Bonzo J.A., Yoo M.H., Krausz K.W., Conrad M., Chen C., Gonzalez F.J., and Hatfield D.L. *Disruption of thioredoxin reductase 1 protects mice from acute acetaminophen-induced hepatotoxicity through enhanced NRF2 activity*. Chem Res Toxicol, 2013. **26**(7): p. 1088-96.
93. Iverson S.V., Eriksson S., Xu J., Prigge J.R., Talago E.A., Meade T.A., Meade E.S., Capecchi M.R., Arner E.S., and Schmidt E.E. *A Txnrd1-dependent metabolic switch alters hepatic lipogenesis, glycogen storage, and detoxification*. Free Radic Biol Med, 2013. **63**: p. 369-80.
94. Kiermayer C., Northrup E., Schrewe A., Walch A., de Angelis M.H., Schoensiegel F., Zischka H., Prehn C., Adamski J., Bekeredjian R., Ivandic B., Kupatt C., and Brielmeier M. *Heart-specific knockout of the mitochondrial thioredoxin reductase (Txnrd2) induces metabolic and contractile dysfunction in the aging myocardium*. J Am Heart Assoc, 2015. **4**(7): p. e002153.
95. Sibbing D., Pfeufer A., Perisic T., Mannes A.M., Fritz-Wolf K., Unwin S., Sinner M.F., Gieger C., Gloeckner C.J., Wichmann H.E., Kremmer E., Schafer Z., Walch A., Hinterseer M., Nabauer M., Kaab S., Kastrati A., Schomig A., Meitinger T., Bornkamm G.W., Conrad M., and von Beckerath N. *Mutations in the mitochondrial thioredoxin reductase gene TXNRD2 cause dilated cardiomyopathy*. Eur Heart J, 2011. **32**(9): p. 1121-33.
96. Geisberger R., Kiermayer C., Homig C., Conrad M., Schmidt J., Zimmer-Strobl U., and Brielmeier M. *B- and T-cell-specific inactivation of thioredoxin reductase 2 does not impair lymphocyte development and maintenance*. Biol Chem, 2007. **388**(10): p. 1083-90.
97. Muri J., Heer S., Matsushita M., Pohlmeier L., Tortola L., Fuhrer T., Conrad M., Zamboni N., Kisielow J., and Kopf M. *The thioredoxin-1 system is essential for fueling DNA synthesis during T-cell metabolic reprogramming and proliferation*. Nat Commun, 2018. **9**(1): p. 1851.
98. Kirsch J., Schneider H., Pagel J.I., Rehberg M., Singer M., Hellfritsch J., Chillo O., Schubert K.M., Qiu J.H., Pogoda K., Kameritsch P., Uhl B., Pircher J., Deindl E., Muller S., Kirchner T., Pohl U., Conrad M., and Beck H. *Endothelial dysfunction, and a prothrombotic,*

- proinflammatory phenotype is caused by loss of mitochondrial thioredoxin reductase in endothelium.* *Arterioscler Thromb Vasc Biol*, 2016. **36**(9): p. 1891-99.
99. Yan J.D., Xu J., Fei Y., Jiang C.S., Zhu W.H., Han Y., and Lu S.M. *TrxR2 deficiencies promote chondrogenic differentiation and induce apoptosis of chondrocytes through mitochondrial reactive oxygen species.* *Exp Cell Res*, 2016. **344**(1): p. 67-75.
 100. Prasad R., Chan L.F., Hughes C.R., Kaski J.P., Kowalczyk J.C., Savage M.O., Peters C.J., Nathwani N., Clark A.J.L., Storr H.L., and Metherell L.A. *Thioredoxin reductase 2 (TXNRD2) mutation associated with familial glucocorticoid deficiency (FGD).* *J Clin Endocrinol Metab*, 2014. **99**(8): p. E1556-63.
 101. Pickering A.M., Lehr M., Gendron C.M., Pletcher S.D., and Miller R.A. *Mitochondrial thioredoxin reductase 2 is elevated in long-lived primate as well as rodent species and extends fly mean lifespan.* *Aging Cell*, 2017. **16**(4): p. 683-92.
 102. Laurent T.C., Moore E.C., and Reichard P. *Enzymatic synthesis of deoxyribonucleotides. Iv. isolation and characterization of thioredoxin, the hydrogen donor from Escherichia coli B.* *J Biol Chem*, 1964. **239**: p. 3436-44.
 103. Martin J.L. *Thioredoxin-a fold for all reasons.* *Structure*, 1995. **3**(3): p. 245-50.
 104. Watson W.H., Pohl J., Montfort W.R., Stuchlik O., Reed M.S., Powis G., and Jones D.P. *Redox potential of human thioredoxin 1 and identification of a second dithiol/disulfide motif.* *J Biol Chem*, 2003. **278**(35): p. 33408-15.
 105. Das K.C. and Das C.K. *Thioredoxin, a singlet oxygen quencher and hydroxyl radical scavenger: redox independent functions.* *Biochem Biophys Res Commun*, 2000. **277**(2): p. 443-47.
 106. Chae H.Z., Kim H.J., Kang S.W., and Rhee S.G. *Characterization of three isoforms of mammalian peroxiredoxin that reduce peroxides in the presence of thioredoxin.* *Diabetes Res Clin Pract*, 1999. **45**(2-3): p. 101-12.
 107. Arner E.S.J. and Holmgren A. *Physiological functions of thioredoxin and thioredoxin reductase.* *Eur J Biochem*, 2000. **267**(20): p. 6102-09.
 108. Hirota K., Murata M., Sachi Y., Nakamura H., Takeuchi J., Mori K., and Yodoi J. *Distinct roles of thioredoxin in the cytoplasm and in the nucleus - A two-step mechanism of redox regulation of transcription factor NF-kappa B.* *J Biol Chem*, 1999. **274**(39): p. 27891-97.
 109. Grippo J.F., Holmgren A., and Pratt W.B. *Proof that the endogenous, heat-stable glucocorticoid receptor-activating factor is thioredoxin.* *J Biol Chem*, 1985. **260**(1): p. 93-97.
 110. Hirota K., Matsui M., Iwata S., Nishiyama A., Mori K., and Yodoi J. *AP-1 transcriptional activity is regulated by a direct association between thioredoxin and Ref-1.* *Proc Natl Acad Sci U S A*, 1997. **94**(8): p. 3633-38.
 111. Moos P.J., Edes K., Cassidy P., Massuda E., and Fitzpatrick F.A. *Electrophilic prostaglandins and lipid aldehydes repress redox-sensitive transcription factors p53 and hypoxia-inducible factor by impairing the selenoprotein thioredoxin reductase.* *J Biol Chem*, 2003. **278**(2): p. 745-50.
 112. Hayashi S., HajiroNakanishi K., Makino Y., Eguchi H., Yodoi J., and Tanaka H. *Functional modulation of estrogen receptor by redox state with reference to thioredoxin as a mediator.* *Nucleic Acids Res*, 1997. **25**(20): p. 4035-40.
 113. Saitoh M., Nishitoh H., Fujii M., Takeda K., Tobiume K., Sawada Y., Kawabata M., Miyazono K., and Ichijo H. *Mammalian thioredoxin is a direct inhibitor of apoptosis signal-regulating kinase (ASK) 1.* *Embo J*, 1998. **17**(9): p. 2596-606.
 114. Haendeler J., Hoffmann J., Tischler V., Berk B.C., Zeiher A.M., and Dimmeler S. *Redox regulatory and anti-apoptotic functions of thioredoxin depend on S-nitrosylation at cysteine 69.* *Nat Cell Biol*, 2002. **4**(10): p. 743-49.

115. Spyrou G., Enmark E., MirandaVizuete A., and Gustafsson J.A. *Cloning and expression of a novel mammalian thioredoxin*. J Biol Chem, 1997. **272**(5): p. 2936-41.
116. Damdimopoulos A.E., Miranda-Vizuete A., Pelto-Huikko M., Gustafsson J.A., and Spyrou G. *Human mitochondrial thioredoxin - Involvement in mitochondrial membrane potential and cell death*. J Biol Chem, 2002. **277**(36): p. 33249-57.
117. Tanaka T., Hosoi F., Yamaguchi-Iwai Y., Nakamura H., Masutani H., Ueda S., Nishiyama A., Takeda S., Wada H., Spyrou G., and Yodoi J. *Thioredoxin-2 (TRX-2) is an essential gene regulating mitochondria-dependent apoptosis*. Embo J, 2002. **21**(7): p. 1695-703.
118. Hansen J.M., Zhang H., and Jones D.P. *Mitochondrial thioredoxin-2 has a key role in determining tumor necrosis factor-alpha-induced reactive oxygen species generation, NF-kappa B activation, and apoptosis*. Toxicol Sci, 2006. **91**(2): p. 643-50.
119. Mitchell D.A. and Marletta M.A. *Thioredoxin catalyzes the S-nitrosation of the caspase-3 active site cysteine*. Nat Chem Biol, 2005. **1**(3): p. 154-58.
120. Mitchell D.A., Morton S.U., Fernhoff N.B., and Marletta M.A. *Thioredoxin is required for S-nitrosation of procaspase-3 and the inhibition of apoptosis in Jurkat cells*. Proc Natl Acad Sci U S A, 2007. **104**(28): p. 11609-14.
121. Shen X.L., Burguillos M.A., Osman A.M., Frijhoff J., Carrillo-Jimenez A., Kanatani S., Augsten M., Saidi D., Rodhe J., Kavanagh E., Rongvaux A., Rraklli V., Nyman U., Holmberg J., Ostman A., Flavell R.A., Barragan A., Venero J.L., Blomgren K., and Joseph B. *Glioma-induced inhibition of caspase-3 in microglia promotes a tumor-supportive phenotype*. Nat Immunol, 2016. **17**(11): p. 1282-90.
122. Matsui M., Oshima M., Oshima H., Takaku K., Maruyama T., Yodoi J., and Taketo M.M. *Early embryonic lethality caused by targeted disruption of the mouse thioredoxin gene*. Dev Biol, 1996. **178**(1): p. 179-85.
123. Nonn L., Williams R.R., Erickson R.P., and Powis G. *The absence of mitochondrial thioredoxin 2 causes massive apoptosis, exencephaly, and early embryonic lethality in homozygous mice*. Mol Cell Biol, 2003. **23**(3): p. 916-22.
124. Harris J.R. *Release of a macromolecular protein component from human erythrocyte ghosts*. Biochim Biophys Acta, 1968. **150**(3): p. 534-37.
125. Flohe L., Toppo S., Cozza G., and Ursini F. *A comparison of thiol peroxidase mechanisms*. Antioxid Redox Signal, 2011. **15**(3): p. 763-80.
126. Rhee S.G., Kang S.W., Chang T.S., Jeong W., and Kim K. *Peroxiredoxin, a novel family of peroxidases*. IUBMB Life, 2001. **52**(1-2): p. 35-41.
127. Cox A.G., Peskin A.V., Paton L.N., Winterbourn C.C., and Hampton M.B. *Redox potential and peroxide reactivity of human peroxiredoxin 3*. Biochemistry, 2009. **48**(27): p. 6495-501.
128. Wood Z.A., Schroder E., Robin Harris J., and Poole L.B. *Structure, mechanism and regulation of peroxiredoxins*. Trends Biochem Sci, 2003. **28**(1): p. 32-40.
129. Stocker S., Maurer M., Ruppert T., and Dick T.P. *A role for 2-Cys peroxiredoxins in facilitating cytosolic protein thiol oxidation*. Nat Chem Biol, 2018. **14**(2): p. 148-55.
130. Rhee S.G. and Woo H.A. *Multiple functions of peroxiredoxins: peroxidases, sensors and regulators of the intracellular messenger H2O2, and protein chaperones*. Antioxid Redox Signal, 2011. **15**(3): p. 781-94.
131. Kang S.W., Chae H.Z., Seo M.S., Kim K.H., Baines I.C., and Rhee S.G. *Mammalian peroxiredoxin isoforms can reduce hydrogen peroxide generated in response to growth factors and tumor necrosis factor-alpha*. J Biol Chem, 1998. **273**(11): p. 6297-302.
132. Neumann C.A., Krause D.S., Carman C.V., Das S., Dubey D.P., Abraham J.L., Bronson R.T., Fujiwara Y., Orkin S.H., and Van Etten R.A. *Essential role for the peroxiredoxin Prdx1 in*

- erythrocyte antioxidant defence and tumour suppression*. Nature, 2003. **424**(6948): p. 561-65.
133. Lv W.P., Li M.X., and Wang L. *Peroxiredoxin 1 inhibits lipopolysaccharide-induced oxidative stress in lung tissue by regulating P38/JNK signaling pathway*. Eur Rev Med Pharmacol Sci, 2017. **21**(8): p. 1876-83.
134. Lee T.H., Kim S.U., Yu S.L., Kim S.H., Park D.S., Moon H.B., Dho S.H., Kwon K.S., Kwon H.J., Han Y.H., Jeong S., Kang S.W., Shin H.S., Lee K.K., Rhee S.G., and Yu D.Y. *Peroxiredoxin II is essential for sustaining life span of erythrocytes in mice*. Blood, 2003. **101**(12): p. 5033-38.
135. Kim J.H., Park S.J., Chae U., Seong J., Lee H.S., Lee S.R., Lee S., and Lee D.S. *Peroxiredoxin 2 mediates insulin sensitivity of skeletal muscles through regulation of protein tyrosine phosphatase oxidation*. Int J Biochem Cell Biol, 2018. **99**: p. 80-90.
136. Park J.G., Yoo J.Y., Jeong S.J., Choi J.H., Lee M.R., Lee M.N., Lee J.H., Kim H.C., Jo H., Yu D.Y., Kang S.W., Rhee S.G., Lee M.H., and Oh G.T. *Peroxiredoxin 2 deficiency exacerbates atherosclerosis in apolipoprotein E-deficient mice*. Circ Res, 2011. **109**(7): p. 739-49.
137. Iuchi Y., Okada F., Tsunoda S., Kibe N., Shirasawa N., Ikawa M., Okabe M., Ikeda Y., and Fujii J. *Peroxiredoxin 4 knockout results in elevated spermatogenic cell death via oxidative stress*. Biochem J, 2009. **419**: p. 149-58.
138. Li L.Q., Shoji W., Takano H., Nishimura N., Aoki Y., Takahashi R., Goto S., Kaifu T., Takai T., and Obinata M. *Increased susceptibility of MER5 (peroxiredoxin III) knockout mice to LPS-induced oxidative stress*. Biochem Biophys Res Commun, 2007. **355**(3): p. 715-21.
139. Zhang Y.G., Wang L., Kaifu T., Li J.M., Li X.Y., and Li L.Q. *Accelerated decline of physical strength in peroxiredoxin-3 knockout mice*. Exp Biol Med, 2016. **241**(13): p. 1395-400.
140. Knoop B., Argyropoulou V., Becker S., Ferte L., and Kuznetsova O. *Multiple roles of peroxiredoxins in inflammation*. Mol Cells, 2016. **39**(1): p. 60-64.
141. Kumin A., Schaefer M., Epp N., Bugnon P., Born-Berclaz C., Oxenius A., Klippel A., Bloch W., and Werner S. *Peroxiredoxin 6 is required for blood vessel integrity in wounded skin*. J Cell Biol, 2007. **179**(4): p. 747-60.
142. Nishiyama A., Matsui M., Iwata S., Hirota K., Masutani H., Nakamura H., Takagi Y., Sono H., Gon Y., and Yodoi J. *Identification of thioredoxin-binding protein-2/vitamin D-3 up-regulated protein 1 as a negative regulator of thioredoxin function and expression*. J Biol Chem, 1999. **274**(31): p. 21645-50.
143. Patwari P., Higgins L.J., Chutkow W.A., Yoshioka J., and Lee R.T. *The interaction of thioredoxin with Txnip - Evidence for formation of a mixed disulfide by disulfide exchange*. J Biol Chem, 2006. **281**(31): p. 21884-91.
144. Lu J. and Holmgren A. *Thioredoxin system in cell death progression*. Antioxid Redox Signal, 2012. **17**(12): p. 1738-47.
145. Minn A.H., Hafele C., and Shalev A. *Thioredoxin-interacting protein is stimulated by glucose through a carbohydrate response element and induces beta-cell apoptosis*. Endocrinology, 2005. **146**(5): p. 2397-405.
146. Patwari P., Chutkow W.A., Cummings K., Verstraeten V.L.R.M., Lammerding J., Schreiter E.R., and Lee R.T. *Thioredoxin-independent regulation of metabolism by the alpha-arrestin proteins*. J Biol Chem, 2009. **284**(37): p. 24996-5003.
147. Chutkow W.A. and Lee R.T. *Thioredoxin regulates adipogenesis through thioredoxin-interacting protein (Txnip) protein stability*. J Biol Chem, 2011. **286**(33): p. 29139-45.
148. Chutkow W.A., Patwari P., Yoshioka J., and Lee R.T. *Thioredoxin-interacting protein (Txnip) is a critical regulator of hepatic glucose production*. J Biol Chem, 2008. **283**(4): p. 2397-406.

149. Chen J., Saxena G., Mungrue I.N., Lusi A.J., and Shalev A. *Thioredoxin-interacting protein - A critical link between glucose toxicity and beta-cell apoptosis*. *Diabetes*, 2008. **57**(4): p. 938-44.
150. Hui T.Y., Sheth S.S., Diffley J.M., Potter D.W., Lusi A.J., Attie A.D., and Davis R.A. *Mice lacking thioredoxin-interacting protein provide evidence linking cellular redox state to appropriate response to nutritional signals*. *J Biol Chem*, 2004. **279**(23): p. 24387-93.
151. Oka S., Liu W.R., Masutani H., Hirata H., Shinkai Y., Yamada S., Yoshida T., Nakamura H., and Yodoi J. *Impaired fatty acid utilization in thioredoxin binding protein-2 (TBP-2)-deficient mice: a unique animal model of Reye syndrome*. *FASEB J*, 2005. **19**(12): p. 121-23.
152. Yoshioka J., Chutkow W.A., Lee S., Kim J.B., Yan J., Tian R., Lindsey M.L., Feener E.P., Seidman C.E., Seidman J.G., and Lee R.T. *Deletion of thioredoxin-interacting protein in mice impairs mitochondrial function but protects the myocardium from ischemia-reperfusion injury*. *J Clin Invest*, 2012. **122**(1): p. 267-79.
153. Parikh H., Carlsson E., Chutkow W.A., Johansson L.E., Storgaard H., Poulsen P., Saxena R., Ladd C., Schulze P.C., Mazzini M.J., Jensen C.B., Krook A., Bjornholm M., Tornqvist H., Zierath J.R., Ridderstrale M., Altshuler D., Lee R.T., Vaag A., Groop L.C., and Mootha V.K. *TXNIP regulates peripheral glucose metabolism in humans*. *Plos Med*, 2007. **4**(5): p. 868-79.
154. Go Y.M. and Jones D.P. *Redox compartmentalization in eukaryotic cells*. *Bba-Gen Subjects*, 2008. **1780**(11): p. 1271-90.
155. Lillig C.H., Berndt C., and Holmgren A. *Glutaredoxin systems*. *Bba-Gen Subjects*, 2008. **1780**(11): p. 1304-17.
156. Beer S.M., Taylor E.R., Brown S.E., Dahm C.C., Costa N.J., Runswick M.J., and Murphy M.P. *Glutaredoxin 2 catalyzes the reversible oxidation and glutathionylation of mitochondrial membrane thiol proteins - Implications for mitochondrial redox regulation and antioxidant defense*. *J Biol Chem*, 2004. **279**(46): p. 47939-51.
157. Taylor E.R., Hurrell F., Shannon R.J., Lin T.K., Hirst J., and Murphy M.P. *Reversible glutathionylation of complex I increases mitochondrial superoxide formation*. *J Biol Chem*, 2003. **278**(22): p. 19603-10.
158. Racker E. *Glutathione reductase from bakers' yeast and beef liver*. *J Biol Chem*, 1955. **217**(2): p. 855-65.
159. Karplus P.A. and Schulz G.E. *Refined structure of glutathione reductase at 1.54 Å resolution*. *J Mol Biol*, 1987. **195**(3): p. 701-29.
160. Deponte M. *Glutathione catalysis and the reaction mechanisms of glutathione-dependent enzymes*. *Biochim Biophys Acta*, 2013. **1830**(5): p. 3217-66.
161. Outten C.E. and Culotta V.C. *Alternative start sites in the *Saccharomyces cerevisiae* GLR1 gene are responsible for mitochondrial and cytosolic isoforms of glutathione reductase*. *J Biol Chem*, 2004. **279**(9): p. 7785-91.
162. Loos H., Roos D., Weening R., and Houwerzijl J. *Familial deficiency of glutathione reductase in human blood cells*. *Blood*, 1976. **48**(1): p. 53-62.
163. Kamerbeek N.M., van Zwieten R., de Boer M., Morren G., Vuil H., Bannink N., Lincke C., Dolman K.M., Becker K., Schirmer R.H., Gromer S., and Roos D. *Molecular basis of glutathione reductase deficiency in human blood cells*. *Blood*, 2007. **109**(8): p. 3560-66.
164. Pretsch W. *Glutathione reductase activity deficiency in homozygous *Gr1a1Neu* mice does not cause haemolytic anaemia*. *Genet Res*, 1999. **73**(1): p. 1-5.
165. Rogers L.K., Tamura T., Rogers B.J., Welty S.E., Hansen T.N., and Smith C.V. *Analyses of glutathione reductase hypomorphic mice indicate a genetic knockout*. *Toxicol Sci*, 2004. **82**(2): p. 367-73.

166. Rogers L.K., Bates C.M., Welty S.E., and Smith C.V. *Diquat induces renal proximal tubule injury in glutathione reductase-deficient mice*. *Toxicol Appl Pharmacol*, 2006. **217**(3): p. 289-98.
167. Eriksson S., Prigge J.R., Talago E.A., Arner E.S.J., and Schmidt E.E. *Dietary methionine can sustain cytosolic redox homeostasis in the mouse liver*. *Nat Commun*, 2015. **6**: p. 6479.
168. Prigge J.R., Coppo L., Martin S.S., Ogata F., Miller C.G., Brusche M.D., Orlicky D.J., Shearn C.T., Kundert J.A., Lytchier J., Herr A.E., Mattsson A., Taylor M.P., Gustafsson T.N., Arner E.S.J., Holmgren A., and Schmidt E.E. *Hepatocyte hyperproliferation upon liver-specific co-disruption of thioredoxin-1, thioredoxin reductase-1, and glutathione reductase*. *Cell Rep*, 2017. **19**(13): p. 2771-81.
169. Berndt C. and Lillig C.H. *Glutathione, glutaredoxins, and iron*. *Antioxid Redox Signal*, 2017. **27**(15): p. 1235-51.
170. Seelig G.F., Simonsen R.P., and Meister A. *Reversible dissociation of gamma-glutamylcysteine synthetase into two subunits*. *J Biol Chem*, 1984. **259**(15): p. 9345-47.
171. Dalton T.P., Dieter M.Z., Yang Y., Shertzer H.G., and Nebert D.W. *Knockout of the mouse glutamate cysteine ligase catalytic subunit (Gclc) gene: embryonic lethal when homozygous, and proposed model for moderate glutathione deficiency when heterozygous*. *Biochem Biophys Res Commun*, 2000. **279**(2): p. 324-29.
172. Yang Y., Dieter M.Z., Chen Y., Shertzer H.G., Nebert D.W., and Dalton T.P. *Initial characterization of the glutamate-cysteine ligase modifier subunit Gclm(-/-) knockout mouse. Novel model system for a severely compromised oxidative stress response*. *J Biol Chem*, 2002. **277**(51): p. 49446-52.
173. Franklin C.C., Backos D.S., Mohar I., White C.C., Forman H.J., and Kavanagh T.J. *Structure, function, and post-translational regulation of the catalytic and modifier subunits of glutamate cysteine ligase*. *Mol Aspects Med*, 2009. **30**(1-2): p. 86-98.
174. Njalsson R. *Glutathione synthetase deficiency*. *Cell Mol Life Sci*, 2005. **62**(17): p. 1938-45.
175. Chen T.S., Richie J.P., Jr., and Lang C.A. *The effect of aging on glutathione and cysteine levels in different regions of the mouse brain*. *Proc Soc Exp Biol Med*, 1989. **190**(4): p. 399-402.
176. Sekhar R.V., McKay S.V., Patel S.G., Guthikonda A.P., Reddy V.T., Balasubramanyam A., and Jahoor F. *Glutathione synthesis is diminished in patients with uncontrolled diabetes and restored by dietary supplementation with cysteine and glycine*. *Diabetes Care*, 2011. **34**(1): p. 162-67.
177. Lu S.C. *Glutathione synthesis*. *Biochim Biophys Acta*, 2013. **1830**(5): p. 3143-53.
178. Griffith O.W. and Meister A. *Origin and turnover of mitochondrial glutathione*. *Proc Natl Acad Sci U S A*, 1985. **82**(14): p. 4668-72.
179. Chen Z. and Lash L.H. *Evidence for mitochondrial uptake of glutathione by dicarboxylate and 2-oxoglutarate carriers*. *J Pharmacol Exp Ther*, 1998. **285**(2): p. 608-18.
180. Mailloux R.J., McBride S.L., and Harper M.E. *Unearthing the secrets of mitochondrial ROS and glutathione in bioenergetics*. *Trends Biochem Sci*, 2013. **38**(12): p. 592-602.
181. Barrett W.C., DeGnore J.P., Konig S., Fales H.M., Keng Y.F., Zhang Z.Y., Yim M.B., and Chock P.B. *Regulation of PTP1B via glutathionylation of the active site cysteine 215*. *Biochemistry*, 1999. **38**(20): p. 6699-705.
182. Klatt P. and Lamas S. *Regulation of protein function by S-glutathiolation in response to oxidative and nitrosative stress*. *Eur J Biochem*, 2000. **267**(16): p. 4928-44.
183. Friesen C., Kiess Y., and Debatin K.M. *A critical role of glutathione in determining apoptosis sensitivity and resistance in leukemia cells*. *Cell Death Differ*, 2004. **11** (Suppl 1): p. S73-85.

184. Kumar C., Igarria A., D'Autreaux B., Planson A.G., Junot C., Godat E., Bachhawat A.K., Delaunay-Moisan A., and Toledano M.B. *Glutathione revisited: a vital function in iron metabolism and ancillary role in thiol-redox control*. *Embo J*, 2011. **30**(10): p. 2044-56.
185. Hider R.C. and Kong X.L. *Glutathione: a key component of the cytoplasmic labile iron pool*. *Biometals*, 2011. **24**(6): p. 1179-87.
186. Meister A. and Anderson M.E. *Glutathione*. *Annu Rev Biochem*, 1983. **52**: p. 711-60.
187. Mills G.C. *Hemoglobin catabolism. I. Glutathione peroxidase, an erythrocyte enzyme which protects hemoglobin from oxidative breakdown*. *J Biol Chem*, 1957. **229**(1): p. 189-97.
188. Ursini F., Maiorino M., Brigelius-Flohe R., Aumann K.D., Roveri A., Schomburg D., and Flohe L. *Diversity of glutathione peroxidases*. *Methods Enzymol*, 1995. **252**: p. 38-53.
189. Brigelius-Flohe R. and Maiorino M. *Glutathione peroxidases*. *Biochim Biophys Acta*, 2013. **1830**(5): p. 3289-303.
190. Esworthy R.S., Ho Y.S., and Chu F.F. *The Gpx1 gene encodes mitochondrial glutathione peroxidase in the mouse liver*. *Arch Biochem Biophys*, 1997. **340**(1): p. 59-63.
191. Ho Y.S., Magnenat J.L., Bronson R.T., Cao J., Gargano M., Sugawara M., and Funk C.D. *Mice deficient in cellular glutathione peroxidase develop normally and show no increased sensitivity to hyperoxia*. *J Biol Chem*, 1997. **272**(26): p. 16644-51.
192. Esworthy R.S., Aranda R., Martin M.G., Doroshov J.H., Binder S.W., and Chu F.F. *Mice with combined disruption of Gpx1 and Gpx2 genes have colitis*. *Am J Physiol-Gastr L*, 2001. **281**(3): p. G848-55.
193. Avissar N., Ornt D.B., Yagil Y., Horowitz S., Watkins R.H., Kerl E.A., Takahashi K., Palmer I.S., and Cohen H.J. *Human kidney proximal tubules are the main source of plasma glutathione-peroxidase*. *Am J Physiol*, 1994. **266**(2): p. C367-75.
194. Takahashi K., Avissar N., Whitin J., and Cohen H. *Purification and characterization of human-plasma glutathione-peroxidase - a selenoglycoprotein distinct from the known cellular enzyme*. *Arch Biochem Biophys*, 1987. **256**(2): p. 677-86.
195. Olson G.E., Whitin J.C., Hill K.E., Winfrey V.P., Motley A.K., Austin L.M., Deal J., Cohen H.J., and Burk R.F. *Extracellular glutathione peroxidase (Gpx3) binds specifically to basement membranes of mouse renal cortex tubule cells*. *Am J Physiol Renal Physiol*, 2010. **298**(5): p. F1244-53.
196. Yant L.J., Ran Q.T., Rao L., Van Remmen H., Shibatani T., Belter J.G., Motta L., Richardson A., and Prolla T.A. *The selenoprotein GPX4 is essential for mouse development and protects from radiation and oxidative damage insults*. *Free Radic Biol Med*, 2003. **34**(4): p. 496-502.
197. Ursini F., Heim S., Kiess M., Maiorino M., Roveri A., Wissing J., and Flohe L. *Dual function of the selenoprotein PHGPx during sperm maturation*. *Science*, 1999. **285**(5432): p. 1393-96.
198. Maiorino M., Conrad M., and Ursini F. *GPx4, lipid peroxidation, and cell death: discoveries, rediscoveries, and open issues*. *Antioxid Redox Signal*, 2018. **29**(1): p. 61-74.
199. Doll S., Proneth B., Tyurina Y.Y., Panzilius E., Kobayashi S., Ingold I., Irmeler M., Beckers J., Aichler M., Walch A., Prokisch H., Trumbach D., Mao G.W., Qu F., Bayir H., Fullekrug J., Scheel C.H., Wurst W., Schick J.A., Kagan V.E., Angeli J.P.F., and Conrad M. *ACSL4 dictates ferroptosis sensitivity by shaping cellular lipid composition*. *Nat Chem Biol*, 2017. **13**(1): p. 91-98.
200. Ghyselinck N.B. and Dufaure J.P. *A mouse cDNA sequence for epididymal androgen-regulated proteins related to glutathione-peroxidase*. *Nucleic Acids Res*, 1990. **18**(23): p. 7144.
201. Dear T.N., Campbell K., and Rabbitts T.H. *Molecular-cloning of putative odorant-binding and odorant-metabolizing proteins*. *Biochemistry*, 1991. **30**(43): p. 10376-82.

202. Holmgren A. *Hydrogen donor system for Escherichia coli ribonucleoside-diphosphate reductase dependent upon glutathione*. Proc Natl Acad Sci U S A, 1976. **73**(7): p. 2275-79.
203. Luthman M. and Holmgren A. *Glutaredoxin from calf thymus. Purification to homogeneity*. J Biol Chem, 1982. **257**(12): p. 6686-90.
204. Holmgren A. *Antioxidant function of thioredoxin and glutaredoxin systems*. Antioxid Redox Signal, 2000. **2**(4): p. 811-20.
205. Yang Y.F. and Wells W.W. *Identification and characterization of the functional amino-acids at the active-center of pig-liver thioltransferase by site-directed mutagenesis*. J Biol Chem, 1991. **266**(19): p. 12759-65.
206. Funato Y., Michiue T., Asashima M., and Miki H. *The thioredoxin-related redox-regulating protein nucleoredoxin inhibits Wnt-beta-catenin signalling through dishevelled*. Nat Cell Biol, 2006. **8**(5): p. 501-08.
207. Hanschmann E.M., Godoy J.R., Berndt C., Hudemann C., and Lillig C.H. *Thioredoxins, glutaredoxins, and peroxiredoxins-molecular mechanisms and health significance: from cofactors to antioxidants to redox signaling*. Antioxid Redox Signal, 2013. **19**(13): p. 1539-605.
208. Rozell B., Barcena J.A., Martinez-Galisteo E., Padilla C.A., and Holmgren A. *Immunochemical characterization and tissue distribution of glutaredoxin (thioltransferase) from calf*. Eur J Cell Biol, 1993. **62**(2): p. 314-23.
209. Pai H.V., Starke D.W., Lesnefsky E.J., Hoppel C.L., and Mieyal J.J. *What is the functional significance of the unique location of glutaredoxin 1 (GRx1) in the intermembrane space of mitochondria?* Antioxid Redox Signal, 2007. **9**(11): p. 2027-33.
210. Nakamura H., Vaage J., Valen G., Padilla C.A., Bjornstedt M., and Holmgren A. *Measurements of plasma glutaredoxin and thioredoxin in healthy volunteers and during open-heart surgery*. Free Radic Biol Med, 1998. **24**(7-8): p. 1176-86.
211. Lundberg M., Fernandes A.P., Kumar S., and Holmgren A. *Cellular and plasma levels of human glutaredoxin 1 and 2 detected by sensitive ELISA systems*. Biochem Biophys Res Commun, 2004. **319**(3): p. 801-09.
212. Gravina S.A. and Mieyal J.J. *Thioltransferase is a specific glutathionyl mixed disulfide oxidoreductase*. Biochemistry, 1993. **32**(13): p. 3368-76.
213. Hashemy S.I., Johansson C., Berndt C., Lillig C.H., and Holmgren A. *Oxidation and S-nitrosylation of cysteines in human cytosolic and mitochondrial glutaredoxins - Effects on structure and activity*. J Biol Chem, 2007. **282**(19): p. 14428-36.
214. Ho Y.S., Xiong Y., Ho D.S., Gao J., Chua B.H.L., Pai H., and Mieyal J.J. *Targeted disruption of the glutaredoxin 1 gene does not sensitize adult mice to tissue injury induced by ischemia/reperfusion and hyperoxia*. Free Radic Biol Med, 2007. **43**(9): p. 1299-312.
215. Aesif S.W., Anathy V., Kuipers I., Guala A.S., Reiss J.N., Ho Y.S., and Janssen-Heininger Y.M.W. *Ablation of glutaredoxin-1 attenuates lipopolysaccharide-induced lung inflammation and alveolar macrophage activation*. Am J Respir Cell Mol Biol, 2011. **44**(4): p. 491-99.
216. Bachschmid M.M., Xu S.Q., Maitland-Toolan K.A., Ho Y.S., Cohen R.A., and Matsui R. *Attenuated cardiovascular hypertrophy and oxidant generation in response to angiotensin II infusion in glutaredoxin-1 knockout mice*. Free Radic Biol Med, 2010. **49**(7): p. 1221-29.
217. Pan S. and Berk B.C. *Glutathiolation regulates tumor necrosis factor-alpha-induced caspase-3 cleavage and apoptosis - Key role for glutaredoxin in the death pathway*. Circ Res, 2007. **100**(2): p. 213-19.

218. Shelton M.D., Kern T.S., and Mieyal J.J. *Glutaredoxin regulates nuclear factor kappa-B and intercellular adhesion molecule in Muller cells: model of diabetic retinopathy*. J Biol Chem, 2007. **282**(17): p. 12467-74.
219. Gladyshev V.N., Liu A., Novoselov S.V., Krysan K., Sun Q.A., Kryukov V.M., Kryukov G.V., and Lou M.F. *Identification and characterization of a new mammalian glutaredoxin (thioltransferase), Grx2*. J Biol Chem, 2001. **276**(32): p. 30374-80.
220. Lundberg M., Johansson C., Chandra J., Enoksson M., Jacobsson G., Ljung J., Johansson M., and Holmgren A. *Cloning and expression of a novel human glutaredoxin (Grx2) with mitochondrial and nuclear isoforms*. J Biol Chem, 2001. **276**(28): p. 26269-75.
221. Lonn M.E., Hudemann C., Berndt C., Cherkasov V., Capani F., Holmgren A., and Lillig C.H. *Expression pattern of human glutaredoxin 2 isoforms: identification and characterization of two testis/cancer cell-specific isoforms*. Antioxid Redox Signal, 2008. **10**(3): p. 547-57.
222. Lillig C.H., Berndt C., Vergnolle O., Lonn M.E., Hudemann C., Bill E., and Holmgren A. *Characterization of human glutaredoxin 2 as iron-sulfur protein: A possible role as redox sensor*. Proc Natl Acad Sci U S A, 2005. **102**(23): p. 8168-73.
223. Berndt C., Hudemann C., Hanschmann E.M., Axelsson R., Holmgren A., and Lillig C.H. *How does iron-sulfur cluster coordination regulate the activity of human glutaredoxin 2?* Antioxid Redox Signal, 2007. **9**(1): p. 151-57.
224. Johansson C., Kavanagh K.L., Gileadi O., and Oppermann U. *Reversible sequestration of active site cysteines in a 2Fe-2S-bridged dimer provides a mechanism for glutaredoxin 2 regulation in human mitochondria*. J Biol Chem, 2007. **282**(5): p. 3077-82.
225. Gallogly M.M., Starke D.W., Leonberg A.K., Ospina S.M., and Mieyal J.J. *Kinetic and mechanistic characterization and versatile catalytic properties of mammalian glutaredoxin 2: implications for intracellular roles*. Biochemistry, 2008. **47**(42): p. 11144-57.
226. Johansson C., Lillig C.H., and Holmgren A. *Human mitochondrial glutaredoxin reduces S-glutathionylated proteins with high affinity accepting electrons from either glutathione or thioredoxin reductase*. J Biol Chem, 2004. **279**(9): p. 7537-43.
227. Zhang H.H., Du Y.T., Zhang X., Lu J., and Holmgren A. *Glutaredoxin 2 reduces both thioredoxin 2 and thioredoxin 1 and protects cells from apoptosis induced by Auranofin and 4-hydroxynonenal*. Antioxid Redox Signal, 2014. **21**(5): p. 669-81.
228. Enoksson M., Fernandes A.P., Prast S., Lillig C.H., Hohngren A., and Orrenius S. *Overexpression of glutaredoxin 2 attenuates apoptosis by preventing cytochrome c release*. Biochem Biophys Res Commun, 2005. **327**(3): p. 774-79.
229. Lillig C.H., Lonn M.E., Enoksson M., Fernandes A.P., and Holmgren A. *Short interfering RNA-mediated silencing of glutaredoxin 2 increases the sensitivity of HeLa cells toward doxorubicin and phenylarsine oxide*. Proc Natl Acad Sci U S A, 2004. **101**(36): p. 13227-32.
230. Lepka K., Volbracht K., Bill E., Schneider R., Rios N., Hildebrandt T., Ingwersen J., Prozorovski T., Lillig C.H., van Horssen J., Steinman L., Hartung H.P., Radi R., Holmgren A., Aktas O., and Berndt C. *Iron-sulfur glutaredoxin 2 protects oligodendrocytes against damage induced by nitric oxide release from activated microglia*. Glia, 2017. **65**(9): p. 1521-34.
231. Brautigam L., Schutte L.D., Godoy J.R., Prozorovski T., Gellert M., Hauptmann G., Holmgren A., Lillig C.H., and Berndt C. *Vertebrate-specific glutaredoxin is essential for brain development*. Proc Natl Acad Sci U S A, 2011. **108**(51): p. 20532-37.
232. Brautigam L., Jensen L.D.E., Poschmann G., Nystrom S., Bannenberg S., Dreij K., Lepka K., Prozorovski T., Montano S.J., Aktas O., Uhlen P., Stuhler K., Cao Y.H., Holmgren A., and Berndt C. *Glutaredoxin regulates vascular development by reversible glutathionylation of sirtuin 1*. Proc Natl Acad Sci U S A, 2013. **110**(50): p. 20057-62.

233. Berndt C., Poschmann G., Stuhler K., Holmgren A., and Brautigam L. *Zebrafish heart development is regulated via glutaredoxin 2 dependent migration and survival of neural crest cells*. Redox Biol, 2014. **2**: p. 673-78.
234. Wu H.L., Yu Y.B., David L., Ho Y.S., and Lou M.F. *Glutaredoxin 2 (Grx2) gene deletion induces early onset of age-dependent cataracts in mice*. J Biol Chem, 2014. **289**(52): p. 36125-39.
235. Mailloux R.J., Xuan J.Y., McBride S., Maharsy W., Thorn S., Holterman C.E., Kennedy C.R., Rippstein P., deKemp R., da Silva J., Nemer M., Lou M., and Harper M.E. *Glutaredoxin-2 is required to control oxidative phosphorylation in cardiac muscle by mediating deglutathionylation reactions*. J Biol Chem, 2014. **289**(21): p. 14812-28.
236. Qi W.B. and Cowan J.A. *Mechanism of glutaredoxin-ISU [2Fe-2S] cluster exchange*. Chem Commun, 2011. **47**(17): p. 4989-91.
237. Fidai I., Wachnowsky C., and Cowan J.A. *Mapping cellular Fe-S cluster uptake and exchange reactions - divergent pathways for iron-sulfur cluster delivery to human ferredoxins*. Metallomics, 2016. **8**(12): p. 1283-93.
238. Frey A.G., Palenchar D.J., Wildemann J.D., and Philpott C.C. *A glutaredoxin.BolA complex serves as an iron-sulfur cluster chaperone for the cytosolic cluster assembly machinery*. J Biol Chem, 2016. **291**(43): p. 22344-56.
239. Witte S., Villalba M., Bi K., Liu Y., Isakov N., and Altman A. *Inhibition of the c-Jun N-terminal kinase/AP-1 and NF-kappaB pathways by PICOT, a novel protein kinase C-interacting protein with a thioredoxin homology domain*. J Biol Chem, 2000. **275**(3): p. 1902-09.
240. Muhlenhoff U., Molik S., Godoy J.R., Uzarska M.A., Richter N., Seubert A., Zhang Y., Stubbe J., Pierrel F., Herrero E., Lillig C.H., and Lill R. *Cytosolic monothiol glutaredoxins function in intracellular iron sensing and trafficking via their bound iron-sulfur cluster*. Cell Metab, 2010. **12**(4): p. 373-85.
241. Haunhorst P., Hanschmann E.M., Brautigam L., Stehling O., Hoffmann B., Muhlenhoff U., Lill R., Berndt C., and Lillig C.H. *Crucial function of vertebrate glutaredoxin 3 (PICOT) in iron homeostasis and hemoglobin maturation*. Mol Biol Cell, 2013. **24**(12): p. 1895-903.
242. Babichev Y. and Isakov N. *Tyrosine phosphorylation of PICOT and its translocation to the nucleus in response of human T cells to oxidative stress*. Adv Exp Med Biol, 2001. **495**: p. 41-45.
243. Cha H., Kim J.M., Oh J.G., Jeong M.H., Park C.S., Park J., Jeong H.J., Park B.K., Lee Y.H., Jeong D., Yang D.K., Bernecker O.Y., Kim D.H., Hajjar R.J., and Park W.J. *PICOT is a critical regulator of cardiac hypertrophy and cardiomyocyte contractility*. J Mol Cell Cardiol, 2008. **45**(6): p. 796-803.
244. Cheng N.H., Zhang W., Chen W.Q., Jin J.P., Cui X.J., Butte N.F., Chan L., and Hirschi K.D. *A mammalian monothiol glutaredoxin, Grx3, is critical for cell cycle progression during embryogenesis*. Febs J, 2011. **278**(14): p. 2525-39.
245. Rodriguez-Manzaneque M.T., Tamarit J., Belli G., Ros J., and Herrero E. *Grx5 is a mitochondrial glutaredoxin required for the activity of iron/sulfur enzymes*. Mol Biol Cell, 2002. **13**(4): p. 1109-21.
246. Wingert R.A., Galloway J.L., Barut B., Foott H., Fraenkel P., Axe J.L., Weber G.J., Dooley K., Davidson A.J., Schmidt B., Paw B.H., Shaw G.C., Kingsley P., Palis J., Schubert H., Chen O., Kaplan J., Zon L.I., and Consortium T.S. *Deficiency of glutaredoxin 5 reveals Fe-S clusters are required for vertebrate haem synthesis*. Nature, 2005. **436**(7053): p. 1035-39.
247. Camaschella C., Campanella A., De Falco L., Boschetto L., Merlini R., Silvestri L., Levi S., and Iolascon A. *The human counterpart of zebrafish shiraz shows sideroblastic-like microcytic anemia and iron overload*. Blood, 2007. **110**(4): p. 1353-58.

248. Kim K.D., Chung W.H., Kim H.J., Lee K.C., and Roe J.H. *Monothiol glutaredoxin Grx5 interacts with Fe-S scaffold proteins Isa1 and Isa2 and supports Fe-S assembly and DNA integrity in mitochondria of fission yeast*. *Biochem Biophys Res Commun*, 2010. **392**(3): p. 467-72.
249. Mannervik B., Board P.G., Hayes J.D., Listowsky I., and Pearson W.R. *Nomenclature for mammalian soluble glutathione transferases*. *Methods Enzymol*, 2005. **401**: p. 1-8.
250. Cesareo E., Parker L.J., Pedersen J.Z., Nuccetelli M., Mazzetti A.P., Pastore A., Federici G., Caccuri A.M., Ricci G., Adams J.J., Parker M.W., and Lo Bello M. *Nitrosylation of human glutathione transferase P1-1 with dinitrosyl diglutathionyl iron complex in vitro and in vivo*. *J Biol Chem*, 2005. **280**(51): p. 42172-80.
251. Droge W. *Free radicals in the physiological control of cell function*. *Physiol Rev*, 2002. **82**(1): p. 47-95.
252. Stewart B.W., Wild C., International Agency for Research on Cancer, and World Health Organization, *World cancer report 2014*. 2014, Lyon, France: WHO Press. p. 630.
253. Anand P., Kunnumakkara A.B., Sundaram C., Harikumar K.B., Tharakan S.T., Lai O.S., Sung B., and Aggarwal B.B. *Cancer is a preventable disease that requires major lifestyle changes*. *Pharm Res*, 2008. **25**(9): p. 2097-116.
254. Hornsveld M. and Dansen T.B. *The hallmarks of cancer from a redox perspective*. *Antioxid Redox Signal*, 2016. **25**(6): p. 300-25.
255. Gorrini C., Harris I.S., and Mak T.W. *Modulation of oxidative stress as an anticancer strategy*. *Nat Rev Drug Discov*, 2013. **12**(12): p. 931-47.
256. Pelicano H., Carney D., and Huang P. *ROS stress in cancer cells and therapeutic implications*. *Drug Resist Updat*, 2004. **7**(2): p. 97-110.
257. Wu L.L., Chiou C.C., Chang P.Y., and Wu J.T. *Urinary 8-OHdG: a marker of oxidative stress to DNA and a risk factor for cancer, atherosclerosis and diabetics*. *Clin Chim Acta*, 2004. **339**(1-2): p. 1-9.
258. Colotta F., Allavena P., Sica A., Garlanda C., and Mantovani A. *Cancer-related inflammation, the seventh hallmark of cancer: links to genetic instability*. *Carcinogenesis*, 2009. **30**(7): p. 1073-81.
259. Chandel N.S., Maltepe E., Goldwasser E., Mathieu C.E., Simon M.C., and Schumacker P.T. *Mitochondrial reactive oxygen species trigger hypoxia-induced transcription*. *Proc Natl Acad Sci U S A*, 1998. **95**(20): p. 11715-20.
260. Cai T., Fassina G., Morini M., Aluigi M.G., Masiello L., Fontanini G., D'Agostini F., De Flora S., Noonan D.M., and Albin A. *N-acetylcysteine inhibits endothelial cell invasion and angiogenesis*. *Lab Invest*, 1999. **79**(9): p. 1151-59.
261. Al-Shabraway M., Bartoli M., El-Remessy A.B., Platt D.H., Matragoon S., Behzadian M.A., Caldwell R.W., and Caldwell R.B. *Inhibition of NAD(P)H oxidase activity blocks vascular endothelial growth factor overexpression and neovascularization during ischemic retinopathy*. *Am J Pathol*, 2005. **167**(2): p. 599-607.
262. Cheng H.W., Lee S.H., and Wu S.Y. *Effects of N-acetyl-L-cysteine on adhesive strength between breast cancer cell and extracellular matrix proteins after ionizing radiation*. *Life Sci*, 2013. **93**(21): p. 798-803.
263. Warburg O. *On respiratory impairment in cancer cells*. *Science*, 1956. **124**(3215): p. 269-70.
264. Warburg O. *On the origin of cancer cells*. *Science*, 1956. **123**(3191): p. 309-14.
265. Weinberg F., Hamanaka R., Wheaton W.W., Weinberg S., Joseph J., Lopez M., Kalyanaraman B., Mutlu G.M., Budinger G.R., and Chandel N.S. *Mitochondrial metabolism and ROS generation are essential for Kras-mediated tumorigenicity*. *Proc Natl Acad Sci U S A*, 2010. **107**(19): p. 8788-93.

266. Chatterjee A., Mambo E., and Sidransky D. *Mitochondrial DNA mutations in human cancer*. *Oncogene*, 2006. **25**(34): p. 4663-74.
267. Davis S., Weiss M.J., Wong J.R., Lampidis T.J., and Chen L.B. *Mitochondrial and plasma membrane potentials cause unusual accumulation and retention of rhodamine 123 by human breast adenocarcinoma-derived MCF-7 cells*. *J Biol Chem*, 1985. **260**(25): p. 13844-50.
268. Nadakavukaren K.K., Nadakavukaren J.J., and Chen L.B. *Increased rhodamine 123 uptake by carcinoma cells*. *Cancer Res*, 1985. **45**(12 Pt 1): p. 6093-99.
269. Heerdt B.G., Houston M.A., and Augenlicht L.H. *Growth properties of colonic tumor cells are a function of the intrinsic mitochondrial membrane potential*. *Cancer Res*, 2006. **66**(3): p. 1591-96.
270. Heerdt B.G., Houston M.A., and Augenlicht L.H. *The intrinsic mitochondrial membrane potential of colonic carcinoma cells is linked to the probability of tumor progression*. *Cancer Res*, 2005. **65**(21): p. 9861-67.
271. Carew J.S., Zhou Y., Albitar M., Carew J.D., Keating M.J., and Huang P. *Mitochondrial DNA mutations in primary leukemia cells after chemotherapy: clinical significance and therapeutic implications*. *Leukemia*, 2003. **17**(8): p. 1437-47.
272. Green D.R. and Reed J.C. *Mitochondria and apoptosis*. *Science*, 1998. **281**(5381): p. 1309-12.
273. Trapp S. and Horobin R.W. *A predictive model for the selective accumulation of chemicals in tumor cells*. *Eur Biophys J*, 2005. **34**(7): p. 959-66.
274. Modica-Napolitano J.S. and Aprille J.R. *Delocalized lipophilic cations selectively target the mitochondria of carcinoma cells*. *Adv Drug Deliv Rev*, 2001. **49**(1-2): p. 63-70.
275. Bernal S.D., Lampidis T.J., Summerhayes I.C., and Chen L.B. *Rhodamine-123 selectively reduces clonal growth of carcinoma cells in vitro*. *Science*, 1982. **218**(4577): p. 1117-19.
276. Lampidis T.J., Bernal S.D., Summerhayes I.C., and Chen L.B. *Selective toxicity of rhodamine 123 in carcinoma cells in vitro*. *Cancer Res*, 1983. **43**(2): p. 716-20.
277. Bernal S.D., Lampidis T.J., Mclsaac R.M., and Chen L.B. *Anticarcinoma activity in vivo of rhodamine 123, a mitochondrial-specific dye*. *Science*, 1983. **222**(4620): p. 169-72.
278. Hickey J.L., Ruhayel R.A., Barnard P.J., Baker M.V., Berners-Price S.J., and Filipovska A. *Mitochondria-targeted chemotherapeutics: the rational design of gold(I) N-heterocyclic carbene complexes that are selectively toxic to cancer cells and target protein selenols in preference to thiols*. *J Am Chem Soc*, 2008. **130**(38): p. 12570-71.
279. Modica-Napolitano J.S., Koya K., Weisberg E., Brunelli B.T., Li Y., and Chen L.B. *Selective damage to carcinoma mitochondria by the rhodacyanine MKT-077*. *Cancer Res*, 1996. **56**(3): p. 544-50.
280. Koya K., Li Y., Wang H., Ukai T., Tatsuta N., Kawakami M., Shishido, and Chen L.B. *MKT-077, a novel rhodacyanine dye in clinical trials, exhibits anticarcinoma activity in preclinical studies based on selective mitochondrial accumulation*. *Cancer Res*, 1996. **56**(3): p. 538-43.
281. Arner E.S.J. *Targeting the Selenoprotein Thioredoxin Reductase 1 for Anticancer Therapy*. *Adv Cancer Res*, 2017. **136**: p. 139-51.
282. Cadenas C., Franckenstein D., Schmidt M., Gehrman M., Hermes M., Geppert B., Schormann W., Maccoux L.J., Schug M., Schumann A., Wilhelm C., Freis E., Ickstadt K., Rahnenfuhrer J., Baumbach J.I., Sickmann A., and Hengstler J.G. *Role of thioredoxin reductase 1 and thioredoxin interacting protein in prognosis of breast cancer*. *Breast Cancer Res*, 2010. **12**(3): p. R44.

283. Lincoln D.T., Al-Yatama F., Mohammed F.M., Al-Banaw A.G., Al-Bader M., Burge M., Sinowatz F., and Singal P.K. *Thioredoxin and thioredoxin reductase expression in thyroid cancer depends on tumour aggressiveness*. *Anticancer Res*, 2010. **30**(3): p. 767-75.
284. Singh S.S., Li Y., Ford O.H., Wrzosek C.S., Mehedint D.C., Titus M.A., and Mohler J.L. *Thioredoxin reductase 1 expression and castration-recurrent growth of prostate cancer*. *Transl Oncol*, 2008. **1**(3): p. 153-57.
285. Tobe R., Carlson B.A., Tsuji P.A., Lee B.J., Gladyshev V.N., and Hatfield D.L. *Differences in redox regulatory systems in human lung and liver tumors suggest different avenues for therapy*. *Cancers (Basel)*, 2015. **7**(4): p. 2262-76.
286. Kahlos K., Soini Y., Saily M., Koistinen P., Kakko S., Paakko P., Holmgren A., and Kinnula V.L. *Up-regulation of thioredoxin and thioredoxin reductase in human malignant pleural mesothelioma*. *Int J Cancer*, 2001. **95**(3): p. 198-204.
287. Cassidy P.B., Honegger M., Poerschke R.L., White K., Florell S.R., Andtbacka R.H., Tross J., Anderson M., Leachman S.A., and Moos P.J. *The role of thioredoxin reductase 1 in melanoma metabolism and metastasis*. *Pigm Cell Melanoma Res*, 2015. **28**(6): p. 685-95.
288. Lincoln D.T., Ali Emadi E.M., Tonissen K.F., and Clarke F.M. *The thioredoxin-thioredoxin reductase system: over-expression in human cancer*. *Anticancer Res*, 2003. **23**(3B): p. 2425-33.
289. Choi J.H., Kim T.N., Kim S., Baek S.H., Kim J.H., Lee S.R., and Kim J.R. *Overexpression of mitochondrial thioredoxin reductase and peroxiredoxin III in hepatocellular carcinomas*. *Anticancer Res*, 2002. **22**(6A): p. 3331-35.
290. Meplan C., Rohrmann S., Steinbrecher A., Schomburg L., Jansen E., Linseisen J., and Hesketh J. *Polymorphisms in thioredoxin reductase and selenoprotein K genes and selenium status modulate risk of prostate cancer*. *PLoS One*, 2012. **7**(11): p. e48709.
291. Topkas E., Cai N., Cumming A., Hazar-Rethinam M., Gannon O.M., Burgess M., Saunders N.A., and Endo-Munoz L. *Auranofin is a potent suppressor of osteosarcoma metastasis*. *Oncotarget*, 2016. **7**(1): p. 831-44.
292. Bu L., Li W., Ming Z.J., Shi J., Fang P., and Yang S.Y. *Inhibition of TrxR2 suppressed NSCLC cell proliferation, metabolism and induced cell apoptosis through decreasing antioxidant activity*. *Life Sci*, 2017. **178**: p. 35-41.
293. Kim H.J., Chae H.Z., Kim Y.J., Kim Y.H., Hwang T.S., Park E.M., and Park Y.M. *Preferential elevation of Prx I and Trx expression in lung cancer cells following hypoxia and in human lung cancer tissues*. *Cell Biol Toxicol*, 2003. **19**(5): p. 285-98.
294. Hedley D., Pintilie M., Woo J., Nicklee T., Morrison A., Birle D., Fyles A., Milosevic M., and Hill R. *Up-regulation of the redox mediators thioredoxin and apurinic/aprimidinic excision (APE)/ref-1 in hypoxic microregions of invasive cervical carcinomas, mapped using multispectral, wide-field fluorescence image analysis*. *Am J Pathol*, 2004. **164**(2): p. 557-65.
295. Han H.Y., Bearss D.J., Browne L.W., Calaluce R., Nagle R.B., and Von Hoff D.D. *Identification of differentially expressed genes in pancreatic cancer cells using cDNA microarray*. *Cancer Res*, 2002. **62**(10): p. 2890-96.
296. Raffel J., Bhattacharyya A.K., Gallegos A., Cui H.Y., Einspahr J.G., Alberts D.S., and Powis G. *Increased expression of thioredoxin-1 in human colorectal cancer is associated with decreased patient survival*. *J Lab Clin Med*, 2003. **142**(1): p. 46-51.
297. Grogan T.M., Fenoglio-Prieser C., Zeheb R., Bellamy W., Frutiger Y., Vela E., Stemmerman G., Macdonald J., Richter L., Gallegos A., and Powis G. *Thioredoxin, a putative oncogene product, is overexpressed in gastric carcinoma and associated with increased proliferation and increased cell survival*. *Hum Pathol*, 2000. **31**(4): p. 475-81.

298. Cha M.K., Suh K.H., and Kim I.H. *Overexpression of peroxiredoxin I and thioredoxin1 in human breast carcinoma*. J Exp Clin Cancer Res, 2009. **28**: p. 93.
299. Whitaker H.C., Patel D., Howat W.J., Warren A.Y., Kay J.D., Sangan T., Marioni J.C., Mitchell J., Aldridge S., Luxton H.J., Massie C., Lynch A.G., and Neal D.E. *Peroxiredoxin-3 is overexpressed in prostate cancer and promotes cancer cell survival by protecting cells from oxidative stress*. Br J Cancer, 2013. **109**(4): p. 983-93.
300. Song I.S., Jeong Y.J., Jeong S.H., Heo H.J., Kim H.K., Bae K.B., Park Y.H., Kim S.U., Kim J.M., Kim N., Ko K.S., Rhee B.D., and Han J. *FOXM1-induced PRX3 regulates stemness and survival of colon cancer cells via maintenance of mitochondrial function*. Gastroenterology, 2015. **149**(4): p. 1006-16.
301. Kim K., Yu M., Han S., Oh I., Choi Y.J., Kim S., Yoon K., Jung M., and Choe W. *Expression of human peroxiredoxin isoforms in response to cervical carcinogenesis*. Oncol Rep, 2009. **21**(6): p. 1391-96.
302. Zhang R., Al-Lamki R., Bai L.F., Streb J.W., Miano J.M., Bradley J., and Min W. *Thioredoxin-2 inhibits mitochondria-located ASK1-mediated apoptosis in a JNK-independent manner*. Circ Res, 2004. **94**(11): p. 1483-91.
303. Andersson M., Holmgren A., and Spyrou G. *NK-lysin, a disulfide-containing effector peptide of T-lymphocytes, is reduced and inactivated by human thioredoxin reductase - Implication for a protective mechanism against NK-lysin cytotoxicity*. J Biol Chem, 1996. **271**(17): p. 10116-20.
304. Shao L.E., Diccianni M.B., Tanaka T., Gribi R., Yu A.L., Pullen J.D., Camitta B.M., and Yu J. *Thioredoxin expression in primary T-cell acute lymphoblastic leukemia and its therapeutic implication*. Cancer Res, 2001. **61**(19): p. 7333-38.
305. Nilsson J., Soderberg O., Nilsson K., and Rosen A. *Thioredoxin prolongs survival of B-type chronic lymphocytic leukemia cells*. Blood, 2000. **95**(4): p. 1420-26.
306. Magnusson C.G.M., Bjornstedt M., and Holmgren A. *Human IgG is substrate for the thioredoxin system: Differential cleavage pattern of interchain disulfide bridges in IgG subclasses*. Mol Immunol, 1997. **34**(10): p. 709-17.
307. Gromer S., Urig S., and Becker K. *The thioredoxin system-from science to clinic*. Med Res Rev, 2004. **24**(1): p. 40-89.
308. Maeda R., Tabata C., Tabata R., Eguchi R., Fujimori Y., and Nakano T. *Is serum thioredoxin-1 a useful clinical marker for malignant pleural mesothelioma?* Antioxid Redox Signal, 2011. **15**(3): p. 685-89.
309. Samudio I., Harmancey R., Fiegl M., Kantarjian H., Konopleva M., Korchin B., Kaluarachchi K., Bornmann W., Duvvuri S., Taegtmeier H., and Andreeff M. *Pharmacologic inhibition of fatty acid oxidation sensitizes human leukemia cells to apoptosis induction*. J Clin Invest, 2010. **120**(1): p. 142-56.
310. Polimeni M., Voena C., Kopecka J., Riganti C., Pescarmona G., Bosia A., and Ghigo D. *Modulation of doxorubicin resistance by the glucose-6-phosphate dehydrogenase activity*. Biochem J, 2011. **439**(1): p. 141-49.
311. Panieri E. and Santoro M.M. *ROS homeostasis and metabolism: a dangerous liason in cancer cells*. Cell Death Dis, 2016. **7**(6): p. e2253.
312. Yoo M.H., Xu X.M., Carlson B.A., Gladyshev V.N., and Hatfield D.L. *Thioredoxin reductase 1 deficiency reverses tumor phenotype and tumorigenicity of lung carcinoma cells*. J Biol Chem, 2006. **281**(19): p. 13005-08.
313. Urig S. and Becker K. *On the potential of thioredoxin reductase inhibitors for cancer therapy*. Semin Cancer Biol, 2006. **16**(6): p. 452-65.

314. Fernandes A.P. and Gandin V. *Selenium compounds as therapeutic agents in cancer*. Bba-Gen Subjects, 2015. **1850**(8): p. 1642-60.
315. Bindoli A., Rigobello M.P., Scutari G., Gabbiani C., Casini A., and Messori L. *Thioredoxin reductase: A target for gold compounds acting as potential anticancer drugs*. Coord Chem Rev, 2009. **253**(11-12): p. 1692-707.
316. Zhang J.M., Li X.M., Han X., Liu R.J., and Fang J.G. *Targeting the thioredoxin system for cancer therapy*. Trends Pharmacol Sci, 2017. **38**(9): p. 794-808.
317. Scalcon V., Bindoli A., and Rigobello M.P. *Significance of the mitochondrial thioredoxin reductase in cancer cells: An update on role, targets and inhibitors*. Free Radic Biol Med, 2018. **127**: p. 62-79.
318. Hill K.E., McCollum G.W., Boeglin M.E., and Burk R.F. *Thioredoxin reductase activity is decreased by selenium deficiency*. Biochem Biophys Res Commun, 1997. **234**(2): p. 293-95.
319. Gromer S., Arscott L.D., Williams C.H., Schirmer R.H., and Becker K. *Human placenta thioredoxin reductase - Isolation of the selenoenzyme, steady state kinetics, and inhibition by therapeutic gold compounds*. J Biol Chem, 1998. **273**(32): p. 20096-101.
320. Nobili S., Mini E., Landini I., Gabbiani C., Casini A., and Messori L. *Gold compounds as anticancer agents: chemistry, cellular pharmacology, and preclinical studies*. Med Res Rev, 2010. **30**(3): p. 550-80.
321. Gasser G., Ott I., and Metzler-Nolte N. *Organometallic anticancer compounds*. J Med Chem, 2011. **54**(1): p. 3-25.
322. Ott I., Koch T., Shorafa H., Bai Z., Poeckel D., Steinhilber D., and Gust R. *Synthesis, cytotoxicity, cellular uptake and influence on eicosanoid metabolism of cobalt-alkyne modified fructoses in comparison to auranofin and the cytotoxic COX inhibitor Co-ASS*. Org Biomol Chem, 2005. **3**(12): p. 2282-86.
323. Cetinkaya B., Cetinkaya E., Kucukbay H., and Durmaz R. *Antimicrobial activity of carbene complexes of rhodium(I) and ruthenium(II)*. Arzneimittelforschung, 1996. **46**(8): p. 821-23.
324. Serebryanskaya T.V., Zolotarev A.A., and Ott I. *A novel aminotriazole-based NHC complex for the design of gold(I) anti-cancer agents: synthesis and biological evaluation*. MedChemComm, 2015. **6**(6): p. 1186-89.
325. Bertrand B., Stefan L., Pirrotta M., Monchaud D., Bodio E., Richard P., Le Gendre P., Warmerdam E., de Jager M.H., Groothuis G.M.M., Picquet M., and Casini A. *Caffeine-based gold(I) N-heterocyclic carbenes as possible anticancer agents: synthesis and biological properties*. Inorg Chem, 2014. **53**(4): p. 2296-303.
326. Engman L., McNaughton M., Gajewska M., Kumar S., Birmingham A., and Powis G. *Thioredoxin reductase and cancer cell growth inhibition by organogold(III) compounds*. Anticancer Drugs, 2006. **17**(5): p. 539-44.
327. Coronello M., Mini E., Caciagli B., Cinellu M.A., Bindoli A., Gabbiani C., and Messori L. *Mechanisms of cytotoxicity of selected organogold(III) compounds*. J Med Chem, 2005. **48**(21): p. 6761-65.
328. Gamberi T., Massai L., Magherini F., Landini I., Fiaschi T., Scaletti F., Gabbiani C., Bianchi L., Bini L., Nobili S., Perrone G., Mini E., Messori L., and Modesti A. *Proteomic analysis of A2780/S ovarian cancer cell response to the cytotoxic organogold(III) compound Aubipy(c)*. J Proteomics, 2014. **103**: p. 103-20.
329. Shaik N., Martinez A., Augustin I., Giovinazzo H., Varela-Ramirez A., Sanau M., Aguilera R.J., and Contel M. *Synthesis of apoptosis-inducing iminophosphorane organogold(III) complexes and study of their interactions with biomolecular targets*. Inorg Chem, 2009. **48**(4): p. 1577-87.

330. Nowak-Sliwinska P., van Beijnum J.R., Casini A., Nazarov A.A., Wagnieres G., van den Bergh H., Dyson P.J., and Griffioen A.W. *Organometallic ruthenium(II) arene compounds with antiangiogenic activity*. J Med Chem, 2011. **54**(11): p. 3895-902.
331. Romero-Canelon I., Pizarro A.M., Habtemariam A., and Sadler P.J. *Contrasting cellular uptake pathways for chlorido and iodido iminopyridine ruthenium arene anticancer complexes*. Metallomics, 2012. **4**(12): p. 1271-79.
332. Jaouen G., Vessieres A., and Top S. *Ferrocifen type anti cancer drugs*. Chem Soc Rev, 2015. **44**(24): p. 8802-17.
333. Fiorina V.J., Dubois R.J., and Brynes S. *Ferrocenyl polyamines as agents for the chemoimmunotherapy of cancer*. J Med Chem, 1978. **21**(4): p. 393-95.
334. Kopf-Maier P., Kopf H., and Neuse E.W. *Ferricenium complexes: a new type of water-soluble antitumor agent*. J Cancer Res Clin Oncol, 1984. **108**(3): p. 336-40.
335. Neuse E.W. *Macromolecular ferrocene compounds as cancer drug models*. J Inorg Organomet Polym, 2005. **15**(1): p. 3-32.
336. Braga S.S. and Silva A.M.S. *A new age for iron: antitumoral ferrocenes*. Organometallics, 2013. **32**(20): p. 5626-39.
337. Top S., Tang J., Vessieres A., Carrez D., Provot C., and Jaouen G. *Ferrocenyl hydroxytamoxifen: A prototype for a new range of oestradiol receptor site-directed cytotoxics*. Chem Commun, 1996. **0**: p. 955-56.
338. Jordan V.C. *The strategic use of antiestrogens to control the development and growth of breast-cancer*. Cancer, 1992. **70**(4): p. 977-82.
339. Hillard E.A., Vessieres A., and Jaouen G. *Ferrocene functionalized endocrine modulators as anticancer agents*. Top Organomet Chem, 2010. **32**: p. 81-117.
340. Hillard E., Vessieres A., Thouin L., Jaouen G., and Amatore C. *Ferrocene-mediated proton-coupled electron transfer in a series of ferrocifen-type breast-cancer drug candidates*. Angew Chem Int Edit, 2006. **45**(2): p. 285-90.
341. Nguyen A., Top S., Vessieres A., Pigeon P., Huche M., Hillard E.A., and Jaouen G. *Organometallic analogues of tamoxifen: Effect of the amino side-chain replacement by a carbonyl ferrocenyl moiety in hydroxytamoxifen*. J Organomet Chem, 2007. **692**(6): p. 1219-25.
342. Citta A., Folda A., Bindoli A., Pigeon P., Top S., Vessieres A., Salmain M., Jaouen G., and Rigobello M.P. *Evidence for targeting thioredoxin reductases with ferrocenyl quinone methides. A possible molecular basis for the antiproliferative effect of hydroxyferrocifens on cancer cells*. J Med Chem, 2014. **57**(21): p. 8849-59.
343. Rigobello M.P., Scutari G., Boscolo R., and Bindoli A. *Induction of mitochondrial permeability transition by auranofin, a gold(I)-phosphine derivative*. Br J Pharmacol, 2002. **136**(8): p. 1162-68.
344. Rigobello M.P., Scutari G., Folda A., and Bindoli A. *Mitochondrial thioredoxin reductase inhibition by gold(I) compounds and concurrent stimulation of permeability transition and release of cytochrome c*. Biochem Pharmacol, 2004. **67**(4): p. 689-96.
345. Rigobello M.P., Messori L., Marcon G., Cinellu M.A., Bragadin M., Folda A., Scutari G., and Bindoli A. *Gold complexes inhibit mitochondrial thioredoxin reductase: consequences on mitochondrial functions*. J Inorg Biochem, 2004. **98**(10): p. 1634-41.
346. Bonomini F., Rodella L.F., and Rezzani R. *Metabolic syndrome, aging and involvement of oxidative stress*. Aging Dis, 2015. **6**(2): p. 109-20.
347. Samson S.L. and Garber A.J. *Metabolic syndrome*. Endocrinol Metab Clin North Am, 2014. **43**(1): p. 1-23.

348. Hohn A., Konig J., and Jung T. *Metabolic syndrome, redox state, and the proteasomal system*. Antioxid Redox Signal, 2016. **25**(16): p. 902-17.
349. Husain K., Hernandez W., Ansari R.A., and Ferder L. *Inflammation, oxidative stress and renin angiotensin system in atherosclerosis*. World J Biol Chem, 2015. **6**(3): p. 209-17.
350. Gilbert C.A. and Slingerland J.M. *Cytokines, obesity, and cancer: new insights on mechanisms linking obesity to cancer risk and progression*. Annu Rev Med, 2013. **64**: p. 45-57.
351. Krawczyk M., Bonfrate L., and Portincasa P. *Nonalcoholic fatty liver disease*. Best Pract Res Clin Gastroenterol, 2010. **24**(5): p. 695-708.
352. May J.M. and de Haen C. *The insulin-like effect of hydrogen peroxide on pathways of lipid synthesis in rat adipocytes*. J Biol Chem, 1979. **254**(18): p. 9017-21.
353. Pignatelli P., Menichelli D., Pastori D., and Violi F. *Oxidative stress and cardiovascular disease: new insights*. Kardiol Pol, 2018. **76**(4): p. 713-22.
354. Amirkhizi F., Siassi F., Djalali M., and Shahraki S.H. *Impaired enzymatic antioxidant defense in erythrocytes of women with general and abdominal obesity*. Obes Res Clin Pract, 2014. **8**(1): p. e26-34.
355. Marseglia L., Manti S., D'Angelo G., Nicotera A., Parisi E., Di Rosa G., Gitto E., and Arrigo T. *Oxidative stress in obesity: a critical component in human diseases*. Int J Mol Sci, 2014. **16**(1): p. 378-400.
356. Palmieri V.O., Coppola B., Grattagliano I., Casieri V., Cardinale G., Portincasa P., Palasciano G., and Di Serio F. *Oxidized LDL receptor 1 gene polymorphism in patients with metabolic syndrome*. Eur J Clin Invest, 2013. **43**(1): p. 41-48.
357. Miwa K., Kishimoto C., Nakamura H., Makita T., Ishii K., Okuda N., Yodoi J., and Sasayama S. *Serum thioredoxin and alpha-tocopherol concentrations in patients with major risk factors*. Circ J, 2005. **69**(3): p. 291-94.
358. Miyamoto S., Kawano H., Hokamaki J., Soejima H., Kojima S., Kudoh T., Nagayoshi Y., Sugiyama S., Sakamoto T., Yoshimura M., Nakamura H., Yodoi J., and Ogawa H. *Increased plasma levels of thioredoxin in patients with glucose intolerance*. Intern Med, 2005. **44**(11): p. 1127-32.
359. Heinonen S., Buzkova J., Muniandy M., Kaksonen R., Ollikainen M., Ismail K., Hakkarainen A., Lundbom J., Lundbom N., Vuolteenaho K., Moilanen E., Kaprio J., Rissanen A., Suomalainen A., and Pietilainen K.H. *Impaired mitochondrial biogenesis in adipose tissue in acquired obesity*. Diabetes, 2015. **64**(9): p. 3135-45.
360. Vanella L., Li M., Rezzani R., Rodella L., Martasek P., Peterson S.J., and Abraham N.G. *Perturbations in redox homeostasis in visceral fat due to decreases in HO-1, adiponectin and pAMPK adversely affects vascular function in obese mice*. Circulation, 2010. **122**(21): p. A19686.
361. Peng X.X., Gimenez-Cassina A., Petrus P., Conrad M., Ryden M., and Arner E.S.J. *Thioredoxin reductase 1 suppresses adipocyte differentiation and insulin responsiveness*. Sci Rep, 2016. **6**: p. 28080.
362. Fisher-Wellman K.H., Mattox T.A., Thayne K., Katunga L.A., La Favor J.D., Neuffer P.D., Hickner R.C., Wingard C.J., and Anderson E.J. *Novel role for thioredoxin reductase-2 in mitochondrial redox adaptations to obesogenic diet and exercise in heart and skeletal muscle*. J Physiol-London, 2013. **591**(14): p. 3471-86.
363. Mansego M.L., Blesa S., Gonzalez-Albert V., Tormos M.C., Saez G., Redon J., and Chaves F.J. *Discordant response of glutathione and thioredoxin systems in human hypertension?* Antioxid Redox Signal, 2007. **9**(4): p. 507-14.

364. Salmon A.B., Flores L.C., Li Y., Van Remmen H., Richardson A., and Ikeno Y. *Reduction of glucose intolerance with high fat feeding is associated with anti-inflammatory effects of thioredoxin 1 overexpression in mice.* Pathobiol Aging Age Relat Dis, 2012. **2**: p. 17101.
365. Widder J.D., Fraccarollo D., Galuppo P., Hansen J.M., Jones D.P., Ertl G., and Bauersachs J. *Attenuation of angiotensin II-induced vascular dysfunction and hypertension by overexpression of Thioredoxin 2.* Hypertension, 2009. **54**(2): p. 338-44.
366. Ebrahimian T., He Y., Schiffrin E.L., and Touyz R.M. *Differential regulation of thioredoxin and NAD(P)H oxidase by angiotensin II in male and female mice.* J Hypertens, 2007. **25**(6): p. 1263-71.
367. Hou X., Song J., Li X.N., Zhang L., Wang X., Chen L., and Shen Y.H. *Metformin reduces intracellular reactive oxygen species levels by upregulating expression of the antioxidant thioredoxin via the AMPK-FOXO3 pathway.* Biochem Biophys Res Commun, 2010. **396**(2): p. 199-205.
368. Aaseth J. and Stoa-Birketvedt G. *Glutathione in overweight patients with poorly controlled type 2 diabetes.* J Trace Elem Exp Med, 2000. **13**(1): p. 105-11.
369. Sundaram R.K., Bhaskar A., Vijayalingam S., Viswanathan M., Mohan R., and Shanmugasundaram K.R. *Antioxidant status and lipid peroxidation in type II diabetes mellitus with and without complications.* Clin Sci, 1996. **90**(4): p. 255-60.
370. Svegliati-Baroni G., Candelaresi C., Saccomanno S., Ferretti G., Bachetti T., Marzioni M., De Minicis S., Nobili L., Salzano R., Omenetti A., Pacetti D., Sigmund S., Benedetti A., and Casini A. *A model of insulin resistance and nonalcoholic steatohepatitis in rats - Role of peroxisome proliferator-activated receptor-alpha and n-3 polyunsaturated fatty acid treatment on liver injury.* Am J Pathol, 2006. **169**(3): p. 846-60.
371. Torzewski M., Ochsenhirt V., Kleschyov A.L., Oelze M., Daiber A., Li H.G., Rossmann H., Tsimikas S., Reifenberg K., Cheng F., Lehr H.A., Blankenberg S., Forstermann U., Munzel T., and Lackner K.J. *Deficiency of glutathione peroxidase-1 accelerates the progression of atherosclerosis in apolipoprotein E-deficient mice.* Arterioscler Thromb Vasc Biol, 2007. **27**(4): p. 850-57.
372. Guo Z., Ran Q., Roberts L.J., Zhou L., Richardson A., Sharan C., Wu D., and Yang H. *Suppression of atherogenesis by overexpression of glutathione peroxidase-4 in apolipoprotein E-deficient mice.* Free Radic Biol Med, 2008. **44**(3): p. 343-52.
373. Pastori D., Pignatelli P., Farcomeni A., Menichelli D., Nocella C., Carnevale R., and Violi F. *Aging-related decline of glutathione peroxidase 3 and risk of cardiovascular events in patients with atrial fibrillation.* J Am Heart Assoc, 2016. **5**(9): p. e003682.
374. Matsuno S., Sasaki H., Yamasaki H., Yamaoka H., Ogawa K., Nakatani M., Hamanishi T., Doi A., Nakano Y., Wakasaki H., Furuta H., Nishi M., Akamizu T., and Nanjo K. *Pro198Leu missense polymorphism of the glutathione peroxidase 1 gene might be a common genetic predisposition of distal symmetric polyneuropathy and macrovascular disease in Japanese type 2 diabetic patients.* J Diabetes Invest, 2011. **2**(6): p. 474-82.
375. Ansari J.A., Bhandari U., Pillai K.K., and Haque S.E. *Effect of rosuvastatin on obesity-induced cardiac oxidative stress in Wistar rats-A preliminary study.* Indian J Exp Biol, 2012. **50**(3): p. 216-22.
376. Chang Y.C., Yu Y.H., Shew J.Y., Lee W.J., Hwang J.J., Chen Y.H., Chen Y.R., Wei P.C., Chuang L.M., and Lee W.H. *Deficiency of NPGPx, an oxidative stress sensor, leads to obesity in mice and human.* Embo Mol Med, 2013. **5**(8): p. 1165-79.
377. Bukowski M.R., Bucklin C., and Picklo M.J. *Quantitation of protein S-glutathionylation by liquid chromatography-tandem mass spectrometry: Correction for contaminating glutathione and glutathione disulfide.* Anal Biochem, 2015. **469**: p. 54-64.

378. Picklo M.J., Idso J.P., and Jackson M.I. *S-glutathionylation of hepatic and visceral adipose proteins decreases in obese rats*. *Obesity*, 2013. **21**(2): p. 297-305.
379. Shao D., Han J.Y., Hou X.Y., Fry J., Behring J.B., Seta F., Long M.T., Roy H.K., Cohen R.A., Matsui R., and Bachschmid M.M. *Glutaredoxin-1 deficiency causes fatty liver and dyslipidemia by inhibiting sirtuin-1*. *Antioxid Redox Signal*, 2017. **27**(6): p. 313-27.
380. Downs K.P., Nguyen H.N., Ahn Y.J., Short J.D., and Asmis R. *Glutaredoxin 1 deficiency causes late-age onset metabolic disease in female C57bl/6 mice, associated with monocyte and macrophage dysfunction*. *Free Radic Biol Med*, 2017. **112**: p. 202.
381. Chalker J., Gardiner D., Kuksal N., and Mailloux R.J. *Characterization of the impact of glutaredoxin-2 (GRX2) deficiency on superoxide/hydrogen peroxide release from cardiac and liver mitochondria*. *Redox Biol*, 2018. **15**: p. 216-27.
382. Luthman M. and Holmgren A. *Rat liver thioredoxin and thioredoxin reductase: purification and characterization*. *Biochemistry*, 1982. **21**(26): p. 6628-33.
383. Prast-Nielsen S., Cebula M., Pader I., and Arner E.S. *Noble metal targeting of thioredoxin reductase-covalent complexes with thioredoxin and thioredoxin-related protein of 14 kDa triggered by cisplatin*. *Free Radic Biol Med*, 2010. **49**(11): p. 1765-78.
384. Mieyal J.J., Starke D.W., Gravina S.A., Dothey C., and Chung J.S. *Thioltransferase in human red blood cells: purification and properties*. *Biochemistry*, 1991. **30**(25): p. 6088-97.
385. Raghavachari N. and Lou M.F. *Evidence for the presence of thioltransferase in the lens*. *Exp Eye Res*, 1996. **63**(4): p. 433-41.
386. Fang J.G., Lu J., and Holmgren A. *Thioredoxin reductase is irreversibly modified by curcumin - A novel molecular mechanism for its anticancer activity*. *J Biol Chem*, 2005. **280**(26): p. 25284-90.
387. Lowry O.H., Rosebrough N.J., Farr A.L., and Randall R.J. *Protein measurement with the Folin phenol reagent*. *J Biol Chem*, 1951. **193**(1): p. 265-75.
388. Clayton D.A. and Shadel G.S. *Isolation of mitochondria from cells and tissues*. *Cold Spring Harb Protoc*, 2014. **2014**(10): p. pdb top074542.
389. Tietze F. *Enzymic method for quantitative determination of nanogram amounts of total and oxidized glutathione: applications to mammalian blood and other tissues*. *Anal Biochem*, 1969. **27**(3): p. 502-22.
390. Anderson M.E. *Determination of glutathione and glutathione disulfide in biological samples*. *Methods Enzymol*, 1985. **113**: p. 548-55.
391. Bersani N.A., Merwin J.R., Lopez N.I., Pearson G.D., and Merrill G.F. *Protein electrophoretic mobility shift assay to monitor redox state of thioredoxin in cells*. *Methods Enzymol*, 2002. **347**: p. 317-26.
392. Du Y.T., Zhang H.H., Lu J., and Holmgren A. *Glutathione and glutaredoxin act as a backup of human thioredoxin reductase 1 to reduce thioredoxin 1 preventing cell death by aurothioglucose*. *J Biol Chem*, 2012. **287**(45): p. 38210-19.
393. Stanley B.A., Sivakumaran V., Shi S., McDonald I., Lloyd D., Watson W.H., Aon M.A., and Paolucci N. *Thioredoxin reductase-2 is essential for keeping low levels of H₂O₂ emission from isolated heart mitochondria*. *J Biol Chem*, 2011. **286**(38): p. 33669-77.
394. Myers D.K. and Slater E.C. *The enzymic hydrolysis of adenosine triphosphate by liver mitochondria. I. Activities at different pH values*. *Biochem J*, 1957. **67**(4): p. 558-72.
395. Amigo I.T., J. Rueda, C. B. *Isolating brain mitochondria by differential centrifugation*. *Bio protocols*, 2016. **6**(10): p. e1809.
396. Bradford M.M. *A rapid and sensitive method for the quantitation of microgram quantities of protein utilizing the principle of protein-dye binding*. *Anal Biochem*, 1976. **72**: p. 248-54.

397. Kofron J.L., Kuzmic P., Kishore V., Colonbonilla E., and Rich D.H. *Determination of kinetic constants for peptidyl prolyl cis trans isomerases by an improved spectrophotometric assay.* Biochemistry, 1991. **30**(25): p. 6127-34.
398. Kozakov D., Brenke R., Comeau S.R., and Vajda S. *PIPER: an FFT-based protein docking program with pairwise potentials.* Proteins, 2006. **65**(2): p. 392-406.
399. Schonbrunner E.R., Mayer S., Tropschug M., Fischer G., Takahashi N., and Schmid F.X. *Catalysis of protein folding by cyclophilins from different species.* J Biol Chem, 1991. **266**(6): p. 3630-35.
400. Jaschke A., Mi H., and Tropschug M. *Human T cell cyclophilin18 binds to thiol-specific antioxidant protein Aop1 and stimulates its activity.* J Mol Biol, 1998. **277**(4): p. 763-69.
401. Lee S.P., Hwang Y.S., Kim Y.J., Kwon K.S., Kim H.J., Kim K., and Chae H.Z. *Cyclophilin a binds to peroxiredoxins and activates its peroxidase activity.* J Biol Chem, 2001. **276**(32): p. 29826-32.
402. Connern C.P. and Halestrap A.P. *Recruitment of mitochondrial cyclophilin to the mitochondrial inner membrane under conditions of oxidative stress that enhance the opening of a calcium-sensitive non-specific channel.* Biochem J, 1994. **302** (Pt 2): p. 321-24.
403. Lin D.T. and Lechleiter J.D. *Mitochondrial targeted cyclophilin D protects cells from cell death by peptidyl prolyl isomerization.* J Biol Chem, 2002. **277**(34): p. 31134-41.
404. Lu J., Chew E.H., and Holmgren A. *Targeting thioredoxin reductase is a basis for cancer therapy by arsenic trioxide.* Proc Natl Acad Sci U S A, 2007. **104**(30): p. 12288-93.
405. Arner E.S.J., Bjornstedt M., and Holmgren A. *1-chloro-2,4-dinitrobenzene is an irreversible inhibitor of human thioredoxin reductase - Loss of thioredoxin disulfide reductase-activity is accompanied by a large increase in NADPH oxidase activity.* J Biol Chem, 1995. **270**(8): p. 3479-82.
406. Eriksson S.E., Prast-Nielsen S., Flaberg E., Szekely L., and Arner E.S. *High levels of thioredoxin reductase 1 modulate drug-specific cytotoxic efficacy.* Free Radic Biol Med, 2009. **47**(11): p. 1661-71.
407. Jarvis R.M., Hughes S.M., and Ledgerwood E.C. *Peroxiredoxin 1 functions as a signal peroxidase to receive, transduce, and transmit peroxide signals in mammalian cells.* Free Radic Biol Med, 2012. **53**(7): p. 1522-30.
408. Sobotta M.C., Liou W., Stocker S., Talwar D., Oehler M., Ruppert T., Scharf A.N.D., and Dick T.P. *Peroxiredoxin-2 and STAT3 form a redox relay for H2O2 signaling.* Nat Chem Biol, 2015. **11**(1): p. 64-70.
409. Fomenko D.E., Koc A., Agisheva N., Jacobsen M., Kaya A., Malinouski M., Rutherford J.C., Siu K.L., Jin D.Y., Winge D.R., and Gladyshev V.N. *Thiol peroxidases mediate specific genome-wide regulation of gene expression in response to hydrogen peroxide.* Proc Natl Acad Sci U S A, 2011. **108**(7): p. 2729-34.
410. Vaseva A.V., Marchenko N.D., Ji K., Tsirka S.E., Holzmann S., and Moll U.M. *p53 opens the mitochondrial permeability transition pore to trigger necrosis.* Cell, 2012. **149**(7): p. 1536-48.
411. Giorgio V., Bisetto E., Soriano M.E., Dabbeni-Sala F., Basso E., Petronilli V., Forte M.A., Bernardi P., and Lippe G. *Cyclophilin D modulates mitochondrial FoF1-ATP synthase by interacting with the lateral stalk of the complex.* J Biol Chem, 2009. **284**(49): p. 33982-88.
412. Crompton M., Virji S., and Ward J.M. *Cyclophilin-D binds strongly to complexes of the voltage-dependent anion channel and the adenine nucleotide translocase to form the permeability transition pore.* Eur J Biochem, 1998. **258**(2): p. 729-35.

413. Leung A.W., Varanyuwatana P., and Halestrap A.P. *The mitochondrial phosphate carrier interacts with cyclophilin D and may play a key role in the permeability transition*. J Biol Chem, 2008. **283**(39): p. 26312-23.
414. Scotcher J., Clarke D.J., Weidt S.K., Mackay C.L., Hupp T.R., Sadler P.J., and Langridge-Smith P.R. *Identification of two reactive cysteine residues in the tumor suppressor protein p53 using top-down FTICR mass spectrometry*. J Am Soc Mass Spectrom, 2011. **22**(5): p. 888-97.
415. Horstkotte J., Perisic T., Schneider M., Lange P., Schroeder M., Kiermayer C., Hinkel R., Ziegler T., Mandal P.K., David R., Schulz S., Schmitt S., Widder J., Sinowatz F., Becker B.F., Bauersachs J., Naebauer M., Franz W.M., Jeremias I., Brielmeier M., Zischka H., Conrad M., and Kupatt C. *Mitochondrial thioredoxin reductase is essential for early postischemic myocardial protection*. Circulation, 2011. **124**(25): p. 2892-902.
416. Hellfritsch J., Kirsch J., Schneider M., Fluege T., Wortmann M., Frijhoff J., Dagnell M., Fey T., Esposito I., Kolle P., Pogoda K., Angeli J.P.F., Ingold I., Kuhlencordt P., Ostman A., Pohl U., Conrad M., and Beck H. *Knockout of mitochondrial thioredoxin reductase stabilizes prolyl hydroxylase 2 and inhibits tumor growth and tumor-derived angiogenesis*. Antioxid Redox Signal, 2015. **22**(11): p. 938-50.
417. Schreiber V., Dantzer F., Ame J.C., and de Murcia G. *Poly(ADP-ribose): novel functions for an old molecule*. Nat Rev Mol Cell Bio, 2006. **7**(7): p. 517-28.
418. Ratnam K. and Low J.A. *Current development of clinical inhibitors of poly (ADP-ribose) polymerase in oncology*. Clin Cancer Res, 2007. **13**(5): p. 1383-88.
419. Wang Y., He Q.Y., Sun R.W., Che C.M., and Chiu J.F. *GoldIII porphyrin 1a induced apoptosis by mitochondrial death pathways related to reactive oxygen species*. Cancer Res, 2005. **65**(24): p. 11553-64.
420. Saggioro D., Rigobello M.P., Paloschi L., Folda A., Moggach S.A., Parsons S., Ronconi L., Fregona D., and Bindoli A. *Gold(III) - Dithiocarbamate complexes induce cancer cell death triggered by thioredoxin redox system inhibition and activation of ERK pathway*. Chem Biol, 2007. **14**(10): p. 1128-39.
421. Liu W.K. and Gust R. *Update on metal N-heterocyclic carbene complexes as potential anti-tumor Metallodrugs*. Coord Chem Rev, 2016. **329**: p. 191-213.
422. Schmidt C., Karge B., Misgeld R., Prokop A., Franke R., Bronstrup M., and Ott I. *Gold(I) NHC complexes: Antiproliferative activity, cellular uptake, inhibition of mammalian and bacterial thioredoxin reductases, and Gram-positive directed antibacterial effects*. Chem-Eur J, 2017. **23**(8): p. 1869-80.
423. Cardoso C.M., Custodio J.B., Almeida L.M., and Moreno A.J. *Mechanisms of the deleterious effects of tamoxifen on mitochondrial respiration rate and phosphorylation efficiency*. Toxicol Appl Pharmacol, 2001. **176**(3): p. 145-52.
424. Rybinskaya M.I., Kreindlin A.Z., and Fadeeva S.S. *On the problem of stabilization of alpha-carbocationic centers in metallocene series - Related interconversions of permethylated alpha-metallocenylcarbocations and metallocenium cation-radicals of the iron sub-group*. J Organomet Chem, 1988. **358**(1-3): p. 363-74.
425. Rybinskaya M.I., Kreindlin A.Z., Struchkov Y.T., and Yanovsky A.I. *On the problem of the stabilization of alpha-metallocenylcarbocation - Synthesis, properties and crystal-structure of [C5Me5Osc5Me4CH2+]BPh4-.CH2Cl2*. J Organomet Chem, 1989. **359**(2): p. 233-43.
426. Desta Z., Ward B.A., Soukhova N.V., and Flockhart D.A. *Comprehensive evaluation of tamoxifen sequential biotransformation by the human cytochrome P450 system in vitro: Prominent roles for CYP3A and CYP2D6*. J Pharmacol Exp Ther, 2004. **310**(3): p. 1062-75.

427. Davies A.M., Malone M.E., Martin E.A., Jones R.M., Jukes R., Lim C.K., Smith L.L., and White I.N.H. *Peroxidase activation of 4-hydroxytamoxifen to free radicals detected by epr spectroscopy*. *Free Radic Biol Med*, 1997. **22**(3): p. 423-31.
428. Do Van B., Gouel F., Jonneaux A., Timmerman K., Gele P., Petrault M., Bastide M., Laloux C., Moreau C., Bordet R., Devos D., and Devedjian J.C. *Ferroptosis, a newly characterized form of cell death in Parkinson's disease that is regulated by PKC*. *Neurobiol Dis*, 2016. **94**: p. 169-78.
429. Folda A., Citta A., Scalcon V., Cali T., Zonta F., Scutari G., Bindoli A., and Rigobello M.P. *Mitochondrial thioredoxin system as a modulator of cyclophilin D redox state*. *Sci Rep*, 2016. **6**: p. 23071.
430. Citta A., Scalcon V., Gobel P., Bertrand B., Wenzel M., Folda A., Rigobello M.P., Meggers E., and Casini A. *Toward anticancer gold-based compounds targeting PARP-1: a new case study*. *Rsc Adv*, 2016. **6**(82): p. 79147-52.
431. Jurgens S., Scalcon V., Estrada-Ortiz N., Folda A., Tonolo F., Jandl C., Browne D.L., Rigobello M.P., Kuhn F.E., and Casini A. *Exploring the theme: Synthesis and biological properties of tridentate cyclometalated gold(III) complexes*. *Bioorg Med Chem*, 2017. **25**(20): p. 5452-60.
432. Karaca O., Scalcon V., Meier-Menches S.M., Bonsignore R., Brouwer J.M.J.L., Tonolo F., Folda A., Rigobello M.P., Kuhn F.E., and Casini A. *Characterization of hydrophilic gold(I) N-heterocyclic carbene (NHC) complexes as potent TrxR inhibitors using biochemical and mass spectrometric approaches*. *Inorg Chem*, 2017. **56**(22): p. 14237-50.
433. Scalcon V., Citta A., Folda A., Bindoli A., Salmain M., Ciofini I., Blanchard S., Cazares-Marinero J.D., Wang Y., Pigeon P., Jaouen G., Vessieres A., and Rigobello M.P. *Enzymatic oxidation of ansa-ferrocifen leads to strong and selective thioredoxin reductase inhibition in vitro*. *J Inorg Biochem*, 2016. **165**: p. 146-51.
434. Scalcon V., Top S., Lee H.Z.S., Citta A., Folda A., Bindoli A., Leong W.K., Salmain M., Vessieres A., Jaouen G., and Rigobello M.P. *Osmocenyl-tamoxifen derivatives target the thioredoxin system leading to a redox imbalance in Jurkat cells*. *J Inorg Biochem*, 2016. **160**: p. 296-304.
435. Scalcon V., Salmain M., Folda A., Top S., Pigeon P., Lee H.Z.S., Jaouen G., Bindoli A., Vessieres A., and Rigobello M.P. *Tamoxifen-like metallocifens target the thioredoxin system determining mitochondrial impairment leading to apoptosis in Jurkat cells*. *Metallomics*, 2017. **9**(7): p. 949-59.